UNIVERSITÉ PARIS-EST

A Study of Well-composedness in n-D

Nicolas Boutry

October 9, 2016

Abstract

Digitization of the real world using real sensors has many drawbacks; in particular, we loose "well-composedness" in the sense that two digitized objects can be connected or not depending on the connectivity we choose in the digital image, leading then to ambiguities. Furthermore, digitized images are arrays of numerical values, and then do not own any topology by nature, contrary to our usual modeling of the real world in mathematics and in physics. Loosing all these properties makes difficult the development of algorithms which are "topologically correct" in image processing: e.g., the computation of the tree of shapes needs the representation of a given image to be continuous and well-composed; in the contrary case, we can obtain abnormalities in the final result. Some well-composed continuous representations already exist, but they are not in the same time n-dimensional and self-dual. n-dimensionality is crucial since usual signals are more and more 3-dimensional (like 2D videos) or 4-dimensional (like 4D Computerized Tomography-scans), and self-duality is necessary when a same image can contain different objects with different contrasts. We developed then a new way to make images well-composed by interpolation in a self-dual way and in n-D; followed with a span-based immersion, this interpolation becomes a self-dual continuous well-composed representation of the initial n-D signal. This representation benefits from many strong topological properties: it verifies the intermediate value theorem, the boundaries of any threshold set of the representation are disjoint union of discrete surfaces, and so on.

Keywords: well-composed, discrete surfaces, digital topology, tree of shapes, mathematical morphology

Contents

1 Introduction 21
2 State-of-the-Art 25
2.1 Mathematical Basics 25
2.2 Well-composed Sets and Images 30
2.3 Topological Reparations and Well-composed Interpolations . . . 48
2.4 Topics related to well-composedness 55
3 Generalization of Well-composedness to Dimension n 72
3.1 The different flavours of n-D WCnesses in brief 72
3.2 Mathematical Basics 74
3.3 n-D EWCness and n-D DWCness 75
3.4 Relations between AWCness, DWCness, and CWCness on cubical grids 98
4 Digitally Well-composed Interpolations in n-D 102
4.1 Self-dual Local Interpolations 103
4.2 A New Self-dual n-D DWC Interpolation 119
5 Some consequences and applications 147
5.1 Pure self-duality 147
5.2 A new representation of digital images 153
5.3 n-D Marching-Cubes-like Algorithms 158
5.4 Tree of shapes of the sign of the DWC morphological Laplacian 162
6 Perspectives 165
6.1 About the equivalence between AWCness and CWCness on cubical grids 165
6.2 Preservation of Digital Well-composedness 166
6.3 Graph-based Characterizations of AWCness and DWCness . . . 176
6.4 n-D Segmentation and Parameterization 186

7 Conclusion 189

Appendices 191
A Proof that $\mathcal{I}_{\min}(u)$ and $\mathcal{I}_{\max}(u)$ are digitally well-composed 192
B Topological Reparation in n-D 195
C Axiomatic Digital Topology 204
D About the equivalence between AWCness and DWCness 238
E Well-composed Interpolations on Polyhedral Complexes 252

List of Figures

2.1 Neighborhoods of a point $p \in \mathbb{Z}^2$. 26
2.2 Square grid using 4-adjacency 27
2.3 Square grid using 8-adjacency 27
2.4 The connectivity paradox using 4-adjacency 28
2.5 The connectivity paradox using 8-adjacency 28
2.6 Different square grids based on 6-adjacency 29
2.7 A 6-curve does not always separates the digital plane even if we use 6-adjacency. 29
2.8 $(4, 8)$-adjacency on the left and $(8, 4)$-adjacency on the right. . 30
2.9 A set which is weakly well-composed but not well-composed [96]. 31
2.10 The (black) sets are well-composed in (a) and (c), but the (black) set in (b) is neither well-composed nor weakly well-composed [96]. 31
2.11 Forbidden patterns into well-composed sets [96]. 32
2.12 The first critical pattern forbidden in 3D well-composed sets and their complement. 35
2.13 The secund critical pattern forbidden in 3D well-composed sets and their complement. 35
2.14 The six possible configurations at a corner point in a 3D well-composed set. 36
2.15 The equivalence of connectivities of a set and its complement does not imply it is well-composed in 3D (p. 171 [98]). 38
2.16 The two forbidden *critical configurations* in the continous analog of 2D well-composed sets. 40
2.17 The flat extension of the dilation operator (p.869 [25]). 43
2.18 Definition of 2D well-composedness on 2D arbitrary grids. . . 44

2.19 A set X where the set of voxels in X (in red) containing the boundary point p (at the center of the cylinder) is face-connected and such that the set of voxels in the complement of X (in blue) is not face-connected. 46
2.20 A truncated octahedra (p. 13 [115]) 46
2.21 A cell complex which would not be well-composed according to Stelldinger [160] 47
2.22 The equivalent in 2D of the repairing method of Gonzalez-Diaz *et al.*. 50
2.23 Repairing of a complex containing a critical edge [64]. 51
2.24 Repairing of a complex containing a critical vertex [64]. 51
2.25 Repairing of more complex forbidden configurations [64]. 52
2.26 Differents configurations using Majority Interpolation [162] . . 53
2.27 A reconstruction based on cubical grids in 3D leads to critical configurations [163]. 56
2.28 Even the digitization of a smooth bordered 3-manifold can contain a 2D critical configuration [163]. 56
2.29 A r-regular object and its reconstrucions [163]: (a) the r-regular object, (b) its reconstruction using a cubic $\frac{r}{2}$-grid, (c) ball union, (d) trilinear interpolation, (e) Majority Interpolation, (f) MMC (modified marching cubes). 57
2.30 An image and its rigid transformation [131]. 58
2.31 Forbidden pattern in regular images [131]. 59
2.32 Patterns that are completely destructured by the rigid transformation [132]. 59
2.33 Modified patterns whose topology is preserved under the rigid transformation [132]. 60
2.34 From seeds to well-composed regions. 61
2.35 Glamorous glue applied to regions results in a well-composed region. 61
2.36 The irreducible thick configuration [8]. 62
2.37 An irreducible gray-level well-composed image and its crest network [113]. 63
2.38 Extraction of the crest network from the irreducible well-composed configurations [113]. 63
2.39 The initial image, the image after the reduced image, and the resulting watershed [113]. 64

2.40 Polyhedral set of a $(4,8)$ digital picture. Its Euler characteristic is equal to 1. 65
2.41 Polyhedral set of a $(8,4)$ digital picture. Its Euler characteristic is equal to 0. 66
2.42 A simple closed curve in $\mathbb{R}^2$ is a Jordan curve. 67
2.43 8-curves and 4-curves are not always Jordan curves in $\mathbb{Z}^2$. . . 67
2.44 A well-composed curve is always a Jordan curve in $\mathbb{Z}^2$. 68
2.45 A simple closed curve in $\mathbb{H}^2$ is a Jordan curve. 69
2.46 Different kinds of simple closed curves according to Wang and Battacharya. 69
2.47 The continuous analog of a not well-composed set. 70
2.48 The continuous analog of a well-composed set. 71
2.49 Non-Jordan Surfaces. 71
2.50 Jordan Surfaces. 71

3.1 The notion of block depends on the space the set lies in. . . . 77
3.2 2D, 3D and 4D blocks. 77
3.3 In the raster scan order: the white points are 1-antagonists, 2-antagonists, 3-antagonists, and 4-antagonists. 77
3.4 The white points on the left draw a 2D primary critical configuration, and the white points on the right draw a secundary 2D critical configuration. 79
3.5 The white points on the left draw a 3D primary critical configuration, and the white points on the right draw a secundary 3D critical configuration. 79
3.6 The white points on the left draw a 4D primary critical configuration, and the white points on the right draw a secundary 4D critical configuration. 80
3.7 Step-by-step construction of the $2n$-path joining the two (red) antagonists into $X \cap S$ into $(\mathbb{Z}/s)^n$. 81
3.8 DWCness implies EWCness. 85
3.9 EWCness does not imply DWCness in n-D ($n \geq 3$). 87
3.10 From single-valued functions to set-valued/interval-valued functions (continuous and discrete cases). 94
3.11 A family of (large upper) threshold sets $\{[U \trianglerighteq \lambda]\}_\lambda$ of an interval-valued image U. We can remark the straightforward inclusion relationship $[U \trianglerighteq \lambda] \subseteq [U \trianglerighteq \lambda - \varepsilon]$ for any $\lambda \in \mathbb{R}$ and $\varepsilon > 0$. 96

3.12 A family of (strict upper) threshold sets $\{[U \rhd \lambda]\}_\lambda$ of an interval-valued image U. We can remark the straightforward inclusion relationship $[U \rhd \lambda] \subseteq [U \rhd \lambda - \varepsilon]$ for any $\lambda \in \mathbb{R}$ and $\varepsilon > 0$. 97
3.13 Possible configurations in 2D. 98
3.14 Possible configurations in 3D. 100
4.1 Subdividing the domain $\mathcal{D}$ into $\mathcal{D}'$ to interpolate. 102
4.2 Illustration of the subdivision process on a block S. 105
4.3 $\mathrm{Subd}(S) \subseteq \left(\frac{\mathbb{Z}}{2}\right)^n$ as a poset. 105
4.4 Parenthood relationship in the graph of a subdivided block. . 107
4.5 Ancesters of the point z at the center of the subdivided block. 108
4.6 Groups of the point z at the center of the subdivided block. . 108
4.7 Ordered computing of the values of the interpolation. 110
4.8 Other kinds of subdivisions/interpolations. 112
4.9 The 3 possible configurations in 2D (modulo reflections and rotations). 115
4.10 $u'\big|_{\mathcal{G}(z)}$ for $z \in \mathbb{E}_2$ for any self-dual local interpolation after the application of f_1 (with m any value $\in \mathbb{R}$). 115
4.11 The Hasse diagrams for the α- and the U-configurations (left) and for the Z-configuration (right). 116
4.12 An image, and its interpolations using the *median*, the *mean/median*, the *min* and the *max* operators respectively. 117
4.13 A counter-example proving that an interpolation satisfying $(\mathcal{P})$ (with only one subdivision and with f_1 the mean operator) cannot ensure digital well-composedness (the values of u' on $\mathbb{E}_0$ are in green, the ones on $\mathbb{E}_1$ are in blue, the ones on $\mathbb{E}_2$ are in red, and the ones on $\mathbb{E}_3$ are in purple). 118
4.14 The initial image u. 120
4.15 The "continuous" interpolation U. 120
4.16 Flattening process. 121
4.17 The interpolation of u. 122
4.18 Computation of the tree of shapes. 123
4.19 The front propagation algorithm applied on a digitally well-composed interval-valued image U. 126
4.20 A situation impossible to obtain with $p, q \in \mathcal{D}$ being $2n$-neighbors in $(\mathbb{Z}/s)^n$. 129

4.21 The 4 possible scenarii when only two $2n$-neighbors p and q in $\mathcal{D}'$ are considered. 130
4.22 Different cases corresponding to Scenario $(1a)$: $u^\flat(p) > \lfloor U \rfloor(q)$ on the left and $u^\flat(p) \leq \lfloor U \rfloor(q)$ on the right. Thanks to $\ell(q) = u^\flat(p)$, $u^\flat(q)$ stays inferior to λ like $u^\flat(p)$. 131
4.23 Different cases corresponding to Scenario $(1b)$: $u^\flat(h) > \lfloor U \rfloor(q)$ on the left and $u^\flat(h) \leq \lfloor U \rfloor(q)$ on the right. Thanks to the enqueuing of p into Q at the level $u^\flat(p) \leq \lambda$, $\ell(q) = u^\flat(h)$ is inferior to λ and then $u^\flat(q)$ stays inferior to λ too. 132
4.24 Different cases corresponding to Scenario $(2a)$: $u^\flat(q) < \lceil U \rceil(p)$ on the left and $u^\flat(q) \geq \lceil U \rceil(p)$ on the right. Thanks to $lcur(p) = u^\flat(q)$, $u^\flat(p)$ stays superior to λ like $u^\flat(q)$. 132
4.25 Different cases corresponding to Scenario $(2b)$: $u^\flat(h) < \lceil U \rceil(p)$ on the left and $u^\flat(h) \geq \lceil U \rceil(p)$ on the right. Thanks to the enqueuing of q into Q at the level $u^\flat(q) > \lambda$, $\ell(p) = u^\flat(h)$ is greater than λ and then $u^\flat(p)$ stays greater than λ too. 133
4.26 Assuming U is digitally well-composed and $u^\flat$ is not digitally well-composed, we obtain the four properties: $u^\flat(p_*) \geq \lambda$, $\lfloor U \rfloor(p_*) < \lambda$, $u^\flat(p'_*) < \lambda$, and $\lceil U \rceil(p'_*) \geq \lambda$ with p_*, p'_* $2n$-neighbors in $\mathcal{D}'$, which lead to a contradiction. 137
4.27 The complete process in detail. 143
4.28 From U_+ to $u^\flat$. 145
4.29 A self-dual digitally well-composed interpolation of image of Figure 4.13. 146

5.1 In the middle, a gray-level image. On the left, its min-tree and max-tree, and on the right its tree of shapes [60]. 148
5.2 Incoherences using 4-connectivity for both upper and lower threshold sets. 148
5.3 Incoherences using 8-connectivity for both upper and lower threshold sets. 148
5.4 An image u, its min/max interpolations, and u_{DWC} which is self-dual. 149
5.5 The tree of shapes of the min, max, and self-dual interpolations. 150
5.6 The initial image u containing a ball and a full torus and its self-dual interpolation. 150
5.7 On the left, u seen from the top, and on the right, u_{DWC} seen from the top. 151

5.8 The tree of shapes of u. 151
5.9 Grain filtering on an image u: our self-dual representation leads to "pure" self-duality. 152
5.10 From u to its underlying graph structure using the dual pair (c_8, c_4). 152
5.11 All the possible cubical connectivity grids are equivalent on a digitally well-composed image. In the raster scan order, the 4-connectivity grid, the 8-connectivity grid, the perfect fusion grid, a 6-connectivity grid, and the Khalimsky grid. 153
5.12 Span-based immersion of $u : [\![0, 1]\!] \times [\![0, 1]\!] \to \mathbb{R}$ into a cubical complex provides continuity properties to the new representation U of u. 155
5.13 $\Delta[U \rhd 0]$, depicted in red, contains a pinch (in yellow). 155
5.14 Our method to obtain an AWC plain map. 156
5.15 Lorensen's Marching Cubes Lookup Table [110] 158
5.16 The "hole problem" using Marching Cubes ([153]) 159
5.17 Lookup tables of Daragon [42, 43] in the 3D case. 161
5.18 n-D approach of Lachaud [94], based on the convex hull. . . . 161
5.19 Summary of the method used by Huyhn *et al.* [80]. 163
5.20 An inclusion tree and its corresponding image [80]. 164

6.1 Morphological dilation does not preserve digital well-composedness using a structuring element based on 4-connectivity. . 166
6.2 Morphological dilation does not preserve digital well-composedness using a structuring element based on 8-connectivity. . 167
6.3 Morphological erosion does not preserve digital well-composedness using a structuring element based on 4-connectivity. . 167
6.4 Morphological erosion does not preserve digital well-composedness using a structuring element based on 8-connectivity. . 167
6.5 The original Barbara image. 171
6.6 The 44417 critical configurations in the original Barbara image. 172
6.7 Our self-dual interpolation of the Barbara image. 172
6.8 A grain filter of the DWC interpolation of the Barbara image with a threshold $\lambda = 10$. 173
6.9 A grain filter of the DWC interpolation of the Barbara image with a threshold $\lambda = 320$. 173
6.10 A grain filter of the DWC interpolation of the Barbara image with a threshold $\lambda = 1280$. 174

6.11 A 3D digitally well-composed binary image, the *mask*, and a marker of the same size. . . . 175
6.12 The geodesic dilation of the marker in the binary image is also digitally well-composed. . . . 175
6.13 A discretized sphere with values on the 2-faces. . . . 177
6.14 How to characterize AWCness in 2D. . . . 179
6.15 Boundaries of the different threshold sets around z^2. . . . 179
6.16 A 3D image which is not AWC. . . . 180
6.17 Some examples of graphs $\mathcal{G}(u, z)$. . . . 181
6.18 Boundary of the well-composed object is a manifold. . . . 187

7.1 Links betweens the different flavors of well-composedness on cubical grids. . . . 190
7.2 A (subdivided) torus and its incidence graph [41] (p.50). . . . 190

B.1 Hierarchical representation of an image: since component boundaries are simple closed curves on well-composed images, two boundaries are either disjoint or in an inclusion relationship; thus, the delimited regions naturally form a tree. Actually it is a sub-part of the tree of shapes [60]. . . . 196
B.2 Number of critical configurations as a function of the size of the image given in number of pixels. . . . 200
B.3 Number of corrections as a function of the number of initial critical configurations. . . . 201
B.4 Original image u. . . . 201
B.5 Zero-crossings of the original Laplacian. . . . 202
B.6 Zero-crossings of the Laplacian modified by the increasing process. . . . 202
B.7 Text segmentation results. . . . 202

C.1 Different representations of the same cubical complex. . . . 212
C.2 The closures $\alpha(x)$, $\alpha(y)$, $\alpha(z)$ in $\mathbb{H}^2$ [41] (p. 34) . . . 214
C.3 The openings $\beta(x)$, $\beta(y)$, $\beta(z)$ in $\mathbb{H}^2$ [41] (p. 34) . . . 214
C.4 The neighborhoods $\theta(x)$, $\theta(y)$, $\theta(z)$ in $\mathbb{H}^2$ [41] (p. 34) . . . 214
C.5 A binary image u_{bin} in $\mathbb{Z}^2$ [41] (p. 31) . . . 215
C.6 u_{bin} [41] (p. 31) supplied with the $(4, 8)$-topology on the left and with the $(8, 4)$-topology on the right (the foreground is in black and the background in white). . . . 215

C.7 Different immersions of u_{bin} into $\mathbb{H}^2$ [41] (p. 31). 216
C.8 A path in $\mathbb{H}^2$ [41] (p.34) 217
C.9 A simple closed curve in $\mathbb{H}^2$ [41] (p.34) 218
C.10 Three examples of orders $|X|, |Y|, |Z|$ ([41], p.37) 220
C.11 The join operator $*$ is not commutative ([41], p.37) 220
C.12 Some order joins representing a *simplicial complex* on the left and a sphere on the right [41] (p.37) 221
C.13 A 2-surface: the sphere $\mathcal{S}_2$ [41] (p.50) 221
C.14 Different kinds of *adherences* of a 2-element in $\mathbb{H}^3$ [41] (p.54) 223
C.15 Examples of simplicial complexes ([41], p.40). 226
C.16 From a subcomplex to its simplicial neighborhood ([41], p.46). 232
C.17 From an order to its chain comples ([41], p.46). 233
C.18 From a simplicial complex to a frontier order ([41], p. 86). . . 233
C.19 A cubical complex and the frontier order of the central square into this order. 234
C.20 From a full subcomplex to its derived neighborhood ([41], p. 98). 236

D.1 A 4D digitally well-composed set (depicted in blue) and its complement (in red). 239
D.2 Bijection between $\mathbb{H}^1$ and $(\mathbb{Z}/2)$ 241
D.3 The subspace $|\beta^{\square}(z)|$ we are working in to study AWCness (2D/3D cases). 242
D.4 Examples of 0-surfaces (in black). 243
D.5 Examples of 1-surfaces. 243
D.6 From a 2D critical configuration in $\mathbb{Z}^2$ to a critical point z^* in $\mathbb{H}^2_0$. 244
D.7 From the 3D critical configuration to the critical point. 246
D.8 Assuming that X is DWC, $|\beta^{\square}_{\mathfrak{N}}(z)|$ is a 0-surface when $\dim(z) = n-2$ $(k=2)$. 247
D.9 Examples of opposites in $\mathbb{H}^2$. 248
D.10 Structure of $\beta^{\square}_{\mathfrak{N}}(z)$ when we have $(n - \dim(z)) = 3$ assuming that $|\beta^{\square}_{\mathfrak{N}}(z)|$ is not connected. 249

E.1 A polyhedral (simplicial) complex (on the left) and its border. 254
E.2 Among these orders, the only bordered 2-surface is the one on the right. 254
E.3 A triangulated Möbius ruban is a bordered 2-manifold. 255

E.4 On the left a topological structure that is not a bordered 2-manifold, and on the right a bordered 2-manifold. Interiors are depicted in black and borders in red. 256
E.5 $[u \leq 0]$ and $[u \leq 1]$ are AWC, but $[u \geq 1]$ is not AWC. 257
E.6 Dual cells. 258
E.7 From a partition of a simplicial complex to its corresponding cell complex (one color by 2-cell). 259
E.8 Families of n-cells: AWC on the left and not AWC on the right. 260
E.9 Functions on cell complexes: AWC on the left and not AWC on the right. 261
E.10 An image defined u on the n-dimensional convex polyhedral domains of a polyhedral complex. 262
E.11 Chain complex of the initial image. 263
E.12 Using derived neighborhoods directly on the initial domain does not lead to a satisfactory result. 264
E.13 Using derived neighborhoods on the chain complex of the domain of u does not lead to a satisfactory result neither. 264
E.14 Using frontier orders on the chain complex of the closure of the domain of the image disconnects the pixels. 265
E.15 Using directly frontier orders on a simplicial complex is not self-dual. 266
E.16 From u defined on the n-cells of a polyhedral complex to U defined on all the faces of the complex. 266
E.17 U' defined on all the 0-faces of the subdivided complex. 267
E.18 The same image U' with an additional border. 267
E.19 $u^\flat_+$ (with the temporary border). 268
E.20 $u^\flat$ (without the temporary border). 268
E.21 $\mathcal{F}([u^\flat \leq 1], \mathcal{C}^{\mathfrak{Pc}^n})$. 269
E.22 $\Delta N^1(\mathcal{F}([u^\flat \leq 0], \mathcal{C}^{\mathfrak{Pc}^n}), \mathcal{C}^{\mathfrak{Pc}^n})$. 270
E.23 $\Delta N^1(\mathcal{F}([u^\flat \leq 1], \mathcal{C}^{\mathfrak{Pc}^n}), \mathcal{C}^{\mathfrak{Pc}^n})$. 270
E.24 $\Delta N^1(\mathcal{F}([u^\flat \leq 0], \mathcal{C}^{\mathfrak{Pc}^n}), \mathcal{C}^{\mathfrak{Pc}^n})$. 270
E.25 The new valued cell complex representing an AWC function. . 271
E.26 Cubical subdivision VS double derived subdivision. 272
E.27 From a cell complex to its hierarchical subdivision. 273
E.28 From the hierarchical subdivision of a polyhedral complex to its chain complex. 274
E.29 The cell complex resulting of the chain complex of the hierarchical subdivision: the geometry of the initial cells is preserved. 274

E.30 From u to U. 275
E.31 The propagation. 275
E.32 A self-dual interpolation of u. 276
E.33 The dual cell resulting from the chain complex of the hierarchical subdivision. 278
E.34 Our self-dual representation on cell complexes. 280

List of Annotations

- AWC: Well-Composed in the sense of Alexandrov,
- CC: Critical Configuration,
- CWC: Continuous Well-Composedness,
- DWC: Digital Well-Composedness,
- EWC: Well-Composed based on the Equivalence of connectivities,
- FPA: Front-Propagation Algorithm,
- IVM: Interval-Valued Map,
- MC: Marching Cubes,
- MM: Mathematical Morphology,
- PL: Piecewise Linear,
- ToS: Tree of Shapes,
- WC: Well-Composed.

List of Symbols

- basics:
  - n is the dimension of the space,
  - $s \geq 1$ is the (domain) subdivision factor,
  - $\mathbb{B} = \{e^1, \ldots, e^n\}$ is the canonical basis of $\mathbb{Z}^n$,
  - x_i is the i^{th} coordinate, $i \in [\![1, n]\!]$, of $x \in \mathbb{R}^n$,
  - $\#$ denotes the cardinal operator,
- single-valued images:
  - $\mathbb{Z}^n$, $\left(\frac{\mathbb{Z}}{2}\right)^n$, $(\mathbb{Z}/s)^n$ are the sets/images spaces,
  - $\mathcal{D} \subseteq (\mathbb{Z}/s)^n$ is the domain of a given image,
  - $\mathbb{V}$ is the value space of a given image,
  - u_{bin} represents a binary image,
  - $\mathbb{I}\text{m}(A, \mathcal{D}, \mathbb{V})$ is the space of all possible images whose space is A, whose domain is $\mathcal{D}$ and whose value space is $\mathbb{V}$,
- interval-valued images:
  - $\lceil U \rceil$ is the upper bound of the interval-valued image U,
  - $\lfloor U \rfloor$ is the lower bound of the interval-valued map U,
- threshold sets:
  - $\lambda \in \mathbb{R}$ is a threshold value belonging to $\mathbb{R}$,
  - $[u \geq \lambda]$ is the large upper threshold set of u for a threshold $\lambda \in \mathbb{R}$,
  - $[u \leq \lambda]$ is the large lower threshold set of u for a threshold $\lambda \in \mathbb{R}$,

- $[u > \lambda]$ is the strict upper threshold set of u for a threshold $\lambda \in \mathbb{R}$,
- $[u < \lambda]$ is the strict lower threshold set of u for a threshold $\lambda \in \mathbb{R}$,
- $[U \trianglerighteq \lambda]$ is the large upper threshold set of U for a threshold $\lambda \in \mathbb{R}$,
- $[U \trianglelefteq \lambda]$ is the large lower threshold set of U for a threshold $\lambda \in \mathbb{R}$,
- $[U \triangleright \lambda]$ is the strict upper threshold set of U for a threshold $\lambda \in \mathbb{R}$,
- $[U \triangleleft \lambda]$ is the strict lower threshold set of U for a threshold $\lambda \in \mathbb{R}$,

- neighborhoods and connectivity:
  - $\mathcal{N}_{2n}(p, A)$ is the $2n$-neighborhood of p in A,
  - $\mathcal{N}^*_{2n}(p, A)$ is the $2n$-neighborhood of p minus p in A,
  - $\mathcal{N}_{3^n-1}(p, A)$ is the $(3^n - 1)$-neighborhood of p in A,
  - $\mathcal{N}^*_{3^n-1}(p, A)$ is the $(3^n - 1)$-neighborhood of p minus p in A,
  - $\mathcal{CC}_{X,A}$ is the set of connected components of $X \subset A$ in A,

- blocks and antagonism:
  - $\mathcal{B}(A)$ is the set of blocks in the space A,
  - $\mathcal{F} = (f^1, \ldots, f^k) \subseteq \mathbb{B}$ is the family of vectors associated to a block,
  - $S_s(z, \mathcal{F})$ is the block associated to z and to the family $\mathcal{F}$ into $(\mathbb{Z}/s)^n$,
  - $S \in \mathcal{B}(A)$ is a block in A,
  - k is the dimension of a block S associated to $\mathcal{F} = (f^1, \ldots, f^k)$,
  - $\text{antag}_S(p)$ is the antagonist in the block S to $p \in S$,

- interval values:
  - $\text{intvl}(a, b)$ is the interval value $[\min(a, b), \max(a, b)]$ of the values $a, b \in \mathbb{R}$,
  - $\text{Span}(V)$ is the span of the (finite) set of values $V \subset \mathbb{R}$,
  - $[\![a, b]\!]$ is the discrete interval $[a, b] \cap \mathbb{Z}$ with $a, b \in \mathbb{Z}$ such that $a \leq b$,
  - $\text{ConvHull}(A)$ is the convex hull of the set $A \subseteq \mathbb{R}^n$,

- interpolations:

  - $\mathcal{I}$ denotes an interpolation method,
  - $\mathcal{I}_{\text{op}}$ denotes an interpolation method based on an operator op,
  - $\mathcal{I}_{\min}$ is the min-based n-D interpolation,
  - $\mathcal{I}_{\max}$ is the max-based n-D interpolation,
  - $\mathcal{I}_{\text{med}}$ is the median-based n-D interpolation,
  - $\mathcal{I}_{\text{Span}}$ is the span-based interval-valued n-D interpolation,

- continuous analogs and boundaries in $\mathbb{R}^n$:
  - $\text{CA}(z)$ is the continuous analog of $z \in \mathbb{Z}^n$ (a cube or radius $\frac{1}{2}$ centered at z),
  - $\text{CA}(X)$ is the union of the continuous analogs of the points of $X \subset \mathbb{Z}^n$,
  - $\text{bdCA}(X)$ is the topological boundary of the continuous analog of $X \subset \mathbb{Z}^n$,
  - $\text{Int}(A)$ is the topological interior of $A \subset \mathbb{R}^n$,
  - $\partial(A)$ is the topological boundary of $A \subset \mathbb{R}^n$,

- mathematical morphology:
  - se is a structuring element,
  - ε is the morphological erosion operator,
  - δ is the morphological dilation operator,
  - $\mathcal{L}$ is the morphological Laplacian operator,
  - δ_{Geod} is the (morphological) geodesic dilation,

- the front-propagation algorithm steb-by-step:
  - u is a single-valued image,
  - U is a set-valued/interval-valued image,
  - U_+ is the interval-valued interpolation with an added border at ℓ_∞,
  - $u^\flat$ is the output image of our n-D self-dual interpolation method before we remove the border,

- u_{DWC} is the output image of our n-D self-dual interpolation method,
- $\mathfrak{FP}$ denotes the output of the front-propagation algorithm,
- ℓ_∞ is the median value of the inner border of the input image in the $\mathfrak{FP}$ algorithm,
- p_∞ is the point corresponding to the exterior in the $\mathfrak{FP}$ algorithm,
- Q is an (hierarchical or not) queue,
- $Q[\ell]$ is the queue at the level ℓ in the $\mathfrak{FP}$ algorithm,
- ℓ is the current level in the $\mathfrak{FP}$ algorithm,
- $\ell(z)$ is the value of ℓ when we enqueue z into the hierarchical queue Q,
- $t(z)$ is the enqueuing time of the point z in the $\mathfrak{FP}$ algorithm,

- remarkable sets of Section 4.1
  - $(\mathcal{P})$ is a set of properties that "usual" well-composed interpolations have to verify,
  - $I_0(u', z)$ corresponds to the set of values that $u'(z)$ can take ensuring in-betweeness of u' in $\mathcal{G}(z)$ using an usual interpolation method,
  - $I_{WC}(u', z)$ corresponds to the set of values that $u'(z)$ can take ensuring well-composedness of u' in $\mathcal{G}(z)$ using an usual interpolation method,
  - $I_{sol}(u', z) = I_0(u', z) \cap I_{WC}(u', z)$ using an usual interpolation method,

- $\left(\frac{\mathbb{Z}}{2}\right)^n$ as a poset:
  - $\mathrm{Subd}(A)$ is the hierarchical subdivision of a bounded hyperrectangle $A \subseteq \mathbb{Z}^n$,
  - $\frac{1}{2}(z)$ is the set of indices of the coordinates of z that are not integers,
  - $\mathbb{E}_i$ is the set of points in $\left(\frac{\mathbb{Z}}{2}\right)^n$ of hierarchical order $i \in [\![0, n]\!]$,
  - $\mathfrak{o}(z)$ is the hierarchical order of $z \in \left(\frac{\mathbb{Z}}{2}\right)^n$,
  - $\mathbb{P}(z)$ are the hierarchical parents of $z \in \left(\frac{\mathbb{Z}}{2}\right)^n$,

- $\mathcal{G}(z)$ is the hierarchical group of $z \in \left(\frac{\mathbb{Z}}{2}\right)^n$,
- $\mathbb{A}(z)$ are the hierarchical ancesters of $z \in \left(\frac{\mathbb{Z}}{2}\right)^n$,
- $\mathrm{opp}(z)$ is the set of couples of opposites relatively to $z \in \left(\frac{\mathbb{Z}}{2}\right)^n$,
- $\mathbb{1}(x)$ is the set of *integral coordinates* of $x \in (\mathbb{Z}/2)^n$,
- $\frac{1}{2}(x)$ is the set of *half coordinates* of $x \in (\mathbb{Z}/2)^n$,

- ordered sets:
  - R is a binary relation,
  - $\mathcal{O}$ represents a set or arbitrary elements,
  - $|\mathcal{O}| = (\mathcal{O}, \alpha_{\mathcal{O}})$ is the set $\mathcal{O}$ supplied with its order relation $\alpha_{\mathcal{O}}$,
  - α is the topological closure operator,
  - $\alpha^{\square}(x) = \alpha(x) \setminus \{x\}$, $\forall x \in \mathcal{O}$,
  - $\alpha_X = \alpha \cap X \times X$,
  - $\alpha(X) = \bigcup_{x \in X} \alpha(x)$,
  - β is the topological opening operator, the inverse of α,
  - $\beta^{\square}(x) = \beta(x) \setminus \{x\}$, $\forall x \in \mathcal{O}$,
  - $\beta_X = \beta \cap X \times X$,
  - $\beta(X) = \bigcup_{x \in X} \beta(x)$,
  - $\theta = \alpha \cap \beta$ is the neighborhood,
  - $\theta^{\square}(x) = \theta(x) \setminus \{x\}$, $\forall x \in \mathcal{O}$,
  - $\theta_X = \theta \cap X \times X$,
  - $\theta(X) = \bigcup_{x \in X} \theta(x)$,

- from $(\mathbb{Z}/2)^n$ to Khalimsky grids:
  - $\mathbb{H}^n$ denotes the Khalimsky grids of dimension n,
  - $\mathbb{H}^n_k$, $k \in [\![0, n]\!]$, denotes the elements of $\mathbb{H}^n$ of dimension k,
  - $\mathcal{Z} : \mathbb{H}^1 \to (\mathbb{Z}/2)$ is the topological isomorphism between $\mathbb{H}^1$ and $(\mathbb{Z}/2)$,
  - $\mathcal{Z}_n : \mathbb{H}^n \to (\mathbb{Z}/2)^n$ is the topological isomorphism between $\mathbb{H}^n$ and $(\mathbb{Z}/2)^n$,

- $\mathcal{H}$ is the inverse of the topological isomorphism $\mathcal{Z}$,
- $\mathcal{H}_n$ is the inverse of the topological isomorphism $\mathcal{Z}_n$,
- $\mathcal{U}_{\mathbb{H}^1}$ is the topology of $\mathbb{H}^1$,
- $\mathcal{U}_{(\mathbb{Z}/2)}$ is the topology associated to $(\mathbb{Z}/2)$ as an isomorph of $\mathbb{H}^1$,
- $\mathcal{U}_{\mathbb{H}^n}$ is the topology of $\mathbb{H}^n$,,
- $\mathcal{U}_{(\mathbb{Z}/2)^n}$ is the topology associated to $(\mathbb{Z}/2)^n$ as an isomorph of $\mathbb{H}^n$

- Khalimsky grids:
  - $a \wedge b = \sup(\alpha(a) \cap \alpha(b))$ is the *infimum* between a and b,
  - $a \vee b = \inf(\beta(a) \cap \beta(b))$ is the *supremum* between a and b,
  - $\dim(f)$ is the dimension of the face $f \in \mathbb{H}^n$,

- Chapter D:
  - $X \subseteq \mathbb{Z}^n$ is a subset of $\mathbb{Z}^n$
  - $Y = \mathbb{Z}^n \setminus X$ is a subset of $\mathbb{Z}^n$
  - $\mathcal{X} = \mathcal{H}_n(X) \subseteq \mathbb{H}^n_n$ is the isomorph of X into the Khalimsky grids,
  - $\mathcal{Y} = \mathcal{H}_n(Y) \subseteq \mathbb{H}^n_n$ is the isomorph of Y into the Khalimsky grids,
  - $\mathcal{IMM}(X) = \mathrm{Int}(\alpha(\mathcal{H}_n(X)))$ is the immersion of X into $\mathbb{H}^n$
  - $\mathfrak{N}$ is the topological boundary of $\mathcal{IMM}(X)$ into $\mathbb{H}^n$
  - $\mathcal{CC}(\mathfrak{N})$ are the connected components of $\mathfrak{N}$,
  - $z^* = \mathcal{H}_n(p) \wedge \mathcal{H}_n(p')$ is a *critical point* when $X \cap S(p, p')$ is a primary/secondary critical configuration,
  - $(\mathcal{P}_k) \equiv \left\{\forall z \in N \cap \mathbb{H}^n_{n-k},\ |\beta^{\square}_{\mathfrak{N}}(z)| \text{ is a } (n-2-\dim(z)) - \text{surface}\right\}.$,
  - $(\mathcal{P}'_k) \equiv \left\{\forall z \in \mathfrak{N} \cap \mathbb{H}^n_{n-k},\ |\beta^{\square}_{\mathfrak{N}}(z)| \text{ is connected}\right\}.$,
  - $\mathcal{I}$ is the family of indices s.t. $\{F_i\}_{i\in\mathcal{I}} = \mathcal{CC}(|\beta^{\square}_{\mathfrak{N}}(z)|)$,
  - $\{F_i\}_{i\in\mathcal{I}}$ are the connected components of $|\beta^{\square}_{\mathfrak{N}}(z)|$,
  - $S(z) \equiv \mathcal{Z}_n(\beta(z) \cap \mathbb{H}^n_n)$ is the block centered at $z \in \mathbb{H}^n$,
  - $\mathcal{T}(u)$ is the set of $(\dim(z)+1)$-faces included into $\alpha(u) \cap \beta^{\square}(z)$,
  - $\mathcal{T}(F_i)$ is the set of $(\dim(z)+1)$-faces of F_i,

- $\mathfrak{a} = \bigvee_{t \in \mathcal{T}(F_1)} t$ and $\mathfrak{b} = \bigvee_{t \in \mathcal{T}(F_2)} t$. (characteristical points)

• Combinatorial and Piecewise Linear topologies:

- C is a simplicial complex,
- Λ_C is the support of the simplicial (sub)complex C,
- $\mathcal{C}^X$ is the chain complex of the order $|X|$,
- $|C_{K/K'}|$ is the frontier order of K into Λ_C relatively to C
- $N(K, C)$ is the simplicial neighborhood of K into C,
- $\Delta(K, C)$ is the border of the derived neighborhood of K into C,
- K^1 or $[K]^1$ is the chain complex of K,
- $N^1(K, C)$ is the derived neighborhood of the subcomplex K into C,
- K^n or $[K]^n$ is the n^{th} derived subdivision of K,
- Char($|X|$) the set of characteristical faces of the order $|X|$,
- ∂X is the border of the order $|X|$,
- Int($|X|$) is the interior of $|X|$,
- $\mathfrak{CC}^n$ is a (simplicial) cell complex,
- $\{S^i\}_{i \in \mathcal{I}}$ is a family of cells of $\mathfrak{CC}^n$
- $\{P^i\}_{i \in \mathcal{I}}$ is a partition of the set of n-cells of $\mathfrak{CC}^n$,
- $\mathfrak{CC}^n_n$ is the set of n-faces of $\mathfrak{CC}^n$.

Chapter 1

Introduction

As told by Rosenfeld in 1979 in [141], "digital pictures are rectangular arrays of non-negative numbers". Effectively, these pictures, which are yet today very common, are simply sets of pixels, that is structures with a position and a value. However, no notion of neighborhood or of continuity are defined on these sets by nature at the contrary to the world we are living in, and which they are assumed to be able to capture.

To give back as much as possible the topology of the plane to these arrays, Rosenfeld considered that two points are neighbours depending on their relative positions in these arrays [138]: roughly speaking, they should be neighbors iff they are "close enough". However, on arrays, there are more than one possible manner to define that two pixels are neighbors: they can be 4-neighbors if their L^1 distance is lower than or equal to one, and they are 8-neighbors if their L^∞ distance is lower than or equal to one (and they are not the only possible connectivities on $\mathbb{Z}^2$).

As we can see, two main drawbacks appear when using this notion: (1) the distance between two different pixels cannot be as small as we want, contrary to the continuous world like Euclidian spaces where the distance between two points can tend toward zero, (2) ambiguities are possible since two pixels can be 8-neighbors but not 4-neighbors.

In Euclidian spaces, a set is said *connected* iff it is not the disjoint union of two open non-empty sets. However, $\mathbb{Z}^2$ is not supplied with a topology by nature, and then connectedness is not possible in that sense. Using sequences of close pixels, Rosenfeld defined then *connectivity-by-path* in digital spaces, which is very useful in practice, but it is not the same definition as

connectivity in the topological sense.

Even the Jordan curve theorem does not usually hold on these "digital spaces" (see the connectivity paradox), that is, a simple closed curve does not always separate the plane into two components. To obviate this problem, we can use *well-composed digital curves*, in the sense that they contain no couple of points which are 8-neighbors but not 4-neighbors, and then they satisfy the Jordan curve theorem. However, they can be difficult to obtain in practice.

For all these reasons, we were looking for a new **representation** for digital images. In fact, we think that *continuity* is crucial for an image, for both its *domain* and its *value domain*: we need to be able to define usual concepts as *open sets*, *neighborhoods*, *closed sets* on the *domain* of the image, and we need to be able to define a distance between two values (or two subsets of) $\mathbb{R}^n$ in the value domain. More precisely, we believe that *set-valued maps* defined on an *Alexandrov space* and whose domain value is either $\mathbb{R}$, or $\mathbb{Z}$, or even $\mathbb{H}^1$ (the *Khalimsky line*), can be very useful in practice.

Such functions, in particular the *plain maps*, verify many classical theorems, like the *intermediate value theorem*, and have many nice topological properties: the "inverse image" of a set preserves the topology of the set, the direct image of a connected set is a connected set, and under some conditions on the domain, the set of *shapes* of this image is a *tree* (the *tree of shapes* is then well-defined), and so on.

Another point was fundamental to us: we need to be n-dimensional. Effectively, common signals are 2D images, but also 2D videos (which are in fact 3D signals), 3D images like Magnetic Resonance images, or even 3D videos like Computed Tomography scans (which are 4D signals).

Also, we wanted our representation to be *well-composed* in the sense that the boundaries of its threshold sets are discrete surfaces; in this case, these boundaries will verify some *separation properties*; in particular, their triangulations using the chain complexes will be (at least) *combinatorial (pseudo)manifolds*, which separate the space into two components, an exterior which is unbounded and an interior which is bounded (which is a digital version of the Jordan-Brouwer separation theorem).

Finally, we wanted our interpolation to be *self-dual*, that is, it must treat in a same way dark components over a bright background or bright components over a dark background; since we do not always know in advance the

contrast of the objects we have to treat, or since we can have several objects of different contrasts to treat at the same time in a same signal, it is salutary to have such a representation.

Our goal was then to find a self-dual (digital) continuous well-composed representation of n-D signals. So our plan in the following.

In the next chapter, we proceed to a state-of-the-art in matter of well-composedness on cubical grids, on Khalimsky grids, and on arbitrary grids, and then in matter of topological reparations and of well-composed interpolations.

After a renaming of the different kinds of well-composednesses on cubical grids, we will present our first main contribution: the generalization of two definitions of well-composednesses, *EWCness* and *DWCness*, to dimension $n \geq 2$, their characterizations, and the proof that DWCness implies EWCness in n-D. We will also recall briefly how these 4 definitions (EWCness, DWCness, *CWCness* and *AWCness*) are known to be related in 2D and 3D in the community of digital topology, and we will summarize their relations in n-D (on cubical grids).

Then, we will present our secund main contribution: the proof that no self-dual local interpolation makes images DWC in n-D under usual contraints. In the continuity of this statement, we will propose our third main contribution: a new (non-local) self-dual local interpolation which makes images DWC on cubical grids in n-D. This theoretical result comes from the fact that applying our front-propagation algorithm on any DWC interval-valued map results in a DWC single-valued map. The proof is provided in this thesis.

The next section presents some consequences of our works in this thesis: (1) a span-based immersion in the Khalimsky grids applied to our self-dual DWC interpolation results in an AWC self-dual representation of n-D signals (at least in 2D and 3D), (2) our self-dual interpolation leads to "pure" self-duality for self-dual operators and to underlying graph structure which do not depend on the values of the new (DWC) representation, (3) a conjecture relating the Marching-Cubes-like algorithms in n-D and DWCness, (4) promising segmentations based on the tree of shapes of the sign of the self-dual DWC interpolation of the morphological Laplacian.

Some embryonic promising researches are also detailed in the perspectives: first we expose that we think that CWCness and AWCness are equiv-

alent on cubical grids, secund we show that well-composedness has been observed to be preserved using monotone plannings, geodesic dilation/erosion, and grain filters, and third we expose a new way to characterize AWCness of images defined on polyhedral complexes.

In the appendices, we provide a proof of the well-known DWCness of the n-D *min* and *max interpolations*. After that, we propose the first n-D method able to topologically repair gray-level images defined on cubical grids. Also, after a recall of the mathematical background necessary for the sequel, we propose a sketch of the proof of the equivalence between AWCness and DWCness on cubical grids in n-D. Then, we propose two new interpolations methods starting from a gray-level image defined on the n-faces of a polyhedral complex and resulting in an image, defined on a *simplicial cell complex*, that we conjecture to be AWC. The first method is based on derived neigborhoods but does not preserve the geometry of the initial cells, and the second uses a new subdivision method that we introduce in this thesis (called *hierarchical subdivision*), which minimizes the deformation of the geometry of the cells. A definition of bordered discrete surface is also introduced and seems very promising.

Chapter 2

State-of-the-Art

In this chapter, we will begin with some recalls about *digital topology* [141, 87]: we will show how the existence of the *connectivity paradoxes* in the digital plane led to use a *dual pair* of connectivities to restore the properties of the (topological) plane in the continuous world (like the Jordan Separation Theorem), how Latecki get rid of this paradox by introducing "well-composed" sets in 2D in [96], and how he extended this concept to 3D in [98]. We will continue with some complements about 2D/3D well-composedness that Latecki brought in [95] when generalizing well-composedness to n-D, $n \geq 2$. The first definition of well-composed 2D gray-level images will also be described. Then we will how Wang and Battacharya [175] extendend 2D well-composedness to arbitrary grids, how Stelldinger [160] extended well-composedness to n-D cellular complexes, and how Najman and Géraud [124] extended n-D well-composedness to Alexandrov spaces.

2.1 Mathematical Basics

In this section, we recall the well-known concepts of digital topology, followed with the connectivity paradoxes and the presentation of the dual pair of adjacencies usually used to get rid of these paradoxes.

2.1.1 Digital topology in $\mathbb{Z}^2$

Here are the basic definitions of *digital topology* [141, 87] when we work in the *digital plane* $\mathbb{Z}^2$.

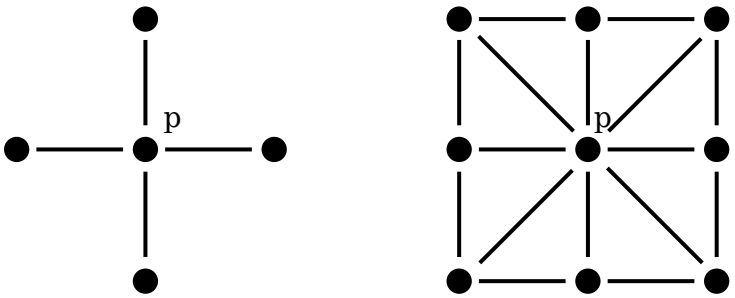

Figure 2.1: Neighborhoods of a point $p \in \mathbb{Z}^2$.

Let S be a subset of the digital plane, the points in S will be termed *foreground* points, while those of its complement in the digital plane, $S^c \equiv \mathbb{Z}^2 \backslash S$, will be termed the *background* points. Note that the background points (respectively the foreground points) will be depicted using white points or black depending on the context.

The *4-neighbors* or *direct neighbors* of a point $(x, y) \in \mathbb{Z}^2$ are its four horizontal and vertical neighbours $(x+1, y)$, $(x-1, y)$, $(x, y+1)$ and $(x, y-1)$. The *8-neighbors* of a point $(x, y) \in \mathbb{Z}^2$ are its four 4-neighbours together with its four *diagonal neighbors* $(x + 1, y + 1)$, $(x + 1, y - 1)$, $(x - 1, y + 1)$ and $(x - 1, y - 1)$.

For $n = 4$ or 8, the *n-neighborhood* of a point $P = (x, y) \in \mathbb{Z}^2$ is the set $\mathcal{N}_n(P)$ consisting of P and its n-neighbors. $\mathcal{N}_n^*(P)$ is the set of all n-neighbors of P without P itself: $\mathcal{N}_n^*(P) = \mathcal{N}_n(P) \setminus \{P\}$. Figure 2.1 depicts on the left the 4-neighborhood and on the right the 8-neighborhood of a point $p \in \mathbb{Z}^2$.

Let P, Q be two points of $\mathbb{Z}^2$. We say that that a sequence of points $(P = P_1, \ldots, P_n = Q)$ of $\mathbb{Z}^2$ is a *n-path*, $n \in \{4, 8\}$, from P to Q iff $P_i \in \mathcal{N}_n^*(P_{i-1})$ for $i \in [\![2, n]\!]$, and it is a *path* if it is a n-path for some $n \in \{4, 8\}$.

A set $X \subseteq \mathbb{Z}^2$ is said *n-connected* iff for every pair of points $P, Q \in X$, there exists a n-path in X from P to Q, and *connected* if it is connected for some $n \in \{4, 8\}$.

A *n-component* of a set $S \subseteq \mathbb{Z}^2$ is a greatest n-connected subset of S. Depending on whether 4− or 8−connectedness is used, we mean 4− or 8−components.

A set $C \subset \mathbb{Z}^2$ is called a *simple closed curve* of *Jordan curve* if it is

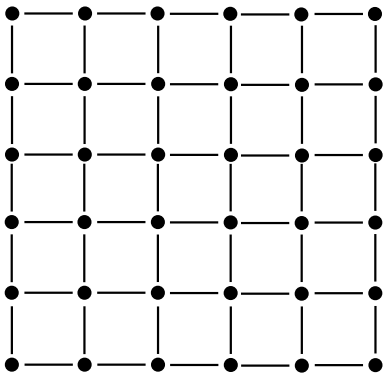

Figure 2.2: Square grid using 4-adjacency

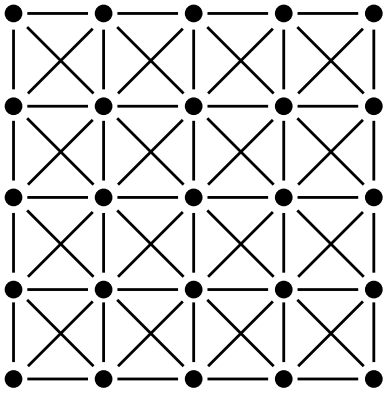

Figure 2.3: Square grid using 8-adjacency

connected and each of its points has exactly two neighbors in C. Depending on wheter we use $4-$ or $8-$neighborhoods, we call C a *4-curve* or a *8-curve*.

Note that to avoid pathological situations [141], we require that a 4-curve contains at least 8 points and that a 8-curve contains at least 4 points.

2.1.2 The connectivity paradox

Let V be equal to the set $\mathbb{Z}^2$, and $E \subset V \times V$ be the irreflexive symmetrical binary relation such that any two points $p, q \in V$ verify $(p, q) \in E$ iff p and q are n-adjacent. We call the points of V the *vertices* and the elements of E the *edges*. We obtain this way a *graph structure* $\mathcal{G} = (V, E)$ based on the n-adjacency. These structures representing the *digital plane* supplied with

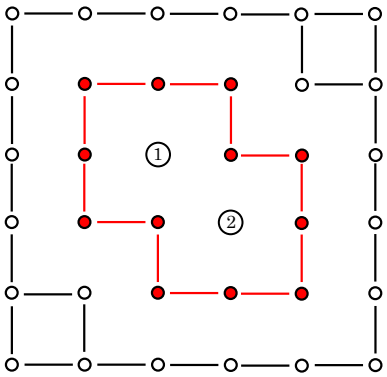

Figure 2.4: The connectivity paradox using 4-adjacency

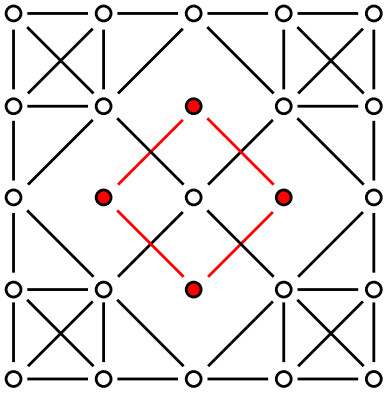

Figure 2.5: The connectivity paradox using 8-adjacency

the n-adjacency can be observed on Figure 2.2 for $n = 4$ and Figure 2.3 for $n = 8$.

Now, assuming that we have a set of foreground points $S \subset \mathbb{Z}^2$ that is given and which depicts a 4- or a 8-curve in $\mathbb{Z}^2$, we could hope that the Jordan Separation Theorem (seen in the introduction) holds as in the continuous world. However, when we draw a 4-curve in the digital plane supplied with the 4-adjacency as shown on Figure 2.4, this curve separates the digital plane into 3 components, two of them are bounded and the third is unbounded. In a certain manner, we have two "interiors". The Jordan Separation Theorem does not hold in discrete spaces using 4-adjacency.

We can also draw an 8-curve in the digital plane, as shown on Figure 2.5, and we obtain that the complement of the 8-curve is an only connected

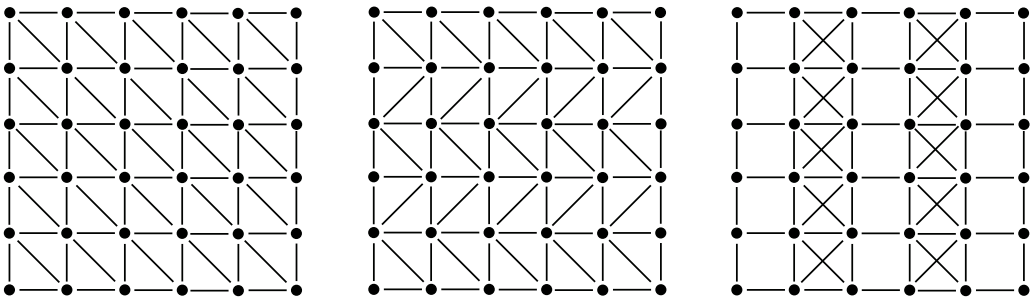

Figure 2.6: Different square grids based on 6-adjacency

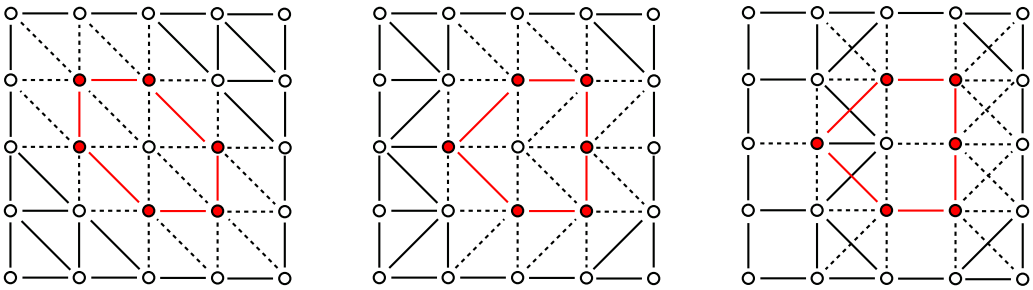

Figure 2.7: A 6-curve does not always separates the digital plane even if we use 6-adjacency.

component. The "interior" and the "exterior" are the same component. Then the Jordan Separation Theorem fails with the 8-adjacency too.

Rosenfeld called these phenomena the *connectivity paradoxes* [147, 87, 96] and explained that this failure follows from the fact that we use the same adjacency for the foreground and the background.

Effectively, we can remark that when we use 6-adjacency such as depicted on Figure 2.6, a 6-curve does not always satisfy the Jordan Separation Theorem (see Figure 2.7): it works using the first grid but not the others. Furthermore, even if these grids are regular, they are not invariant by translation or rotation. For these reasons, we will not use 6-adjacency in this thesis.

2.1.3 Dual pair of adjacencies

Using a *dual pair of adjacencies*, as recommended in [46] for the first time, can be salutary. The $(8, 4)$-adjacency, meaning that we use 8-adjacency for the foreground and 4-adjacency for the background, or the $(4, 8)$-ajacency,

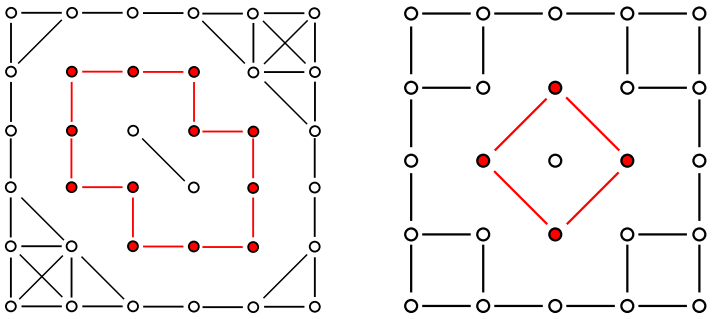

Figure 2.8: $(4, 8)$-adjacency on the left and $(8, 4)$-adjacency on the right.

meaning that we use 4-adjacency for the foreground and 8-adjacency for the background, make the Jordan Separation Theorem true. This is depicted on Figure 2.8: on the left, the 4-curve separates the plane into two 8-components, and on the right, the 8-curve separates the plane into two 4-components.

However, using a dual pair of connectivities is efficient but has a main drawback: the result depends on the chosen couple of adjacencies. In other words, we have to choose, depending on the application, one couple of adjacencies or its dual, and we are not always able to know *a priori* which couple is the most adapted to our needs and will give the expected results. Effectively, a set of connected components of a given set clearly depends on the chosen couple of adjacencies, and then the consequences can be dramatical in some applications as in *object counting* [87].

Another consequence of dual adjacencies is that we cannot attribute adjacencies to more than two colors: even if this method can be effective using binary images, we could be stuck using *multilabel images*. It seems then natural to look for another manner to make true the JST.

2.2 Well-composed Sets and Images

Let us now recall the seminal definitions of well-composednesses.

2.2.1 Well-composedness on $\mathbb{Z}^2$

In 1995, Latecki *et al.* introduced in [96] a class of subsets of $\mathbb{Z}^2$ which are free from topological paradoxes like the connectivity paradoxes developed above,

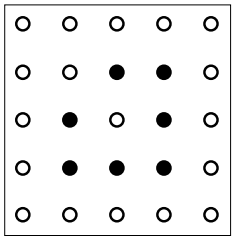

Figure 2.9: A set which is weakly well-composed but not well-composed [96].

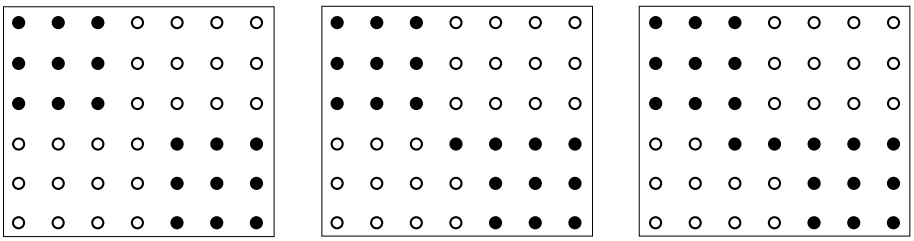

Figure 2.10: The (black) sets are well-composed in (a) and (c), but the (black) set in (b) is neither well-composed nor weakly well-composed [96].

and which allow to obtain the same results whatever the chosen connectivities for the foregound and for the background.

Furthermore, these sets have many nice topological properties [96]: the Jordan Separation Theorem holds for them, their Euler characteristic are locally computable (by a counting process of local patterns), the problems of irreducible thick disappear, and so on.

So, let us begin with the seminal definitions of *well-composed sets* in the digital plane $\mathbb{Z}^2$.

Definition 1 (Weakly Well-composed sets [96])**.** *Let S be a subset of $\mathbb{Z}^2$. S is said* weakly well-composed *iff any 8-component is a 4-component.*

For example, as shown on Figure 2.9 [96], this set is weakly well-composed, since it is made of one 8-component (in black) which is also a 4-component. Since this definition is not *self-dual*, that is, S weakly well-composed does not imply that its complementary is well-composed, Latecki strenghtened this definition in the following manner [96]:

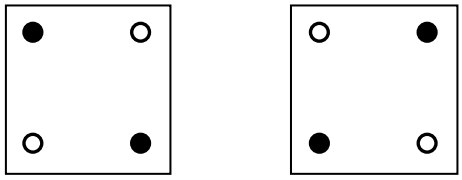

Figure 2.11: Forbidden patterns into well-composed sets [96].

Definition 2 (Well-composed sets [96]). *Let S be a subset of $\mathbb{Z}^2$. S is said* well-composed *iff S and its complement S^c in $\mathbb{Z}^2$ are both weakly well-composed.*

As shown on Figure 2.10, the (black) set S on Subfigure (a) is made of two 8-components which are also 4-components. The set on Subfigure (c) is made of one only 8-component which is also a 4-component. At the contrary, the set on Subfigure (b) is made of one only 8-component which is made of two 4-components, and then is neither weakly well-composed nor well-composed.

Then Latecki reformulated the notion of well-composedness using *local 4-connectivity*.

Definition 3 (Local 4-connectivity [96]). *A set $S \subseteq \mathbb{Z}^2$ is said* locally 4-connected *iff the points of S in the 8-neighborhood of any point of S are 4-connected, i.e., $S \cap \mathcal{N}_8(P)$ is 4-connected for every point P in S.*

Notice that this notion is self-dual, even if the definition relies on S and not on both S and S^c.

Proposition 1 (Self-duality of local 4-connectivity [96]). *Let S be a subset of $\mathbb{Z}^2$. If S is locally 4-connected, then S^c is locally 4-connected.*

Then we come to the theorem linking local 4-connectivity to well-composedness.

Theorem 1 (Local 4-connectivity [96]). *A set $S \subseteq \mathbb{Z}^2$ is well-composed iff it is locally 4-connected.*

Using Theorem 1, it is clear that the patterns, called "critical configurations", depicted on Figure 2.11 and representing two points which are 8-adjacent but not 4-adjacent, cannot occur in a well-composed set.

Now we can come to an essential proposition stating that, in well-composed sets, "the connectivities are equivalent".

Proposition 2 (Equivalence of connectivities [96]). *Let S be a well-composed subset of $\mathbb{Z}^2$. Then S is 4-connected iff it is 8-connected.*

Since a set is not always connected, Latecki generalized this proposition to any well-composed set in the digital plane.

Proposition 3 (Equivalence of connectivities [96]). *Let S be a well-composed subset of $\mathbb{Z}^2$. Then every 4-component of S is a 8-component of S and vice versa.*

A remarkable property should be noticed: the local criteria of Proposition 7 is equivalent to the global criteria of Proposition 3.

Obviously, considering a digital set $X \subset \mathbb{Z}^2$ or a *binary digital image* $(\mathbb{Z}^2, X)$, such that it is the characteristical function of X, is rigorously equivalent, which means that all the theory relative to well-composed sets holds for binary images.

2.2.2 Well-composedness on $\mathbb{Z}^3$

As we have seen just before, a 2D well-composed set is a set such that its 8-components and its 4-components are the same. Therefore we could imagine that it is also the case for 3D sets: a subset of $\mathbb{Z}^3$ whould be well-composed iff its components are the same whatever the chosen connectivity. However it is not the case: the equivalence of connectivities in 3D is not strong enough to obtain the same nice topological properties as in the 2D case.

Let us recall what is *well-composedness* for 3D sets according to Latecki [98].

A *three-dimensional digital set* is a finite subset of $\mathbb{Z}^3$. Then, the *continuous analog* $\mathrm{CA}(p)$ of a point $p \in \mathbb{Z}^3$ is the closed unit cube centered at this point with faces parallel to the coordinate planes:

$$\mathrm{CA}(p) = \{q \in \mathbb{R}^3 \ ; \ \|p - q\|_\infty \leq 1/2\}$$

where for any $(x, y, z) \in \mathbb{R}^3$, $\|(x, y, z)\|_\infty \equiv \max\{|x|, |y|, |z|\}$.

This operator is fundamental since it allows to go from the discrete space $\mathbb{Z}^3$ to the continuous (Euclidian) space $\mathbb{R}^3$.

The *continuous analog* $CA(X)$ *of a (digital) set* $X \subset \mathbb{Z}^3$ is the union of the continuous analogs of the points belonging to the set X:

$$\mathrm{CA}(X) = \bigcup_{p \in X} \mathrm{CA}(p).$$

Note that the function $\mathrm{CA} : \mathcal{P}(\mathbb{Z}^3) \to \mathcal{P}(\mathbb{R}^3)$ admits an inverse which is the (subset) digitization operator $\mathrm{Dig}_\in : \mathcal{P}(\mathbb{R}^3) \to \mathcal{P}(\mathbb{Z}^3)$ defined such that for any set $Y \subset \mathbb{R}^3$, $\mathrm{Dig}_\in(Y) = \{p \in \mathbb{Z}^3 \ ; \ p \in Y\}$. Effectively, for any $X \subset \mathbb{Z}^3$,

$$\mathrm{Dig}_\in(CA(X)) = X.$$

However the inverse is not always true: $\mathrm{CA}(\mathrm{Dig}_\in(Y)) = Y$ iff Y is an union of unit cubes centered at points of $\mathbb{Z}^3$.

Then we will denote $\mathrm{bdCA}(X)$ the topological boundary of $\mathrm{CA}(X)$:

$$\mathrm{bdCA}(X) = \mathrm{CA}(X) \setminus \mathrm{Int}(\mathrm{CA}(X)),$$

where Int(.) is the *interior operator*.

Latecki noticed in [98] that the topological boundary is rigorously equal to the *face boundary* defined as the union of the set of closed faces, that is, the unit closed squares in $\mathbb{R}^3$ which are parallel to one of the coordinate planes, each of which is the common face of a cube in $\mathrm{CA}(X)$ and a cube not in $\mathrm{CA}(X)$. For the interested reader, some additionnal equivalent definitions can be found in [98].

Summarily, as developed in [98, 9, 78, 146], a point of a 3D digital set can be interpreted as a unit cube in $\mathbb{R}^3$, a digital object can be interpreted as a connected set of cubes in $\mathbb{R}^3$, and the surface of an object in $\mathbb{R}^3$ is the set of faces of the cubes that separate the object from its complement.

Definition 4 (3D well-composed sets [98])**.** *Let* X *be a subset of* $\mathbb{Z}^3$*. We say that* X *is a* 3D well-composed set *iff the boundary of its continuous analog* $\mathrm{bdCA}(X)$ *is a 2-manifold, that is, if for any point* $p \in X$*, the (open) neighborhood of* p *in* $\mathrm{bdCA}(X)$ *is homeomorphic to* $\mathbb{R}^2$*.*

Note that this definition is self-dual: for any $X \subset \mathbb{Z}^3$, $\mathrm{bdCA}(X) = \mathrm{bdCA}(X^c)$ and then X is well-composed iff X^c is well-composed.

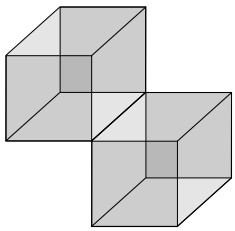

Figure 2.12: The first critical pattern forbidden in 3D well-composed sets and their complement.

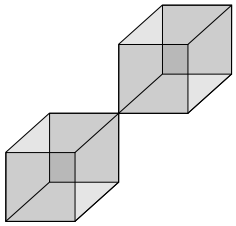

Figure 2.13: The secund critical pattern forbidden in 3D well-composed sets and their complement.

Like for the 2D case, well-composedness can be characterized using local patterns based on adjacencies. Two points $p, q \in \mathbb{Z}^3$ are said to be *face-adjacent* iff their continuous analogs $\mathrm{CA}(p)$ and $\mathrm{CA}(q)$ share a face, that is, a unit closed square which is parallel to one of the coordinate planes, which is equivalent to say that p and q have all their coordinates equal but one which differ from one. Two points $p, q \in \mathbb{Z}^3$ are said to be *edge-adjacent* iff their continuous analogs $\mathrm{CA}(p)$ and $\mathrm{CA}(q)$ share an edge, that is, a line segment parallel to one of the coordinate axes, but not a face, which is equivalent to say that one their coordinate is equal and the two others differ from one. Two points $p, q \in \mathbb{Z}^3$ are said to be *corner-adjacent* iff their continuous analogs $\mathrm{CA}(p)$ and $\mathrm{CA}(q)$ share a point (but not an edge), which is equivalent to say that their three coordinates differ from one.

This way, Latecki [98] defined the local pattern corresponding to a set of two points that are edge-adjacent as the *first type of critical configuration* $\begin{pmatrix} 1 & 0 \\ 0 & 1 \end{pmatrix}$ (see Figure 2.12) and the local pattern corresponding to a set of two points that are corner-adjacent as the *secund type of critical configuration* $\left(\begin{array}{cc|cc} 1 & 0 & 0 & 0 \\ 0 & 0 & 0 & 1 \end{array}\right)$ (see Figure 2.13). This leads to the (local) characterization

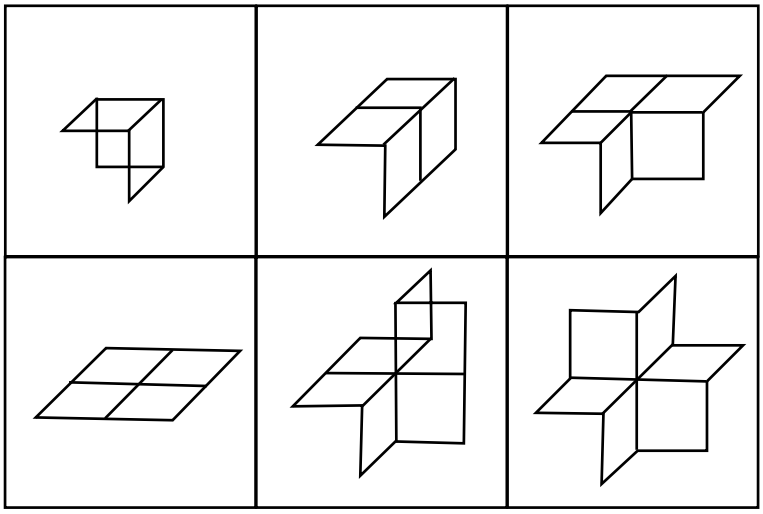

Figure 2.14: The six possible configurations at a corner point in a 3D well-composed set.

of 3D well-composedness:

Proposition 4 (Characterization of 3D WC sets [98])**.** *Let S be a digital set in $\mathbb{Z}^3$. S is well-composed iff there is no occurence neither of the first nor of the second critical configurations in S or its complement in $\mathbb{Z}^3$ (modulo 90 degrees rotations and translations).*

The complete proof is in [98] (pp. 166-167). Summarily, it relies on the fact that any set containing one of these critical configurations contains a "pinch" such that at these critical locations, no point of the boundary owns an open neighborhood homeomorphic to an open disk, and then to $\mathbb{R}^2$. Conversely, if the set S does not contain any critical configuration of any type, then at each point belonging to the interior of a face, any neighborhood which is small enough will be homeomorphic to an open disk, at any point belonging to the interior of the union of two adjacent faces of the boundary sharing an edge, the neighborhood of this point is homeomorphic to an open disk (whatever if the two faces are parallel or perpendicular), and at the corners of the faces included in the boundary, only 6 configurations are possible (see Figure 2.14). In the six cases the corner admits a neighborhood homeomorphic to an open disk, which concludes the proof of Latecki.

However we can denote that this study has been processed case-by-case and then seems difficult to extend in higher dimensions.

Reformulated using closed surfaces, it can be said that a digital set $X \subset \mathbb{Z}^3$ is well-composed iff each connected component of the boundary of its continuous analog is a *simple closed surface*, which means that each connected component of the boundary of the continuous analog of a 3D well-composed set satisfies the *Jordan-Brouwer Separation Theorem*, stating that a simple closed surface in $\mathbb{R}^3$ separates the 3D space into two components: the interior which is bounded and the exterior which is unbounded.

Another direct consequence is that the continuous analog of any (finite) 3D well-composed set is a *bordered 3-manifold*, that is, a set such that any point belonging to its interior has a neighborhood homeomorphic to a relatively open subset of a closed half-space in $\mathbb{R}^3$.

Latecki also introduced a characterization of 3D well-composed sets using m-adjacencies. Two points are said *6-adjacent (6-neighbors)* iff their continuous analog share a face, *18-adjacent (18-neighbors)* iff their continuous analogs share a face or an edge, and *26-adjacent (26-neighbors)* iff their continuous analogs share a face, an edge, or a corner (of a unit cube centered at a point of $\mathbb{Z}^3$). For any $p \in \mathbb{Z}^3$, $\mathcal{N}_{18}(p)$ and $\mathcal{N}_{26}(p)$ correspond obviously to the set of the 18-neighbors or p and to the set of the 26-neighbors of p respectively.

Using these definitions, the following proposition holds:

Proposition 5 (3D WCness and adjacencies [98])**.** *Let X be a digital subset of $\mathbb{Z}^3$. Assume now that $X_1 = X$ and $X_0 = X^c$. Then, X is well-composed iff the two following conditions hold for $\kappa \in \{0, 1\}$:*

- *for every two 18-adjacent points x and y in X_κ, there exists a 6-path joining x to y into $\mathcal{N}_{18}(x) \cap \mathcal{N}_{18}(y) \cap X_\kappa$,*
- *for every two 26-adjacent points x and y in X_κ, there exists a 6-path joining x to y into $\mathcal{N}_{26}(x) \cap \mathcal{N}_{26}(y) \cap X_\kappa$.*

Using this proposition, we clearly understand that local 18/26-connectivities in well-composed sets imply 6-connectivity. Let us recall that for $m \in \{6, 18, 26\}$, a m-component of a set X is a greater connected subset of X based on the m-connectivity (by path).

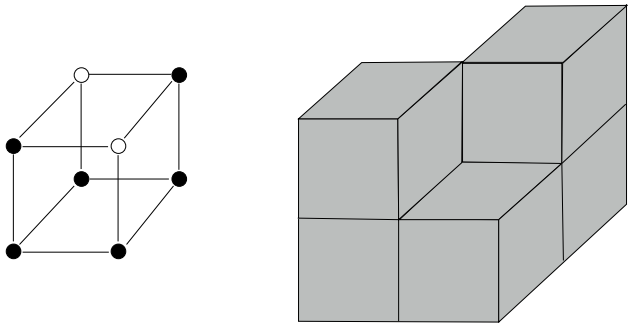

Figure 2.15: The equivalence of connectivities of a set and its complement does not imply it is well-composed in 3D (p. 171 [98]).

Proposition 6 (3D WCness and 6-connectivity [98])**.** *Let X be a digital subset of $\mathbb{Z}^3$ and assume we use the notation of the proposition presented before. Then each 26-component of X_κ is a 6-component of X_κ, and each 18-component of X_κ is a 6-component of X_κ.*

In other words, 3D well-composed sets (and their complement in $\mathbb{Z}^3$) have their connectivities equivalent. However, it is important to notice that the converse is not always true: there exist non-well-composed 3D sets such that the set of their 26-components is the same as the set of their 6-components and such that the set of the 26-components of their complementary is the same as the set of the 6-components of the complementary. For that, see the set $\left(\begin{array}{cc|cc} 0 & 1 & 1 & 1 \\ 1 & 0 & 1 & 1 \end{array}\right)$ depicted on Figure 2.15.

Like for 2D sets, considering a digital set $X \subset \mathbb{Z}^3$ or a *binary digital image* $(\mathbb{Z}^3, X)$ such that it is the *characteristical function* of X is rigorously equivalent.

2.2.3 Well-composedness on $\mathbb{Z}^n$

In [95], Latecki generalized the notion of well-composedness to digital sets is discrete spaces $\mathbb{Z}^n$ of dimension n, with n a integer greater than or equal to 2.

The *continuous analog* of a point $p = (p_1, \ldots, p_n) \in \mathbb{Z}^n$ is the cartesian product:

$$\mathrm{CA}((p_1, \ldots, p_n)) = [p_1 - 1/2, p_1 + 1/2] \times \cdots \times [p_n - 1/2, p_n + 1/2],$$

which can also be reformulated in this equivalent manner:

$$\mathrm{CA}(p) = \{q \in \mathbb{R}^3 \ ; \ \|p - q\|_\infty \leq 1/2\}.$$

Then it follows that as before the *continuous analog* $\mathrm{CA}(X)$ *of a set* $X \subset \mathbb{Z}^n$ is the union of the continuous analogs of the points of the set X, and the topological boundary of this set in $\mathbb{R}^n$ is called for short $\mathrm{bdCA}(X)$.

Now let us recall some basis about topology in Euclidian spaces: we call *n-dimensional bordered manifold* a subset of $\mathbb{R}^n$ such that each point in it admits a neighborhood which is homeomorphic to a relatively open subset of a closed half-space in $\mathbb{R}^n$, and such that this set is not a n-manifold without boundary. Each connected component of a n-dimensional bordered manifold is called a *n-dimensional surface*.

Then Latecki defined in [95] (p. 99) *well-composedness* for sets in n-D spaces using the notion of bordererd manifolds as well:

Definition 5 (n-D WCness [95])**.** *Let $X \subset \mathbb{Z}^n$ be a digital set. X is said to be* well-composed *iff* $\mathrm{CA}(X)$ *is a n-dimensional bordered manifold.*

For this reason, well-composed sets are sometimes called *digital bordered manifolds* [95].

This can be reformulated with an equivalent definition using only the boundary of the continuous analog:

Definition 6 (n-D WCness [95])**.** *Let $X \subset \mathbb{Z}^n$ be a digital set. X is said to be well-composed iff* $\mathrm{bdCA}(X)$ *is a $(n-1)$-dimensional manifold (without boundary).*

The equivalence of these two definitions follows from the fact that a set which is an union of n-dimensional cubes is an n-dimensional bordered manifold iff its boundary is a $(n-1)$-manifold.

Let us notice that a manifold has not to be connected, contrary to surfaces, and then a well-composed set has not to be connected.

Even if Latecki defined well-composedness for n-D, its main works about well-composedness [96, 98, 95, 48, 72, 97, 99, 100, 153, 154, 162, 163] focus on 2D and 3D sets (on regular cubical grids).

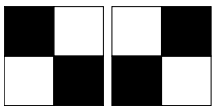

Figure 2.16: The two forbidden *critical configurations* in the continous analog of 2D well-composed sets.

2.2.4 Well-composed segmented digital images

We can mention the existence of *segmented digital images* [95] which are a $(k+2)$-uple $(\mathbb{Z}^n, X_0, X_1, \ldots, X_k)$ such that $X_i \cap X_j = \emptyset$ for $0 \leq i < j \leq k$ and each $X_i \subseteq \mathbb{Z}^n$ is finite or its complement X_i^c is finite for $i \in [\![0, k]\!]$. Then a segmented digital image is said *well-composed* iff each set X_i for $i \in [\![0, k]\!]$ is well-composed.

For example, an usual binary image $(\mathbb{Z}^n, X)$ is a particular case of segmented digital image, where $\mathbb{Z}^n$ is partitioned into only two components, the foreground and the background.

Let us recall that the union of two different sets extracted from a well-composed segmented digital image is generally not well-composed, because the well-composedness is not preserved by the union operator.

2.2.5 Complementing the framework in 2D and in 3D

In [96], Latecki asserted that a 2D digital set which is well-composed cannot contain neither the pattern $\begin{pmatrix} 1 & 0 \\ 0 & 1 \end{pmatrix}$ nor its 90 degrees rotation because a well-composed set is locally 4-connected. But it was not clear that a set which does not contain any of these patterns was well-composed. In 2000, he finally confirmed this intuition using Theorem 1 (p.101 of [95]):

Proposition 7. *Let $S \subseteq \mathbb{Z}^2$ be a digital set. X is well-composed (in the sense of Definition 6) iff its continuous analog* $\mathrm{CA}(X)$ *does not contain the* critical configurations *depicted on Figure 2.16.*

In other words, this set is well-composed iff the (local) patterns $\begin{pmatrix} 0 & 1 \\ 1 & 0 \end{pmatrix}$ and $\begin{pmatrix} 1 & 0 \\ 0 & 1 \end{pmatrix}$ do not occur in S.

Thanks to the self-duality of these local patterns, this definition is self-dual.

Then Latecki asserted that, in 2D, Definition 6 and Definition 2 of well-composed sets are equivalent:

Proposition 8 (Equivalence of connectivities of 2D WC sets [95])**.** *A set $X \subset \mathbb{Z}^2$ is well-composed (in the sense of Definition 6) iff every 8-component of X is a 4-component of X and every 8-component of X^c is a 4-component of X^c.*

All these definitions of 2D well-composedness are then equivalent.

In the 3D case, as stated by the Proposition 5 in [95] (p.105), a digital set $X \subseteq \mathbb{Z}^3$ is well-composed in the sense of Definition 6 iff the critical configurations of type one or two do not occur in neither $\mathrm{CA}(X)$ not $\mathrm{CA}(X^c)$.

Some propositions in [95] have to be noticed since they rely on the equivalence of connectivities at a local level.

Proposition 9. *A digital set $X \subset \mathbb{Z}^2$ is well-composed iff for every two points $x, y \in X$ such that they are 8-adjacent, there exists $z \in X$ such that z is 4-adjacent to both x and y.*

Thanks to the topology of the plane, it is equivalent to say that for every two points $x, y \in X^c$ such that they are 8-adjacent, there exists $z \in X^c$ such that z is 4-adjacent to both x and y, which simplifies Proposition 9. However, in 3D, Latecki observed that:

Proposition 10. *A digital set $X \subset \mathbb{Z}^3$ is well-composed iff the following conditions hold for $\kappa \in \{0, 1\}$ (we recall that $X_0 = X^c$ and that $X_1 = X$):*

- *for every two 18-adjacent points but not 6-adjacent $x, y \in X_\kappa$, there exists a point z in X_κ that is 6-adjacent to x and y,*
- *for every two 26-adjacent points but not 18-adjacent $x, y \in X_\kappa$, there exists a 6-path in X_κ joining x and y into $\mathcal{N}_{26}(x) \cap \mathcal{N}_{26}(y) \cap X_\kappa$.*

In this case, the property has to be true in both cases, that is, for X and X^c.

2.2.6 Well-composed gray-level images in 2D

As we have seen before, a 2D digital (binary) image [95] (p.102) is a 4-uple $(\mathbb{Z}^2, X, k, l)$ where X is a subset of $\mathbb{Z}^2$ such that either X or X^c is finite. X corresponds to the *foreground* and is associated to the k-adjacency, and $X^c \equiv \mathbb{Z}^2 \setminus X$ the *background* of the image and is associated to the l-adjacency. To avoid the connectivity paradox, the couple (k, l) is generally a dual pair of adjacencies. Equivalenty, this image can be interpreted as the characteristical function of the set X in $\mathbb{Z}^2$, that is, a mapping I from $\mathbb{Z}^2$ to $\{0, 1\}$ such that $I(p) = 1$ if $p \in X$ and $I(p) = 0$ if $p \in X^c$.

A 2D gray-level image is then a couple $I = (\mathbb{Z}^2, u)$ where $u : \mathbb{Z}^2 \to [\![0, 255]\!]$ is a mapping from $\mathbb{Z}^2$ to $[\![0, 255]\!]$. This image I is generally identified with its mapping u since these two concepts are rigorously equivalent.

Then we can apply a very straightforward operation called *binarization* of a gray-level image relatively to a given threshold. Given a gray-level image $u : \mathbb{Z}^2 \to [\![0, 255]\!]$ and a threshold $\lambda \in \mathbb{Z}$, the resulting *binarization* of u relatively to λ is equal to the binary image $u_{\text{bin}} : \mathbb{Z}^2 \to \{0, 1\}$ defined for any $p \in \mathbb{Z}^2$ such that $u_{\text{bin}}(p) = 1$ if $u(p) \geq \lambda$ and $u_{\text{bin}}(p) = 0$ if $u(p) < \lambda$.

Now that we have defined what is a binarization of a gray-level image, we can recall the seminal definition of *well-composed 2D gray-level images* of Latecki [95]:

Definition 7. *A gray-level image is said* well-composed *iff for every threshold a binarization of the gray values results in a binary well-composed image.*

Latecki introduced also a characterization of 2D well-composed gray-level images, which shows how much the different binarizations are intercorrelated:

Proposition 11 ([95])**.** *A gray-level image $I = (\mathbb{Z}^2, u)$ is well-composed iff for any restriction of u to a 2×2 square, denoted by $\begin{pmatrix} a & b \\ c & d \end{pmatrix}$, the diagonal intervals have a non-empty intersection:*

$$[\min(a, d), \max(a, d)] \cap [\min(b, c), \max(b, c)] \neq \emptyset.$$

We will see later how much this characterization is powerfull, useful, and how it can be extended to n-D gray-level images.

Note that this notion of binarization by a given threshold comes from *cross-section topology* [118, 21, 17, 18] and is also much used in mathematical morphology [25, 148, 76, 77, 137], because this interpretation of an image

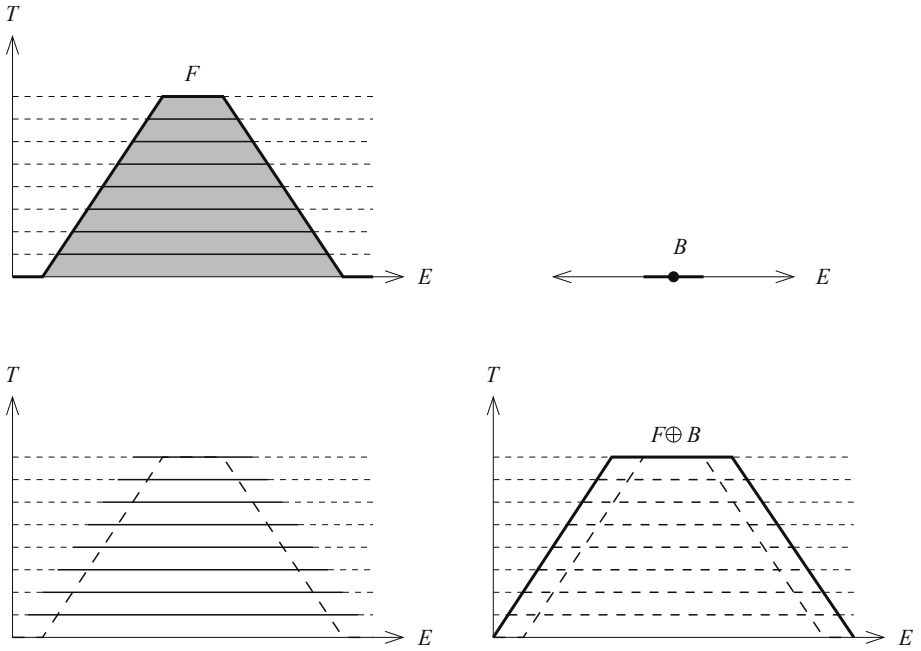

Figure 2.17: The flat extension of the dilation operator (p.869 [25]).

gives access to many powerful operators on gray-level images that can be obtained using a very simple procedure as depicted on Figure 2.17: starting from a set operator ϕ, we decompose the image by computing its binarizations, we apply on each binarization the operator ϕ, and then we use a *stacking* procedure to obtain the resulting image $\phi^T(u)$. This way, an operator on gray-level images has been computed/defined.

2.2.7 Well-composedness on arbitrary grids in 2D

According to Wang and Battacharya [175], we can extend the definition of well-composedness coming from the rectangular grids to arbitrary grids in 2D in the following manner. We assume that we have a (locally finite) arbitrary grid system of (closed) pixels paving the topological space $\mathbb{R}^2$ such that the boundary of each pixel is a Jordan curve, as depicted on Figure 2.18.

A set X of pixel in then said *well-composed* iff for any point p belonging to the boundary of X, the set of pixels of X adjacent to p is *edge-connected* [175], which means that for any two pixels in this set, there exists a sequence of pixels of this set going from the first to the second such that two consecutive

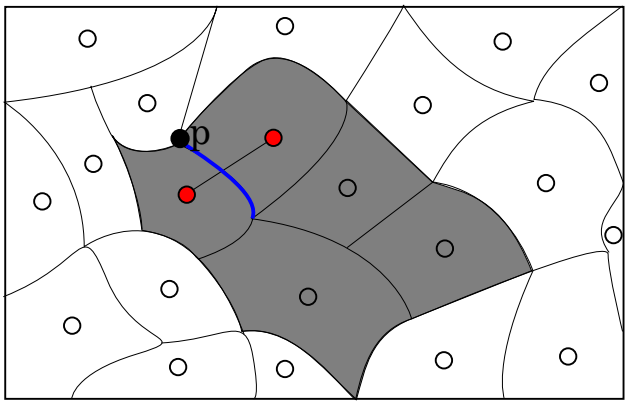

Figure 2.18: Definition of 2D well-composedness on 2D arbitrary grids.

elements share an edge. Figure 2.18 depicts a well-composed set in dark gray: at each boundary point p of X, the set made of the pixels containing p in X is edge-connected (the edge shared by the two pixels is in blue).

Effectively, in the case of rectangular pixels, we obtain that a set X is well-composed in the sense of Latecki [96] iff 8-connectivity (vertex-connectedness) implies 4-connectivity (edge-connectedness).

A particular grid system is the hexagonal grid where every set of pixels is well-composed [175], which is obviously not the case of the rectangular grid.

Serra and Kiran [151] worked on this last topic: $\mathbb{R}^n$ is partitioned into a set of regular open sets, called a *tessellation*, and the complement in $\mathbb{R}^n$ of its union, called the *net*. In this framework [151], they recall an observation of Fedorov [55] which states that the only possible tessellations (inherited from a Voronoï grid system) such that its elements are identical (up to a translation) are in 2D the square and the hexagonal grid systems, and in 3D the cube, the hexagonal prism, the truncated octahedron[1], and the two elongated and rhombic dodecahedra.

Among them, only the hexagonal grid system and the truncated octahedron verify that any two elements of the tessellation such that their adherence are adjacent share a face of dimension $(n-1)$, *i.e.* an edge in 2D and a (2D) face in 3D. In other words, any (finite) set of elements of these tessellations

[1]The Voronoï polyhedron of a body-centered cubic grid, also called *BCC grid* [164] is well-known for its guarantees in matter of topology preservation.

is *strongly adjacent*: there exists a small open disk/ball in 2D/3D such that any intersection of adherences of two adjacent elements of X contains this disk/ball.

Then the link between the works of Wang and Battacharya [175] and Serra and Kiran [151] is straightforward: the strong adjacency is similar to well-composedness on arbitrary grids but the difference relies on the fact that strong adjacency is based on open sets and that well-composedness on arbitrary grids is based on closed sets.

Furthermore, if we consider a tessellation and an arbitrary grid system which are *isomorphic* in the sense that they have the same topological structure up to a closure/opening, every subset of this tessellation which is strongly adjacent has its isomorph in the arbitrary grid system which is well-composed, and conversely. For this reason, these definitions seem "equivalent".

We could easily extend the definition of well-composedness of Wang and Battacharya on a (locally finite) arbitrary grid in n-D such that boundaries of the *voxels* covering $\mathbb{R}^n$ are *connected* $(n-1)$*-manifolds* (see [71, 109, 90, 3] for complements about the Jordan-Brouwer theorem in n-D). Then, we could say that any set X of voxels is *well-composed on an arbitrary grid in* $\mathbb{R}^n$ iff for any face f of dimension $k \in [\![0, n-1]\!]$ belonging to the boundary of X, the set Y of voxels of X containing f (respectively the set Y' of voxels not in X and containing f) are *face-connected*, which means that for any two voxels in this set Y (respectively Y'), there exists a sequence of voxels of this same set going from the first to the second such that two consecutive elements share a face of dimension $(n-1)$.

Note that self-duality in the n-dimensional case is ensured because of the double condition, the first relative to X and the second relative to the complement of X (see Figure 2.19).

This way, we obtain that, in the grid system made of truncated octahedra (see Figure 2.20) covering $\mathbb{R}^3$, every set of voxels is well-composed. Effectively, as stated by L. Mazo in his thesis [115], two voxels in such a grid system share either a face of dimension 2 or nothing. This means that two voxels which belong to a set X and which are connected in this set X are face-connected in this same set X, and that the converse is true for X^c. This way, every set in such a space is well-composed.

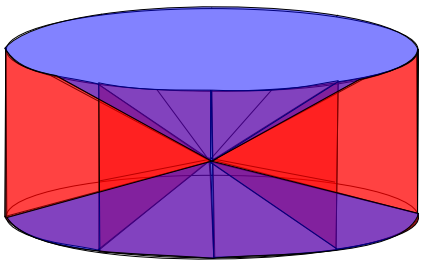

Figure 2.19: A set X where the set of voxels in X (in red) containing the boundary point p (at the center of the cylinder) is face-connected and such that the set of voxels in the complement of X (in blue) is not face-connected.

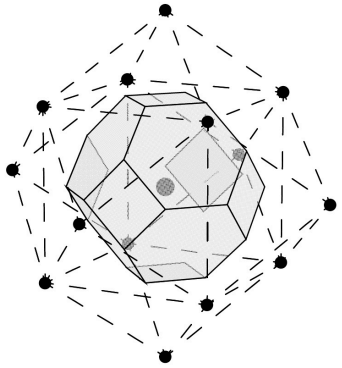

Figure 2.20: A truncated octahedra (p. 13 [115])

This adjacency is known as $2(2^n - 1)$ adjacency in n-D (6-adjacency in 2D, 14-adjacency in 3D, and so on), but shows a strong anisotropy on the graph of the covered domain [115].

2.2.8 Well-composedness on cell complexes in $\mathbb{R}^n$

As defined in Stelldinger's book [160], a *cell complex in* $\mathbb{R}^n$ is a set of *convex polyhedra* in $\mathbb{R}^n$, called *cells*, such that every face of each cell belongs to this complex, and such that for any two faces of the complex, their intersection is a common face of both these two faces.

The *dimension* of a cell is the maximum number of contained independent vectors after translating the cell so that it covers the origin, and a cell of dimension $m \geq 0$ is called a *m-cell*. The *dimension* of a cell complex is the

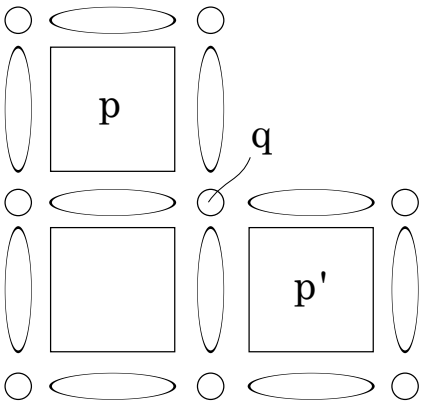

Figure 2.21: A cell complex which would not be well-composed according to Stelldinger [160]

maximal dimension of its cells.

Two cells of a complex are said *m-ajdacent* if their intersection is a m'-cell with $m' \geq m$. Two cells are *adjacent* iff they are adjacent for some m. They are *incident* iff they are adjacent and of different dimensions (then one cell is subset of the other). A *complete cell complex of dimension* m is a cell complex where each cell of dimension $m' < m$ is incident to at least one cell with dimension m.

A cell complex is called *well-composed* if it is complete, of dimension n, and if any two adjacent n-cells are $(n-1)$-adjacent. A set in $\mathbb{R}^n$ is said *well-composed* iff there exists a well-composed cell complex such that the union of its cells is equal to this set.

According to Stelldinger [160], this definition extends the ones of Latecki [98, 95] and Wang and Bhattacharya [175] for arbitrary cell complexes in any dimension.

However, it seems that the cell complex such as depicted o Figure 2.21 made of three edge-connected unit squares depicting a "L", plus their faces, depicts a cell complex which would be well-composed according to Latecki, since the boundary of the complex is a simple closed curve. However it would not be well-composed according to Stelldinger, since this set contains two squares p and p' which share a vertex q, and then are adjacent, but which do not share any edge. The definition of Latecki and Stelldinger seems then not to be equivalent.

2.2.9 Well-composedness in Alexandrov spaces in n-D

Well-composedness exists also in *Alexandrov spaces*, that is, topological spaces that verify the $T0$ separation axiom and that are *discrete spaces* (these notions are detailed is Chapter C).

Effectively, let $\mathcal{X}$ be a finite subset of an Alexandrov space $\mathcal{A}$, then this set is said to be *well-composed* iff its topological boundary $\mathfrak{N} = \alpha(\mathcal{X}) \cap \alpha(\mathcal{A} \setminus \mathcal{X})$, where α is the *closure operator*, is a disjoint union of *discrete surfaces* [89, 52].

To extend this notion to *set-valued maps* defined on Alexandrov spaces, we have to recall what are *threshold sets* of such functions; let $U : \mathcal{A} \rightsquigarrow \mathbb{R}$ be a set-valued map, then for any $\lambda \in \mathbb{R}$, the following sets:

$$
\begin{aligned}
[U \trianglerighteq \lambda] &= \{\, z \in \mathcal{A} \;\big|\; \exists\, v \in U(z),\, v \geq \lambda \,\}, \\
[U \triangleright \lambda] &= \{\, z \in \mathcal{A} \;\big|\; \forall\, v \in U(z),\, v > \lambda \,\}, \\
[U \triangleleft \lambda] &= \{\, z \in \mathcal{A} \;\big|\; \forall\, v \in U(z),\, v < \lambda \,\}, \\
[U \trianglelefteq \lambda] &= \{\, z \in \mathcal{A} \;\big|\; \exists\, v \in U(z),\, v \leq \lambda \,\}.
\end{aligned}
$$

are called *threshold sets* of the set-valued map U.

This notion of well-composedness has also been extended to *plain maps*, a particular subclass of *set-valued maps*: a plain map is said *well-composed* iff its threshold sets are well-composed.

As we will see later, we renamed this definition into "well-composedness in the sense of Alexandrov" or "AWCness", to differentiate it from well-composedness on $\mathbb{Z}^n$ when the used Alexandrov space correspond to the *Khalimsky grids*.

2.3 Topological Reparations and Well-composed Interpolations

Two main approaches exist to make a set or an image well-composed on a cubical grid: *topological reparations* and *well-composed interpolations*.

The first one is often called *topological reparation*, because we consider that we give back to the objects in the image the topological properties they

had before the digitization process; mainly, digitized objects should have a boundary which is a $(n-1)$-manifold.

The second approach correspond to *interpolations*, since their restriction to the initial domain is then assumed to be exactly the initial image. However, without constraints, there is no guarantee that the interpolation has the same topology as the initial image. For example, the 1D image • • represents two connected pixels, valued at 1. One non-constrained interpolation can then be • ∘ •, where ∘ denotes a pixel valued at 0. The two black points are then disconnected. For this reason, we will consider only what we call *in-between interpolations*, that is, interpolations such that the secondary pixels have values that are between the values of the primary pixels. They have the property not to create new extrema in the image when the interpolation is done. This way, in-between interpolations preserve the topology of the initial image.

2.3.1 Topological repairing on cubical grids

Digital images resulting from a convenient digitization should be well-composed, assuming that the digitization procedure preserves the topology of the initial object. Effectively, real objects, or the most of us, have a boundary which is a (topological) manifold.

However, it is well-known that it is not always the case in image processing: the choice of digitization is not always adapted, the resolution of the digitization can be too large, and so on. Moreover, it has been shown that even using the digitization by intersection, which results in well-composed images in 2D for a sufficient resolution, does not provide bordered 3-manifolds by reconstruction using cubical voxels, whatever the chosen resolution.

It seems then useful to know how to make digital images well-composed in n-D if we want to give back to the objects the property such that their boundary is a manifold. Latecki [99, 95] called this procedure "topological repairing", and introduced the first method in 2D able to do it. As usual, the ones correspond to the object/foreground and the zeros to the background. Its method proceeds then by changing the zeros where critical configurations occur into the binary initial image into ones. Also, depending on the neighborhood surrounding the critical configuration and the possible propagation of the critical configuration, a different method is chosen to eliminate

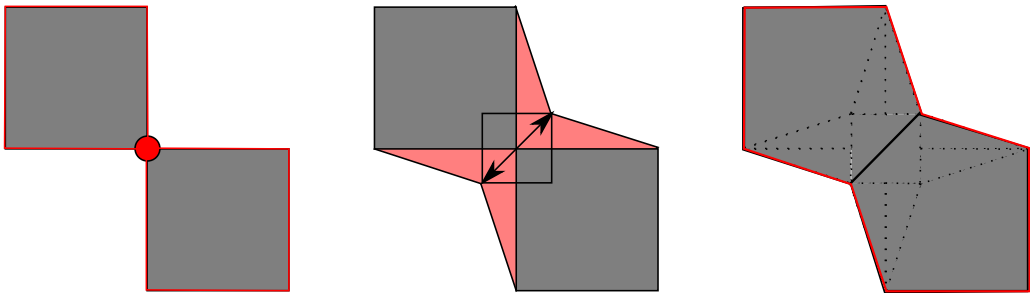

Figure 2.22: The equivalent in 2D of the repairing method of Gonzalez-Diaz *et al.*.

the critical configurations in this neighborhood. This method is translation-invariant and 90 degrees rotation invariant, and guarantees that the number of modifications is minimal.

Then, Siqueira *et al.* [153, 154] proposed a 3D randomized method which makes any 3D binary image well-composed in the sense that the boundary of the continuous analog of the resulting object (made with cubical voxels) will be a 2-manifold. Since no assumption is made on the topology of the initial object, no topological equivalence is ensured, but a theoretical bound ensures that the maximal number of new critical configurations which will appear during the elimination of the m initial configurations is inferior than or equal to $m/2$.

Siqueira *et al.* [153, 154] also developed an algorithm able to make 3D multilabel images well-composed following this same principle of "topological repairing".

Topological repairing of cubical complexes Gonzalez-Diaz *et al.* [64] introduced in 2011 a method able to topologically repair a cubical complex associated to a 3D binary digital image into a polyhedral complex which is homotopy equivalent and well-composed, that is, whose boundary is a 2-manifold. The polyhedron of the geometric realization of the boundary of this interpolation is then made of simple closed surfaces in $\mathbb{R}^3$, on which cohomological information [68, 69, 62, 63, 67] is computable. The proposed (local) method is homotopy preserving, such that the resulting cohomological informations can be used to recognition or characterization tasks.

Their method would be this way in 2D: on a 2D cubical complex, as

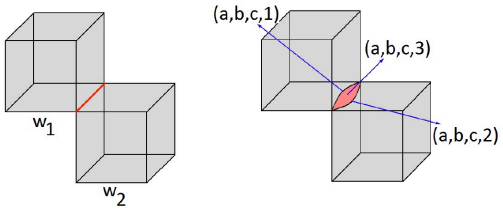

Figure 2.23: Repairing of a complex containing a critical edge [64].

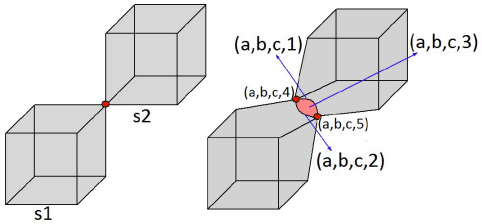

Figure 2.24: Repairing of a complex containing a critical vertex [64].

shown on Figure 2.22, the aera of the surface of each "critical point" would be "increased" such that there is no more pinch into the boundary of the complex (in dark gray), which would lead to a 2D well-composed polyhedral complex (in dark grey too) whose boundary (in red) is made of simple closed curves.

In 3D, the *critical faces* in the complex, that is, the faces in the combinatorial structure corresponding to the pinch in to the geometrical realization, are "stretched" such that the pinch disappears: Figure 2.23 shows how a critical edge shared by two edge-adjacent cubes w_1 and w_2 is replaced by a face of dimension 2 plus two bordering edges, and Figure 2.24 shows how a critical vertex, shared by to vertex-adjacent cubes s_1 and s_2, is replaced by a combinatorial structure made of one 2-face, two bordering edges, and their common vertices. More complicated structures are used to repair the other problematic configurations (see Figure 2.25). Note that this method is not self-dual.

An efficient coding of this family of polyhedral complexes, called *ECM representation* [65, 66] and using 3D images has been developed to store this family of repaired and well-composed complexes into images.

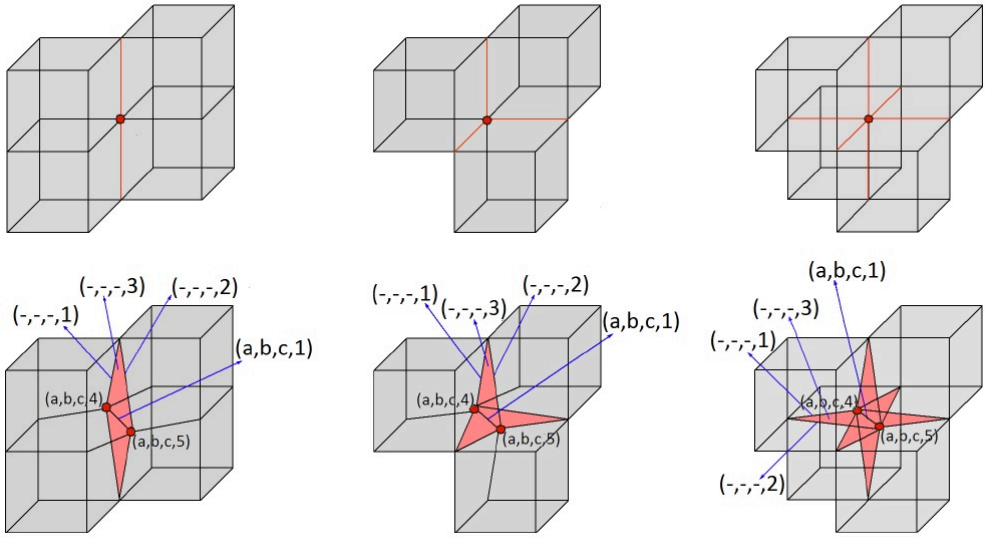

Figure 2.25: Repairing of more complex forbidden configurations [64].

2.3.2 Well-composed Interpolations

In 1998, Rosenfeld, Kong and Nakamura [145] developed the first well-composed 2D interpolation, that is a method able to compute an image on a bigger domain than the one of the initial image, such that its restriction to the initial domain equals the original image and such that the resulting interpolation is well-composed.

This method can be decomposed in two steps . First an *image magnification* [145], which is equivalent to replacing each pixel of the original image by a set of $(k+1)*(k+1)$ pixels (where $k \geq 1$ is given) of the same value and which replaces the original pixel. Secondly, a modification step removes the critical configurations of the magnified image by changing one of the values of the 4 (simple) points of the critical configuration (from 0 to 1 or the converse). Since the magnification process and the modifications are *simple deformations* [145], they preserve the topology (in the sense that the two images have the same adjacency tree), and then the final image is a well-composed image topologically equivalent.

Then in 2000, Latecki [95] developed an alternative method to make a 2D binary image well-composed. This new method is based on the *image*

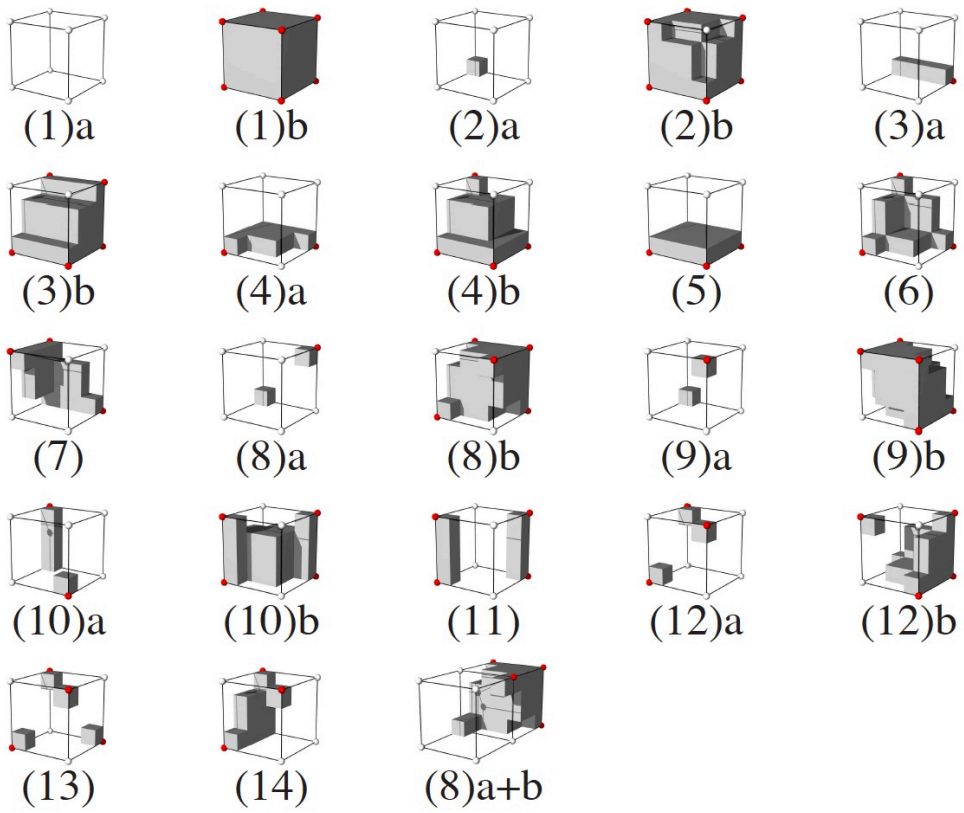

Figure 2.26: Differents configurations using Majority Interpolation [162]

expansion of Köthe [91], and consists in doubling the resolution of the square grid of the initial image by adding new pixels (the so-called "secondary" pixels) between the original pixels (the "primary" pixels). A secondary pixel added between two edge-connected pixels will take the value of these primary pixels iff they have the same value. In the contrary case, they will be labeled as "boundary points". A secondary pixel added at the center of a square of 4 vertex-connected pixels will take the value of these pixels iff they all have the same value. In the converse case, they will be labeled boundary points. Finally, we obtain 3 sets, a set of zeros, a set of ones, and a set of boundary points, each of them being well-composed.

We can denote the difference between these two first algorithms: the one of Rosenfeld *et al.* is based on simple deformations so it ensures topological

equivalence, but the one of Latecki is based on a "counting process", which ensures well-composedness but no topological equivalence.

Then in 2006, Stelldinger proposed a method called *Majority Interpolation* [162], shown on Figure 2.26, which can be seen as a slightly modified 3D extension of the method of Latecki [95], since it is also based on the counting of primary/secondary voxels that are set at the value one to decide the values at the secondary voxels of the subdivided cubical grid. The resulting binary image is always well-composed in the sense that the resulting boundary in the interpolated image is a 2-manifold, but this method is not self-dual.

In 2000, Latecki [95] developed the first gray level well-composed interpolation method in 2D. Starting with the same image expansion as the one used for the binary interpolation, the new pixels are valued based on bilinear interpolation: a pixel added between 2 primary pixels is valued at the mean of these two pixels, and at the center of a square of primary pixel, the new pixel is set a the mean of the values of these 4 pixels if the restriction of the image to these four pixels was well-composed, and at the median of these same values either.

This last method has been slightly modified by Géraud [59] in 2015 where the new pixels added at the center of a square of 4 pixels is always the median of these four primary pixels, since the median is always the good solution in 2D to make an image well-composed. This method does not create any extrema.

We can notice that these gray-level interpolation methods are self-dual in the sense that they do not overemphasize bright components of the dark ones, nor the converse. The counterpart of this powerful property is that the initial images having a integer-based value space, the value space of the new images is $\mathbb{Z}/4$ for the method of Latecki and $\mathbb{Z}/2$ for the method of Géraud.

As noticed by the author [26], extending 2D well-composed interpolations to n-D is not so easy when we want to ensure self-duality using a local interpolation with usual constraints. Effectively, Mazo [116] developed a method able to interpolated any image in n-D into a well-composed one, based on the connectivity function where $\varepsilon = 1$ correspond to the *max interpolation* and $\varepsilon = 1$ corresponds to the *min interpolation*. Even if this method is initially for binary images defined on Khalimsky grids, its extension to $\mathbb{Z}^n$ and to gray level images is well-known and frequently used. However this method is not

self-dual, contrary to the one we are going to present in this thesis in a next chapter.

2.4 Topics related to well-composedness

Now let us see the numerous topics in image processing and mathematics that are related to well-composedness.

2.4.1 About digitization of regular images

In image analysis, many real objects are assumed to be smooth. More exactly, they are assumed to be closed in $\mathbb{R}^2/\mathbb{R}^3$, to have a compact boundary, and such that at each point of their boundary, their tangent line/plane are well-defined [72]. This way, these subsets of $\mathbb{R}^2/\mathbb{R}^3$ are *r-regular*, that is, there exists a value $r > 0$ such that, at each point of their boundary, they admit an inside (respectively an outside) open *osculating disk/ball* of radius superior than or equal to r lying entirely in this set (respectively its complementary). This class of sets has been introduced in 1982 [134, 150] and then used by Latecki *et al.* [100, 99, 96] and by Tajine and Ronse [167].

Then, by *digitization*, some topological properties may be preserved depending on the chosen digitalization (as the *subset digitization* [99], the *Gauss digitization*, the *intersection digitization*, the *threshold-based digitizations*, and so on). This also depends on the chosen *reconstruction method* following the digitization process used to reproduce the shape of the original object as good as possible thanks to *continuous analogs* like Voronoï cells, cubes, or balls (centered at the voxels of the digitization and *tessellating* $\mathbb{R}^n$).

Then the real object and its reconstruction can be homeomorphic (in the sense of the topological equivalence of Pavlidis [134]), or *homotopy equivalent*, or they can have the same *homotopy tree*, they can bee *strongly r-similar* (that is their *morphing distance* [161] is inferior or equal to r), and so on.

Well-composedness for a set X means that its reconstruction using unit cubic voxels has a boundary which is made of a 1-manifold if the 2D case and is made of a 2-manifold if the 3D case. In other words, manifoldness of the boundary of a real-object is preserved iff its digitization is well-composed, assuming that we used unit centered cubes for the reconstruction step.

Figure 2.27: A reconstruction based on cubical grids in 3D leads to critical configurations [163].

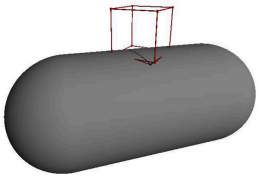

Figure 2.28: Even the digitization of a smooth bordered 3-manifold can contain a 2D critical configuration [163].

In 2D, according to Gross and Latecki [72], if the initial object is r-regular, then its *digitization by intersection* that is, if the space is tessellated with squares and the squared pixels whose interior intersect the initial set are set at 1 and the others at 0, is a well-composed 2D set when using a square grid of diameter r, and then manifoldness of the initial object has been preserved.

In 3D, it has been shown by Stelldinger *et al.* in [163, 161] that using cubical grids, whatever the regularity of the initial object and the resolution of the cubical grid, we cannot ensure that the reconstructed object is well-composed (see Figure 2.27).

Effectively, even digitizations of very regular objects can contain some particular configurations, the famous "critical configurations" of Latecki, which result in pinches in the reconstruction using cubic centered voxels (see Figure 2.27).

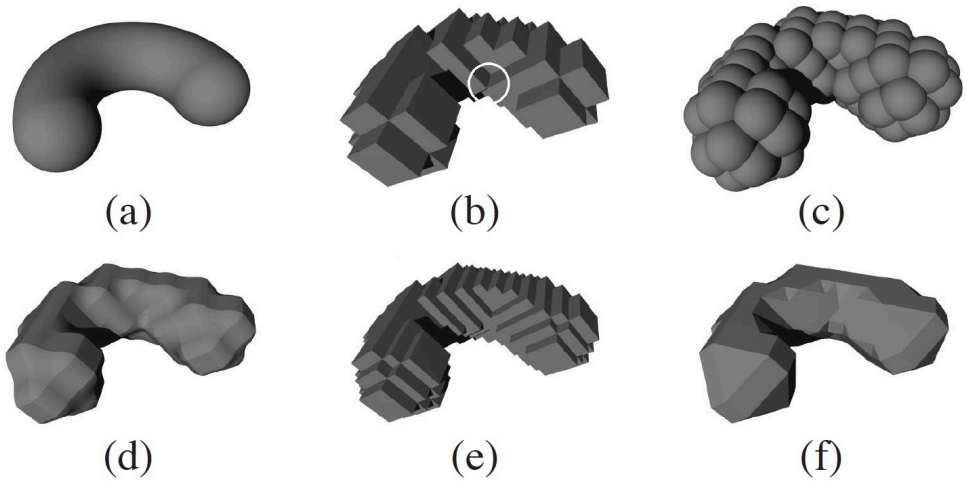

Figure 2.29: A r-regular object and its reconstrucions [163]: (a) the r-regular object, (b) its reconstruction using a cubic $\frac{r}{2}$-grid, (c) ball union, (d) trilinear interpolation, (e) Majority Interpolation, (f) MMC (modified marching cubes).

The same reasoning can be extended to greater dimensions.

Since r-regularity is a very strong constraint, we could imagine that some other kinds of geometric/topological constraints could allow to obtain well-composedness, however it has been shown than r-regularity is a very good assumption to model real objets, since it is a necessary and sufficient condition for many topology preserving theorems [161].

The only possibility seems then to be to change either the grid where the digitization is realized (1), or the digitization itself (2), or the reconstruction procedure (3). In the first case, we can refer to the works of Stelldinger and Strand [164] which show that any digitization on a *body-centered-cubic* (BCC) or*face-centered-cubic* (FCC) grid ensure topology preservation if the digitization is dense enough, and then that the boundary of the reconstruction is a 2-manifold. In the second case, only the 2D digitization by intersection seems promising yet to ensure well-composedness but the other digitizations do not give any guarantees. In the third case, many very efficient techniques exist and ensure that the resulting boundary is a manifold whatever the given input (see Figure 2.29: *majority interpolation* [162], *ball union* [163],

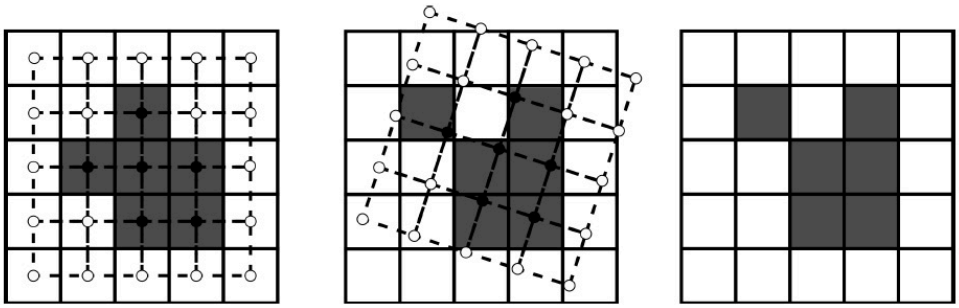

Figure 2.30: An image and its rigid transformation [131].

the *Marching Cubes algorithm* [110] (under some constraints), the *trilinear interpolation* [163], the *smooth surface representation* [163]. Note that this list may be not exhaustive.

2.4.2 Rigid transformations and preservation of well-composedness

In the continuous world, topological properties are preserved by *rigid transformations*, that is, compositions of a translation and a rotation. They are much used in *remote sensing* [157], *medical imaging* [135], *image registration* [12], and *image warping* [54]. This is not anymore the case in the discrete world [129, 130]: starting from a binary image defined on a square grid, it is often mandatory to discretize the result of a continuous rigid transformation of this image since its domain must behave to $\mathbb{Z}^2$ (see Figure 2.30).

This results in the loss of digital topological properties, especially based on connectivities, like the well-composedness or the *adjacency tree* [140] (a tree-based representation of the nested relationship between the connected components in the image), which is no longer isomorphic to the one of the original image. This way, the two images cannot be topologically equivalent [145].

Fortunately, Ngo *et al.* [131, 132] proved that if the initial image is *regular* (a criterion based on some forbidden patterns described on Figure 2.31) including the usual critical configurations of Latecki [96]), then the resulting rigid transformation is well-composed and the adjacency trees of the two images are isomorphic. In that sense, they are "topologically equivalent".

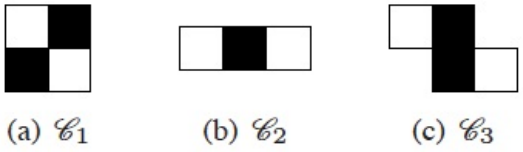

Figure 2.31: Forbidden pattern in regular images [131].

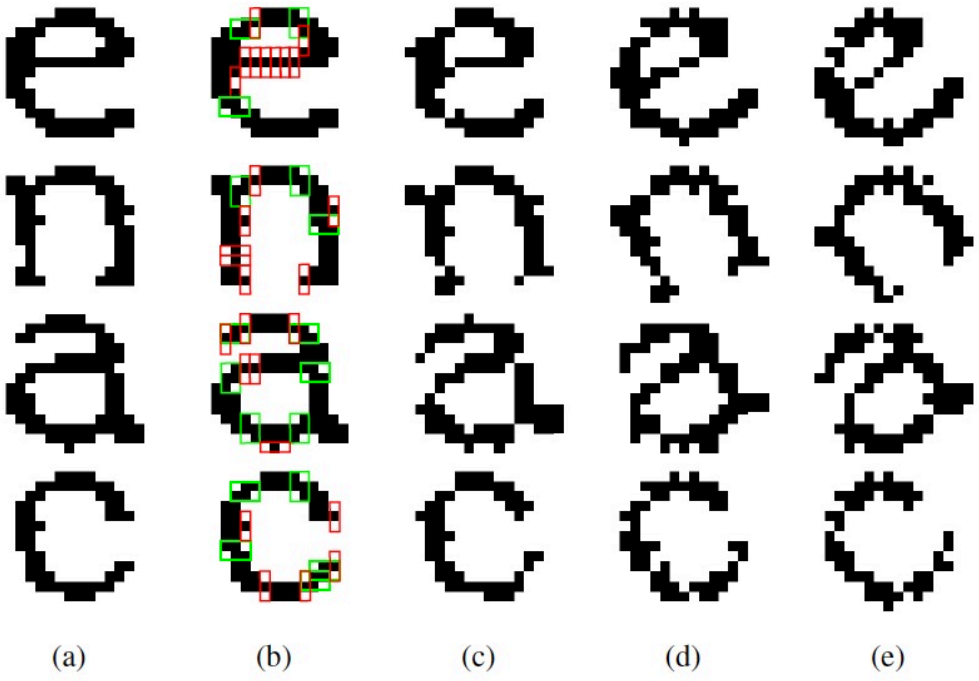

Figure 2.32: Patterns that are completely destructured by the rigid transformation [132].

Making regular any image is then straightforward, using for example a super-resolution strategy [131] able to make any well-composed image regular. Figure 2.32 shows letters whose topology is lost under rigid transformation due to the local critical patterns depicted in red: 4-connected components are decomposed into several other 4-connected components, and the 8-components corresponding to the holes are merged with the background. Figure 2.33

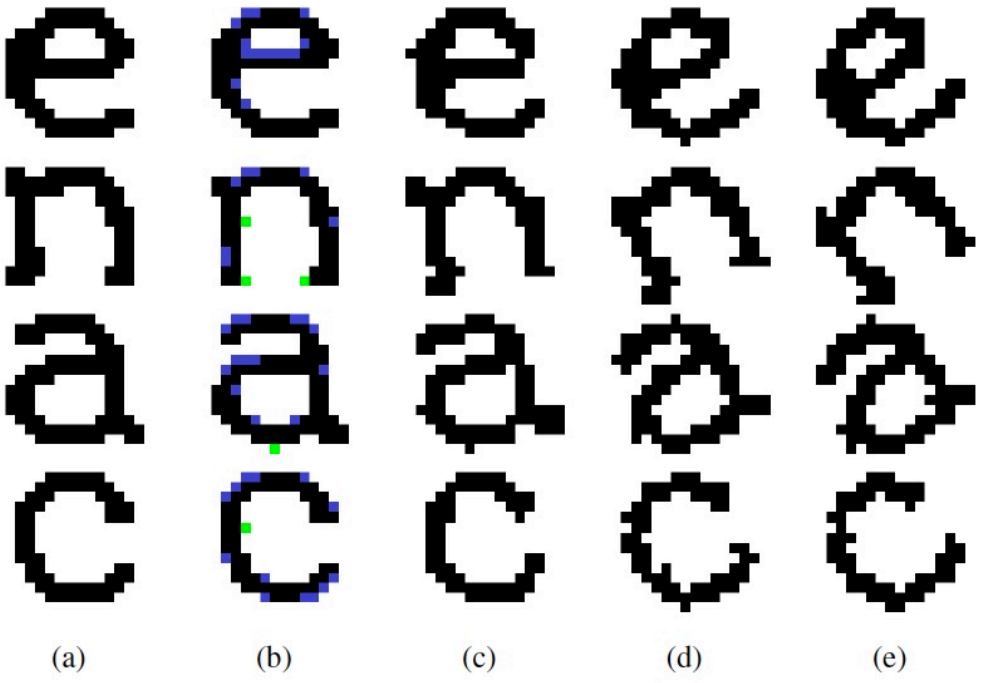

Figure 2.33: Modified patterns whose topology is preserved under the rigid transformation [132].

shows the same letters, modified such that no critical pattern happens, the rigid transformation preserves well-composedness and adjacency tree. Nowadays, no result about the 3D case has been published.

2.4.3 Front propagation and well-composed segmentations

Among the family of topology constrained front propagation methods [33, 6, 166, 101, 75, 149], [75] and [149] rely on *simple points* [14, 87, 15], that is, points such that their add or remove to the component will not change the topology of the image. They start from initial seeds distributed in the areas of interest in the space of the image, and then modify these (connected) components by adding/removing simple points. It can also be interesting to use *multisimple points* [149], that is points such that their add/remove do not create/delete handles in the image.

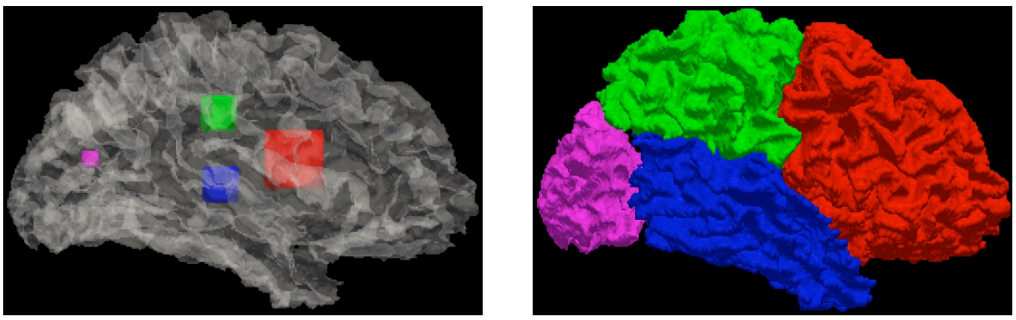

Figure 2.34: From seeds to well-composed regions.

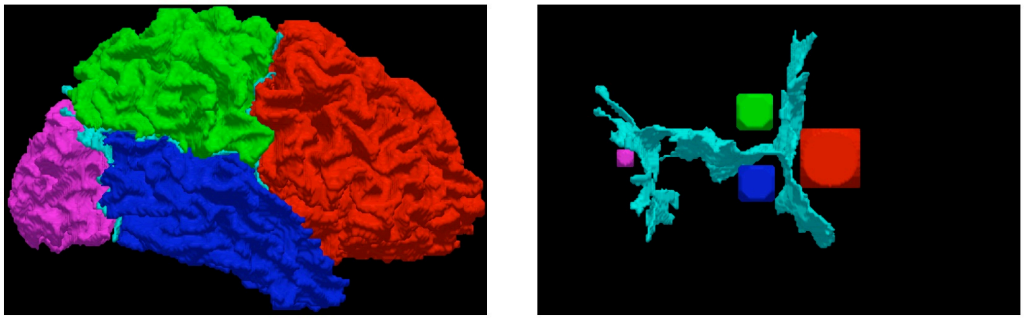

Figure 2.35: Glamorous glue applied to regions results in a well-composed region.

Tustison proposed then in [169] a new method based on two simultaneous criteria: the preservation of the topology, but also the preservation of the well-composedness [96, 98, 99] of the seeds. This procedure is based on the identification using *topological numbers* [19] of points, which preserves the well-composedness and the topology of the image: these *topological well-composed points* are then the only points allowed to be added to the front to make it evolve. This results in a set of connected components and in an interface which are well-composed (see Figure 2.34): the adjacency relations are then (4,4) in 2D and (6,6) in 3D.

Since the interface between two near components will satisfy the Digital Jordan Separation Theorem [127, 99] (DJST) thanks to their well-composedness, these components can be iteratively *glued* together by adding elegantly the part of the Jordan surface separating them to constitute a final segmentation which is well-composed (see Figure 2.35). Then, they can be visualized us-

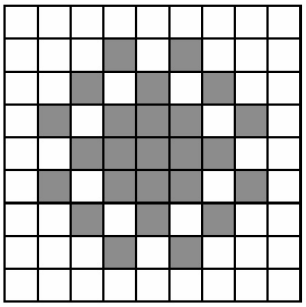

Figure 2.36: The irreducible thick configuration [8].

ing the MC algorithm [110]: the use of the CCMC (Connectivity-Consistent Marching Cubes) algorithm [74] generally used to resolve the ambiguous cases is not required anymore.

2.4.4 Thin topological maps thanks to well-composedness

A discrete image can be seen as the digitization of a piecewise continuous function. This way, we can represent the underlying piecewise continuous function of a discrete image using a topological map where faces correspond to the smooth regions and where the contours made of edges and vertices correspond to the discontinuities of this underlying function. Note that this representation using faces, edges and vertices is not new [56, 92]. However, *consistency problems*, like the "irreducible thick configuration" of [8] on Figure 2.36 or [18, 87], are encountered when we work on cubical grids in this context: there is then no guarantee that the extracted crest network is thin.

To obviate this problem, Marchadier *et al.* [113] propose to use well-composedness [96, 17, 95] to avoid the connectivity problem and to obtain a coherent topological map where the resulting *crest network* is thin. The proposed method is the following. Starting from a given 2D grayscale image, they compute the gradient that they make well-composed using some topological repairing method [113]. Then they apply a *leveling method* of Bertrand [18] which combines the well-composed-preserving thinning of Latecki [96] and deletion of the *peaks*, to obtain finally an *irreducible well-composed gray level image* (see Figure 2.37).

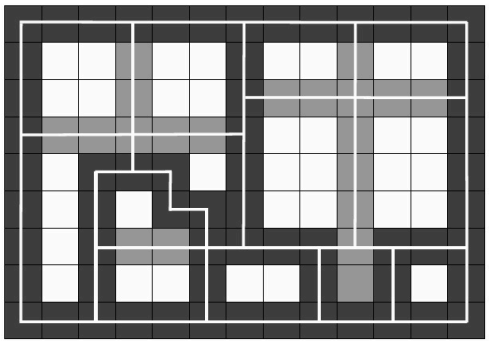

Figure 2.37: An irreducible gray-level well-composed image and its crest network [113].

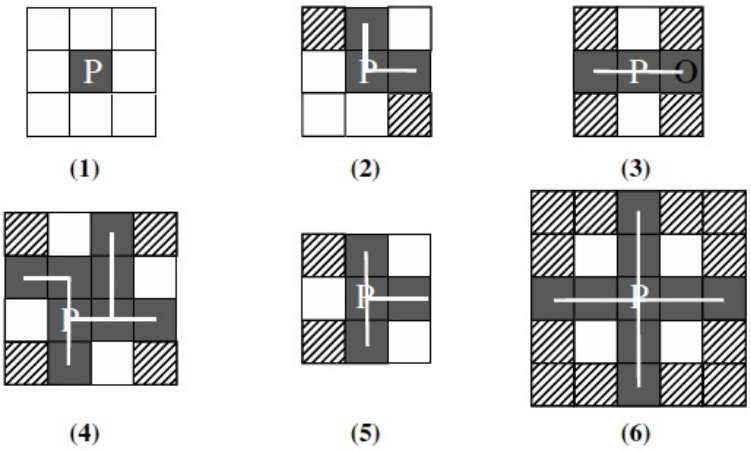

Figure 2.38: Extraction of the crest network from the irreducible well-composed configurations [113].

In fact, we can see see this resulting image as a *watershed transform* [20, 123, 125, 136] of the gradient of the initial image. Effectively, the *quasi-minima* of this image represent the *catchment bassins*. Then, by a configuration-base study, a thin crest network is computed on the complement of these quasi-minima using a linking method [118, 44], with no ambiguities since this image is well-composed (see Figure 2.38). This way, Marchadier obtains a coherent topological map [29, 57] (see Figure 2.39) representing the underlying piecewise continuous function of the given discrete image.

Figure 2.39: The initial image, the image after the reduced image, and the resulting watershed [113].

2.4.5 Locally computable Euler characteristic thanks to well-composedness

The *Euler number/characteristic* [87] or *genus* is a topological invariant used in many applications [111, 176]: *computer graphics*, *image analysis*, object counting, *visual inspection* [158, 180], *License Plates Characters and Numbers Regnition tasks* [1], *real-time thresholding* [155].

A subset X of the plane or of the 3D space is said to be *polyhedral* iff it is expressible as a finite union of vertices (0-faces), edges (1-faces), triangles (2-faces), and tetrahedra (3-faces). We also say that C is the *simplicial decomposition* of X. The *Euler characteristic* is defined by the following axioms:

- $\xi(\emptyset) = 0$,
- $\xi(S) = 1$ if S is non-empty and convex,
- for any polyhedral sets S^1, S^2, $\xi(S^1 \cup S^2) = \xi(S^1) + \xi(S^2) - \xi(S^1 \cap S^2)$,

and does not depend on the triangulation C of X.

According to [168, 87], the *(face) Euler number* of the polyhedral set S can be formulated such that:

$$\xi(S) = n_0 - n_1 + n_2 - n_3,$$

where n_k, $k \in [\![0, 3]\!]$, denotes the number of k-faces in the simplicial decomposition. Note that the value of the face Euler number depends on the chosen connectivity [168].

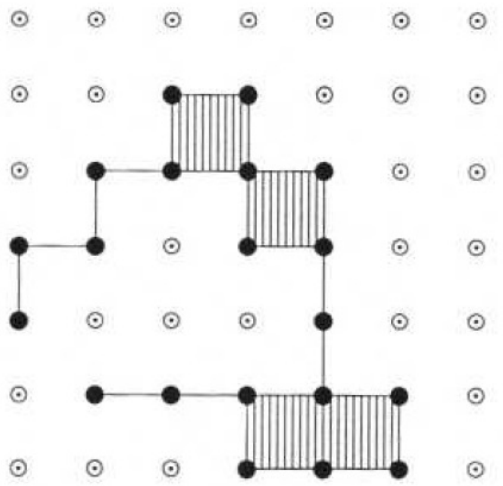

Figure 2.40: Polyhedral set of a $(4, 8)$ digital picture. Its Euler characteristic is equal to 1.

By the *Euler-Poincaré Formula*, we obtain the formula of the *volume Euler number*:

$$\varepsilon = b_0 - b_1 + b_2,$$

where b_k is the *k-dimensional Betti number*. More exactly, b_0 equals the number of 1-components, b_1 equals the number of holes in all 1-components, and b_2 equals the number of cavities in all 1-components. For a given binary image F, the sum of the volume Euler numbers of all connected components in F is called the *volume Euler number* of the image F.

In fact, in the case of a planar polyhedral set, the Euler characteristic is equal to the number of connected components minus the number of holes, which permits to define easily the Euler characteristic of a 2D image where the continuous analog of the ones is represented by its corresponding planar polyhedral set, which is always possible on a rectangular grid for a digital, and then finite, set (which is detailed hereafter).

Assume that any 2D binary digital (m, n)-image P, where (m, n) belongs to $\{(4, 8), (8, 4)\}$, is given, and that we define, as in [87], C_0 as the black point set in the image, C_1 as the union of the black segments whose endpoints are m-adjacent black points. If $(m, n) = (4, 8)$ (respectively if $(m, n) = (8, 4)$), we define C_2 as the union of the unit squares (respectively the $(1, 1, \sqrt{2})$

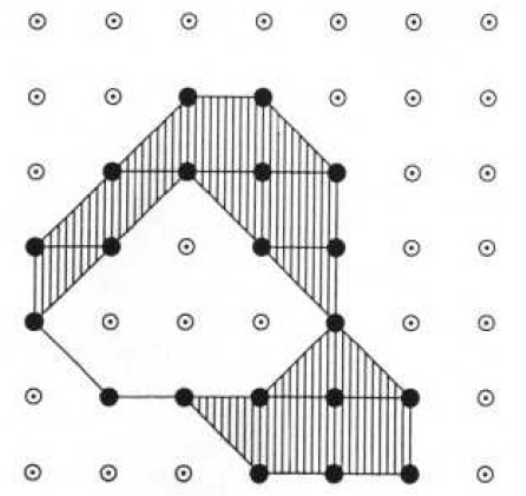

Figure 2.41: Polyhedral set of a $(8, 4)$ digital picture. Its Euler characteristic is equal to 0.

triangles) whose sides are contained in C_1. Then we obtain $C(P) = C_0 \cup C_1 \cup C_2$, that is, the polyhedral set of the image P. The Euler characteristic of P is then obtained by computing the number of connected components of $C(P)$ minus the number of holes in $C(P)$.

Figure 2.40 and Figure 2.41 depict two binary images with the same set of points. Figure 2.40 depicts an image whose Euler characteristic is equal to one, when Figure 2.41 depicts an image whose Euler characteristic is equal to zero. Effectively, the Euler characteristic depends on the chosen connectivity. For this reason, if the given digital picture is well-composed, the choice of the adjacencies does not import, and the Euler characterisitic is unique.

Furthermore, it has been observed that using dual adjacencies on arbitrary binary digital image, this characteristic can be computed locally [133, 88] by an enumeration of some local patterns (see also [70, 159] for different approaches). Since using any pair of dual adjacencies on a well-composed image leads to the same result, Latecki deduced then in [96] that the Euler characteristic is also locally computable on well-composed sets. This results in much faster algorithms, which shows one more time powerfulness of well-composedness.

The 3D case is obviously also important and hade been treated in [34, 45, 35, 173, 47, 22, 103]. In particular, in [102], the used method is local.

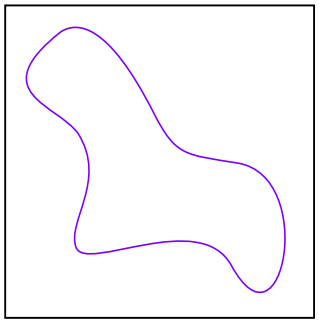

Figure 2.42: A simple closed curve in $\mathbb{R}^2$ is a Jordan curve.

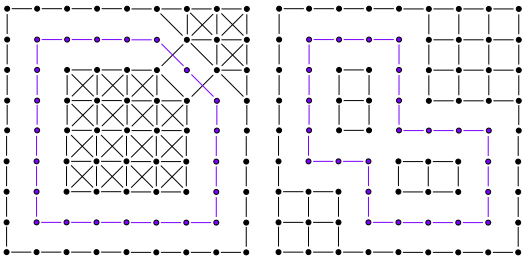

Figure 2.43: 8-curves and 4-curves are not always Jordan curves in $\mathbb{Z}^2$.

Benefits of well-composedness come mainly from the fact that the number of possible configurations is reduced, and then the calculus are simplified and the computations are faster.

2.4.6 Well-composed Jordan curves separate the plane

The Jordan Separation Theorem [128] (JST) states that a simple closed curve S in the continuous plane $\mathbb{R}^2$ separates it into two components, a bounded part that we call the "interior" and a unbounded part that we call the "exterior", and that this curve is the common boundary of these two parts (see Figure 2.42). In this case, S is said to be a *Jordan curve*. However it is well-known that when we work into the discrete analog of the plane, like on *rectangular grids*, we loose some topological properties of the continuous world.

For example, a simple closed curve based on *digital connectivity* [70, 81, 121, 122, 140, 142, 143, 144, 182], does not always separate the space into two components anymore: Figure 2.43 shows on the left a curve based on the

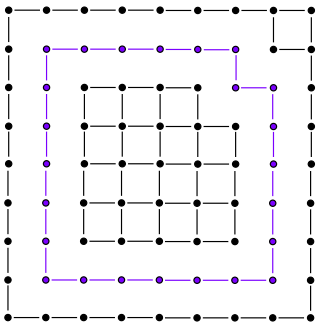

Figure 2.44: A well-composed curve is always a Jordan curve in $\mathbb{Z}^2$.

8-connectivity and on the right a curve based on the 4-connectivity; none of them separates the digital plane $\mathbb{Z}^2$.

In fact, it is related to the connectivity paradox of Rosenfeld [147], developed in Subsection 2.1.2, which can happen when we choose the same connectivity in $\mathbb{Z}^n$ for a set and its complement. To obviate this problem, we can use dual pair of connectivities, and then we obtain the Digital Jordan Separation Theorem [165, 141, 139, 138] which states that a *digital 4-connected simple closed curve* (whose each point has two 4-neighbors in the curve) separates the plane into two 8-connected components. Conversely a *digital 8-connected simple closed curve* (whose each point has two 8-neighbors in the curve) separates the plane into two 4-components.

Another way to obviate the connectivity paradox is to use *well-composed simple closed curves*, for which 4-connectivity and 8-connectivity are equivalent: in this manner no ambiguity is possible and the connectivity paradox cannot occur anymore. Figure 2.44 shows an example of well-composed simple closed curve, which is then a Jordan curve in the sense that it separates the digital plane into two components.

Note that another way to preserve the separation property proper to the plane is to work in *Khalimsky Grids* [73] (see Figure 2.45), where simple closed curves, also called 1-*surfaces* [89, 52], separate the Khalimsky grid $\mathbb{H}^2$. However in this case, the neighborhood of a point in $\mathbb{H}^2$ depends on its coordinates, and then the grid structure of $\mathbb{H}^2$ is different from the usual ones of $\mathbb{Z}^2$.

On arbitrary grids, Wang and Battacharya [175] proposed an interesting generalization of the DJST, considering that two pixels are *direct edge-*

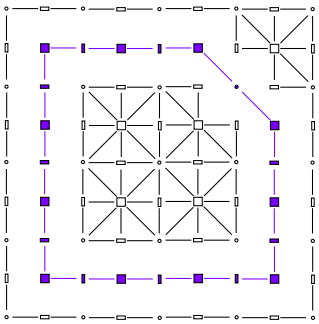

Figure 2.45: A simple closed curve in $\mathbb{H}^2$ is a Jordan curve.

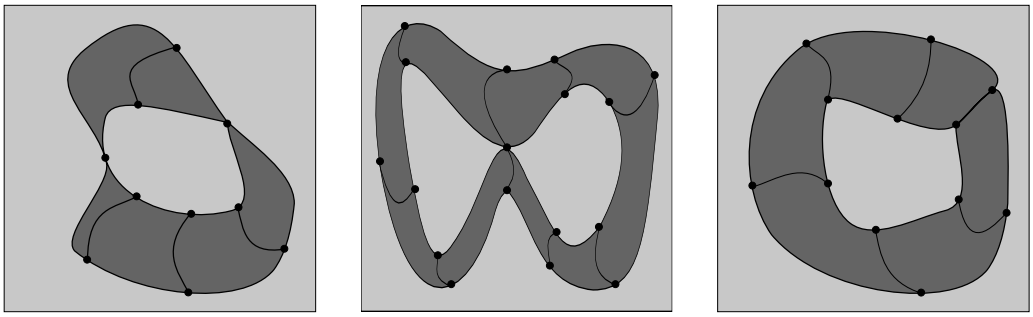

Figure 2.46: Different kinds of simple closed curves according to Wang and Battacharya.

connected if they share an edge, *direct vertex-connected* if they share a vertex, and *direct mix-connected* if they share an edge or a vertex. This way, their equivalent of the Jordan Separation Theorem on arbitrary grids is the following: a finite *edge-connected* simple closed curve (of pixels) separates the plane into two mix-connected (respectively edge-connected) components. Furthermore, a *well-composed simple closed curve* (of pixels) in the sense of [175], that is, such that *(direct) vertex-connectedness* implies *(direct) edge-connectedness*, separates $\mathbb{R}^2$ into two edge-connected components. Figure 2.46 shows on the left a mix-connected simple closed curve, separating the plane into two edge-connected parts, the curve in the middle is an edge-connected simple closed curve separating the plane into two mix-connected components, and on the right, we can see a well-composed simple closed curve which separates the plane into two components, whatever the chosen connectivity. Well-composedness is then used here to give back to the JST the "natural" topological property verified in the continuous plane.

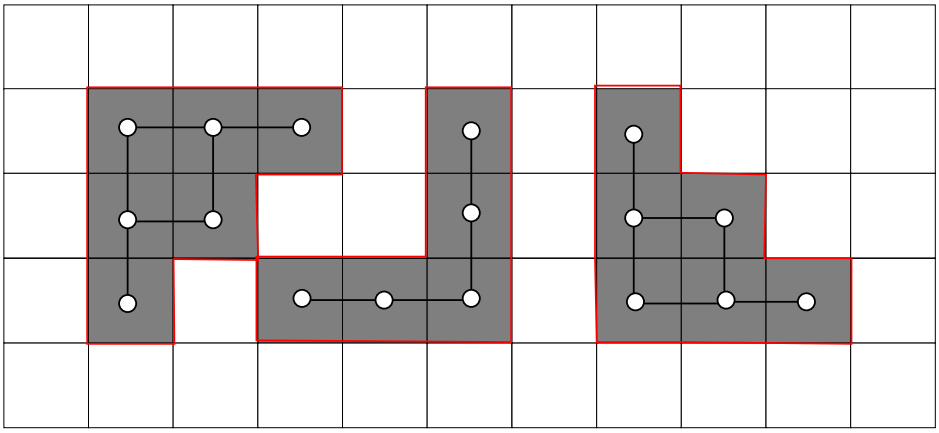

Figure 2.47: The continuous analog of a not well-composed set.

2.4.7 Jordan separation theorem and well-composedness

Well-composedness is deeply related to *Jordan curves* and *Jordan surfaces*.

We recall that the *Jordan curve theorem* [82, 13, 170, 23] (resp. the *Jordan-Brouwer Separation theorem* [3, 71, 109, 90]) states that a simple closed curve (resp. a simple closed surface) in the continuous plane $\mathbb{R}^2$ (resp. in the continuous space $\mathbb{R}^3$) separates the plane (resp. the space) into two components, one which is bounded, called the *interior*, and one which is unbounded, called the *exterior*, and that their common boundary is this curve (resp. this surface). In the first case, we call it a *Jordan curve*, and in the second case, we call it a *Jordan surface*.

Effectively, as stated in [95], it is equivalent to say that a 2D subset X of $\mathbb{Z}^2$ is *well-composed* or to say that the boundary of its *continuous analog* is a 1-manifold, which means that it is made of disjoint simple closed curves. Figure 2.47 shows a set which is not well-composed, since one of the connected components of its boundary is not a simple closed curve, and Figure 2.48 shows a well-composed set, since each connected component of its boundary is a simple closed curve.

Take care not to amalgamate the fact that a simple closed curve is well-composed and the fact that the boundary of a 2D set is a simple closed curve. The first concept is a property of well-composed curves as a set (in this case, the whole set is a Jordan curve), when the second one is the property of any boundary of any 2D well-composed set (in this case, the Jordan curves are

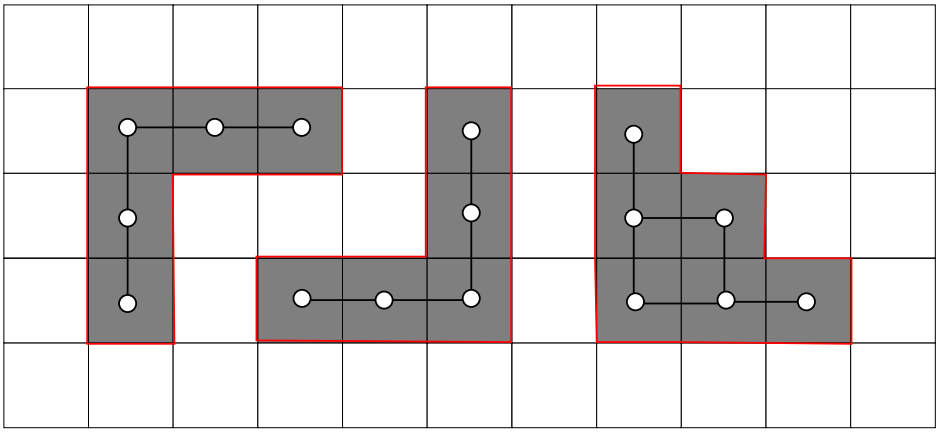

Figure 2.48: The continuous analog of a well-composed set.

the boundaries).

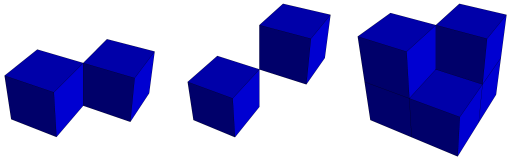

Figure 2.49: Non-Jordan Surfaces.

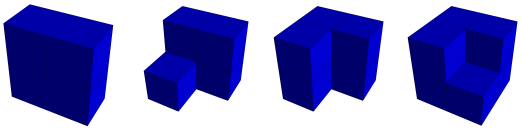

Figure 2.50: Jordan Surfaces.

Also, a digital 3D set $X \subset \mathbb{Z}^3$ said *well-composed* [98, 95] iff the boundary of its continuous analog is a 2-manifold, that is, is made of disjoint simple closed surfaces, which strongly relates the Jordan-Brouwer separation theorem to well-composedness. Figure 2.49 shows the boundaries of continuous analogs which are not Jordan surfaces, and Figure 2.50 shows at the contrary boundaries of continuous analogs of well-composed sets which are then 2-manifolds.

Chapter 3

Generalization of Well-composedness to Dimension n

In this chapter, we expose our contributions in matter of well-composedness. In particular, we explain how we renamed the different kinds of well-composednesses: since they are not always equivalent, this justifies the terminology we introduced to differentiate them. Also we will study how they are related, and how we propose to extend these definitions to gray-level/real-valued images. We will also show how we propose to characterize real-valued digitally well-composed images in n-D, extending the 2D characterization of Latecki in [95]. We will end with the computation of the complexity of this verification process, able to check if an image is digitally well-composed or not. Note that the dimension $n \in \mathbb{N}^*$ of the space we are working in is assumed to be greater than or equal to 2 and finite.

3.1 The different flavours of n-D WCnesses in brief

As we have seen in Section 2.2, Latecki introduced in 2D well-composedness for sets such that a set is well-composed iff its connectivities are equivalent, that is to say that we have the same sets of components whatever the chosen connectivity for this set and its complement in $\mathbb{Z}^2$. However, in 3D, the definition of well-composedness is not the natural extension of the 2D one:

a 3D set is said well-composed iff the boundary of the continuous analog is a 2-manifold. This is a stronger condition since it implies that a 3D set and its complement in $\mathbb{Z}^n$ have their connectivities equivalent, but the converse is not true (see Figure 2.15). Furthermore, alternative definitions of well-composednesses appeared in 1997 in 2D arbitrary grids [175], in 2008 in [160] in the cellular complexes, and in 2013 in [124] in Alexandrov spaces (like the *Khalimsky grids*). Since in our case, we were mainly interested in cubical grids, we renamed these definitions and properties in the following manner:

- A (digital) set $X \subset \mathbb{Z}^n$ is said *EWC* or *well-composed based on the equivalence of its connectivities* iff any $(3^n - 1)$ component of X (respectively of X^c) is a $2n$-component and *vice versa*.
- A (digital) set $X \subset \mathbb{Z}^n$ is said *CWC* or *well-composed in the continuous sense* iff the (topological) boundary of its continuous analog is a $(n-1)$-manifold.
- A (digital) set $X \subset \mathbb{Z}^n$ is said *DWC* or *well-composed in the digital sense* iff it does not contain any *k-D critical configuration*, with $k \in [\![2, n]\!]$.
- A (digital) set $X \subset \mathbb{Z}^n$ is said *AWC* or *well-composed in the Alexandrov sense* iff the connected components of the topological boundary of its immersion $\mathcal{IMM}(X)$ in the Khalimsky grids $\mathbb{H}^n$ are discrete $(n-1)$-surfaces (see Chapter D for more details). By identification, we will say equivalently that $\mathcal{IMM}(X)$ is AWC or that X is AWC.

Notice that we did not take into account well-composedness on arbitrary grids or arbitrary cellular complexes, since we are mainly intrested in cubical grids. Also, we generalized these notions to n-D, since we focus on n-D signals, $n \geq 2$. Considering that digital well-composedness makes sense on $\mathbb{Z}^n$, but also on a subdivided version of $\mathbb{Z}^n$ like $\left(\frac{\mathbb{Z}}{2}\right)^n$ or more generally $(\mathbb{Z}/s)^n$ with $s \in \mathbb{N}^*$, we will define our generalizations of well-composedness into $(\mathbb{Z}/s)^n$. Effectively, an interpolation on a cubical grid starts usually from an image whose domain is in $\mathbb{Z}^n$ and outputs an image whose domain is in $\left(\frac{\mathbb{Z}}{2}\right)^n$, as we will see in the next chapter.

3.2 Mathematical Basics

Let $n \geq 2$ be a (finite) integer called the *dimension* and $s \geq 1$ be an integer called the *subdivision factor*.

Now, let $\mathbb{B} = \{e^1, \ldots, e^n\}$ be the (orthonormal) canonical basis of $(\mathbb{Z}/s)^n$. We use the notation x_i, where i belongs to $[\![1, n]\!]$, to determine the i^{th} coordinate of the vector $x \in \mathbb{Z}^n$. We recall that the L^1-*norm* of a point $x \in \mathbb{Z}^n$ is denoted by $\|.\|_1$ and is equal to $\sum_{i \in [\![1,n]\!]} |x_i|$ where $|.|$ is the *absolute value*. Also, the L^∞-*norm* is denoted by $\|.\|_\infty$ and is equal to $\max_{i \in [\![1,n]\!]} |x_i|$.

For a given point $x \in (\mathbb{Z}/s)^n$, the set of the $2n$-*neighborhood* in $(\mathbb{Z}/s)^n$ is noted $\mathcal{N}_{2n}(x, (\mathbb{Z}/s)^n)$ and is equal to $\{y \in (\mathbb{Z}/s)^n \ ; \ \|x - y\|_1 \leq 1/s\}$. In other words,

$$\mathcal{N}_{2n}(x, (\mathbb{Z}/s)^n) = \{x\} \cup \{x - \frac{e^1}{s}, x + \frac{e^1}{s}, \ldots, x - \frac{e^n}{s}, x + \frac{e^n}{s}\}.$$

An element of the $2n$-neighborhood of $x \in (\mathbb{Z}/s)^n$ is called a $2n$-*neighbor* of x in $(\mathbb{Z}/s)^n$. The *starred* $2n$-*neighborhood* of $x \in (\mathbb{Z}/s)^n$ is noted $\mathcal{N}^*_{2n}(x, (\mathbb{Z}/s)^n)$ and is equal to $\mathcal{N}_{2n}(x, (\mathbb{Z}/s)^n) \setminus \{x\}$. Two points $x, y \in (\mathbb{Z}/s)^n$ such that $x \in \mathcal{N}^*_{2n}(y, (\mathbb{Z}/s)^n)$ or equivalently $y \in \mathcal{N}^*_{2n}(x, (\mathbb{Z}/s)^n)$ are said to be $2n$-*adjacent* in $(\mathbb{Z}/s)^n$.

Then, for a given point $x \in (\mathbb{Z}/s)^n$, the set of the $(3^n - 1)$-*neighborhood* in $(\mathbb{Z}/s)^n$ is noted $\mathcal{N}_{3^n-1}(x, (\mathbb{Z}/s)^n)$ and is equal to $\{y \in (\mathbb{Z}/s)^n \ ; \ \|x-y\|_\infty \leq 1/s\}$. In other words,

$$\mathcal{N}_{3^n-1}(x, (\mathbb{Z}/s)^n) = \left\{ x + \sum_{i \in [\![1,n]\!]} \lambda_i e^i \ ; \ \lambda_i \in \{-1/s, 0, 1/s\}, \forall i \in [\![1, n]\!] \right\}.$$

An element of the $(3^n - 1)$-neighborhood of $x \in (\mathbb{Z}/s)^n$ in $(\mathbb{Z}/s)^n$ is called a $(3^n - 1)$-*neighbor* of x in $(\mathbb{Z}/s)^n$. The *starred* $(3^n - 1)$-*neighborhood* of $x \in (\mathbb{Z}/s)^n$ in $(\mathbb{Z}/s)^n$ is noted $\mathcal{N}^*_{3^n-1}(x, (\mathbb{Z}/s)^n)$ and is equal to $\mathcal{N}_{3^n-1}(x, (\mathbb{Z}/s)^n) \setminus \{x\}$. Two points $x, y \in (\mathbb{Z}/s)^n$ such that $x \in \mathcal{N}^*_{3^n-1}(y, (\mathbb{Z}/s)^n)$ or equivalently $y \in \mathcal{N}^*_{3^n-1}(x, (\mathbb{Z}/s)^n)$ are said to be $(3^n - 1)$-*adjacent* in $(\mathbb{Z}/s)^n$.

Let x, y be two points in $(\mathbb{Z}/s)^n$ and X be a subset of $(\mathbb{Z}/s)^n$. A (finite) $2n$-*path* (respectively a (finite) $(3^n - 1)$-*path*) joining x to y into X as a subset of $(\mathbb{Z}/s)^n$ is a sequence $(p^0 = x, p^1, \ldots, p^{k-1}, p^k = y)$ such that for any $i \in [\![0, k]\!]$, p^i belongs to X and such that for any $i \in [\![0, k-1]\!]$, $p^{i+1} \in$

$\mathcal{N}^*_{2n}(p^i, (\mathbb{Z}/s)^n)$ (respectively $p^{i+1} \in \mathcal{N}^*_{3^n-1}(p^i, (\mathbb{Z}/s)^n)$). Such paths are said to be of *length* k.

A subset X of $(\mathbb{Z}/s)^n$ such that its cardinal $\mathrm{Card}(X)$ is finite is said to be a *digital set*. A (digital) set $X \subset (\mathbb{Z}/s)^n$ is said $2n$-*connected* (respectively (3^n-1)-connected) into $(\mathbb{Z}/s)^n$ iff for any couple of points $x, y \in X$, there exists a $2n$-path (respectively a (3^n-1)-path) joining them into X as a subset of $(\mathbb{Z}/s)^n$. A subset C of X which is $2n$-connected (respectively (3^n-1)-connected) into $(\mathbb{Z}/s)^n$ and which is *maximal in the inclusion sense*, that is, there is no subset of X which is greater than C and which is connected into $(\mathbb{Z}/s)^n$, is said to be a $2n$-*component* (respectively a (3^n-1)-*component*) of X in $(\mathbb{Z}/s)^n$.

A point $x \in (\mathbb{Z}/s)^n$ is said to be $2n$-*connected* (respectively (3^n-1)-*connected*) to a set $Y \subseteq (\mathbb{Z}/s)^n$ into $(\mathbb{Z}/s)^n$ iff there exists a point $y \in Y$ such that x and y are $2n$-neighbors (respectively (3^n-1)-neighbors) in $(\mathbb{Z}/s)^n$. Two sets $X, Y \subseteq (\mathbb{Z}/s)^n$ are said to be $2n$-*connected* (respectively (3^n-1)-*connected*) in $(\mathbb{Z}/s)^n$ iff there exists $x \in X$ such that x and Y are $2n$-connected (respectively (3^n-1)-connected) in $(\mathbb{Z}/s)^n$.

The set of connected components in $(\mathbb{Z}/s)^n$ of a set $X \subset (\mathbb{Z}/s)^n$ based on the ξ-connectivity, $\xi \in \{2n, 3^n-1\}$, is denoted by $\mathcal{CC}_\xi(X, (\mathbb{Z}/s)^n)$. Assuming that a point $x \in (\mathbb{Z}/s)^n$ belongs to a set $X \subset (\mathbb{Z}/s)^n$, the connected component of X in $(\mathbb{Z}/s)^n$ based on the ξ-connectivity, $\xi \in \{2n, 3^n-1\}$, is denoted by $\mathcal{CC}_\xi(X, x, (\mathbb{Z}/s)^n)$; in the contrary case, $\mathcal{CC}_\xi(X, x, (\mathbb{Z}/s)^n) = \emptyset$.

3.3 n-D EWCness and n-D DWCness

In this section, we extend naturally the seminal definition of EWCness to n-D, we define DWCness in n-D and we show how we can characterize a DWC set using $2n$-connectivity, and we study the correlation between EWCness and DWCness.

3.3.1 n-D EWCness

Now that we have defined the basics in matter of connectivity in digital topology, we can define well-composedness based on the equivalence of connectivities.

Definition 8. *Let X be (digital) set in $(\mathbb{Z}/s)^n$. X is said to be* EWC *or* well-composed based on the equivalence of its connectivities *iff the two following conditions hold:*

- *any of its $2n$-component in $(\mathbb{Z}/s)^n$ is also one of its (3^n-1)-components in $(\mathbb{Z}/s)^n$ and vice versa.*
- *any $2n$-component of X^c in $(\mathbb{Z}/s)^n$ is also a (3^n-1)-component of X^c in $(\mathbb{Z}/s)^n$ and vice versa.*

We can underline that this definition is clearly self-dual, and since the connectivity does not matter for this class of sets, we will sometimes say that their connectivities (and the ones of their complement in $(\mathbb{Z}/s)^n$) are *equivalent*. Also, this definition is the "natural" extension of the one of Latecki in [96] for 2D sets.

3.3.2 n-D DWCness

In this subsection, we introduce a notion of *digital well-composedness* for sets in $\mathbb{Z}^n$, that we call in this way because it is based on patterns called "k-dimensional critical configurations", $k \in [\![2, n]\!]$, and these patterns can only occur in subsets of $\mathbb{Z}^n$. So let us introduce the basic mathematical background which will allow us to generalize the notion of well-composedness based on critical configurations to dimension $n \geq 2$.

Like usual, $\mathbb{B} = \{e^1, \ldots, e^n\}$ is the canonical basis of $\mathbb{Z}^n$.

Definition 9. *Given a point $z \in (\mathbb{Z}/s)^n$ and a family of vector $\mathcal{F} = (f^1, \ldots, f^k) \subseteq \mathbb{B}$, we define the* block *of $(\mathbb{Z}/s)^n$ associated to the couple $(z, \mathcal{F})$ in this way:*

$$S_s(z, \mathcal{F}) = \left\{ z + \sum_{i \in [\![1,k]\!]} \lambda_i f^i \;\middle|\; \lambda_i \in \{0, 1/s\}, \forall i \in [\![1, k]\!] \right\}.$$

Let us denote that a set which is a 2D block in $\mathbb{Z}^2$ is not a 2D block in $(\mathbb{Z}/2)^2$, as depicted on Figure 3.1.

A subset $S \subset (\mathbb{Z}/s)^n$ is called a *block of* $(\mathbb{Z}/s)^n$ iff there exists a couple $(z, \mathcal{F}) \in (\mathbb{Z}/s)^n \times \mathcal{P}(\mathbb{B})$ such that $S = S_s(z, \mathcal{F})$. Note that a block of $(\mathbb{Z}/s)^n$ which is associated to a family $\mathcal{F} \in \mathcal{P}(\mathbb{B})$ of cardinal $k \in [\![0, n]\!]$ is said to be of *dimension* k, what will be denoted by $\dim(S) = k$. Figure 3.2 shows 2D,

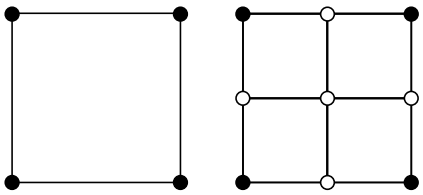

Figure 3.1: The notion of block depends on the space the set lies in.

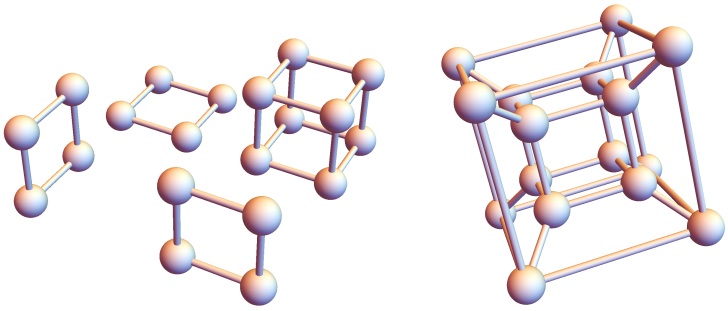

Figure 3.2: 2D, 3D and 4D blocks.

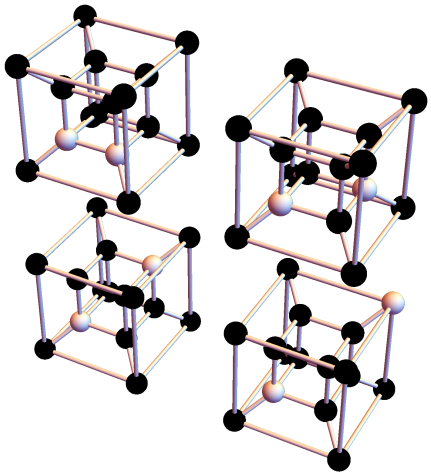

Figure 3.3: In the raster scan order: the white points are 1-antagonists, 2-antagonists, 3-antagonists, and 4-antagonists.

3D and 4D blocks. We can remark that their dimension does not depend on the space they lie in. We will denote the set of blocks of $(\mathbb{Z}/s)^n$ by $\mathcal{B}((\mathbb{Z}/s)^n)$.

Using this notion of blocks, we can define *antagonism*. Two points p, q belonging to a block $S \in \mathcal{B}((\mathbb{Z}/s)^n)$ are said to be *antagonist* in S iff their distance equals the maximal distance using the L^1 norm between two points into S. In other words, two points p and q in $(\mathbb{Z}/s)^n$ are antagonist in $S \in \mathcal{B}((\mathbb{Z}/s)^n)$ iff $p, q \in S$ such that:

$$\|p - q\|_1 = \max\{\|x - y\|_1 \ ; \ x, y \in S\},$$

and in this case we write that $q = \text{antag}_S(p)$ or equivalently $p = \text{antag}_S(q)$. The antagonist of a point p in a block $S \in \mathcal{B}((\mathbb{Z}/s)^n)$ containing p exists and is unique. Sometimes we will use the notation $S_s(p, q)$ where $p, q \in (\mathbb{Z}/s)^n$ are $(3^n - 1)$-neighbors into $(\mathbb{Z}/s)^n$ to indicate the block in $\mathcal{B}((\mathbb{Z}/s)^n)$ such that p and q are antagonist in this block.

Also, two points which are antagonist in a block of $(\mathbb{Z}/s)^n$ of dimension $k \in [\![0, n]\!]$ are said *k-antagonist*. In this case, k of their coordinates differ, and they differ from a value $1/s$, the other coordinates being equal. Two points which are 0-antagonist are equal, two points which are 1-antagonist in a block of $(\mathbb{Z}/s)^n$ are $2n$-neighbours in $(\mathbb{Z}/s)^n$, and two points which are n-antagonist in a block $S \in \mathcal{B}((\mathbb{Z}/s)^n)$ are $(3^n - 1)$-neighbors in $(\mathbb{Z}/s)^n$. See Figure 3.3 for different possible couple of antagonists (in white) in a 4D space.

Now we are able to define *critical configurations* of dimension $k \in [\![2, n]\!]$ in a n-D space:

Definition 10. *A set of two points $\{p, q\} \in (\mathbb{Z}/s)^n$ such that p and q are antagonist in a block $S \in \mathcal{B}((\mathbb{Z}/s)^n)$ of dimension $k \in [\![2, n]\!]$ is called a* primary critical configuration *in $(\mathbb{Z}/s)^n$ of dimension k. Any set equal to a block $S \in \mathcal{B}((\mathbb{Z}/s)^n)$ of dimension $k \in [\![2, n]\!]$ minus two points which are antagonist into S is called a* secundary critical configuration *in $(\mathbb{Z}/s)^n$ of dimension k. More generally, a* critical configuration *(of dimension $k \in [\![2, n]\!]$) in $(\mathbb{Z}/s)^n$ is either a primary or a secondary critical configuration (of dimension k) in $(\mathbb{Z}/s)^n$.*

In other words, the set of primary critical configurations can be written as following:

$$\{\{p, \text{antag}_S(p)\} \ ; \ S \in \mathcal{B}((\mathbb{Z}/s)^n), \ p \in S, \ \dim(S) \geq 2\},$$

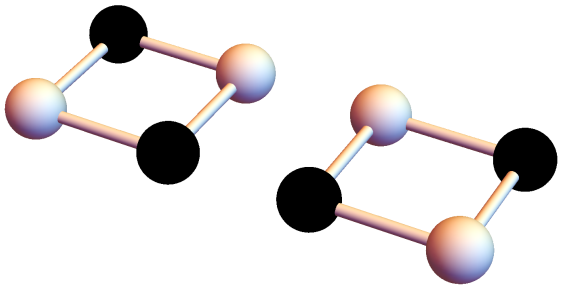

Figure 3.4: The white points on the left draw a 2D primary critical configuration, and the white points on the right draw a secundary 2D critical configuration.

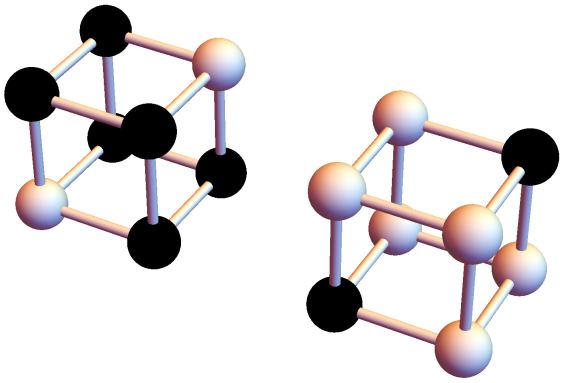

Figure 3.5: The white points on the left draw a 3D primary critical configuration, and the white points on the right draw a secundary 3D critical configuration.

and the set of the secondary critical configurations can be written in this way:

$$\{S \setminus \{p, \mathrm{antag}_S(p)\} \; ; \; S \in \mathcal{B}((\mathbb{Z}/s)^n), \; p \in S, \; \dim(S) \geq 2\} \, .$$

Figures 3.4, 3.5 and 3.6 depict 2D, 3D, and 4D critical configurations.

There comes our definition of digitally well-composed sets:

Definition 11. *A (digital) set $X \subset (\mathbb{Z}/s)^n$ is said* digitally well-composed *or* DWC *iff it does not contain any critical configurations, that is, for any block*

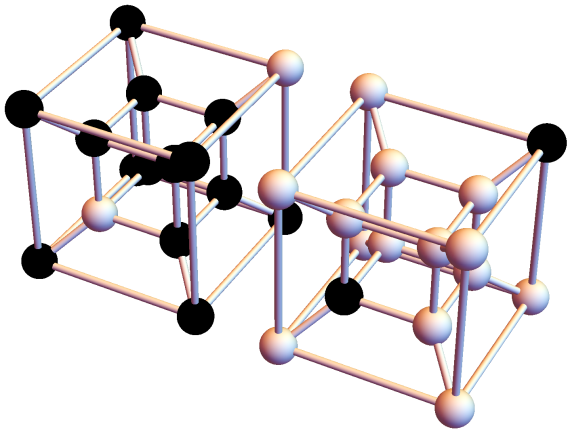

Figure 3.6: The white points on the left draw a 4D primary critical configuration, and the white points on the right draw a secundary 4D critical configuration.

$S \in \mathcal{B}((\mathbb{Z}/s)^n)$, the restriction $X \cap S$ is neither a primary nor a secundary critical configuration in $(\mathbb{Z}/s)^n$.

Obviously, this definition is self-dual, since a set $X \subset (\mathbb{Z}/s)^n$ contains a primary (respectively a secondary) critical configuration in the block $S \in \mathcal{B}((\mathbb{Z}/s)^n)$ iff its complement X^c contains a secondary (respectively a primary) critical configuration in this same block S.

Note that this definition is based on local patterns, at the contrary of well-composedness based on the equivalence of connectivities which is based on connected components, and then is global.

Also, Latecki remarked that in 2D and 3D, we can express well-composedness using $2n$-paths in restricted areas. Effectively, we can reformulate digital well-composedness based on $2n$-paths in dimension 2, 3, but also in dimension $n \geq 4$ as showed by our n-D theorem:

Theorem 2. *A set $X \subset (\mathbb{Z}/s)^n$ is digitally well-composed iff, for any block $S \in \mathcal{B}((\mathbb{Z}/s)^n)$ and for any couple of points $(p, \text{antag}_S(p))$ such that they belong to $X \cap S$ (resp. $S \setminus X$), p and $\text{antag}_S(p)$ are $2n$-connected in $X \cap S$ (resp. in $S \setminus X$) as subsets of $(\mathbb{Z}/s)^n$.*

Proof: Let us begin by the converse implication. If X is not digitally well-composed, there exists some block $S \subset (\mathbb{Z}/s)^n$ such as $X \cap S$ is a primary or

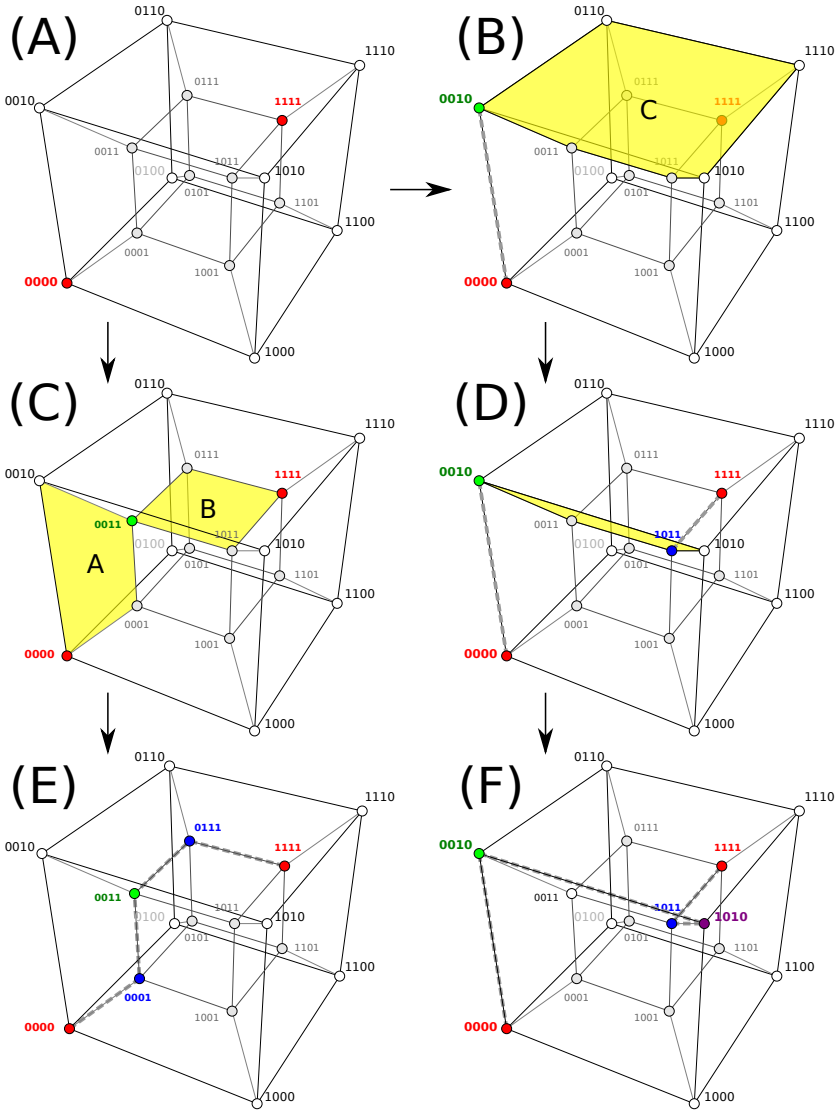

Figure 3.7: Step-by-step construction of the $2n$-path joining the two (red) antagonists into $X \cap S$ into $(\mathbb{Z}/s)^n$.

a secondary critical configuration in $(\mathbb{Z}/s)^n$. In the primary case, $\mathrm{Card}(X \cap S) = 2$, what contradicts that $\mathrm{Card}(X \cap S) \geq k+1$ due to the fact that every couple of antagonists (p, p') in this block is connected by a $2n$-path in $(\mathbb{Z}/s)^n$. In the secondary case, $\mathrm{Card}(X^c \cap S) = 2$, what contradicts that $\mathrm{Card}(X^c \cap S) \geq k+1$ for the same reason.

Concerning the direct implication, let us prove firstly that for two antagonists p and p' in some block $S \in \mathcal{B}((\mathbb{Z}/s)^n)$ of dimension $k \in [\![1, n]\!]$ such that $p, p' \in X$, there exists a $2n$-path in $X \cap S$ joining them as a subset of $(\mathbb{Z}/s)^n$ when X is digitally well-composed.

Initialization ($k = 1$) : the $2n$-path joining p and p' into $X \cap S$ as a subset of $(\mathbb{Z}/s)^n$ is simply $\pi = (p, p')$.

Induction ($k \in [\![2, n-1]\!]$): let us assume that this property is true for every $l \in [\![1, k]\!]$. Now, let us assume that there exists a couple of points p and p' of X such as they are antagonist in a block $S \in \mathcal{B}((\mathbb{Z}/s)^n)$ of dimension $(k+1)$. We know that X is digitally well-composed and then does not contain any primary critical configuration. Consequently, there exists one point $q \in X \cap S$ such as $q \neq p$ and $q \neq p'$. That means that p and q are antagonist in some block $S' \in \mathcal{B}((\mathbb{Z}/s)^n)$ of dimension l strictly lower than $k+1$, and then they are connected by a $2n$-path $\pi_{pq} = (p, \ldots, q)$ in $X \cap S' \subset X \cap S$ as as subset of $(\mathbb{Z}/s)^n$. For the same reason, q and p' are connected by a $2n$-path $\pi_{qp'} = (q, \ldots, p') \subseteq X \cap S$ in $(\mathbb{Z}/s)^n$. Consequently, by joining the two paths π_{pq} and $\pi_{qp'}$ we obtain a $2n$-path $\pi_{pp'}$ in $X \cap S$ joining p and p' into $(\mathbb{Z}/s)^n$.

A similar reasoning will prove that the non existence of secondary critical configurations in X (and then the non existence of primary critical configurations in X^c) implies that for any couple of points (p, p') of X^c and antagonist in some block $S \in \mathcal{B}((\mathbb{Z}/s)^n)$, there exists some $2n$-path joining them in $X^c \cap S$. □

This proof is illustrated on Figure 3.7 (here we have $s = 1$): two antagonists, depicted in red in the block S (the tesseract), are assumed to belong to a digitally well-composed set $X \subset \mathbb{Z}^n$, which is shown on Subfigure (A). Since the two red points $(0, 0, 0, 0)$ and $(1, 1, 1, 1)$ belong to X and are 4-antagonist in S, there exists at least one more point in the block S belonging to X (in the contrary case, X contains a critical configuration, which is impossible by hypothesis). A first possibility is shown on Subfigure (B), and a second possiblity is shown on Subfigure (C), where the green point depicts this additional point. Let us treat first the case corresponding to Subfigure (B): since the points $(0, 0, 1, 0)$ and $(1, 1, 1, 1)$ are 3-antagonist in the 3D block C depicted in yellow, there must be at least one more point in this block which belongs to X (for the same reason as before), and then we obtain that the blue point $(1, 0, 1, 1)$ belongs to X, which is shown on

Subfigure (D). Applying recursively the reasoning until X does not contain any critical configuration, we obtain that the point $(1, 0, 1, 0)$ also belongs to X, which is shown in purple on Subfigure (F). Finally, we obtain a $2n$-path joining the two red points $(0, 0, 0, 0)$ to $(1, 1, 1, 1)$ into $X \cap S$. Let us now treat the case corresponding to Subfigure (C): if $(0, 0, 0, 0)$ and $(0, 0, 1, 1)$, which are 2-antagonist, are the only points of X in the block A, $X \cap A$ is a critical configuration, then there exists an additional point among $(0, 0, 1, 0)$ and $(0, 0, 0, 1)$ which belongs to X. The same thing happens in the block B where at least $(0, 0, 1, 1)$ and $(1, 1, 1, 1)$ belongs to X: at least $(0, 1, 1, 1)$ or $(1, 0, 1, 1)$ must belong to X. Let us assume that $(0, 0, 0, 1)$ and $(0, 1, 1, 1)$ belong to X, we obtain Subfigure (E) where a $2n$-path joins the two red points $(0, 0, 0, 0)$ to $(1, 1, 1, 1)$ in $X \cap S$. Obvioulsy, the reasoning is similar when $(0, 0, 0, 0)$ and $(1, 1, 1, 1)$ belong to X^c. In this case, we obtain that a $2n$-path joins these two points in $X^c \cap S$, thanks to self-duality of digital well-composedness.

3.3.3 Link between EWCness and DWCness

Let us recall that EWCness in a global phenomenon, since it is based on connected components, and that DWCness is based on local properties, that is, there is no critical configurations. That shows that the link between DWCness and EWCness is not so obvious. Before proving that DWCness implies EWCness in any (finite) dimension n, $n \geq 2$, let us announce some lemmas.

Lemma 1. *Let $X \subset (\mathbb{Z}/s)^n$ be a digitally well-composed set in $(\mathbb{Z}/s)^n$. Then the $(3^n - 1)$-components of X in $(\mathbb{Z}/s)^n$, respectively of X^c in $(\mathbb{Z}/s)^n$, are digitally well-composed in $(\mathbb{Z}/s)^n$.*

Proof: We need first to prove that any element of $\mathcal{CC}_{3^n-1}(X, (\mathbb{Z}/s)^n)$ is DWC. Let C be an element of $\mathcal{CC}_{3^n-1}(X, (\mathbb{Z}/s)^n)$. Assume that C is not digitally well-composed, that means that there exists a block $S \in \mathcal{B}((\mathbb{Z}/s)^n)$ of dimension $k \geq 2$ such that $C \cap S$ is either a primary critical configuration or a secundary critical configuration. Let us begin with the primary case: there exists $p \in S$ such that $C \cap S = \{p, \text{antag}_S(p)\}$. Then we remark that any point different from p or $\text{antag}_S(p)$ belonging in S is a $(3^n - 1)$-neighbour of both p and p'. In other words, if there exists $q \in S$, $q \notin \{p, \text{antag}_S(p)$, belonging to X, it belongs also to C since this is a $(3^n - 1)$-component of X. Then $X \cap S = C \cap S$, and this way X contains a critical configuration

in $(\mathbb{Z}/s)^n$, which is impossible. The reasoning is the same for the secondary case. We have proven that the (3^n-1)-connected components of a DWC set are DWC. Now we need to prove that any element of $\mathcal{CC}_{3^n-1}(X^c,(\mathbb{Z}/s)^n)$ is DWC. Since X digitally well-composed in $(\mathbb{Z}/s)^n$ implies that X^c is digitally well-composed in $(\mathbb{Z}/s)^n$, the proof is done. □

Lemma 2. *Let $p,p' \in (\mathbb{Z}/s)^n$ be two points in a digitally well-composed set $X \subset (\mathbb{Z}/s)^n$. If p and p' are (3^n-1)-connected into X, they are also $2n$-connected into X.*

Proof: Let p,p' be two points in $X \subset (\mathbb{Z}/s)^n$ which is digitally well-composed in $(\mathbb{Z}/s)^n$. Assuming that p and p' are (3^n-1)-connected into X as a subset of $(\mathbb{Z}/s)^n$, there exists a (3^n-1)-path $\pi=(q^0=p,q^1,\ldots,q^{k-1},q^k=p')$ of length $k \geq 0$ joining them into X as a subset of $(\mathbb{Z}/s)^n$. For any $i \in [\![0,k-1]\!]$, q^i and q^{i+1} are (3^n-1)-adjacent into $(\mathbb{Z}/s)^n$, and then antagonist in a block $S_s(q^i,q^{i+1})$. Since X is digitally well-composed in $(\mathbb{Z}/s)^n$ and q^i and q^{i+1} belong to X, by Theorem 2, there exists a $2n$-path joining q^i and q^{i+1} into $X \cap S(q^i,q^{i+1})$ as a subset of $(\mathbb{Z}/s)^n$, such that these two points are $2n$-connected into X as a subset of $(\mathbb{Z}/s)^n$. By transitivity, p and p' are then $2n$-connected into X as a subset of $(\mathbb{Z}/s)^n$. □

Note that the converse is true, as stated by the following proposition.

Proposition 12. *Let $X \subset (\mathbb{Z}/s)^n$ be a digital set. Let us assume that each connected component of X in $(\mathbb{Z}/s)^n$, that is, any element of $\mathcal{CC}_{3^n-1}(X,(\mathbb{Z}/s)^n)$, and each connected component of X^c in $(\mathbb{Z}/s)^n$, that is, any element of $\mathcal{CC}_{3^n-1}(X^c,(\mathbb{Z}/s)^n)$, are digitally well-composed in $(\mathbb{Z}/s)^n$. Then, X is digitally well-composed in $(\mathbb{Z}/s)^n$.*

Proof: Let us assume that X is not digitally well-composed in $(\mathbb{Z}/s)^n$. There exists some block $S \in \mathcal{B}((\mathbb{Z}/s)^n)$ of dimension $k \in [\![2,n]\!]$ such that $X \cap S$ is a critical configuration of dimension k in $(\mathbb{Z}/s)^n$. Let us treat first the primary case. If $X \cap S = \{p,p'\}$ with $p' = \text{antag}_S(p)$, obviously p and p' are (3^n-1)-neighbors in $(\mathbb{Z}/s)^n$ since $\|p-p'\|_\infty \leq 1/s$ (they are antagonist), and then the connected component $C_X = \mathcal{CC}_{3^n-1}(X,p,(\mathbb{Z}/s)^n)$ contains also p'. This way, $C_X \cap S \supseteq \{p,p'\}$, and since $C_X \subseteq X$, $C_X \cap S = \{p,p'\}$, which contradicts that C_X is digitally well-composed into $(\mathbb{Z}/s)^n$. Now let us proceed to the secondary case. If X contains a secondary critical configuration in S as a subset of $(\mathbb{Z}/s)^n$, it means that $X^c \cap S = \{p,p'\}$ with $p' = \text{antag}_S(p)$. One more time, p and p' are (3^n-1)-neighbors into $(\mathbb{Z}/s)^n$,

and then the connected component $C_{X^c} = \mathcal{CC}_{3^n-1}(X^c, p, (\mathbb{Z}/s)^n)$ contains also p'. Then, $C_{X^c} \cap S \supseteq \{p, p'\}$, and since $C_{X^c} \subseteq X^c$, $C_{X^c} \cap S = \{p, p'\}$, which contradicts that C_{X^c} is digitally well-composed in $(\mathbb{Z}/s)^n$. □

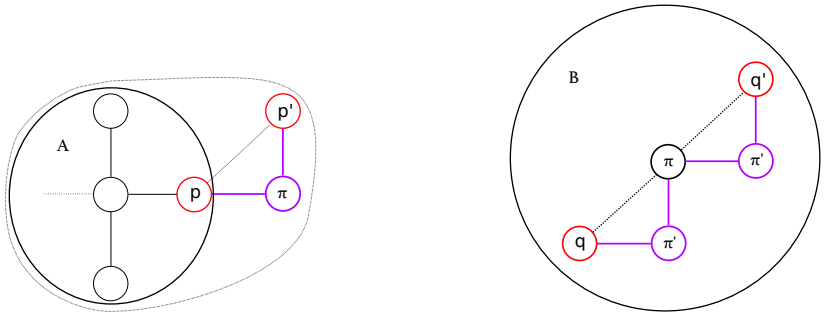

(a) In a digitally well-composed set, a $2n$-component is also a $(3^n - 1)$-component.

(b) In a digitally well-composed set, a $(3^n - 1)$-component is also a $2n$-component.

Figure 3.8: DWCness implies EWCness.

Theorem 3 (DWC ⇒ EWC)**.** *Let $X \subset (\mathbb{Z}/s)^n$ be a digitally well-composed set in $(\mathbb{Z}/s)^n$. Then, X and X^c are well-composed based on the equivalence of connectivities (EWC) in $(\mathbb{Z}/s)^n$.*

Proof: Let us prove in a first time that each $2n$-component in $(\mathbb{Z}/s)^n$ of a set $X \subset (\mathbb{Z}/s)^n$ wich is digitally well-composed in $(\mathbb{Z}/s)^n$ is also a $(3^n - 1)$-component of X in $(\mathbb{Z}/s)^n$ (see Figure 3.8a). Let A be any (non-empty) $2n$-component of a set $X \subset (\mathbb{Z}/s)^n$ which is digitally well-composed in $(\mathbb{Z}/s)^n$. It is obvious that A is $(3^n - 1)$-connected in $(\mathbb{Z}/s)^n$, the $2n$-connectivity implying the $(3^n - 1)$-connectivity. Let us prove now that A is maximal for the $(3^n - 1)$-connectivity by *reductio ad absurdum*: if A is not maximal for the $(3^n - 1)$-connectivity into $(\mathbb{Z}/s)^n$, there exists $A' \in \mathcal{CC}_{3^n-1}(X, (\mathbb{Z}/s)^n)$ such that $A \subset A'$. Then there exists $p, p' \in (\mathbb{Z}/s)^n$ such that $p \in A$ and $p' \in A' \setminus A$. These points belong both to A' and then are $(3^n - 1)$-connected in A as a subset of $(\mathbb{Z}/s)^n$. Also, A' is digitally well-composed in $(\mathbb{Z}/s)^n$ because it is a $(3^n - 1)$-component of a set which is digitally well-composed in $(\mathbb{Z}/s)^n$ (see Lemma 1). By Lemma 2, p and p' are $2n$-connected into A' as a subset of $(\mathbb{Z}/s)^n$, and then p' belongs to A, which leads to a contradiction. Then A is also a $(3^n - 1)$-component in $(\mathbb{Z}/s)^n$.

Let us now proceed to the converse implication. Let B be a (3^n-1)-component of X as a subset of $(\mathbb{Z}/s)^n$ (see Figure 3.8b). We need to prove that B is a $2n$-component of X as a subset of $(\mathbb{Z}/s)^n$, *i.e.*, B is $2n$-connected in $(\mathbb{Z}/s)^n$ and maximal for the $2n$-connectivity in the inclusion sense. Let us first prove that B is $2n$-connected into $(\mathbb{Z}/s)^n$. B is a (3^n-1) component of a set which is digitally well-composed into $(\mathbb{Z}/s)^n$, and then is digitally well-composed into $(\mathbb{Z}/s)^n$ by Lemma 1. Let $q, q' \in (\mathbb{Z}/s)^n$ be two points of B, then they are (3^n-1)-connected into B as a subset of $(\mathbb{Z}/s)^n$, and then they are also $2n$-connected by Lemma 2 into B as as subset of $(\mathbb{Z}/s)^n$. B is then $2n$-connected into $(\mathbb{Z}/s)^n$. Let us now assume that B is not maximal for the $2n$-connectivity. Then there exists some point $p \in X$ which is $2n$-connected to B in $(\mathbb{Z}/s)^n$ and which does not belong to B. Since the $2n$-connectivity implies the (3^n-1)-connectivity, this point belongs then to B. We have a contradiction. Then B is maximal for the $2n$-connectivity.

The fact that X^c is well-composed based on the equivalence of connectivities follows from the fact that X digitally well-composed implies X^c digitally well-composed and then X^c is well-composed based on the equivalence of connectivities. □

Now that we know that each (3^n-1)-component in $(\mathbb{Z}/s)^n$ of a set which is digitally well-composed into $(\mathbb{Z}/s)^n$ is also one of its $2n$-component in $(\mathbb{Z}/s)^n$ and conversely, we can deduce easily the following corollary.

Corollary 1. *Let $X \subset (\mathbb{Z}/s)^n$ be a digitally well-composed set in $(\mathbb{Z}/s)^n$. Then we have:*

$$\mathcal{CC}_{2n}(X, (\mathbb{Z}/s)^n) = \mathcal{CC}_{3^n-1}(X, (\mathbb{Z}/s)^n),$$

and

$$\mathcal{CC}_{2n}(X^c, (\mathbb{Z}/s)^n) = \mathcal{CC}_{3^n-1}(X^c, (\mathbb{Z}/s)^n).$$

Recall that the converse of Theorem 3 is not true in 3D (and in higher dimensions) (see Figure 3.9): a 3D subset of $(\mathbb{Z}/s)^n$ can be EWC in $(\mathbb{Z}/s)^n$ whithout being DWC in $(\mathbb{Z}/s)^n$, since the (3^n-1)-components in$(\mathbb{Z}/s)^n$ and the $2n$-components in $(\mathbb{Z}/s)^n$ of this set are equal, but it contains a 2D critical configuration at the top and then is not DWC (the reasoning holds for any $n \geq 3$).

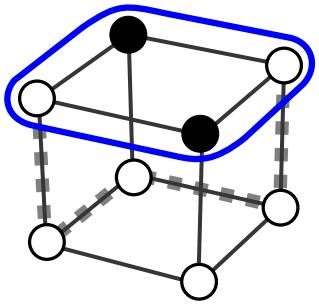

Figure 3.9: EWCness does not imply DWCness in n-D ($n \geq 3$).

Lemma 3. *Let $X \subset (\mathbb{Z}/s)^n$ be a digitally well-composed set in $(\mathbb{Z}/s)^n$. Then the $2n$-components of X, respectively of X^c, in $(\mathbb{Z}/s)^n$ are digitally well-composed.*

Proof: Since X is digitally well-composed in $(\mathbb{Z}/s)^n$, its $(3^n - 1)$ components in $(\mathbb{Z}/s)^n$ and the ones of its complement X^c in $(\mathbb{Z}/s)^n$ are digitally well-composed in $(\mathbb{Z}/s)^n$ by Lemma 1. Then, by Corollary 1, each $(2n)$-component of X or X^c is digitally well-composed in $(\mathbb{Z}/s)^n$. This concludes the proof. □

Finally, for sets which are digitally well-composed in $(\mathbb{Z}/s)^n$, it does not care if we consider either the $(3^n - 1)$-components or the $2n$-components of this set (respectively of its complement) since they are the same. Furthermore, these components are digitally well-composed in $(\mathbb{Z}/s)^n$.

3.3.4 Well-composed gray-level n-D images

In [95], Latecki told explicitely that a (digital) binary image $(\mathbb{Z}^2, X)$ is such that the set $X \subset \mathbb{Z}^2$ is finite or its complement is finite. Then it is obvious that we can store this kind of set in a matrix on a computer, this matrix representing the smallest rectangle $[\![x_{\min}, x_{\max}]\!] \times [\![y_{\min}, y_{\max}]\!]$ containing at least all the elements of X is the set of ones is finite, or containing at least all the elements of X^c is the set of zeros is finite. The resulting matrix contains then zeros and ones is finite number and represent rigorously the set X. However in the case of a gray-level image, there is no explicit assumption about which value (or group of value) is in finite number. To obviate ambiguities, we propose the definition below (see Definition 12), which is as general as possible: it allows to define images using real values, since today

we do not work anymore with quantificated images such that their values are in $[\![0, 255]\!]$ (they can be floating points, or negative, and so on). This definition also handles the different kinds of well-composednesses, since they are not equivalent in n-D, $n \geq 2$. But let us come back to some basics.

Let us assume that the integers $n \geq 2$ and $s \geq 1$ exist. From now on, we will say that a 4-uple $(A, \mathcal{D}, \mathbb{V}, u)$, representing the mapping $u : \mathcal{D} \subseteq A \to \mathbb{V}$, is an *image* defined on $\mathcal{D} \subseteq A$. In this case, A is called the *space* of the image, $\mathcal{D} \subseteq A$ is called the *domain* of the image, and $\mathbb{V} \subseteq \mathbb{R}$ is the *value space* of the image. Note that $(A, \mathcal{D}, \mathbb{V}, u)$ will be generally identified to u. Also, u will be said to be a *digital image* iff its space is equal to $(\mathbb{Z}/s)^n$ for some s and if its domain $\mathcal{D} \subset (\mathbb{Z}/s)^n$ is finite. Moreover, $(A, \mathcal{D}, \mathbb{V}, u)$ will be called a *(digital) gray-level* image if it is a digital image and if $\mathbb{V} = \mathbb{N}$.

Also we will use the following notation where A denotes any space and $\mathbb{V}$ denotes any value space:

$$\mathbb{I}\mathrm{m}(A, \mathcal{D}, \mathbb{V}) = \{u : \mathcal{D} \subseteq A \to \mathbb{V}\},$$

and:

$$\mathbb{I}\mathrm{m}(A, \mathbb{V}) = \{u : \mathcal{D} \subseteq A \to \mathbb{V} \ ; \ \mathcal{D} \subseteq A\}.$$

Now let us recall the definition of *threshold sets*, coming from the cross-section topology [118, 21, 17, 18]. Let $u \in \mathbb{I}\mathrm{m}((\mathbb{Z}/s)^n, \mathcal{D}, \mathbb{R})$ be an image and let be $\lambda \in \mathbb{R}$ a given threshold, a *large upper threshold set* is defined as:

$$[u \geq \lambda] = \{x \in \mathcal{D} \ ; \ u(x) \geq \lambda\},$$

a *strict upper threshold set* is defined as:

$$[u > \lambda] = \{x \in \mathcal{D} \ ; \ u(x) > \lambda\},$$

a *large lower threshold set* is defined as:

$$[u \leq \lambda] = \{x \in \mathcal{D} \ ; \ u(x) \leq \lambda\},$$

and a *strict lower threshold set* is defined as:

$$[u < \lambda] = \{x \in \mathcal{D} \ ; \ u(x) < \lambda\}.$$

Also, an *hyperrectangle* in $(\mathbb{Z}/s)^n$ is defined as the *cartesian product* in $(\mathbb{Z}/s)^n$, denoted by $\prod$, of the discrete intervals $[m_i, M_i] \cap \frac{\mathbb{Z}}{s}$ for all $i \in [\![1, n]\!]$ denoted by:

$$\prod_{i \in [\![1,n]\!]} [m_i, M_i] \cap \frac{\mathbb{Z}}{s},$$

where $m \in (\mathbb{Z}/s)^n$, its *lower bound*, and $M \in (\mathbb{Z}/s)^n$, its *upper bound*, are given and such that $\forall i \in [\![1, n]\!], m_i \leq M_i$. A *bounded hyperrectangle* in $(\mathbb{Z}/s)^n$ is an hyperrectangle such that the n coordinates of its lower bounds and of its upper bounds are finite.

Definition 12 (Well-composedness(es) of n-D images)**.** *A digital image $u : \mathcal{D} \subseteq (\mathbb{Z}/s)^n \to \mathbb{R}$ is said* X-WC*, where X belongs to $\{E, D, C, A\}$, in $(\mathbb{Z}/s)^n$ iff for every threshold $\lambda \in \mathbb{R}$, all the threshold sets of u are X-WC sets in $(\mathbb{Z}/s)^n$. This same image is said* X-WC*, where X belongs to $\{E, D, C, A\}$, on a domain $\mathcal{D}' \subseteq \mathcal{D}$ iff for every threshold $\lambda \in \mathbb{R}$, all the threshold sets of u restricted to the domain $\mathcal{D}'$ are X-WC sets in $(\mathbb{Z}/s)^n$.*

Note that we will not treat the case where the domain of a given image u is infinite because we want to ensure the property that the cardinal of the inverse image of any value taken in the value space of the image is finite. Moreover, 2D images defined on cubical grids are generally defined on rectangular domains, 3D images on rectangular parallelepipeds, and so on. This justifies our restriction to bounded hyperrectangles for images defined on a cubical grid.

3.3.5 Characterizing DWC real-valued n-D images

Now let us remark that in the case of a real-valued image defined on a bounded hyperrectangle, we are able to detect the digital well-composedness of this image only using the upper (respectively lower) threshold sets, as proved using the following Lemmas.

Lemma 4. *Let $u \in \mathbb{I}\mathrm{m}((\mathbb{Z}/s)^n, \mathcal{D}, \mathbb{R})$ be a gray-level image such that $\mathrm{Card}(\mathcal{D}) < +\infty$. Then u is digitally well-composed on $\mathcal{D}$ iff for any $\lambda \in \mathbb{R}$, $[u \leq \lambda]$ and $[u > \lambda]$ are both digitally well-composed (or equivalently iff $[u \geq \lambda]$ and $[u < \lambda]$ are both digitally well-composed).*

Proof: The direct implication is obvious. For the converse implication, let us proceed in two parts. Let us define $\mathbb{V}(u) = \{u(z) \mid z \in \mathcal{D}\}$ and:

$$\varepsilon = \min\{|u(p) - u(q)| \mid p, q \in \mathcal{D},\ u(p) \neq u(q)\}.$$

Firstly, we can observe that for any $\lambda \in \mathbb{R}$, every threshold set $[u < \lambda]$ can be rewritten $[u \leq f(\lambda)]$ with $f : \mathbb{R} \to \mathbb{R}$ defined such that:

$$f(\lambda) = \begin{cases} \lambda - \varepsilon/2 & \text{if } \lambda \in \mathbb{V}(u), \\ \lambda & \text{either.} \end{cases}$$

That means that every threshold set $[u < \lambda]$ is equal to $[u \leq \lambda']$ for some $\lambda' \in \mathbb{R}$.

Secundly, we can observe that every threshold set $[u \geq \lambda]$ can be rewritten $[u > f(\lambda)]$ using this same function f. That means that every threshold set $[u \geq \lambda]$ is equal to $[u > \lambda']$ for some $\lambda' \in \mathbb{R}$.

Finally, all the threshold sets $[u \leq \lambda]$ and $[u > \lambda]$ are digitally well-composed, then u is digitally well-composed. The reasoning is dual for the proposition in brackets. □

We have previously defined blocks in $(\mathbb{Z}/s)^n$. The extension to *blocks of a domain* $\mathcal{D} \subseteq (\mathbb{Z}/s)^n$ is straightforward. For a given domain $\mathcal{D} \subset (\mathbb{Z}/s)^n$, the *set of blocks in* $\mathcal{D}$ is denoted $\mathcal{B}(\mathcal{D}, (\mathbb{Z}/s)^n)$ and is such that:

$$\mathcal{B}(\mathcal{D}, (\mathbb{Z}/s)^n) = \{S \in \mathcal{B}((\mathbb{Z}/s)^n) \; ; \; S \subseteq \mathcal{D}\}.$$

Lemma 5. *Let $n \geq 2$ and $s \geq 1$ be two integers and H be a bounded hyperrectangle in $(\mathbb{Z}/s)^n$. Let X and Y be two sets of $(\mathbb{Z}/s)^n$ such as: $X \cap Y = \emptyset$ and $X \cup Y = H$ (i.e., (X, Y) is a* partition of H*). Then, X is digitally well-composed in $(\mathbb{Z}/s)^n$ iff Y is digitally well-composed in $(\mathbb{Z}/s)^n$. In other words, hyperrectangles preserve self-duality of digital well-composedness by avoiding side effects.*

Proof: Let us assume that X contains a primary critical configuration in $(\mathbb{Z}/s)^n$. It means that there exists some block $S \in \mathcal{B}(H, (\mathbb{Z}/s)^n)$ such that $X \cap S = \{p, p'\}$ with p and p' antagonist in S. Because X and Y are complementary in H, $X \cap S$ and $Y \cap S$ are complementary in $S \subseteq H$. The consequence is that $Y \cap S = S \setminus \{p, p'\}$, i.e., Y contains a secondary critical configuration in S as a subset of $(\mathbb{Z}/s)^n$.

So, we have proven that X contains a primary critical configuration iff Y contains a secondary critical configuration, and by a symetrical reasoning, we can prove that X contains a secondary critical configuration iff Y contains a primary critical configuration. That finally means that X is digitally well-composed in $(\mathbb{Z}/s)^n$ iff Y is digitally well-composed in $(\mathbb{Z}/s)^n$. □

Lemma 6. *Let $n \geq 2$ and $s \geq 1$ be two integers and H be a bounded hyperrectangle in $(\mathbb{Z}/s)^n$. Let $u : \mathcal{D} \to \mathbb{R}$ be a gray-level image. Then, u is digitally well-composed iff for any $\lambda \in \mathbb{R}$ the threshold set $[u \leq \lambda]$ is digitally well-composed in $(\mathbb{Z}/s)^n$ (or equivalently iff for any $\lambda \in \mathbb{R}$ the threshold set $[u \geq \lambda]$ is digitally well-composed in $(\mathbb{Z}/s)^n$).*

Proof: Using Lemma 4 and because the cardinal of H is finite, we know that u is digitally well-composed in $(\mathbb{Z}/s)^n$ iff for any $\lambda \in \mathbb{R}$, $[u \leq \lambda]$ and $[u > \lambda]$ are digitally well-composed in $(\mathbb{Z}/s)^n$. Furthermore, using Lemma 5, and because $[u \leq \lambda] \cap [u > \lambda] = \emptyset$ and $[u \leq \lambda] \cup [u > \lambda] = H$ (with H an hyperrectangle), we know that $[u \leq \lambda]$ is digitally well-composed in $(\mathbb{Z}/s)^n$ iff $[u > \lambda]$ is digitally well-composed in $(\mathbb{Z}/s)^n$. We can conclude that u is digitally well-composed in $(\mathbb{Z}/s)^n$ iff $[u \leq \lambda]$ is digitally well-composed in $(\mathbb{Z}/s)^n$. □

Like exposed in [27], there exists a characterization for gray-level digitally well-composed images defined on bounded hyperrectangles. It is the natural extension of the characterization of Latecki for 2D images in [95].

Proposition 13. *Let $n \geq 2$ and $s \geq 1$ be two integers and H be a bounded hyperrectangle in $(\mathbb{Z}/s)^n$. A real-valued image $u : \mathcal{D} \subset \mathbb{Z}^n \to \mathbb{R}$ is digitally well-composed in $(\mathbb{Z}/s)^n$ iff for any block $S \in \mathcal{B}(\mathcal{D}, (\mathbb{Z}/s)^n)$ such that $\dim(S) \geq 2$ and for any couple of points $(p, p') \in S \times S$ such that $p' = \text{antag}_S(p)$, the following relation is true:*

$$\text{intvl}(u(p),\, u(p')) \;\cap\; \text{Span}\{\, u(p'') \;\big|\; p'' \in S \setminus \{p,\, p'\}\,\} \;\neq\; \emptyset.$$

Proof: Effectively, let us assume that there exists a block $S \in \mathcal{B}(\mathcal{D}, (\mathbb{Z}/s)^n)$ and a couple of points $(p, p') \in S \times S$ such that this intersection is empty, then either:

$$\max\{\, u(p'') \;\big|\; p'' \in S \setminus \{p,\, p'\}\,\} < \min(u(p),\, u(p')),$$

and in this case $[u \geq \min(u(p),\, u(p'))] \cap S$ is equal to $\{p, p'\}$ which is a primary critical configuration, or:

$$\max(u(p),\, u(p')) < \min\{\, u(p'') \;\big|\; p'' \in S \setminus \{p,\, p'\}\,\},$$

and:

$$[u \geq \min\{\, u(p'') \;\big|\; p'' \in S \setminus \{p,\, p'\}\,\}] \cap S = S \setminus \{p,\, p'\},$$

which is a secundary critical configuration. In both cases, u is obviously not digitally well-composed. Conversely, if there exists a value $\lambda \in \mathbb{R}$ such that $[u \geq \lambda]$ contains a critical configuration in a block $S \in \mathcal{B}(\mathcal{D})$, either $[u \geq \lambda] \cap S$ is a primary critical configuration (1), or it is a secundary critical configuration (2). In case (1), there exists $p, p' \in S$ such that $p' = \text{antag}_S(p)$ and $[u \geq \lambda] \cap S = \{p, p'\}$, which means that $\min\{u(p), u(p')\} \geq \lambda$, and in parallel we have $[u < \lambda] \cap S = S \setminus \{p, p'\}$, which means that $\max\{\, u(p'') \;\big|\; p'' \in S \setminus \{p,\, p'\}\} < \lambda$, and then the intersection we are looking for is empty. In case (2), there exists $p, p' \in S$ such that $p' = \text{antag}_S(p)$ and $[u \geq \lambda] \cap S = S \setminus \{p, p'\}$, which means that $\min\{\, u(p'') \;\big|\; p'' \in S \setminus \{p,\, p'\}\} \geq \lambda$, and in parallel we have $[u < \lambda] \cap S = \{p, p'\}$, which means that $\max\{u(p), u(p')\} < \lambda$, and then the intersection we are looking for is still empty. This concludes the proof. □

Practically, this characterization means that for a given and finite dimension $n \geq 2$, we can check if an image defined on a domain $\mathcal{D}$ is digitally well-composed or not in $(\mathbb{Z}/s)^n$ by a very simple algorithm by checking at each block $S \in \mathcal{B}(\mathcal{D})$ if the image is digitally well-composed. Furthermore, the complexity of this algorithm is for a fixed dimension in linear time relatively to the number of blocks in the domain $\mathcal{D}$, which means that it is very fast, in particular for small dimensions.

We propose Algorithm 1 which works in n-D and verifies that a given image does not contain any critical configurations.

For sake of simplicity, let us compute the complexity of this algorithm assuming that the subdivision factor is equal to 1.

Let us begin with the 2D case: if we assume that we have a real-valued image u defined on a rectangular domain $\mathcal{D} = [\![0, s_1]\!] \times [\![0, s_2]\!] \subset \mathbb{Z}^2$, we have a total number of $s_1 \times s_2$ 2D blocks in $\mathcal{D}$. In each block, we have a total of $\text{Card}(S)$ possible points p. Then, for each p, we compute in constant time its antagonist p' in the block. The computation of m_1, m_2, M_1, M_2 are each one in $O(\text{Card}(S))$. The comparison $(M_1 < m_2) \;||\; (M_2 < m_1)$ is in constant time. Finally, we obtain a complexity in $O(s_1 \times s_2 \times \text{Card}(S)^2) = O(s_1 \times s_2)$ since the size of the block is a constant in this context.

Now, let us consider that the dimension is a parameter that we have to take into account for the computation of the complexity. Assuming that the given image u if of dimension $n \geq 2$, then its domain can be written $\mathcal{D} = \prod_{i=1}^{n} [\![0, s_i]\!]$ where s_i is a non-nul integer for any $i \in [\![1, n]\!]$. Then we

Algorithm 1: An algorithm able to check the digital well-composedness of a n-D image.

```
CheckImage (n, u, D) : isDWC;
begin
    for S ∈ B(D) s.t. dim(S) ≥ 2 do
        for p ∈ S do
            p' ← antag_S(p);
            m1 ← min(u(p), u(p'));
            M1 ← max(u(p), u(p'));
            m2 ← min{ u(p'') | p'' ∈ S \ {p, p'} };
            M2 ← max{ u(p'') | p'' ∈ S \ {p, p'} };
            if (M1 < m2) || (M2 < m1) then
                return false;
    return true;
```

have a total number of C_n^k families of k vectors among n (with $k \in [\![2, n]\!]$). For each family of dimension $k \in [\![2, n]\!]$, we have a total number of associated blocks (of dimension k) which is lower than $\prod_{i=1}^{n}(s_i + 1)$. For each block, we have a total number of 2^{k-1} couples of antagonists, and for each couple, we have to compute m_1 and M_1, which can be computed simultaneously with only one comparison, and m_2 and M_2, which need each $2^k - 3$ comparisons. Also, the comparisons $M_1 < m_2$ and $M_2 < m_1$ constitute 2 operations. We obtain that we need less than 2^{k+1} comparisons for each couple of antagonists, which means less than 4^k comparisons for each block, and then less than $\prod_{i=1}^{n}(s_i + 1) \times 4^k$ for each family. We obtain then a total complexity equal to:

$$T(n, \{s_i\}) \leq \prod_{i=1}^{n}(s_i + 1) \times \sum_{k=2}^{n} C_n^k 4^k.$$

Using the binomial formula $\sum_{k=0}^{n} C_n^k x^k = (1 + x)^n$, we obtain finally:

$$T(n, \{s_i\}) \leq 5^n \times \prod_{i=1}^{n}(s_i + 1).$$

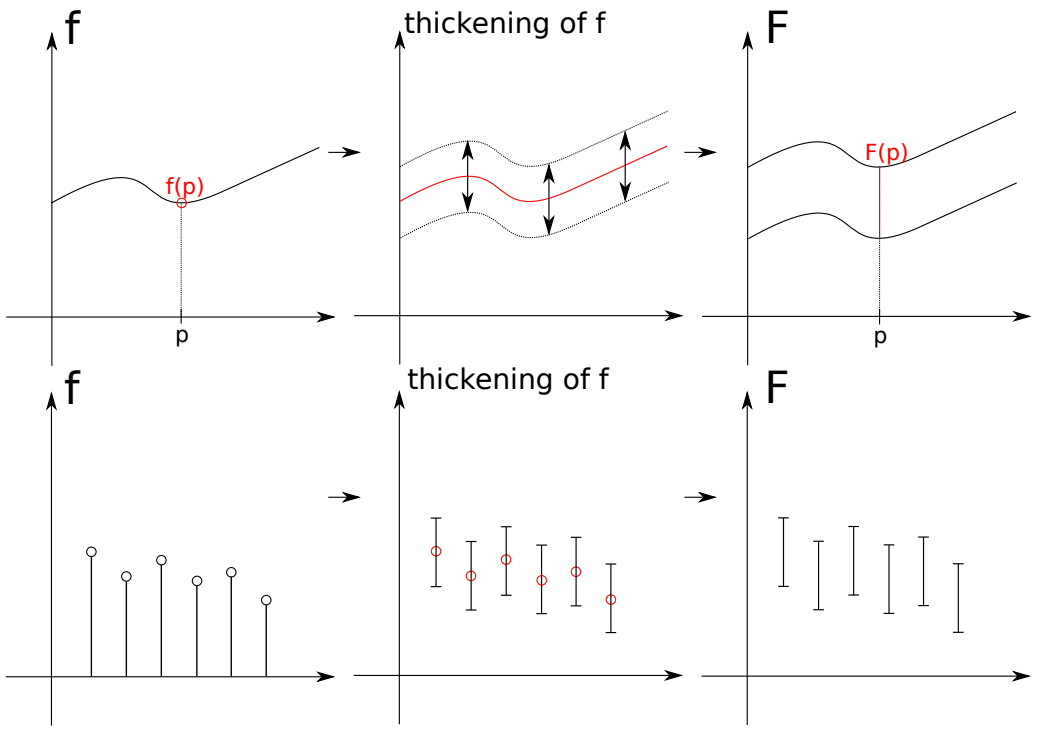

Figure 3.10: From single-valued functions to set-valued/interval-valued functions (continuous and discrete cases).

3.3.6 DWCness for interval-valued maps

We have seen what means digital well-composedness for single-valued maps, that is, maps such that for a point p belonging to their domain $\mathcal{D}$, the value at p is a real value belonging to $\mathbb{R}$. However, as seen in the book of Aubin [10] which introduces *set-valued analysis*, we can define *set-valued maps*, that is, maps such that for a point p belonging to their domain $\mathcal{D}$, the value at p is a subset of $\mathbb{R}$. We will be particularily interested in *interval-valued maps*, a class of set-valued maps such that the value at each point of the domain is an interval $[a, b] \subset \mathbb{R}$.

These set-valued maps can be interpreted in the following manner: let us imagine we have a single-valued function $f : \mathcal{D} \to \mathbb{R}$. By stretching/thickening the function as depicted on top of Figure 3.10, we obtain a new function $F : \mathcal{D} \to 2^{\mathbb{R}}$ (also written $F : \mathcal{D} \rightsquigarrow \mathbb{R}$), that is, a function such that at each point $p \in \mathcal{D}$, $F(p)$ is a set and then has potentially a

thickness not equal to zero. For this reason, F is said to be a *set-valued function*. We can easily extend this thickening to discrete images, as shown on the bottom of Figure 3.10, to obtain discrete set-valued images.

Effectively, these functions will be very useful to define a new kind of digital well-composedness and will be used as intermediary maps to prove that the final real-valued interpolation we present in Section 4.2 is digitally well-composed: when an interval-valued map is digitally well-composed (see the definition hereafter), the output of our front-propagation algorithm applied on this map is a digitally well-composed single-valued image. In other words, if we interpolate a given image u into an interval-valued image U which is digitally well-composed, we know that the output image u_{DWC} (with U as input) is also digitally well-composed. The fact that u_{DWC} interpolates the original image u is detailed later.

Let us now introduce the definition of digital well-composedness for interval-valued images [27] defined on discrete spaces as $(\mathbb{Z}/s)^n$, where $n \geq 2$ is the dimension and $s \geq 1$ is the subdivision factor. Note that we drew from the definition of well-composed interval-valued maps of Najman and Géraud [124] in Alexandrov spaces.

Definition 13. *A* set-valued map $U : \mathcal{D} \subseteq X \rightsquigarrow Y$ *is a function from a topological space X to a topological space Y such that for any $p \in X$, $p \in \mathcal{D} \Leftrightarrow U(p) \neq \emptyset$ ($\mathcal{D}$ is called the* domain *of U) and such that $\forall p \in \mathcal{D}, U(p) \subseteq Y$.*

Definition 14. *An* interval-valued map $U : \mathcal{D} \subseteq X \rightsquigarrow Y$ *is a set-valued map such that for any $p \in \mathcal{D}$, $U(p)$ is an* interval *of the topological space $Y \subseteq \mathbb{R}^n$, that is, $U(p)$ can be written $[a, b] \cap Y$ for some $a, b \in \mathbb{R}$ such that $a \leq b$.*

Now that we have defined interval-valued maps, we can define their *threshold sets* (see Figures 3.11 and 3.12).

Definition 15. *For a given interval-valued map $U : \mathcal{D} \subseteq (\mathbb{Z}/s)^n \rightsquigarrow \mathbb{R}$, we define for any $\lambda \in \mathbb{R}$ respectively the* large upper, the strict upper, the strict

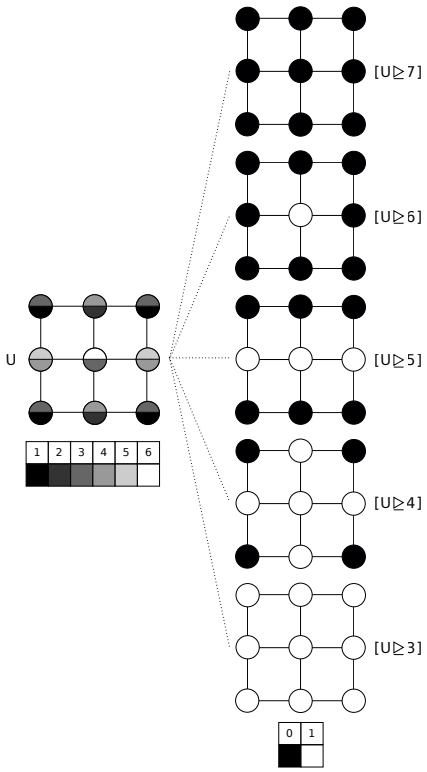

Figure 3.11: A family of (large upper) threshold sets $\{[U \trianglerighteq \lambda]\}_\lambda$ of an interval-valued image U. We can remark the straightforward inclusion relationship $[U \trianglerighteq \lambda] \subseteq [U \trianglerighteq \lambda - \varepsilon]$ for any $\lambda \in \mathbb{R}$ and $\varepsilon > 0$.

lower, the large lower threshold sets *as well:*

$$
\begin{aligned}
[U \trianglerighteq \lambda] &= \{\, z \in \mathcal{D} \;\big|\; \exists\, v \in U(z),\, v \geq \lambda \,\}, \\
[U \triangleright \lambda] &= \{\, z \in \mathcal{D} \;\big|\; \forall\, v \in U(z),\, v > \lambda \,\}, \\
.[U \triangleleft \lambda] &= \{\, z \in \mathcal{D} \;\big|\; \forall\, v \in U(z),\, v < \lambda \,\}, \\
[U \trianglelefteq \lambda] &= \{\, z \in \mathcal{D} \;\big|\; \exists\, v \in U(z),\, v \leq \lambda \,\}.
\end{aligned}
$$

Using the threshold sets like in [124], we can define digital well-composedness on $(\mathbb{Z}/s)^n$:

Definition 16. *An n-D interval-valued map* $U : \mathcal{D} \subseteq (\mathbb{Z}/s)^n \to \mathbb{I}_\mathbb{R}$*, where*

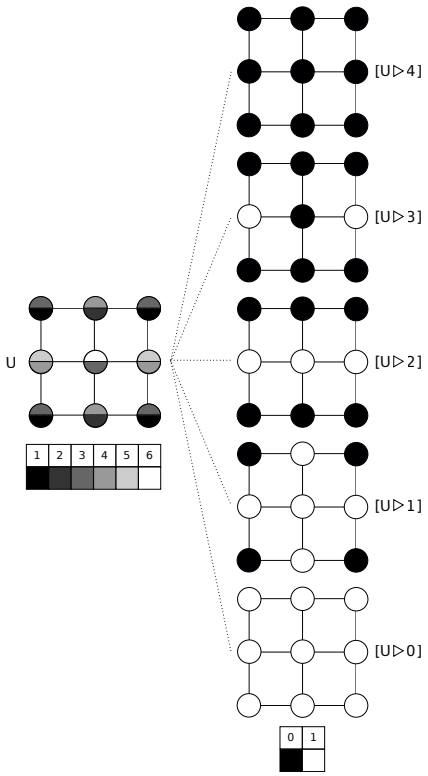

Figure 3.12: A family of (strict upper) threshold sets $\{[U \rhd \lambda]\}_\lambda$ of an interval-valued image U. We can remark the straightforward inclusion relationship $[U \rhd \lambda] \subseteq [U \rhd \lambda - \varepsilon]$ for any $\lambda \in \mathbb{R}$ and $\varepsilon > 0$.

$\mathbb{I}_\mathbb{R}$ *is the set of intervals of* $\mathbb{R}$*, is said* digitally well-composed *on* $(\mathbb{Z}/s)^n$ *iff all its threshold sets are digitally well-composed on* $(\mathbb{Z}/s)^n$*.*

Now, let us define the *upper/lower bounds* of an interval-valued map. They will be useful to characterize interval-valued digitally well-composed maps.

Definition 17. *For an nD interval-valued map* $U : \mathcal{D} \subseteq (\mathbb{Z}/s)^n \to \mathbb{I}_\mathbb{R}$*, the* upper bound $\lceil U \rceil$ *and the* lower bound $\lfloor U \rfloor$ *are defined such that for any* $p \in \mathcal{D}$*,* $\lceil U \rceil(p) = \max(U(p))$ *and* $\lfloor U \rfloor(p) = \min(U(p))$*.*

Then a simple characterization follows.

Proposition 14. *An nD interval-valued map* $U : \mathcal{D} \subseteq (\mathbb{Z}/s)^n \to \mathbb{I}_\mathbb{R}$ *defined on a bounded hyperrectangle* $\mathcal{D}$ *is digitally well-composed in* $(\mathbb{Z}/s)^n$ *iff both*

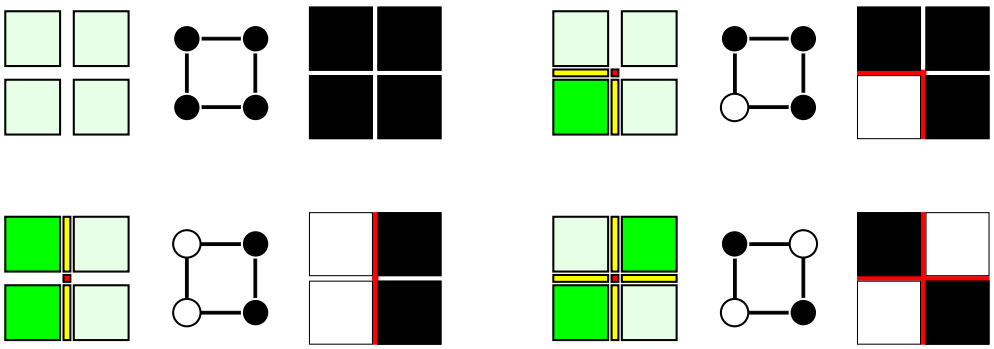

Figure 3.13: Possible configurations in 2D.

$\lceil U \rceil : \mathcal{D} \to \mathbb{R}$ and $\lfloor U \rfloor : \mathcal{D} \to \mathbb{R}$ are nD images which are digitally well-composed in $(\mathbb{Z}/s)^n$.

Proof: Effectively, for any $\lambda \in \mathbb{R}$, we have the remarkable equalities:

$$\begin{cases} [U \rhd \lambda] = [\lfloor U \rfloor > \lambda], & (1) \\ [U \lhd \lambda] = [\lceil U \rceil < \lambda], & (2) \\ [U \trianglerighteq \lambda] = [\lceil U \rceil \geq \lambda], & (3) \\ [U \trianglelefteq \lambda] = [\lfloor U \rfloor \leq \lambda]. & (4) \end{cases}$$

This way, if U is digitally well-composed in $(\mathbb{Z}/s)^n$, then for any $\lambda \in \mathbb{R}$, $[U \trianglerighteq \lambda]$ and $[U \trianglelefteq \lambda]$ are digitally well-composed in $(\mathbb{Z}/s)^n$, and then by (3) and (4), $\lceil U \rceil$ and $\lfloor U \rfloor$ are digitally well-composed in $(\mathbb{Z}/s)^n$. Conversely, if both $\lceil U \rceil$ and $\lfloor U \rfloor$ are digitally well-composed in $(\mathbb{Z}/s)^n$, then for any $\lambda \in \mathbb{R}$, $[\lfloor U \rfloor > \lambda]$, $[\lceil U \rceil < \lambda]$, $[\lceil U \rceil \geq \lambda]$, and $[\lfloor U \rfloor \leq \lambda]$ are digitally well-composed in $(\mathbb{Z}/s)^n$ and then by (1) to (4), U is digitally well-composed in $(\mathbb{Z}/s)^n$. □

3.4 Relations between AWCness, DWCness, and CWCness on cubical grids

Note that in this section, we talk about subsets in $\mathbb{Z}^n$, but these properties hold for subsets of $(\mathbb{Z}/s)^n$.

The proof of the equivalence between EWCness, CWCness, and DWCness in 2D being already in [96, 95], let us expose briefly why AWCness and

DWCness are equivalent (a study of the equivalence between AWCness and DWCness in n-D, $n \geq 2$, is provided in Chapter D).

On Figure 3.13, the middle of the subfigure represents the restriction of a set to a 2D block in $\mathbb{Z}^2$ (the white points correspond to the foreground), the left of the subfigures represents the representation in Khalimsky Grids of this same set up to an isomorphism (the foreground is depicted by the green squares and the boundary is depicted by the yellow edges and the red point), and the right of the subfigures represents the continuous analog of the restriction of this set in $\mathbb{R}^2$ (the foreground is in white and the boundary in red).

In the raster scan order, we observe then the following possibilities by comparing the two first columns of the subfigures:

1. if the restriction of the set is made of four black points, that is, no point of X belongs to the block, and then there is no boundary in this part of the Khalimsky grid, we have then nothing to prove,

2. if the restriction of the set is made of only one point, we can observe that the red point belonging to the discrete boundary has only two neighbors into the boundary: the two yellow edges,

3. if this resctriction is made of two 4-adjacent white points, the red point belonging to the discrete boundary has one more time two yellow edges as neighbors into the boundary,

4. if this restriction is made of two white points which are 8-adjacent but not 4-adjacent, that is, when we have a critical configuration, then we obtain that the red point has four neighbors, the four yellow edges.

Then the red points of the boundary of the representation of the set in Khalimsky grids admit only two neighbors iff the set is digitally well-composed. Since the yellow edges admits always two neighbors, because a boundary is closed (and thein contains its vertices in the Khalimsky grid) by construction, we obtain finally that every set which is AWC is DWC and conversely in 2D.

The equivalence in 2D between DWCness/AWCness and CWCness is also depicted on Figure 3.13, to favor the understanding and the link between these three kinds of well-composednesses.

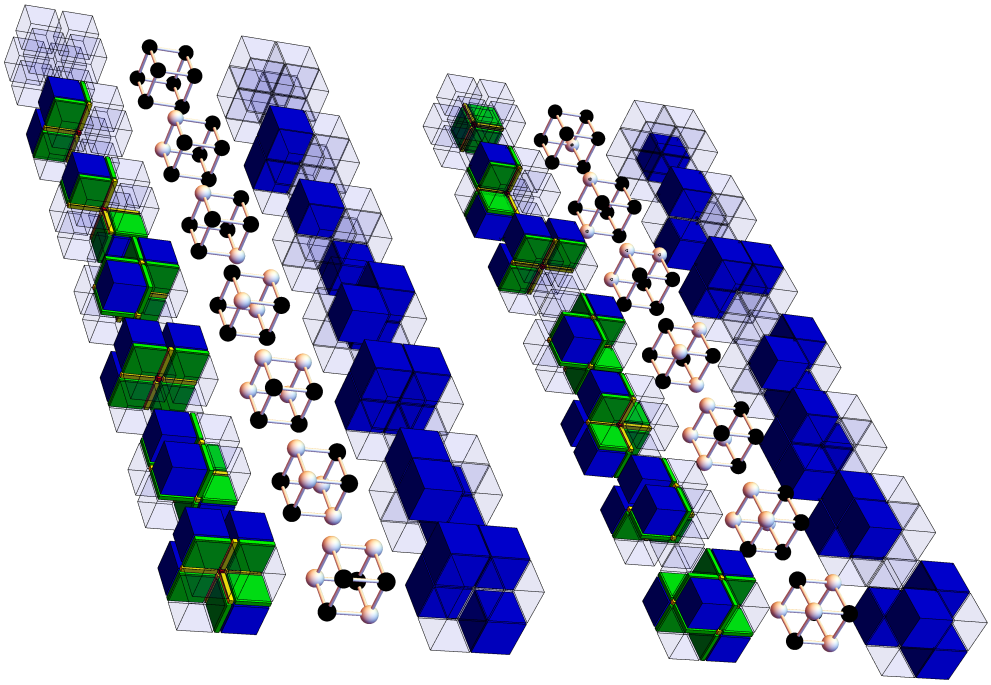

Figure 3.14: Possible configurations in 3D.

Since it is well-known that EWCness, DWCness, AWCness and CWCness are equivalent for (digital) sets in $\mathbb{Z}^2$, they are also equivalent for 2D (digital) binary or gray-level images.

In 3D, Latecki has proven that DWCness and CWCness are equivalent, and has also shown that they imply EWCness. However the proof of the equivalence of AWCness and DWCness in 3D, even if well-known and admitted in the community of digital topology, has not been published to our knowledge. That is why we propose to recall in brief why it is true (the detailed study in n-D, $n \geq 2$, is in Chapter D).

Looking at Figure 3.14, with the same reasoning as for the 2D case, we obtain that there is no critical configurations in the restriction $X \cap S$, where S is a 3D block, if and only if the boundary $\partial\mathcal{IMM}(X)$ (made of green squares, yellow edges, and red points) of the *immersion* $\mathcal{IMM}(X)$ (such that white points in $\mathbb{Z}^3$ become blue cubes) of X is locally a simple closed curve. At the contrary, in the cases containing one or more 2D critical configurations or a 3D critical configuration, $\partial\mathcal{IMM}(X)$ is not locally a simple closed curve: it

2D:	**EWC** **1995** [96]	$\Leftrightarrow$	DWC	$\Leftrightarrow$	AWC	$\Leftrightarrow$	CWC
3D:	EWC	$\Leftarrow$	DWC	$\Leftrightarrow$	AWC	$\Leftrightarrow$	**CWC** **1997** [98]
nD:	**EWC** **2015** [27]	$\Leftarrow$	**DWC** **2015** [27]	$\overset{?}{\Leftrightarrow}$	**AWC** **2013** [124]	$\overset{?}{\Leftrightarrow}$	**CWC** 2000 [95]

Table 3.1: The different "flavors" of well-composedness and their relationship on cubical grids (our contributions are emphasized in yellow).

contains a "pinch" at a yellow edge in the case of a 2D critical configuration and at a red point in the case of a 3D critical configuration. Note that the cases that we can obtain by complementarity have been omitted since well-composedness is self-dual. This gives the intuition of why AWCness and DWCness are equivalent in 3D.

Obviously, the equivalence between AWCness, DWCness, and CWCness in 3D is also true for (digital) binary or gray-level images by extension.

Finally, thanks to Latecki, 3D CWCness implies 3D EWCness (for sets), and then each kind of WCness among AWCness, CWCness, and DWCness implies in 3D EWCness for sets, binary images, and gray-level images.

In n-D, it is more complicated, because the case-by-case study is impossible: the different possible cases depend on the given n. However, we have proven that DWCness in n-D implies EWCness for digital sets and then for binary and gray-level images.

We summarized all these relations in Table 3.1. Note that the relation between n-D DWCness, AWCness and CWCness has a "?" on the equivalence relationships because the proof of the equivalence between AWCness and DWCness remains not verified at this moment, and because the equivalence between AWCness and CWCness (exposed later) is a conjecture.

Obviously, all the equivalences or relations cited in this section hold for $(\mathbb{Z}/s)^n$.

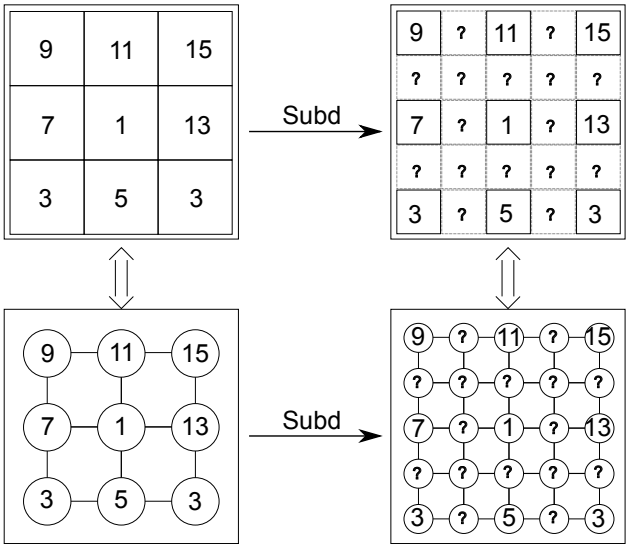

Figure 4.1: Subdividing the domain $\mathcal{D}$ into $\mathcal{D}'$ to interpolate.

Chapter 4

Digitally Well-composed Interpolations in n-D

Let us begin with the definition of the interpolation of a digital image.

Definition 18. *An* interpolation *of an image* $(\mathbb{R}^n, \mathcal{D}, \mathbb{R}, u)$ *defined on a (bounded hyperrectangular) domain* $\mathcal{D} \subset \mathbb{Z}^n$ *is an image* $(\mathbb{R}^n, \mathcal{D}', \mathbb{R}, u')$ *such that its domain* $\mathcal{D}'$ *contains* $\mathcal{D}$ *and such that the restriction of the interpolation* u' *to the domain* $\mathcal{D}$ *of the initial image* u *is equal to* u *(see Figure 4.1).*

In this chapter, we are going to show that making an interpolation is not so easy when some criterias are required: digital well-composedness, *self-duality*, n-dimensionality, *in-betweeness*, and so on. In particular, we are going to show in Section 4.1 that *local interpolations* fail to produce 3D digitally well-composed interpolations satisfying all these constraints, and that another approach has to be found. In Section 4.2, we will expose the interpolation that we propose to this aim.

Note that in the sequel, we will always assume that the given images are defined on a bounded hyperrectangular domain $\prod_{i\in[\![1,n]\!]}[m_i, M_i] \cap \mathbb{Z}^n$ where $\prod$ is the *cartesian product* and where m, M are the *minimal bound* and *maximal bound* of the domain respectively. Interpolations will be defined on *subdivisions* of these domains defined as $\prod_{i\in[\![1,n]\!]}[m_i, M_i] \cap \left(\frac{\mathbb{Z}}{2}\right)^n$.

4.1 Self-dual Local Interpolations

After having recall some preliminary vocabulary related to *hierarchical subdividions*, the usual process used to subdivide $\mathbb{Z}^n$ into $\left(\frac{\mathbb{Z}}{2}\right)^n$, we will show that an "usual" interpolation of an digital image is simply a numerical scheme with some constraints. In particular, when we combine *orderedness*, invariance by 90 degrees rotations, translations and axial symmetries, *in-betweenness*, and digital well-composedness, we can characterize our interpolation method by a set of "interpolating functions" that are used one by one to construct the interpolation in such a way that it is digitally well-composed on all its domain at the end of the interpolation (if no impossible case is encountered). Finally we will observe that our counter-example shows that every self-dual interpolation verifying the properties above fail in 3D and higher dimensions.

4.1.1 Subdivisions and Interpolations

A block of $\mathbb{Z}^n$ can be *subdivided* into blocks of $(\mathbb{Z}/s)^n$ using the following procedure that we call the *subdividing rule*:

Definition 19 (Hierarchical Subdivision of a block)**.** *Let us assume that a value $s \in \mathbb{N}^*$ is given. Let $S \in \mathcal{B}(\mathbb{Z}^n)$ be a block associated to a point $z \in \mathbb{Z}^n$ and a family of vector $\mathcal{F} = (f^1, \dots, f^k) \subseteq \mathbb{B}$. Then the* subdivision *of S is*

denoted by $\mathrm{Subd}(S)$ *and is equal to:*

$$\mathrm{Subd}(S) = \left\{ z + \sum_{i \in [\![1,k]\!]} \lambda_i f^i \ ; \ \forall i \in [\![1,k]\!], \lambda_i \in \{0, 1/s, 2/s, \ldots, 1\} \right\}.$$

Note that the subdivision of a block of dimension 0 is this same block, that a block of dimension 1 is subdivided into s blocks of same dimension, that a block of dimension 2 is subdivided into s^2 blocks of dimension 2, and so on.

In the case where s is even, like when $s = 2$, we will sometimes speak about the *center* of a subdivided block. For a given block $S \in \mathcal{B}(\mathbb{Z}^n)$, the *center* of the block S is defined as $(p+q)/2$ where p and q are two antagonists in this block. Obviously, this point belongs to $\left(\frac{\mathbb{Z}}{2}\right)^n$ and is unique (in the sense that it does not depend on the couple of antagonist that has been chosen to compute it).

Let us define now the *subdivision* of a domain:

Definition 20 (Hierarchical subdivision of a bounded hyperrectangle)**.** *Let us assume that a value $s \in \mathbb{N}^*$ is given. Let $\mathcal{D} \subseteq \mathbb{Z}^n$ be a bounded hyperrectangle. Then the subdivision of this domain is the union of the subdivision of the blocks of $\mathbb{Z}^n$ that are subset of this domain:*

$$\mathrm{Subd}(\mathcal{D}) = \bigcup_{S \in \mathcal{B}\mathcal{D}} \mathrm{Subd}(S).$$

Obviously, $\mathrm{Subd}(\mathcal{D}) \subseteq (\mathbb{Z}/s)^n$.

Now that we have defined the subdivision of a domain, we can define an interpolation of an image defined on a cubical grid.

Definition 21 (Interpolations)**.** *Let $(\mathbb{Z}^n, \mathcal{D}, \mathbb{R}, u)$ be a given image (with $\mathcal{D}$ a bounded hyperrectangle). We call* real-valued (digital) interpolation of u *any image $(\left(\frac{\mathbb{Z}}{2}\right)^n, \mathrm{Subd}(\mathcal{D}), \mathbb{R}, u')$ such that its restriction to $\mathcal{D}$ is equal to u:*

$$u'\big|_{\mathcal{D}} = u.$$

For example, on Figure 4.2, we can see an image defined on a 2D block and that can be represented as a 2D matrix by $\begin{pmatrix} a & b \\ c & d \end{pmatrix}$. On its right side,

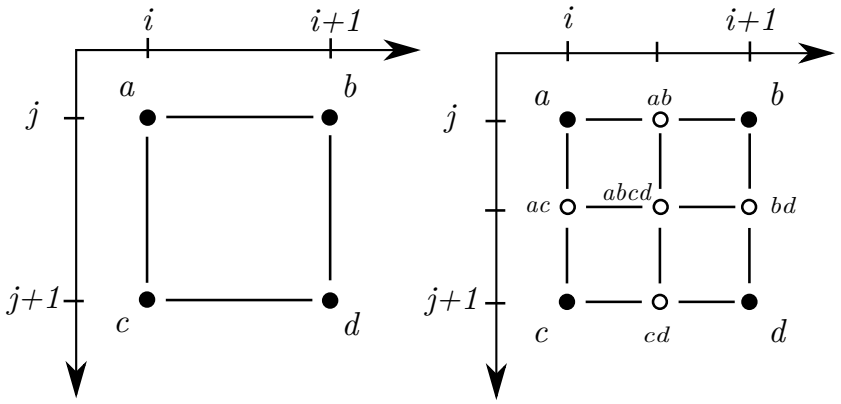

Figure 4.2: Illustration of the subdivision process on a block S.

we can observe the interpolation of this image $\begin{pmatrix} a & ab & b \\ ac & abcd & bd \\ c & cd & d \end{pmatrix}$ where the pixels (i, j, a),$(i+1, j, b)$,$(i, j+1, c)$, and $(i+1, j+1, d)$, the *primary pixels*, preserved their positions, and where $(i+1/2, j, ab)$,$(i, j+1/2, ac)$,$(i+1, y+1/2, bd)$,$(i+1/2, j+1, cd)$ and $(i+1/2, j+1/2, abcd)$, the *secondary pixels*, are "inserted" between the primary ones.

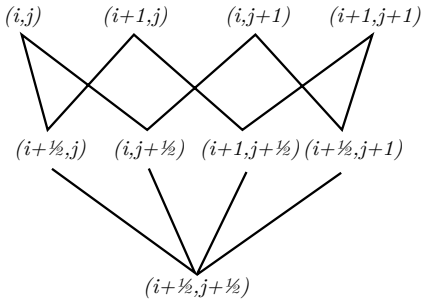

Figure 4.3: $\mathrm{Subd}(S) \subseteq \left(\frac{\mathbb{Z}}{2}\right)^n$ as a poset.

Now let us observe that the hierarchical subdivision (of a block) of $\mathbb{Z}^n$ when $s = 2$ induces an *relation order*, that is, a binary relation $R : \left(\frac{\mathbb{Z}}{2}\right)^n \to \{0, 1\}$ which is *reflexive* $(\forall a, aRa)$, *antisymmetrical* $(\forall a, b, aRb \wedge bRa \Rightarrow a = b)$, and *transitive* $(\forall a, b, c, aRb \wedge bRc \Rightarrow aRc)$. For that, let us define the mapping $\circledcirc : \left(\frac{\mathbb{Z}}{2}\right)^n \to \mathbb{N}$, called the *order*, defined such that $\forall p \in \mathbb{Z}$, $\circledcirc(p) = 0$, such that for each point $q \in \left(\frac{\mathbb{Z}}{2}\right)^n$ inserted at the middle between two points

of order 0 whose distance L^1 equals 1, $\circledcirc(q) = 1$, and such that for each point $r \in \left(\frac{\mathbb{Z}}{2}\right)^n$ which is not of order 0 nor 1 and which is inserted at the middle between two points of order 1 whose distance L^1 equals 1, $\circledcirc(r) = 2$, and so on. This way, we can define the binary relation $R : \left(\frac{\mathbb{Z}}{2}\right)^n \to \{0, 1\}$ such that $p, q \in \left(\frac{\mathbb{Z}}{2}\right)^n$ verify pRq which is said "p is *parent* of q" iff $\circledcirc(p) \leq \circledcirc(q)$ and $\|p - q\|_\infty \leq 1/2$. The couple $(\mathbb{Z}^n, R)$ which represents $\mathbb{Z}^n$ supplied with the order relation R is called a *partial order* or *poset*. Also, a point $p \in \left(\frac{\mathbb{Z}}{2}\right)^n$ is said to be a *direct parent* of $q \in \left(\frac{\mathbb{Z}}{2}\right)^n$ iff pRq and there exists no point into $\left(\frac{\mathbb{Z}}{2}\right)^n \setminus \{p, q\}$ such that pRr and rRq. Figure 4.3 shows this parenthood relationship between the points of a 2D block $S((i, j), (e^1, e^2))$ by linking a point of the 2D block and its direct parent(s) in this block. Based on this figure, we can also obtain the following matrix of orders corresponding to this subdivided block:

$$\begin{pmatrix} 0 & 1 & 0 \\ 1 & 2 & 1 \\ 0 & 1 & 0 \end{pmatrix}.$$

A generalization to dimension $n \geq 2$ is proposed in the next subsection.

Note that a similar relation exists using the Khalimsky grids, where the order relation is based on the inclusion, but we do not have any inclusion right here since we are working on graphs made of vertices and edges.

4.1.2 Notations Specific to Hierarchical Subdibisions

As we have seen before, we can associate an order to a position in $\left(\frac{\mathbb{Z}}{2}\right)^n$ assuming that this space results from the subdivision of $\mathbb{Z}^n$. Let us define this notion more formally.

Definition 22. *We denote by $\frac{1}{2}(z)$ the set of the coordinates of the point $z \in \left(\frac{\mathbb{Z}}{2}\right)^n$ such that they are not integers:*

$$\frac{1}{2}(z) = \left\{ i \in [\![1, n]\!] \; ; \; z_i \in \frac{\mathbb{Z}}{2} \setminus \mathbb{Z} \right\}.$$

This notation, even if looking much simple, will be very useful in the following, because it permits to classify the points of $\left(\frac{\mathbb{Z}}{2}\right)^n$ just based on the number of integral coordinates.

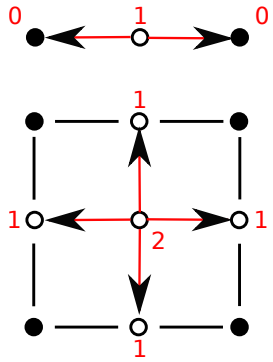

Figure 4.4: Parenthood relationship in the graph of a subdivided block.

Definition 23 (Order)**.** *We denote by* $\mathbb{E}_k$ *with* $k \in [\![0, n]\!]$ *the set of points in* $\left(\frac{\mathbb{Z}}{2}\right)^n$ *such that they have* $(n-k)$ *integral coordinates:*

$$\mathbb{E}_k = \left\{ z \in \left(\frac{\mathbb{Z}}{2}\right)^n \; ; \; \text{Card}\left(\frac{1}{2}(z)\right) = k \right\}.$$

Then, we call order *of a point* $z \in \left(\frac{\mathbb{Z}}{2}\right)^n$ *the value* k *such that* $z \in \mathbb{E}_k$*.*

The sets of parents can then be defined very easily:

Definition 24 (Parents)**.** *Let* z *be an element of* $\left(\frac{\mathbb{Z}}{2}\right)^n \setminus \mathbb{Z}^n$*. The set of* (direct) parents *(see Figure 4.4) of* z *is denoted by* $\mathbb{P}(z)$ *and equal to:*

$$\mathbb{P}(z) = \bigcup_{i \in \frac{1}{2}(z)} \left\{ z + \frac{e^i}{2}, z - \frac{e^i}{2} \right\}.$$

With z *an element of* $\left(\frac{\mathbb{Z}}{2}\right)^n$*, we define the* 0^{th} *order parents of* z *denoted* $\mathbb{P}^0(z)$ *and equal to* $\{z\}$*. Also, we define recursively, for any* z *element of* $\left(\frac{\mathbb{Z}}{2}\right)^n \setminus \mathbb{Z}^n$*, and for* $k \geq 1$*:*

$$\mathbb{P}^k(z) = \bigcup_{p \in \mathbb{P}(z)} \mathbb{P}^{k-1}(p).$$

Note that a point of $\mathbb{Z}^n$ does not have parents if it corresponds to a primary pixel. However points of order 1 have parents of order 0, points of order 2 have parent of order 1, and so on. Also we can remark that $\{\mathbb{E}_k\}_{k \in [\![0,n]\!]}$ represents a *(hierarchichal) partition* of $\left(\frac{\mathbb{Z}}{2}\right)^n$.

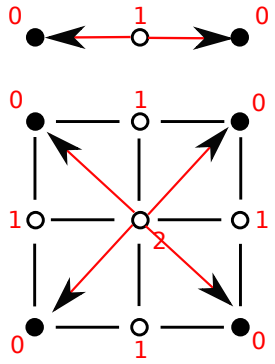

Figure 4.5: Ancesters of the point z at the center of the subdivided block.

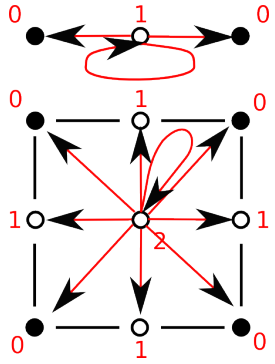

Figure 4.6: Groups of the point z at the center of the subdivided block.

Now we define a category of points that we call *ancesters* (of a point $p \in \left(\frac{\mathbb{Z}}{2}\right)^n$). They are very useful because they represent the set of positions of the pixels whose depends directly the value of the interpolation at p (see Figure 4.5) when using *local interpolations*.

Definition 25 (Ancesters)**.** *Let z be an element of $\left(\frac{\mathbb{Z}}{2}\right)^n$. The set of the* ancesters of p *is denoted by $\mathbb{A}(p)$ and is defined such that:*

$$\mathbb{A}(p) = \mathbb{P}^{\mathfrak{o}(z)}(z).$$

Note that $\mathbb{A}(p)$ is a subset of $\mathbb{Z}^n$.

Definition 26 (Groups)**.** *Let z be an element of $\left(\frac{\mathbb{Z}}{2}\right)^n$. The* group of p *denoted by $\mathcal{G}(p)$ is defined such that:*

$$\mathcal{G}(p) = \bigcup_{k \in [\![0, \mathfrak{o}(z)]\!]} \mathbb{P}^k(z),$$

and represents the set of all the parents of any order of z in $\left(\frac{\mathbb{Z}}{2}\right)^n$.

The usefulness of *groups* (see Figure 4.6) of a point $z \in \left(\frac{\mathbb{Z}}{2}\right)^n$ will be seen later.

A last notation is useful when we work with *in-between interpolations*.

Definition 27 (Opposites)**.** *Let z be an element of $\left(\frac{\mathbb{Z}}{2}\right)^n \setminus \mathbb{Z}^n$. The set of* opposites *of z is the family of pairs or points:*

$$\mathrm{opp}(z) = \bigcup_{i \in \frac{1}{2}(z)} \left\{ \left\{ z - \frac{e^i}{2}, z + \frac{e^i}{2} \right\} \right\}.$$

Let a, b, z be three points of $\left(\frac{\mathbb{Z}}{2}\right)^n$, we say that a is opposite to b relatively to *z iff $\{a, b\} \in \mathrm{opp}(z)$.*

Now that we have defined the mathematical basics in matter of hierarchical subdivisions, we are able to define the different properties that an "usual" local interpolation has to satisfy on a cubical grid.

4.1.3 "Usual" Local Interpolations

We have seen that an image $u' \in \mathbb{Im}(\left(\frac{\mathbb{Z}}{2}\right)^n, \mathbb{R})$ defined on a domain $\mathcal{D}' \subset \left(\frac{\mathbb{Z}}{2}\right)^n$ is an interpolation of an image $u \in \mathbb{Im}(\mathbb{Z}^n, \mathbb{R})$ defined on a given domain $\mathcal{D} \subset \mathbb{Z}^n$ iff $\mathcal{D} \subseteq \mathcal{D}'$ and the restriction of u' to $\mathcal{D}$, noted $u'\big|_{\mathcal{D}}$, is equal to u, that is, for any $p \in \mathcal{D}$, $u'(p) = u(p)$.

Definition 28. *An operator $\mathcal{I} : \mathbb{Im}(\mathbb{Z}^n, \mathbb{R}) \to \mathbb{Im}(\left(\frac{\mathbb{Z}}{2}\right)^n, \mathbb{R})$ is said to be a* cubical (real-valued) interpolation method *iff for any image $u \in \mathbb{Im}(\mathbb{Z}^n, \mathbb{R})$ defined on a bounded hyperrectangle $\mathcal{D} \subseteq \mathbb{Z}^n$, $\mathcal{I}(u) : \mathrm{Subd}(\mathcal{D}) \to \mathbb{R}$ is an interpolation of u.*

Definition 29 (Self-duality)**.** *A cubical real-valued interpolation method $\mathcal{I} : \mathbb{Im}(\mathbb{Z}^n, \mathbb{R}) \to \mathbb{Im}(\left(\frac{\mathbb{Z}}{2}\right)^n, \mathbb{R})$ is said* self-dual *iff for any image $u \in \mathbb{Im}(\mathbb{Z}^n, \mathbb{R})$, we have the relation:*

$$\mathcal{I}(-u) = -\mathcal{I}(u)$$

In other words, if we denote by u'_+ the interpolation by $\mathcal{I}$ of u and by u'_- the interpolation by $\mathcal{I}$ of $(-u)$, both of domain $\mathcal{D}' \subseteq \left(\frac{\mathbb{Z}}{2}\right)^n$, we have for any $p \in \mathcal{D}'$ the relation:

$$u'_+(p) = -u'_-(p).$$

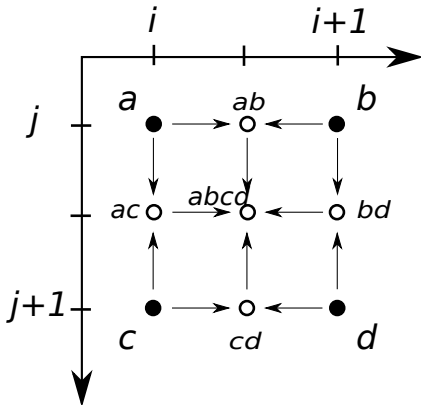

Figure 4.7: Ordered computing of the values of the interpolation.

Self-duality is much important to us, and in image analysis in general, because it represents that an image will be treated in the same manner whatever if it contains bright components over a dark background or dark components over a bright background.

Definition 30 (Ordered)**.** *Let $\mathcal{D}$ be a bounded hyperrectangle in $\mathbb{Z}^n$. A cubical real-valued interpolation method:*

$$\mathcal{I} : \mathbb{I}\mathrm{m}(\mathbb{Z}^n, \mathcal{D}, \mathbb{R}) \to \mathbb{I}\mathrm{m}(\left(\frac{\mathbb{Z}}{2}\right)^n, \mathrm{Subd}(\mathcal{D}), \mathbb{R})$$

is said ordered *iff for any image $u \in \mathbb{I}\mathrm{m}(\mathbb{Z}^n, \mathbb{R})$, at each point $p \in \mathrm{Subd}(\mathcal{D})$, the value $u'(p)$ of the interpolation $\mathcal{I}(u)$ at p is computed based only on the values of u at the parents of p in $\left(\frac{\mathbb{Z}}{2}\right)^n$. In other words, the values at the centers of the subdivided "edges" depend only on the values at the vertices of the initial edges, the values at the center of the subdivided "squares" depend only on the values at the centers of its edges, and so on.*

As depicted on Figure 4.7 illustrating orderedness of an interpolation method, on the image $\begin{pmatrix} a & ab & b \\ ac & abcd & bd \\ c & cd & d \end{pmatrix}$, ab is a function of a and b, ac is a function of a and c, bd is a function of b and d, cd is a function of c and d, and $abcd$ is a function of ab, ac, bd and cd, and then also a function of a,b,bc and d. In other words, the values of the secundary pixels depend on the value of their ancesters. In this manner, an interpolation method which is ordered is also *local*:

Definition 31 (Local)**.** *Let $\mathcal{D}$ be a bounded hyperrectangle in $\mathbb{Z}^n$. A cubical real-valued interpolation method $\mathcal{I} : \mathbb{I}\mathrm{m}(\mathbb{Z}^n, \mathcal{D}, \mathbb{R}) \to \mathbb{I}\mathrm{m}(\left(\frac{\mathbb{Z}}{2}\right)^n, \mathrm{Subd}(\mathcal{D}), \mathbb{R})$ is said* local *iff for any image $u \in \mathbb{I}\mathrm{m}(\mathbb{Z}^n, \mathcal{D}, \mathbb{R})$, at each point $p \in \mathrm{Subd}(\mathcal{D})$, the value $u'(p)$ of the interpolation $\mathcal{I}(u)$ at p is computed based only on the values $u\big|_{\mathbb{A}(p)}$.*

Definition 32 (In-between)**.** *A cubical real-valued interpolation method $\mathcal{I} : \mathbb{I}\mathrm{m}(\mathbb{Z}^n, \mathbb{R}) \to \mathbb{I}\mathrm{m}(\left(\frac{\mathbb{Z}}{2}\right)^n, \mathbb{R})$ is said* in-between *iff for any image $u \in \mathbb{I}\mathrm{m}(\mathbb{Z}^n, \mathbb{R})$ defined on a domain $\mathcal{D} \subseteq \mathbb{Z}^n$ which is a bounded hyperectangle, its interpolation $u' = \mathcal{I}(u)$ defined on the domain $\mathcal{D}' = \mathrm{Subd}(\mathcal{D})$ is such that at each point $p \in \mathcal{D}' \setminus \mathcal{D}$, the value $u'(p)$ satisfies the relation:*

$$u'(p) \in \bigcap_{\{z^-, z^+\} \in \mathrm{opp}(p)} \mathrm{intvl}(u'(z^+), u'(z^-)).$$

Note that this relation is recursive. Also, this property is very interesting because it implies that we do not create any extrema in the image when we proceed to the interpolation.

Definition 33 (DWC interpolations)**.** *A cubical real-valued interpolation method $\mathcal{I} : \mathbb{I}\mathrm{m}(\mathbb{Z}^n, \mathbb{R}) \to \mathbb{I}\mathrm{m}(\left(\frac{\mathbb{Z}}{2}\right)^n, \mathbb{R})$ is said* digitally well-composed (DWC) *iff for any image $u \in \mathbb{I}\mathrm{m}(\mathbb{Z}^n, \mathbb{R})$ defined on a domain $\mathcal{D} \subseteq \mathbb{Z}^n$ which is a bounded hyperrectangle, its interpolation $u' = \mathcal{I}(u)$ defined on the domain $\mathcal{D}' = \mathrm{Subd}(\mathcal{D})$ is digitally well-composed.*

Note that we make the difference between an interpolation, which is a digitally well-composed image, and an interpolation method, which is an operator which produces digitally well-composed images.

Now we can express the set of properties that "usual" local interpolations on cubical grids satisfy in general. We call this set of properties $(\mathcal{P})$:

$$(\mathcal{P}) \equiv \begin{cases} \mathcal{I} \text{ is a cubical real-valued interpolation} \\ \mathcal{I} \text{ is invariant by translations, } \frac{\pi}{2}\text{'s rotations and axial symmetries} \\ \mathcal{I} \text{ is ordered} \\ \mathcal{I} \text{ is in-between} \\ \mathcal{I} \text{ is self-dual} \\ \mathcal{I} \text{ is digitally well-composed} \end{cases}$$

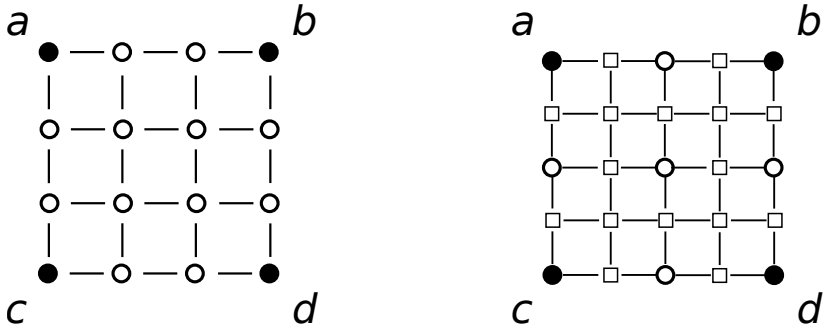

(a) Atypic subdivision. (b) Double interpolation.

Figure 4.8: Other kinds of subdivisions/interpolations.

Note that there exists other manners to subdivide the domain before proceeding to the interpolation. Effectively, the interpolation could be done on a domain such that we added more than one pixel between each pixel. Also, we could imagine an "double" interpolation, that is, made of two succesive interpolations, which could lead to primary, secundary, and then ternary pixels. See Figure 4.8 for an illustration of these two methods. In our study, we will limit ourselves to "simple" interpolations which subdivide only once the original domain, as described for the cubical real-valued interpolation methods using the operator Subd.

4.1.4 Constrained Interpolation Methods

We are going to show in this subsection that taking into account the set of properties $(\mathcal{P})$ for an interpolation method is equivalent to solve a system of equations.

Lemma 7. *Any cubical real-valued interpolation method* $\mathcal{I} : \mathbb{Im}(\mathbb{Z}^n, \mathbb{R}) \to \mathbb{Im}(\left(\frac{\mathbb{Z}}{2}\right)^n, \mathbb{R})$ *verifying* $(\mathcal{P})$ *can be characterized by a set of functions* $\{f_k\}_{k\in[\![1,n]\!]}$ *constraining* $u' = \mathcal{I}(u)$ *such that:*

$$\forall\, z \in \left(\frac{\mathbb{Z}}{2}\right)^n,\ u'(z) = \begin{cases} u(z) & \text{if } z \in \mathbb{E}_0 \\ f_k(u\big|_{\mathbb{A}(z)}) & \text{if } z \in \mathbb{E}_k,\ k \in [1,n] \end{cases}$$

We denote such an interpolation method $\mathcal{I}_{f_1,\dots,f_n}$.

Proof: The interpolation u' at the center of a subdivided 1D block depends only on the values of u at the points of $\mathbb{E}_0$. Furthermore, this method

has to be invariant by translations, 90 degrees rotations and then does not depend on the position or on the orientation of the 1D block. It does not depend neither on the order of these two values because the process is invariant by symmetries. Hence, there is an unique function f_1 characterizing this method on subdivisions of 1D blocks, and this function must be symmetrical. On a subdivision of a 2D block, the only unknown value is at its center, since the values belonging to $\mathbb{E}_0$ or $\mathbb{E}_1$ in the subdivided domain are already valued. Since the method in invariant by translations and 90 degrees rotations, the function that value the center of the subdivided 2D block does not depend on the position or on the rotation, and then there exists one only function f_2 used to compute this value. We can follow iteratively the reasoning for the subdivisions of blocks of greater dimensions until n. □

Notice that this Lemma is an implication and not an equivalence: an interpolation verifying this numerical scheme does not always verify all the properties in $(\mathcal{P})$.

Definition 34 (I_0)**.** *Let $(\mathbb{Z}^n, \mathcal{D}, \mathbb{R}, u)$ be an image and let be a cubical real-valued interpolation method $\mathcal{I} : \mathbb{I}\mathrm{m}(\mathbb{Z}^n, \mathbb{R}) \to \mathbb{I}\mathrm{m}(\left(\frac{\mathbb{Z}}{2}\right)^n, \mathbb{R})$, such that we obtain the interpolation $u' = \mathcal{I}(u)$ defined on the domain $\mathcal{D}' = \mathrm{Subd}(\mathcal{D})$. In this case, we can define the set $I_0(u', z)$ representing the set of possible values $u'(z)$ at $z \in \mathcal{D}' \setminus \mathcal{D}$ such that $\mathcal{I}$ is in-between:*

$$I_0(u', z) = \bigcap_{\{z^-, z^+\} \in \mathrm{opp}(z)} \mathrm{intvl}(u'(z^+), u'(z^-)).$$

In this manner, $\mathcal{I}$ is in-between iff $\forall z \in \mathcal{D}' \setminus \mathcal{D}$, $u'(z) \in I_0(u', z)$.

Definition 35 (I_{WC})**.** *Let $(\mathbb{Z}^n, \mathcal{D}, \mathbb{R}, u)$ be an image and let be a cubical real-valued interpolation method $\mathcal{I} : \mathbb{I}\mathrm{m}(\mathbb{Z}^n, \mathbb{R}) \to \mathbb{I}\mathrm{m}(\left(\frac{\mathbb{Z}}{2}\right)^n, \mathbb{R})$ such that we obtain the interpolation $u' = \mathcal{I}(u)$ defined on the domain $\mathcal{D}' = \mathrm{Subd}(\mathcal{D})$. In this case, we define the set $I_{WC}(u', z)$ such that for any $z \in \mathbb{E}_1 \cap \mathcal{D}'$, $I_{WC}(u', z) = \mathbb{R}$ and for any $z \in \mathbb{E}_k \cap \mathcal{D}'$ with $k \in [\![2, n]\!]$:*

$$I_{WC}(u', z) \;=\; \{\, v \in \mathbb{R} \;\mid\; u'(z) = v \;\Rightarrow\; u'\big|_{\mathcal{G}(z)} \text{ is } DWC \,\}$$

Now, we can see that the restriction of u' to $\mathcal{G}(z) \setminus \{z\}$ makes the algorithm able to decide how to value $u'(z)$ such that the restriction of u' will be DWC on $\mathcal{G}(z)$. This way, if no unsolvable case is encountered, u' will be digitally well-composed on the whole domain $\mathcal{D}'$ as a subset of $\left(\frac{\mathbb{Z}}{2}\right)^n$ at the end of the interpolation.

Definition 36 (I_{sol}). *Let $(\mathbb{Z}^n, \mathcal{D}, \mathbb{R}, u)$ be an image and let be a cubical real-valued interpolation method $\mathcal{I} : \mathbb{Im}(\mathbb{Z}^n, \mathbb{R}) \to \mathbb{Im}(\left(\frac{\mathbb{Z}}{2}\right)^n, \mathbb{R})$ such that we obtain the interpolation $u' = \mathcal{I}(u)$ defined on the domain $\mathcal{D}' = \mathrm{Subd}(\mathcal{D})$. In this case, we define the set $I_{sol}(u', z)$ such that for any $z \in \mathcal{D}' \setminus \mathcal{D}$:*

$$I_{sol}(u', z) \;=\; I_0(u', z) \cap I_{WC}(u', z).$$

The set $I_{sol}(u', z)$ takes into account at the same time the fact that $\mathcal{I}$ must be digitally well-composed in $(\mathbb{Z}/s)^n$, in-between, and ordered.

Theorem 4. *Let $(\mathbb{Z}^n, \mathcal{D}, \mathbb{R}, u)$ be an image and let be a cubical real-valued interpolation method $\mathcal{I} : \mathbb{Im}(\mathbb{Z}^n, \mathbb{R}) \to \mathbb{Im}(\left(\frac{\mathbb{Z}}{2}\right)^n, \mathbb{R})$ such that we obtain the interpolation $u' = \mathcal{I}(u)$ defined on the domain $\mathcal{D}' = \mathrm{Subd}(\mathcal{D})$. In this case, if $\mathcal{I}$ satisfies $(\mathcal{P})$, then we have:*

$$\forall z \in \left(\frac{\mathbb{Z}}{2}\right)^n, u'(z) = \begin{cases} u(z) & \text{if } z \in \mathbb{E}_0, \\ f_k(u\big|_{\mathbb{A}(z)}) \in I_{sol}(u, z) & \text{if } z \in \mathbb{E}_k, k \in [1, n]. \end{cases}$$

Proof: It is the direct consequence of Lemma 7 and Definition 36. □

Notice that, this way, such a local interpolation method $\mathcal{I}$ is ordered, in-between, digitally well-composed, but not necessarily self-dual, and then this numerical scheme is not sufficient to ensure that $\mathcal{I}$ satisfies $(\mathcal{P})$.

Now that we have proven that the set of functions $\{f_1, \ldots, f_n\}$ is characteristic of such interpolations, let us determine them.

4.1.5 Determining f_1

Let us begin with the study of f_1, *i.e.*, the function setting the values at the centers of the subdivided blocks of dimension 1. This function has to be self-dual, symmetrical, and in-between due to $(\mathcal{P})$. We choose one of the most common function satisfying these constraints: the mean operator $f_1 : \mathbb{R}^2 \mapsto \mathbb{R} : (v_1, v_2) \mapsto f_1(v_1, v_2) = (v_1 + v_2)/2$.

Note that we do not prove here that this function is the only possible way to satisfy all these constraints, but it is well-known in the community that other possibilites are not convenient in practice, and that the mean operator, satisfying self-duality, symmetry, and in-betweenness, is the most natural way to interpolate in 1D because it corresponds to a linear interpolation.

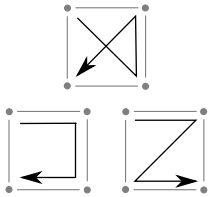

Figure 4.9: The 3 possible configurations in 2D (modulo reflections and rotations).

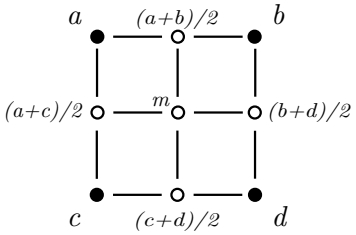

Figure 4.10: $u'\big|_{\mathcal{G}(z)}$ for $z \in \mathbb{E}_2$ for any self-dual local interpolation after the application of f_1 (with m any value $\in \mathbb{R}$).

4.1.6 Equations of f_2

Concerning f_2, *i.e.*, the function which sets the values of u' at the centers of the subdivided blocks of dimension 2, let us compute $I_0(u', z)$ and $I_{WC}(u', z)$ for any given $z \in \mathbb{E}_2$ to deduce $I_{sol}(u', z)$.

However, since their values depend on the configurations of $u\big|_{\mathbb{A}(z)}$, let us examine which configurations are possible in the 2D case. Let us assume that $u\big|_{\mathbb{A}(z)} = \begin{pmatrix} a & b \\ c & d \end{pmatrix}$. Then a total of $4! = 24$ configurations are possible. Modulo 90 degrees rotations, axial symmetries and reflections, it remains only 3 possible configurations: the *α-configurations* which correspond to the relation $a \leq d < b \leq c$, the *U-configurations* which corresponds to $a \leq b \leq d \leq c$, and the *Z-configurations* which corresponds to $a \leq b \leq c \leq d$ (see Figure 4.9).

Proposition 15. *Let $\left(\left(\frac{\mathbb{Z}}{2}\right)^n, \mathcal{D}, \mathbb{R}, u\right)$ be a given real-valued image, and let z be a point in $z \in \mathbb{E}_2 \cap \mathrm{Subd}(\mathcal{D})$. Modulo 90 degrees rotations and symmetries, an α-configuration implies that $u\big|_{\mathbb{A}(z)}$ is not digitally well-composed in $\mathbb{Z}^n$, whereas a U- or Z-configuration implies that $u\big|_{\mathbb{A}(z)}$ is digitally well-composed in $\mathbb{Z}^n$.*

Proof: Let us assume that an image $u : \mathcal{D} \subseteq \mathbb{Z}^n \to \mathbb{R}$ is given. For the given $z \in \mathbb{E}_2 \cap \mathrm{Subd}(\mathcal{D})$, let us denote by $u\big|_{\mathbb{A}(z)} = \begin{pmatrix} a & b \\ c & d \end{pmatrix}$ the restriction of u to the 2D block $\mathbb{A}(z)$ in $\mathbb{Z}^n$. If this restriction corresponds to an α-configuration, that is, $a \leq d < b \leq c$ (next to a 90 degrees rotation or axial

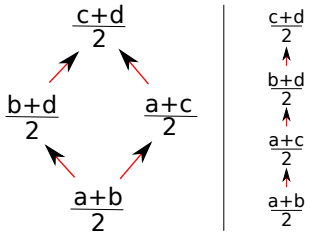

Figure 4.11: The Hasse diagrams for the α- and the U-configurations (left) and for the Z-configuration (right).

symmetry), then clearly $[u \geq b] \cap \mathbb{A}(z)$ is a critical configuration in $\mathbb{Z}^n$ and then the restriction of u to $\mathbb{A}(z)$ is not digitally well-composed in $\mathbb{Z}^n$. If we have an U-configuration, we have $a \leq b \leq d \leq c$ (next to a 90 degrees rotation or axial symmetry) and then $\text{intvl}(a,d) \cap \text{intvl}(b,c) = \text{intvl}(b,d) \neq \emptyset$, and then the restriction of u to $\mathbb{A}(z)$ is digitally well-composed in $\mathbb{Z}^n$. And if we have a Z-configuration, we have $a \leq b \leq c \leq d$ (next to a 90 degrees rotation or axial symmetry), and then $\text{intvl}(a,d) \cap \text{intvl}(b,c) = \text{intvl}(b,c) \neq \emptyset$ and the restriction of u to $\mathbb{A}(z)$ is digitally well-composed in $\mathbb{Z}^n$. □

Theorem 5. *Given an image $u : \mathcal{D} \subseteq \mathbb{Z}^n \to \mathbb{R}$, any cubical real-valued interpolation $\mathcal{I}_{f_1,\ldots,f_n}$ satisfying $(\mathcal{P})$ and such that f_1 is the mean operator is such that $\forall\, z \in \text{Subd}(\mathcal{D}) \cap \mathbb{E}_2$:*

$$\begin{cases} f_2(u|_{\mathbb{A}(z)}) & = \text{med}\{u|_{\mathbb{A}(z)}\} & \text{if } u|_{\mathbb{A}(z)} \text{ is not DWC,} \\ f_2(u|_{\mathbb{A}(z)}) & \in I_0(u,z) & \text{otherwise.} \end{cases}$$

Proof: Let us begin with the computation of $I_0(u',z)$ for $z \in \mathbb{E}_2$. From the values already set in u' on $\mathbb{P}(z) \subseteq \mathbb{E}_1$ by f_1 during the recursive process (see Figure 4.10), we can compute $I_0(u',z)$ using the Hasse diagram of each configuration (see Figure 4.11). Recall that a *Hasse diagram* is a representation of a finite partially ordered sets where greater elements are at a higher position in the diagram. We obtain finally that $I_0(u',z) = \text{intvl}(\frac{a+c}{2}, \frac{b+d}{2})$ for the three configurations, with one remarkable property: the median value of $u|_{\mathbb{A}(z)}$ always belongs to $I_0(u',z)$.

Let us follow with the computation of $I_{WC}(u',z)$, where $u'|_{\mathcal{G}(z)}$ (see Figure 4.10) satisfies the four conditions:

$$\begin{cases} \text{intvl}(a,m) \cap \text{intvl}((a+b)/2,(a+c)/2) & \neq \emptyset, \quad (1) \\ \text{intvl}((a+b)/2,(b+d)/2) \cap \text{intvl}(m,b) & \neq \emptyset, \quad (2) \\ \text{intvl}((a+c)/2,(c+d)/2) \cap \text{intvl}(m,c) & \neq \emptyset, \quad (3) \\ \text{intvl}(m,d) \cap \text{intvl}((c+d)/2,(b+d)/2) & \neq \emptyset. \quad (4) \end{cases}$$

In the case of the α-configuration in $\mathbb{Z}^n$, (2) $\Rightarrow m \leq \frac{b+d}{2}$ and (4) $\Rightarrow m \geq \frac{b+d}{2}$. That implies that $m = \frac{b+d}{2}$, which also satisfies (1) and (3). Consequently, $I_{WC}(u',z) = \{\text{med}\{u\big|_{\mathbb{A}(z)}\}\}$, and because $I_{WC}(u',z) \subseteq I_0(u',z)$, $I_{sol}(u',z) = \{\text{med}\{u\big|_{\mathbb{A}(z)}\}$ in the not digitally well-composed case.

In the cases of the U- and the Z-configurations in $\mathbb{Z}^n$, we obtain that $I_{WC}(u',z) = [\frac{a+b}{2}, \frac{c+d}{2}] \supseteq I_0(u',z)$, so we conclude that $I_{sol}(u',z) = I_0(u',z)$. □

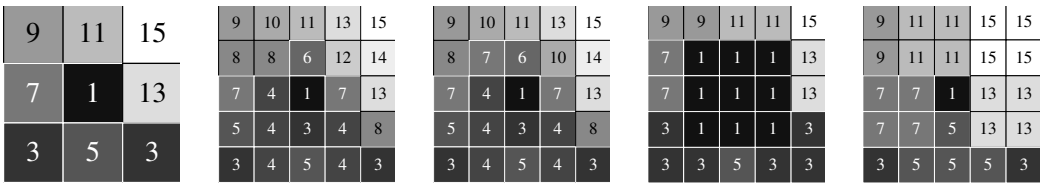

Figure 4.12: An image, and its interpolations using the *median*, the *mean/median*, the *min* and the *max* operators respectively.

Let us remark that all the well-known self-dual interpolations making 2D images well-composed are particular cases of interpolations characterized by the two first interpolation functions f_1 and f_2. They all use the mean operator for f_1. Furthermore, let z be a point in $\mathbb{E}_2$ belonging to the subdivision of the domain of the original image. The *median method* (see Figure 4.12), consists in setting the value $u'(z)$ at $\text{med}\{u\big|_{\mathbb{A}(z)}\}$ (in this case f_2 is an operator and not only a function). The *mean/median method of Latecki* [95] consisting in setting the value $u'(z)$ at $\text{mean}\{u\big|_{\mathbb{A}(z)}\}$ if the restriction of the image to the 2D block is digitally well-composed and to $\text{med}\{u\big|_{\mathbb{A}(z)}\}$ otherwise. And the *min/max method*, consisting in setting the value $u'(z)$ at $\frac{1}{2}(\min\{u\big|_{\mathbb{A}(z)}\} + \max\{u\big|_{\mathbb{A}(z)}\})$ in the digitally well-composed case and to $\text{med}\{u\big|_{\mathbb{A}(z)}\}$ otherwise. Take care not to amalgamate the min method, the max method and the min/max method.

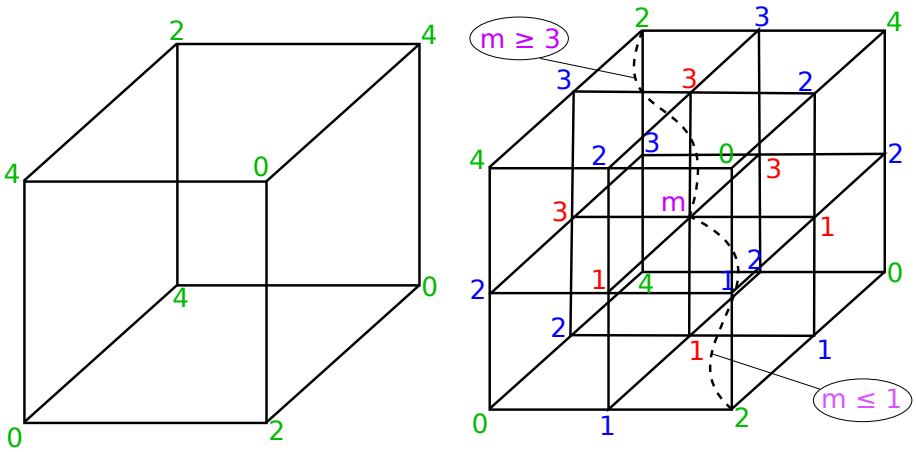

Figure 4.13: A counter-example proving that an interpolation satisfying $(\mathcal{P})$ (with only one subdivision and with f_1 the mean operator) cannot ensure digital well-composedness (the values of u' on $\mathbb{E}_0$ are in green, the ones on $\mathbb{E}_1$ are in blue, the ones on $\mathbb{E}_2$ are in red, and the ones on $\mathbb{E}_3$ are in purple).

4.1.7 Equations of f_3 for local self-dual interpolations

Theorem 6. *No (local) interpolation satisfies $(\mathcal{P})$ for $n \geq 3$ with one subdivision when we choose the mean operator to interpolate in 1D.*

Proof: Let z be the center of the subdivided block of dimension 3 such that we have $u'\big|_{\mathbb{A}(z)}$ as in Figure 4.13: the initial valued 3D block is on the left, its "in-process interpolation" is on the right. We apply the first interpolating function f_1, *i.e.*, we set the values of u' at the centers of the 1D blocks at the mean of the values of the initial block. Then we apply the second interpolating function f_2, which fixes the values of u' at the centers of the subdivided 2D blocks at the median of the values of u' at the initial 2D blocks because u is not digitally well-composed on them. Finally, since we want that u' is digitally well-composed on the 3D blocks in the initial cube, we need to have for any of this block S_3 and for any point $p \in S_3$ and $p' = \mathrm{antag}_{S_3}(p)$:

$$\mathrm{intvl}(u'(p),\, u'(p')) \;\cap\; \mathrm{Span}\{\, u'(p'') \;\big|\; p'' \in S_3 \setminus \{p,\, p'\}\,\} \;\neq\; \emptyset.$$

This results in a set of two equations $m \geq 3$ and $m \leq 1$, where $m \in \mathbb{R}$ is the value of u' at the center of the 3D block, that are impossible to satisfy

simultaneously. Then, no interpolation can satisfy the set of constraints $(\mathcal{P})$ as soons as we reach $n \geq 3$. □

Finally, assuming that an *usual interpolation* is a cubic real-valued interpolation method that starts from an image defined on a bounded hyperectangle in $\mathbb{Z}^n$, such that it satisfies the set of properties $(\mathcal{P})$, and such that its function f_1 is the mean operator, we have shown that no usual local interpolation is able to make digitally well-composed images in 3D (and higher dimensions) in $\left(\frac{\mathbb{Z}}{2}\right)^n$.

4.2 A New Self-dual n-D DWC Interpolation

In Section 3.1, we have seen that it is usual to develop cubical real-valued digitally well-composed interpolation methods $\mathcal{I}$ such that:

$$\begin{cases} \mathcal{I} \text{ is self-dual} & (1) \\ \mathcal{I} \text{ is in-between} & (1) \\ \mathcal{I} \text{ subdivides the domain only once} & (3) \\ \mathcal{I} \text{ has a subdivision factor of 2} & (4) \\ \mathcal{I} \text{ is invariant by translations, } \frac{\pi}{2}\text{'s rotations and axial symmetries} & (5) \\ \mathcal{I} \text{ is ordered} & (6) \\ \mathcal{I} \text{ is local} & (7) \\ \mathcal{I} \text{ uses the mean operator at the centers of edges} & (8) \end{cases}$$

This list of properties is ordered by order of priority. Effectively self-duality is mandatory because it is our main objective: as we have seen, min- and max-interpolations already exist, and they favorize bright components over dark ones or the converse. In-betweeness is important too, because it ensures that we preserve the contours in the image in the sense that we do not create new extrema. The third and fourth constraints are not necessary but they mean that we interpolate the image by adding the minimal number of pixels in the new image (assuming we want a regular grid as output and that we want that the domain of the interpolation does not depend on the input image). The fifth condition means that we want that the result does not depend on a possible translation/rotation/symmetry. The sixth, seventh, eighth conditions are finally of low priority: effectively life is easier when we proceed to an ordered interpolation, because we know in advance the order at which we value the domain of the interpolation, it is more "systematic".

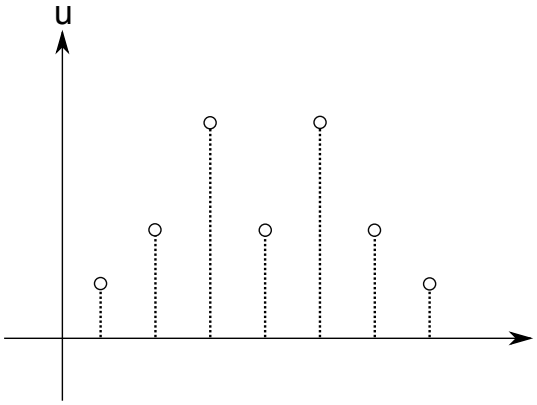

Figure 4.14: The initial image u.

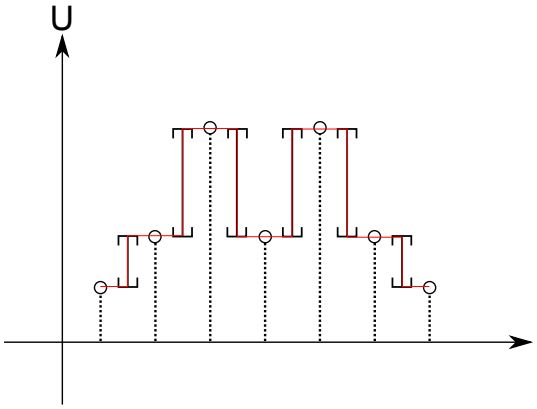

Figure 4.15: The "continuous" interpolation U.

But as we will see, there exists (at least) an interpolation that verifies the constraints (1) to (5) without being ordered, since this interpolation is even not local.

4.2.1 A Front-Popagation Algorithm (FPA)

Effectively, if we consider that orderedness and locality are not so much necessary, we can use a front-propagation algorithm (FPA). More exactly, we proceed in two steps. First we make the input image u depicted on Figure 4.14 "continuous" by adding secondary pixels between the primary pixels; their values are not single values but intervals as depicted on Figure 4.15. We call

this new map the *interval-valued interpolation* U.

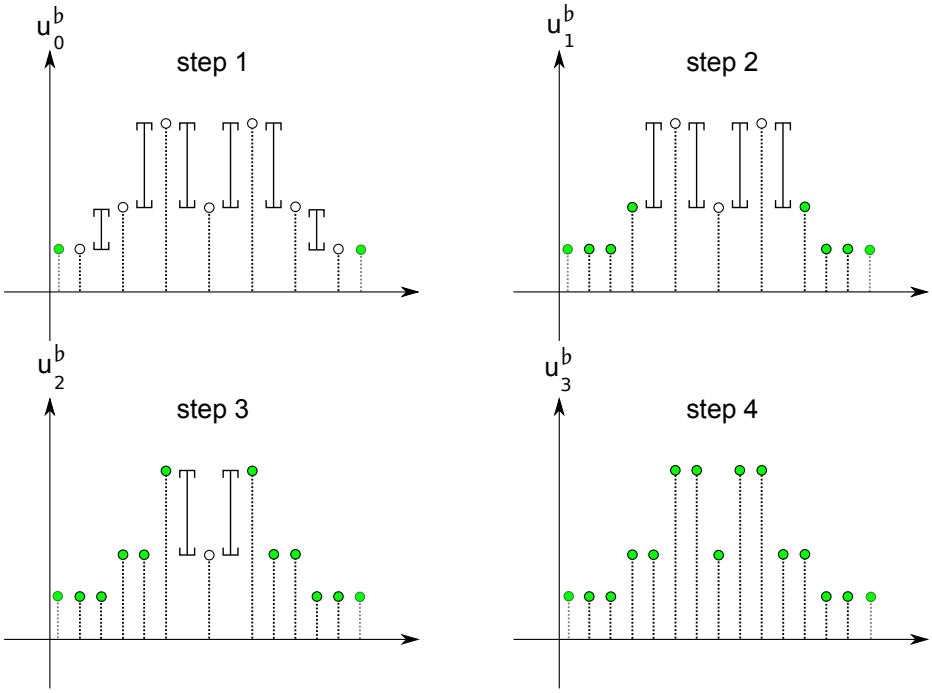

Figure 4.16: Flattening process.

And then, since the new function has some non-zero "thickness", we can use a FPA which flattens this function to make a third map $u^\flat$ which has new topological properties thanks to the "regularization" properties of the FPA in n-D (we call them the *intrinsic properties* of the FPA and we will detail them later).

We depicted the step-by-step process on Figure 4.16 starting from the interval-valued interpolation U: we add a border that we consider as being the initial front (for this reason, we depict it using green points), to ensure that the propagation starts from the contour. Then we propagate the front deeper and deeper in the image until the front, made of the green points, recovers all the domain of U. The new image is called $u^\flat$ because it correspond to U which has been flattened. Then, we remove the temporary border (see Figure 4.17) to obtain an interpolation which is "smoother" than the original image u.

Applying this algorithm in n-D, $n \geq 2$, leads to digitally well-composed

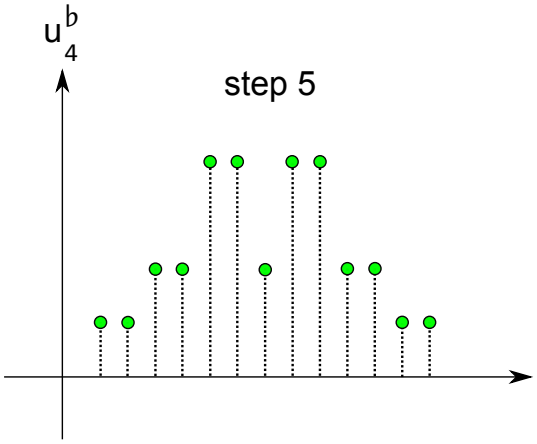

Figure 4.17: The interpolation of u.

images, as we are going to prove in the following subsections.

4.2.2 Origin of the FPA

The front propagation algorithm studied in the next subsection is related to the algorithm proposed in [60, 40], which computes in quasi-linear time the morphological tree of shapes [32] of a nD image. Schematically, the tree of shapes computation algorithm is composed of 4 steps as depicted in Figure 4.18. The input is an integer-valued image u, defined on the nD cubical grid. First an immersion step creates an interval-valued map U, defined on a larger space $\mathcal{K}$. A front propagation step, based on a hierarchical queue, takes U and produces two outputs: an image $u^\flat$ and an array $\mathcal{R}$ containing the elements of $\mathcal{K}$. In this array, the elements are sorted so that the next step, an union-find-based tree computation, produces $\mathcal{T}(u^\flat)$ the tree of shapes of $u^\flat$. Actually $u^\flat\big|_{\mathbb{Z}^n} = u$ and $\mathcal{T}(u^\flat)\big|_{\mathbb{Z}^n} = \mathcal{T}(u)$. The last step, the emersion, removes from $\mathcal{T}(u^\flat)$ all the elements of $\mathcal{K} \setminus \mathbb{Z}^n$, and also performs a canonicalization of the tree. So $\mathcal{T}(u)$, the tree of shapes of u, is obtained [60].

The front propagation step (highlighted in red in the schematic description) acts as a *flattening* of an interval-valued map U into a function $u^\flat$, because we have $\forall\, z,\ \ u^\flat(z) \in U(z)$ [60]. In the following, we will denote by $\mathfrak{FP}$ both the front propagation algorithm (the part highlighted in red in Figure 4.18) and the mathematical operator $\mathfrak{FP} : U \mapsto u^\flat$.

Last, let us give two important remarks. **1.** We are going to reuse the

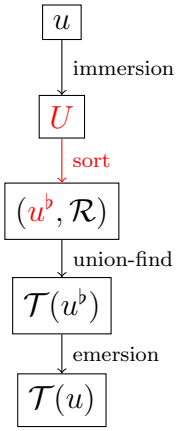

Figure 4.18: Computation of the tree of shapes.

front propagation algorithm $\mathfrak{FP}$, yet in a *very different* way than it is used in the tree of shapes computation algorithm. Indeed, its input U will be different (both the structure and the values of U will be different), and its purpose also will be different (flattening versus sorting). **2.** Actually, the front propagation algorithm is *just a part* of the solution that we present to make nD functions digitally well-composed.

4.2.3 An explanation of the FPA

Let us now explain shortly the $\mathfrak{FP}$ algorithm, which is recalled in Algorithm 3. The basic procedures used to handle the hierarchical queue are recalled in Algorithm 2 . The reader can also refer to [60] for the original version. This algorithm uses a classical front propagation on the definition domain of U. This propagation is based on a hierarchical queue, denoted by Q and the current (queue) level is denoted by ℓ. There are two notable differences with the well-known hierarchical-queue-based propagation. First the values of U are interval-valued so we have to decide at which (single-valued) level to enqueue the domain points. The solution is to enqueue a point h at the value of the interval $U(h)$ that is the closest to ℓ (see the procedure PRIORITY_PUSH). The image $u^\flat$ actually stores the *enqueuing level* of the points. Second, when the queue at the current level, $Q[\ell]$, is empty (and when the hierarchical queue Q is not yet empty), we shall decide what is the next current level. We have the choice of taking the next level, either less or greater than ℓ, such that the queue at that level is not empty (see the

Algorithm 2: Handling of an hierarchical is ensured thanks to PRIORITY_PUSHand PRIORITY_POP.

```
PRIORITY_PUSH(Q, h, U, ℓ)
/* modifies Q */
begin
    [lower, upper] ← U(h)
    if lower > ℓ then
        ℓ' ← lower
    else if upper < ℓ then
        ℓ' ← upper
    else
        ℓ' ← ℓ
    PUSH(Q[ℓ'], h)

PRIORITY_POP(Q, ℓ) : H
/* modifies Q, and sometimes ℓ */
begin
    if Q[ℓ] is empty then
        ℓ' ← level next to ℓ such as Q[ℓ'] is not empty
        ℓ ← ℓ'
    return POP(Q[ℓ])
```

procedure PRIORITY_POP). Practically, choosing going up or down the levels does not change the resulting image $u^\flat$. The neighborhood $\mathcal{N}_{2n}$ used by the propagation corresponds to the $2n$-connectivity into $(\mathbb{Z}/s)^n$.

Like in [60], the initialization of the front propagation relies on the definition of a point, p_∞ (first point enqueued), and of a value $\ell_\infty \in U(p_\infty)$, which is the initial value of the current level ℓ. Similarly to the case of the tree of shapes computation, p_∞ is taken in the outer boundary of the definition domain of U. The initial level ℓ_∞ is set at the median value of the points belonging to the inner boundary of the definition domain of U; more precisely, when the interval-valued U is constructed from an integer-valued function u, ℓ_∞ is computed from the values of the inner boundary of u. Using the median operator ensures that ℓ_∞ is set in a self-dual way: schematically $\ell_\infty(-u) = -\ell_\infty(u)$. An example is given later in Section 4.2.4.

Algorithm 3: Computation of the function $u^\flat$ from an interval-valued map U defined on $(\mathbb{Z}/s)^n$.

```
𝔉𝔓(U) : Image ;
/* computes u^♭ */;
begin
    for all h do
        deja_vu(h) ← false;
    PUSH(Q[ℓ_∞], p_∞);
    deja_vu(p_∞) ← true;
    ℓ ← ℓ_∞   /* start from root level */ ;
    while Q is not empty do
        h ← PRIORITY_POP(Q, ℓ);
        u^♭(h) ← ℓ;
        for all n ∈ 𝒩_2n(h, (ℤ/s)^n) such as deja_vu(n) = false do
            PRIORITY_PUSH(Q, n, U, ℓ);
            deja_vu(n) ← true;
    return u^♭
```

4.2.4 An illustration of the FPA

Let us now illustrate this algorithm on a simple run, depicted in Figure 4.19. The initial interval-valued image U is displayed in (i). A square filled in gray indicates the points that have already been processed in previous iterations. A circle filled in orange indicates the point h being processed, and the value displayed in the circle is the current level ℓ; it means that we have just executed the line "$u^\flat(h) \leftarrow \ell$" of the algorithm. A dashed circle filled in green, say at a point p, indicates that this point is in the hierarchical queue Q; the value displayed in this circle, say v, is the queue level of this point, i.e., we have $p \in Q[v]$. When no symbol is displayed at a point, it means that this point is not yet processed and is not in Q; we then depict its value in U.

The input interval-valued image U is shown in (i). In the following, the point coordinates are (*row*, *column*); for instance we have $U(2,1) = U(2,3) = [4,5]$.

The initialization step is depicted by (ii). We assume that we have $p_\infty = (1,1)$ and $\ell_\infty = 2$. The initialization thus adds p_∞ in $Q[2]$, and sets $\ell \leftarrow \ell_\infty$,

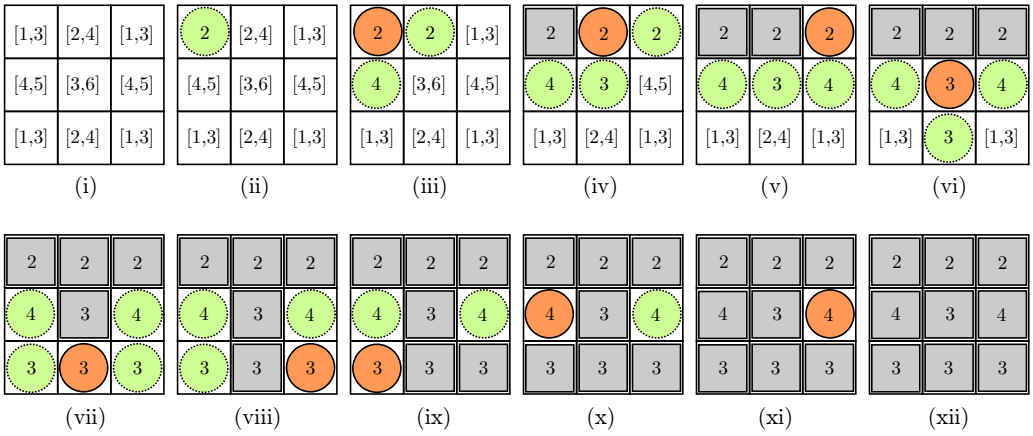

Figure 4.19: The front propagation algorithm applied on a digitally well-composed interval-valued image U.

so the current level ℓ is 2.

The first iteration of the 'while' loop is depicted by (iii). It pops the point $h = (1, 1)$, and performs the assignment $u^\flat(h) \leftarrow \ell$, precisely $u^\flat(1, 1) \leftarrow 2$. It then pushes its neighboring points $(1, 2)$ and $(2, 1)$ into Q, respectively with level **2** and **4**. Indeed, we have $U(1, 2) = [\mathbf{2}, 4]$ and $U(2, 1) = [\mathbf{4}, 5]$ so PRIORITY_PUSH respectively chooses in these intervals the levels that are the closest to the current level $\ell = 2$.

The second iteration is depicted by (iv). Since the queue $Q[\ell]$ is not empty, the current level does not change, and the point $h = (1, 2)$ is popped. $u^\flat(h) \leftarrow \ell$ is performed; precisely $u^\flat((1, 2)) \leftarrow 2$. Then the points $(1, 3)$ and $(2, 2)$ are pushed respectively in $Q[\mathbf{2}]$ and $Q[\mathbf{3}]$ since $\ell = 2$, $U(1, 3) = [1, 3] = \{1, \mathbf{2}, 3\}$, and $U(2, 2) = [\mathbf{3}, 6]$.

The third iteration is depicted by (v), popping $(1, 3)$ from $Q[2]$ (the current level does not change), and pushing $(2, 3)$ in $Q[\mathbf{4}]$ since $U(2, 3) = [\mathbf{4}, 5]$.

For the fourth iteration, depicted by (vi), the current level is $\ell = 2$, and the queue corresponding to the current level, namely $Q[\mathbf{2}]$, is empty. Indeed, the hierarchical queue is only composed of $Q[\mathbf{3}] \cup Q[4]$; the four points depicted with circles in (vi) only contains the values 3 and 4. The procedure PRIORITY_POP thus changes the current level to the closest level whose queue is not empty, so $\ell \leftarrow 3$. The point $h = (2, 2)$ is then popped from $Q[3]$, the assignment $u^\flat(2, 2) \leftarrow 3$ is performed, and the neighbor point $(3, 2)$ of h is

pushed in $Q[\mathbf{3}]$ since $U(3,2) = [2,4] = \{2, \mathbf{3}, 4\}$.

The following iterations, depicted by the sub-figures (vii) to (xi), lead to the final integer-valued image $u^\flat$, depicted by (xii). This resulting image is such as:

$$\forall\ z \in \mathcal{D},\ \ u^\flat(z) \in U(z).$$

This front propagation algorithm thus flattens an interval-valued map U into the integer-valued image $u^\flat = \mathfrak{FP}(U)$.

4.2.5 Intrinsic continuity properties of the FPA

Two main continuity properties of the FPA are of major interest for the sequel. Both properties relate the values of the flattened image $u^\flat$ at two pixels p and q of the domain $\mathcal{D}' \subset (\mathbb{Z}/s)^n$ of U which are neighbors in $(\mathbb{Z}/s)^n$ depending on the values $U(p)$ and $U(q)$. We say that these properties are *intrinsic* in the sense that they are a direct result of the internal functioning of the algorithm. But let us introduce first some additional notations concerning the FPA.

We define $\ell : \mathcal{D}' \to \mathbb{R}$ as the real-valued *map of levels*: for a given point $z \in \mathcal{D}'$, $\ell(z) \in \mathbb{R}$ is the value of ℓ when we enqueue z into the hierarchical queue Q during the front propagation. Note that it is different from the "enqueuing level" ℓ' presented just before in the algorithm. Also, we define the *enqueuing time map* $t : \mathcal{D}' \to \mathbb{N}$ such that, for any point $z \in \mathcal{D}'$, $t(z)$ is the time at which the point z has been enqueued into Q during the front propagation. We say that a position $p \in \mathcal{D}'$ is being *processed* while the current position h is equal to p. Obviously, for any $p \in \mathcal{D}'$, we use the notation $u^\flat(p)$ assuming that this pixel has been valued yet by the front propagation algorithm (we recall that each pixel of $u^\flat$ is valued only once).

Now let us begin with a preliminary lemma which correlates the values of the initial interval-valued image U, the interpolation $u^\flat$ and the map of levels $\ell : \mathcal{D}' \to \mathbb{R}$. This lemma will be necessary to prove the first main intrinsic continuity property detailed after.

Lemma 8. *Let $U : \mathcal{D}' \subseteq (\mathbb{Z}/s)^n \rightsquigarrow \mathbb{R}$ be an nD interval-valued map, and let $u^\flat = \mathfrak{FP}(U) : \mathcal{D}' \to \mathbb{R}$ be the real-valued function resulting from the front*

propagation algorithm applied on U. Now, let r be a point of $\mathcal{D}'$, we can observe the two following implications:

$$\begin{cases} u^\flat(r) < \lceil U \rceil(r) \Rightarrow \ell(r) \leq u^\flat(r) & (1) \\ \\ u^\flat(r) > \lfloor U \rfloor(r) \Rightarrow \ell(r) \geq u^\flat(r) & (2) \end{cases}$$

Proof: By a case-by-case study, we can establish a correlation between $\ell(r)$ and $u^\flat(r)$ for any given point $r \in \mathcal{D}'$. The possible cases are $\ell(r) < \lfloor U \rfloor(r)$ (1), $\ell(r) \in U(r)$ (2), and $\ell(r) > \lceil U \rceil(r)$ (3):

1. we obtain that $\ell(r) < u^\flat(r)$ because $u^\flat(r) \in U(r)$, and at the same time, $u^\flat(r)$ is equal to $\lfloor U \rfloor(r)$ because it is the nearest value to $\ell(r)$ in $U(r)$.

2. we obtain that $u^\flat(r) = \ell(r)$ because the nearest value to $\ell(r)$ in $U(r)$ is $\ell(r)$ itself, and at the same time we obtain simply the initial property $u^\flat(r) \in U(r)$ (no additionnal assumption is possible).

3. we obtain that $\ell(r) > u^\flat(r)$ because $u^\flat(r) \in U(r)$, and at the same time $u^\flat(r) = \lceil U \rceil(r)$ because this is the nearest value to $\ell(r)$ into $U(r)$.

Finally, we obtain this table:

Case	Relation 1	Relation 2
$(1) : \ell(r) < \lfloor U \rfloor(r)$	$\ell(r) < u^\flat(r)$	$u^\flat(r) = \lfloor U \rfloor(r)$
$(2) : \ell(r) \in U(r)$	$\ell(r) = u^\flat(r)$	$u^\flat(r) \in U(r)$
$(3) : \ell(r) > \lceil U \rceil(r)$	$\ell(r) > u^\flat(r)$	$u^\flat(r) = \lceil U \rceil(r)$

Then we can observe that if $u^\flat(r) < \lceil U \rceil(r)$, that is, if $u^\flat(r) \neq \lceil U \rceil(r)$, we are then either in the case (1) or in the case (2) and then we obtain that $\ell(r) \leq u^\flat(r)$.

Conversely, if $u^\flat(r) > \lfloor U \rfloor(r)$, that is, if $u^\flat(r) \neq \lfloor U \rfloor(r)$, we are then either in the case (2) or in the case (3) and then we obtain that $\ell(r) \geq u^\flat(r)$. □

There follows the first intrinsic property of the FPA, which is also the key to understand why a digitally well-composed interval-valued image results in a digitally well-composed single-valued image.

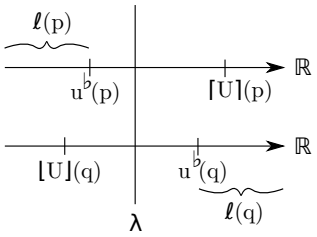

Figure 4.20: A situation impossible to obtain with $p, q \in \mathcal{D}$ being $2n$-neighbors in $(\mathbb{Z}/s)^n$.

Lemma 9. *Let $U : \mathcal{D}' \subseteq (\mathbb{Z}/s)^n \rightsquigarrow \mathbb{R}$ be an nD interval-valued map, and let $u^\flat = \mathfrak{FP}(U) : \mathcal{D}' \to \mathbb{R}$ be the real-valued function resulting from the front propagation algorithm applied on U. Let $p, q \in \mathcal{D}'$ be two $2n$-neighbors in $(\mathbb{Z}/s)^n$ and $\lambda \in \mathbb{R}$. Then, it is impossible to get the following set of properties together:*

$$\begin{cases} u^\flat(p) & \leq & \lambda, & (\mathcal{H}1) \\ \lceil U \rceil(p) & > & \lambda, & (\mathcal{H}2) \\ u^\flat(q) & > & \lambda, & (\mathcal{H}3) \\ \lfloor U \rfloor(q) & \leq & \lambda. & (\mathcal{H}4) \end{cases}$$

Now, let p, q be two $2n$-neighbors in $\mathcal{D}'$ and let us assume that there exists a value $\lambda \in \mathbb{R}$ verifying $(\mathcal{H}1)$, $(\mathcal{H}2)$, $(\mathcal{H}3)$ and $(\mathcal{H}4)$.

We can observe easily thanks to $(\mathcal{H}1)$ and $(\mathcal{H}2)$ that $u^\flat(p) < \lceil U \rceil(p)$ and then by Lemma 8, we obtain:

$$\ell(p) \leq u^\flat(p) \quad (\mathcal{H}5).$$

Also, thanks to $(\mathcal{H}3)$ and $(\mathcal{H}4)$, we obtain $u^\flat(q) > \lfloor U \rfloor(q)$ and using Lemma 8, this results in:

$$\ell(q) \geq u^\flat(q) \quad (\mathcal{H}6).$$

Taking into consideration the two $2n$-neighbors p and q, we have 4 possible scenarii as depicted on Figure 4.21:

1. either p is enqueued before q, then two subcases are possible:
   (a) either q is enqueued when p is the current position,
   (b) or q is enqueued before p is the current position.

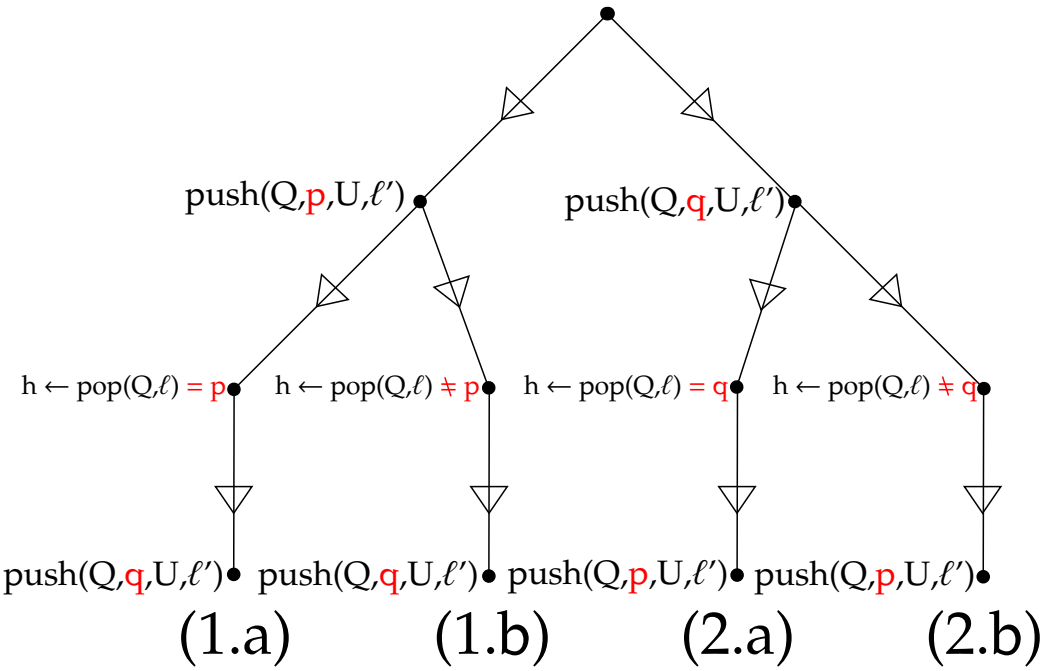

Figure 4.21: The 4 possible scenarii when only two $2n$-neighbors p and q in $\mathcal{D}'$ are considered.

2. either q is enqueued before p, then two subcases are possible:

   (a) either p is enqueued when q is the current position,

   (b) or p is enqueued before q is the current position.

Let us notice that since p and q are $2n$-neighbors, q cannot been enqueued after p is the current position, and similarly p cannot been enqueued after q is the current position (all the $2n$-neighbors of the current position will have been enqueued when it has been processed).

Now let us show that whatever the scenario we choose, we always obtain a contradiction.

$(1.a)$: p is enqueued before q, and then q is enqueued when p is the current position. It means that $\ell(q) = u^\flat(p)$. However, we have seen that $u^\flat(p) \leq \lambda$ by $(\mathcal{H}1)$, and that $\ell(q) \geq u^\flat(q) > \lambda$ by $(\mathcal{H}6)$ and $(\mathcal{H}3)$. This leads to a contradiction.

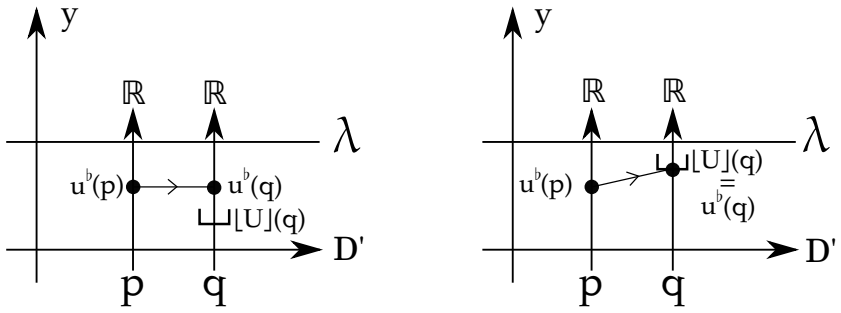

Figure 4.22: Different cases corresponding to Scenario $(1a)$: $u^\flat(p) > \lfloor U \rfloor(q)$ on the left and $u^\flat(p) \leq \lfloor U \rfloor(q)$ on the right. Thanks to $\ell(q) = u^\flat(p)$, $u^\flat(q)$ stays inferior to λ like $u^\flat(p)$.

$(1.b)$: p is enqueued before q, and q is enqueued before the current position is set at p. This way, since the current level ℓ at $t(p)$ is equal to $\ell(p) \leq u^\flat(p)$, it is equal to $\ell(q) \leq u^\flat(p)$ at $t(q)$ (no jump of the non-empty queue level $Q[u^\flat(p)]$ is allowed by the algorithm). This means by $(\mathcal{H}1)$ that $\ell(q) \leq \lambda$. However, by $(\mathcal{H}6)$ and $(\mathcal{H}3)$, $\ell(q) > \lambda$. This leads to a contradiction.

$(2.a)$ is the symmetrical case of $(1.a)$ and $(2.b)$ is the one of $(1.b)$ and then they lead also to contradictions.

The conclusion is that whatever the scenario (and one of these scenarii happens during the computation of the interpolation), the combination of hypotheses $(\mathcal{H}1)$, $(\mathcal{H}2)$, $(\mathcal{H}3)$ and $(\mathcal{H}4)$ leads only to a contradiction. These hypotheses are then incompatible.

□

Since this Lemma can be a little difficult, let us expose an intuitive explanation of this incompatibility by a scenario-by-scenario study.

In Scenario $(1.a)$, p is enqueued at the level $u^\flat(p)$ and at its pop, while the current position is p, the algorithm enqueues q into Q such that $\ell(q) = u^\flat(p)$. This way, by $(\mathcal{H}1)$ $(u^\flat(p) \leq \lambda)$ and $(\mathcal{H}4)$ $(\lfloor U \rfloor(q) \leq \lambda)$, we obtain that $u^\flat(q) \leq \lambda$ (see Figure 4.22), contradicting $(\mathcal{H}3)$.

In Scenario $(1.b)$, q is enqueued after p and before p is the current position. This way, there exists a third point $h \in \mathcal{D}'$ such that $\ell(q) = u^\flat(h) \leq \lambda$ thanks to $(\mathcal{H}1)$ and $(\mathcal{H}2)$ (see the proof above), and then using $(\mathcal{H}4)$ $(\lfloor U \rfloor(q) \leq \lambda)$, we obtain that $u^\flat(q) \leq \lambda$ (see Figure 4.23), contradicting $(\mathcal{H}3)$.

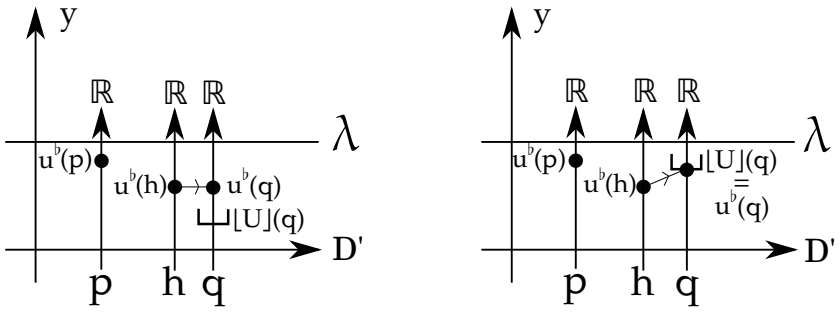

Figure 4.23: Different cases corresponding to Scenario (1*b*): $u^\flat(h) > \lfloor U \rfloor(q)$ on the left and $u^\flat(h) \leq \lfloor U \rfloor(q)$ on the right. Thanks to the enqueuing of p into Q at the level $u^\flat(p) \leq \lambda$, $\ell(q) = u^\flat(h)$ is inferior to λ and then $u^\flat(q)$ stays inferior to λ too.

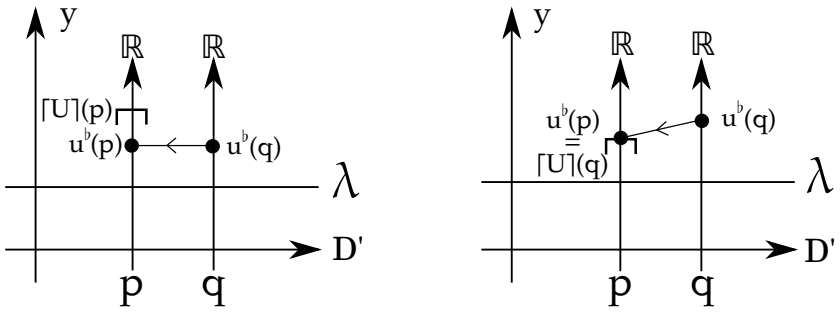

Figure 4.24: Different cases corresponding to Scenario (2*a*): $u^\flat(q) < \lceil U \rceil(p)$ on the left and $u^\flat(q) \geq \lceil U \rceil(p)$ on the right. Thanks to $lcur(p) = u^\flat(q)$, $u^\flat(p)$ stays superior to λ like $u^\flat(q)$.

In Scenario (2.*a*), q is enqueued at the level $u^\flat(q)$ and at its pop, while the current position is q, the algorithm enqueues p into Q such that $\ell(p) = u^\flat(q)$. This way by $(\mathcal{H}3)$ $(u^\flat(q) > \lambda)$ and $(\mathcal{H}2)$ $(\lceil U \rceil(p) > \lambda)$, we obtain that $u^\flat(p) > \lambda$ (see Figure 4.24), contradicting $(\mathcal{H}1)$.

In Scenario (2.*b*), p is enqueued after q and before q is the current position. This way, there exists a third point $h \in \mathcal{D}'$ such that $\ell(p) = u^\flat(h) > \lambda$ thanks to $(\mathcal{H}3)$ and $(\mathcal{H}4)$ (see the proof above), and then using $(\mathcal{H}2)$ $(\lceil U \rceil(p) > \lambda)$, we obtain that $u^\flat(p) > \lambda$ (see Figure 4.25), contradicting $(\mathcal{H}1)$.

Finally, whatever the chosen scenario, the values $u^\flat(p)$ and $u^\flat(q)$ are always on the same side of the line $\{y = \lambda\}$ (either both above, or both below). That is what we call *the first (intrinsic) property of continuity of the FPA.*.

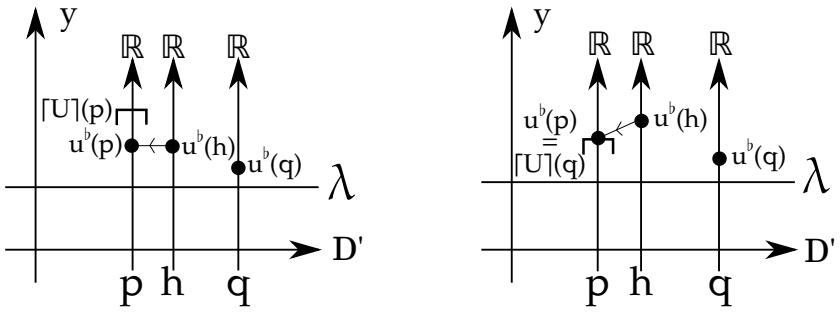

Figure 4.25: Different cases corresponding to Scenario (2*b*): $u^\flat(h) < \lceil U \rceil(p)$ on the left and $u^\flat(h) \geq \lceil U \rceil(p)$ on the right. Thanks to the enqueuing of q into Q at the level $u^\flat(q) > \lambda$, $\ell(p) = u^\flat(h)$ is greater than λ and then $u^\flat(p)$ stays greater than λ too.

Now, let us expose the secund intrinsic continuity property of the FPA that we will use later to prove that the interpolation method used in this thesis is *in-between*.

Lemma 10. *Let $U : \mathcal{D}' \subseteq (\mathbb{Z}/s)^n \rightsquigarrow \mathbb{R}$ be an nD interval-valued map, and let $u^\flat = \mathfrak{FP}(U) : \mathcal{D}' \to \mathbb{R}$ be the real-valued function resulting from the front propagation algorithm applied on U. Now, let $a, m \in \mathcal{D}'$ be $2n$-neighbours in $(\mathbb{Z}/s)^n$ such that $U(a) \subseteq U(m)$. Then $u^\flat(m) < u^\flat(a)$ implies that $u^\flat(a) = \lfloor U \rfloor(a)$ and $u^\flat(m) > u^\flat(a)$ implies that $u^\flat(a) = \lceil U \rceil(a)$.*

Proof: Let us begin with the case $t(a) < t(m)$, that is, a has been enqueued before m. Three cases are possible.

The first subcase corresponds to $\ell(a) > \lceil U \rceil(a)$. Then $u^\flat(a) = \lceil U \rceil(a)$, $Q[u^\flat(a)] \supseteq \{a\}$ at $t = t(a)$, and the current level ℓ remains greater than or equal to $u^\flat(a)$ until a has been processed, because no jump of non-empty queue level is allowed. Since m is enqueued after a (by hypothesis) and at the latest during the processing of a (because a and m are $2n$-neighbors), $\ell(m) \geq u^\flat(a)$. Since $\lceil U \rceil(m) \geq \lceil U \rceil(a) \geq u^\flat(a)$, we obtain finally the relation $u^\flat(m) \geq u^\flat(a)$ (Case 1.1).

The second subcase corresponds to $\ell(a) \in U(a)$. In this subcase, $u^\flat(a) = \ell(a)$, $Q[u^\flat(a)] \supseteq \{a\}$ at time $t = t(a)$, and the current level ℓ stays at the value $u^\flat(a)$ until a is processed (at least). Since a and m are $2n$-neighbors, and since m is enqueued after a, m is enqueued after $t(a)$ and at the latest

while a is processed. This way, $\ell(m) = u^\flat(a)$ and then $u^\flat(m) = u^\flat(a)$ since $U(a) \subseteq U(m)$ (Case 1.2).

The third subcase corresponds to $\ell(a) < \lfloor U \rfloor(a)$. We reason by symmetry and we obtain that $u^\flat(a) = \lfloor U \rfloor(a)$ and $u^\flat(m) \leq u^\flat(a)$ (Case 1.3).

Let us follow with the case $t(a) > t(m)$. Then five subcases are possible.

If $\ell(m) > \lceil U \rceil(m)$, then $u^\flat(m) = \lceil U \rceil(m)$, $Q[u^\flat(m)] \supseteq \{m\}$ at $t = t(m)$, and the current level ℓ remains greater than or equal to $u^\flat(m)$ until m has been processed, because no jump of non-empty queue level is allowed. Since a is enqueued after m (by hypothesis) and at the latest during the processing of m (because a and m are $2n$-neighbors), $\ell(a) \geq u^\flat(m)$. Then two subcases are possible: either $\lceil U \rceil(m) > \lceil U \rceil(a)$ and $u^\flat(a) = \lceil U \rceil(a) < u^\flat(m)$ (Case 2.1.a), or $\lceil U \rceil(m) = \lceil U \rceil(a)$ and $u^\flat(a) = \lceil U \rceil(a) = u^\flat(m)$ (Case 2.1.b).

If $\ell(m) \in]\lceil U \rceil(a), \lceil U \rceil(m)]$, assuming that $\lceil U \rceil(a) < \lceil U \rceil(m)$, $u^\flat(m) = \ell(m)$, $Q[u^\flat(m)] \supseteq \{m\}$ at $t = t(m)$, and the current level ℓ stays at the value $u^\flat(m)$ until m is processed (at least). Since a and m are $2n$-neighbors, and since a is enqueued after m, a is enqueued after $t(m)$ and at the latest while m is processed. This way, $\ell(a) = u^\flat(m)$, and then $u^\flat(a) = \lceil U \rceil(a) < u^\flat(m)$ (Case 2.2).

If $\ell(m) \in U(a)$, $u^\flat(m) = \ell(m)$ (since $U(a) \subseteq U(m)$) and $Q[u^\flat(m)] \supseteq \{m\}$ at $t = t(m)$. Then the current level ℓ stays at the value $u^\flat(m)$ until m is processed (at least). Since a and m are $2n$-neighbors, and since a is enqueued after m, a is enqueued after $t(m)$ and at the latest while m is processed. This way, $\ell(a) = u^\flat(a)$ and then $u^\flat(a) = u^\flat(m)$ (Case 2.3).

If $\ell(m) \in [\lfloor U \rfloor(m), \lfloor U \rfloor(a)[$ (assuming that $\lfloor U \rfloor(m) < \lfloor U \rfloor(a)$), we reason by symmetry and we obtain that $u^\flat(a) = \lfloor U \rfloor(a) > u^\flat(m)$ (Case 2.4).

If $\ell(m) < \lfloor U \rfloor(m)$, we reason again by symmetry and we obtain that either $\lfloor U \rfloor(m) < \lfloor U \rfloor(a)$ and $u^\flat(a) = \lfloor U \rfloor(a) > u^\flat(m)$ (Case 2.5a), or $\lfloor U \rfloor(m) = \lfloor U \rfloor(a)$ and $u^\flat(a) = \lfloor U \rfloor(a) = u^\flat(m)$ (Case 2.5b).

Let us summarize the different cases:

Case	Relation 1	Relation 2	Relation 3
(1.1)	$t(a) < t(m)$	$u^\flat(a) = \lceil U \rceil(a)$	$u^\flat(m) \geq u^\flat(a)$
(1.2)	$t(a) < t(m)$	$u^\flat(a) \in U(a)$	$u^\flat(m) = u^\flat(a)$
(1.3)	$t(a) < t(m)$	$u^\flat(a) = \lfloor U \rfloor(a)$	$u^\flat(m) \leq u^\flat(a)$
(2.1.a)	$t(m) < t(a)$	$u^\flat(a) = \lceil U \rceil(a)$	$u^\flat(m) > u^\flat(a)$
(2.1.b)	$t(m) < t(a)$	$u^\flat(a) = \lceil U \rceil(a)$	$u^\flat(m) = u^\flat(a)$
(2.2)	$t(m) < t(a)$	$u^\flat(a) = \lceil U \rceil(a)$	$u^\flat(m) > u^\flat(a)$
(2.3)	$t(m) < t(a)$	$u^\flat(a) \in U(a)$	$u^\flat(m) = u^\flat(a)$
(2.4)	$t(m) < t(a)$	$u^\flat(a) = \lfloor U \rfloor(a)$	$u^\flat(m) < u^\flat(a)$
(2.5.a)	$t(m) < t(a)$	$u^\flat(a) = \lfloor U \rfloor(a)$	$u^\flat(m) < u^\flat(a)$
(2.5.b)	$t(m) < t(a)$	$u^\flat(a) = \lfloor U \rfloor(a)$	$u^\flat(m) = u^\flat(a)$

We obtain finally that $u^\flat(a) < u^\flat(m)$ implies that we are in Case 1.1, 2.1.a, or 2.2 and then $u^\flat(a) = \lceil U \rceil(a)$, and that $u^\flat(a) > u^\flat(m)$ implies that we are in Case 1.3, 2.4, or 2.5.a, and then $u^\flat(a) = \lfloor U \rfloor(a)$. This concludes the proof. □

4.2.6 Fundamental properties of the FPA

Thanks to Lemma 9, the FPA presents a very strong property: if the input image U is a digitally well-composed interval-valued image, the output image $u^\flat = \mathfrak{FP}(U)$ is digitally well-composed, whatever the chosen value ℓ_∞ at which is set the inner boundary of the definition domain of U before the front propagation. This result can be observed on Figure 4.19.

Theorem 7 ($\mathfrak{FP}(U)$ is DWC if U is DWC)**.** *If the nD interval-valued map $U : \mathcal{D}' \subset \left(\frac{\mathbb{Z}}{2}\right)^n \rightsquigarrow \mathbb{R}$, defined on a bounded hyperrectangle $\mathcal{D}'$, is digitally well-composed, the resulting nD function $u^\flat = \mathfrak{FP}(U)$ is digitally well-composed.*

Let us assume that $u^\flat$ is not digitally well-composed. Then, there exists some $\lambda \in \mathbb{R}$ such that $[u^\flat \geq \lambda]$ contains a critical configuration of primary or secondary type. Let us begin with the primary case.

If $[u^\flat \geq \lambda]$ contains a critical configuration of primary type, that means that there exists some block $S \subseteq \mathcal{D}'$ of dimension k (with $2 \leq k \leq n$) such that $[u^\flat \geq \lambda] \cap S = \{p, p'\}$ where p and p' are two antagonists in S. In

other words, we have:

$$\begin{cases} u^\flat(p) & \geq & \lambda \\ u^\flat(p') & \geq & \lambda \\ u^\flat(p'') & < & \lambda,\ \forall\, p'' \in S \setminus \{p,\, p'\}. \end{cases}$$

We know that $u^\flat(p'') < \lambda$ implies that $\lfloor U \rfloor(p'') < \lambda,\ \forall\, p'' \in S \setminus \{p, p'\}$. This way, we obtain the following relation:

$$\max\{\, \lfloor U \rfloor(p'') \;\big|\; p'' \in S \setminus \{p, p'\}\,\} \;<\; \lambda.$$

Moreover, $\lfloor U \rfloor$ is digitally well-composed (since U is digitally well-composed). The characterization of a digitally well-composed single-valued function implies that $\mathrm{intvl}(\lfloor U \rfloor(p), \lfloor U \rfloor(p'))$ intersects $\mathrm{Span}\{\lfloor U \rfloor(p'') \;\big|\; p'' \in S \setminus \{p, p'\}\}$, so there exists some $p_* \in \{p, p'\}$ such that:

$$\lfloor U \rfloor(p_*) < \lambda.$$

Also, we have:

$$\begin{cases} \lceil U \rceil(p_*) \geq \lambda, \\ \lceil U \rceil(\mathrm{antag}_S(p_*)) \geq \lambda. \end{cases}$$

This means that these two antagonists in S belong to the set $[\lceil U \rceil \geq \lambda]$ which is digitally well-composed. Then, there exists a $2n$-path connecting them into $[\lceil U \rceil \geq \lambda] \cap S$. Consequently, there exists some point $p'_* \in \mathcal{N}_{2n}(p_*) \cap S$ such that:

$$\lceil U \rceil(p'_*) \geq \lambda.$$

We thus end up with the four properties: $u^\flat(p_*) \geq \lambda$, $\lfloor U \rfloor(p_*) < \lambda$, $u^\flat(p'_*) < \lambda$, and $\lceil U \rceil(p'_*) \geq \lambda$ with p_*, p'_* $2n$-neighbors in $\mathcal{D}'$ (see Figure 4.26). Thanks to Lemma 9, we obtain a contradiction.

For the secondary case, the hypothesis such as $[u^\flat \geq \lambda]$ contains a secondary critical configuration is equivalent to have $[u^\flat < \lambda]$ containing a primary critical configuration. With a symmetrical reasoning, we obtain that $u^\flat(p_*) < \lambda$, $\lceil U \rceil(p_*) \geq \lambda$, $u^\flat(p'_*) \geq \lambda$, and $\lfloor U \rfloor(p'_*) < \lambda$, which is impossible too.

□

Since we are much interested in self-duality, there is another fundamental property of our algorihm.

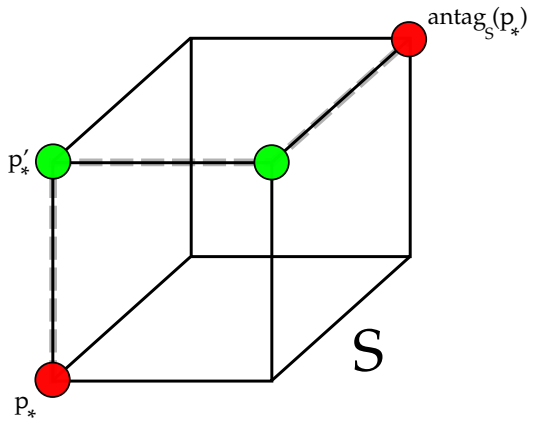

Figure 4.26: Assuming U is digitally well-composed and $u^\flat$ is not digitally well-composed, we obtain the four properties: $u^\flat(p_*) \geq \lambda$, $\lfloor U \rfloor(p_*) < \lambda$, $u^\flat(p'_*) < \lambda$, and $\lceil U \rceil(p'_*) \geq \lambda$ with p_*, p'_* $2n$-neighbors in $\mathcal{D}'$, which lead to a contradiction.

Conjecture 1. *For any nD interval-valued map U, and whatever p_∞ and $\ell_\infty \in U(p_\infty)$ now considered as parameters, we have:*
$\mathfrak{FP}_{(p_\infty, \ell_\infty)}(U) = -\mathfrak{FP}_{(p_\infty, -\ell_\infty)}(-U)$*, so* $\mathfrak{FP}$ *is* self-dual.

The fact that this algorithm is self-dual is part of the proof that the tree of shapes computation algorithm is self-dual. It is not published yet.

Now, there is a property of Algorithm 3, which is related to the determinism of the FPA.

Conjecture 2. *Once given p_∞ and ℓ_∞, the front propagation algorithm $\mathfrak{FP}$ (Algorithm 3) is deterministic with respect to its input, the nD interval-valued map U.*

The fact that this algorithm is deterministic is part of the proof that the tree of shapes computation algorithm is correct. It is not published yet.

4.2.7 Making an nD function digitally well-composed

In this subsection, we explain the full process which starts from a given single-valued image and ends up with a digitally well-composed interpolation of this image.

Our interpolation in details

We start from a gray-level image $u : \mathcal{D} \subset \mathbb{Z}^n \to \mathbb{Z}$ defined on a bounded hyperrectangle $\mathcal{D}$. We *subdivide* the domain of the image by computing the smallest hyperrectangle $\mathcal{D}' \subset \left(\frac{\mathbb{Z}}{2}\right)^n$ containing $\mathcal{D}$ and we define a new function on the domain $\mathcal{D}'$ such that the restriction of this function to $\mathcal{D}$ is equal to u, that is, this function *interpolates* u. With $B = \{-\frac{1}{2}, 0, \frac{1}{2}\}^n$, where B_z is the translation of B by z, and with "op" an operator on (finite) subsets of $\mathbb{R}$, we define the following interpolation:

Definition 37. *Let $u : \mathcal{D} \to \mathbb{R}$ with $\mathcal{D} \subset \mathbb{Z}^n$ a bounded hyperrectangle. We define the* operator-based interpolation $\mathcal{I}_{\mathrm{op}}(u) : \mathcal{D}' = \mathrm{Subd}(\mathcal{D}) \to \mathbb{R}$ *such that, for any $z \in \mathcal{D}'$:*

$$(\mathcal{I}_{\mathrm{op}}(u))(z) \;=\; \begin{cases} \mathrm{op}\{\, u(z) \,\} & \text{if } z \in \mathcal{D}, \\ \mathrm{op}\{\, u(z'),\ z' \in B_z \cap \mathcal{D} \,\} & \text{otherwise.} \end{cases}$$

This interpolation is said *local* since it is computed at each point $p \in \mathcal{D}'$ using only the nearest neighbors of p in $\left(\frac{\mathbb{Z}}{2}\right)^n$.

The following proposition, which could also be derived from [116], follows easily.

Proposition 16. *For any $u : \mathcal{D} \subset \mathbb{Z}^n \to \mathbb{Z}$, the nD real-valued functions $\mathcal{I}_{\min}(u)$ and $\mathcal{I}_{\max}(u)$ are digitally well-composed, and the interpolation operators $\mathcal{I}_{\min}$ and $\mathcal{I}_{\max}$ are dual* (i.e. $\forall\, u,\ \mathcal{I}_{\min}(u) = -\mathcal{I}_{\max}(-u)$*).*

Proof: The proof is in Chapter A. □

Let us recall the definition of the Span operator: $\forall\, V \subset \mathbb{V}$,

$$\mathrm{Span}(V) \;=\; [\,\min(V), \max(V)\,] \;\cap\; \mathbb{V}.$$

Using this operator on the interpolations $\mathcal{I}_{\min}(u)$ and $\mathcal{I}_{\max}(u)$, we obtain the following *span-based interpolation* of u that we call $\mathcal{I}_{\mathrm{Span}}(u)$, defined such that:

$$\begin{cases} \lfloor \mathcal{I}_{\mathrm{Span}}(u) \rfloor &= \mathcal{I}_{\min}(u) \\ \lceil \mathcal{I}_{\mathrm{Span}}(u) \rceil &= \mathcal{I}_{\max}(u). \end{cases}$$

Since this interpolation is interval-valued, we say it is an *immersion* of u. The property of $\mathcal{I}_{\mathrm{Span}}(u)$ is then obvious:

Proposition 17. *For any* $u : \mathcal{D} \subset \mathbb{Z}^n \to \mathbb{Z}$*, the* n*D interval-valued function* $\mathcal{I}_{\mathrm{Span}}(u) : \mathcal{D}' \subset \left(\frac{\mathbb{Z}}{2}\right)^n \rightsquigarrow \mathbb{Z}$ *is digitally well-composed, and the interpolation operator* $\mathcal{I}_{\mathrm{Span}}$ *is self-dual (it verifies* $\forall\, u,\ \mathcal{I}_{\mathrm{Span}}(u) = -\mathcal{I}_{\mathrm{Span}}(-u)$*).*

Proof: It follows from the fact that the two functions $\mathcal{I}_{\min}(u)$ and $\mathcal{I}_{\max}(u)$ are (single-valued) digitally well-composed images and that an interval-valued is digitally well-composed iff its upper and lower bounds are digitally well-composed.

□

Then, starting from $\mathcal{I}_{\mathrm{Span}}(u) : \mathcal{D}' \subset \left(\frac{\mathbb{Z}}{2}\right)^n \rightsquigarrow \mathbb{Z}$ as developed above, we add an outer border to the hyperrectangle $\mathcal{D}'$, which becomes $\mathcal{D}'_+$, and we define $U_+ : \mathcal{D}'_+ \rightsquigarrow (\mathbb{Z}/2)$ such that $\forall p \in \mathcal{D}',\ U_+(p) = (\mathcal{I}_{\mathrm{Span}}(u))(p)$, and $\forall p \in \mathcal{D}'_+ \setminus \mathcal{D}', U(p) = \{\ell_\infty(u)\}$. This way, we preserved digital well-composedness of the interpolation, since adding an outer border valued by a constant to an image defined on a bounded hyperrectangle preserves digital well-composedness. Effectively, we have the following proposition:

Proposition 18 (Adding a (constant-valued) border preserves DWCness)**.** *Let* $U_0 : \mathcal{D} \subset \left(\frac{\mathbb{Z}}{2}\right)^n \rightsquigarrow \mathbb{Z}$ *be a DWC set-valued map defined on a bounded hyperrectangle* $\mathcal{D}$ *in* $\left(\frac{\mathbb{Z}}{2}\right)^n$*. Now, let* $U_1 : \mathcal{D}' \subset \left(\frac{\mathbb{Z}}{2}\right)^n \rightsquigarrow \mathbb{Z}$ *be another set-valued map defined on a bounded hyperrectangle* $\mathcal{D}'$ *in* $\left(\frac{\mathbb{Z}}{2}\right)^n$ *such that* $\delta(\mathcal{D}, \mathrm{se}) \subseteq \mathcal{D}'$ *where* δ *is the dilation operator and* se *is the structuring element defined such as* $\{p \in \left(\frac{\mathbb{Z}}{2}\right)^n\ ;\ ||p||_\infty \leq 1/2\}$*, and such that* $U_1|_{\mathcal{D}} = U_0$ *and for any* $p \in \mathcal{D}' \setminus \mathcal{D}$*,* $U'(p) = \{c\}$ *(where* c *in a given constant in* $\mathbb{R}$*). Then,* U_1 *is a DWC set-valued map.*

Proof: We can prove that every block $S \in \mathcal{B}(\mathcal{D}')$ of dimension $k \geq 2$ which intersects $\mathcal{D}$ and $\mathcal{D}' \setminus \mathcal{D}$ contains at least two elements of $\mathcal{D}' \setminus \mathcal{D}$ which are $2n$-neighbors in $\left(\frac{\mathbb{Z}}{2}\right)^n$. Let us now assume that U_1 is not DWC. There exists then a block $S \in \mathcal{B}(\mathcal{D}', \left(\frac{\mathbb{Z}}{2}\right)^n)$ of dimension $k \geq 2$ such that $U_1|_S$ is not DWC. Three cases are then possible: either $S \subseteq \mathcal{D}$ (which is impossible since $U_1|_S = U_0|_S$ which is DWC), or $S \subseteq \mathcal{D}' \setminus \mathcal{D}$ (which is impossible since $U_1|_S = \{c\}$ which is DWC), or S intersects at the same time $\mathcal{D}$ and $\mathcal{D}' \setminus \mathcal{D}$. In this last case, there exists two different elements $q^1, q^2 \in \mathcal{D}' \setminus \mathcal{D}$ that belong to S and which are $2n$-neighbors in $\left(\frac{\mathbb{Z}}{2}\right)^n$. Since these two elements belong to $\mathcal{D}' \setminus \mathcal{D}$, $U_1(q^1) = U_1(q^2)$ and then U_1 is DWC on the block S, which leads to a contradiction. □

Then we apply the front propagation on U_+ with p_∞ belonging to the outer border of $\mathcal{D}'_+$. We obtain the single-valued image $u^\flat : \mathcal{D}'_+ \to \mathbb{Z}/2$, which

is digitally well-composed, at which we remove the border. Since removing the outer border preserves digital well-composedness, we obtain the final interpolation $u_{\mathrm{DWC}} : \mathcal{D}' \to \mathbb{Z}/2$ of u, which is digitally well-composed too.

With $\alpha \in \mathbb{R}$, let us denote by b_α the operator which adds an outer border set at $\{\alpha\}$ to a interval-valued image defined on an hyperrectangle, and b^- the operator which removes the outer border to a single-valued image defined on an hyperrectangle. We can then define our interpolation in this way:

$$u_{\mathrm{DWC}} = \mathfrak{I}_{\mathrm{DWC}}(u),$$

where the *digitally well-composed interpolation operator* is defined such that:

$$\mathfrak{I}_{\mathrm{DWC}} = b^- \circ \mathfrak{FP} \circ b_{\ell_\infty(.)} \circ \mathcal{I}_{\mathrm{Span}}.$$

u_{DWC} is digitally well-composed

Combining the properties of the immersion and of the FPA, we obtain the following proposition:

Proposition 19. *Let $u : \mathcal{D} \subset \mathbb{Z}^n \to \mathbb{Z}$ be a given image. Then the image $u_{\mathrm{DWC}} = \mathfrak{I}_{\mathrm{DWC}}(u)$ is digitally well-composed.*

u_{DWC} interpolates u

Since for each $p \in \mathcal{D}$, $U_+(p) = (\mathcal{I}_{\mathrm{Span}}(u))(p) = \{u(p)\}$, the FPA cannot choose another value than $u(p)$ at the point p during the flattenning process, and then $u_{\mathrm{DWC}}(p) = u^\flat(p) = u(p)$. This way, the following proposition is straightforward:

Proposition 20. *Let $u : \mathcal{D} \subset \mathbb{Z}^n \to \mathbb{R}$ be a given image. Then the image $u_{\mathrm{DWC}} = \mathfrak{I}_{\mathrm{DWC}}(u)$ interpolates u.*

u_{DWC} is self-dual

Since the immersion step and the front propagation are self-dual, the complete process is self-dual, and then we obtain the following statement:

Conjecture 3. *Let $u : \mathcal{D} \subset \mathbb{Z}^n \to \mathbb{R}$ be a given image. Then the image $u_{\mathrm{DWC}} = \mathfrak{I}_{\mathrm{DWC}}(u)$ interpolates u in a self-dual way.*

u_{DWC} is in-between

Let us recall the Definition 32 establishes what is an in-between interpolation. This notion is much important because it represents that the interpolation method outputs an image with no new extrema compared to the input image.

Proposition 21. *Let $u : \mathcal{D} \subset \mathbb{Z}^n \to \mathbb{Z}$ be a given image. Then the image $u_{\mathrm{DWC}} : \mathcal{D}' \subset \left(\frac{\mathbb{Z}}{2}\right)^n \to \mathbb{Z}/2$ defined such that $u_{\mathrm{DWC}} = \mathfrak{I}_{\mathrm{DWC}}(u)$ is an in-between interpolation of u.*

Proof: Let $u : \mathcal{D} \to \mathbb{Z}$ be a given image, and $u_{\mathrm{DWC}} = \mathfrak{I}_{\mathrm{DWC}}(u)$ be its interpolation. This way, we know that $\forall z \in \mathcal{D}$, $u_{\mathrm{DWC}}(p) = u(p)$. Let us assume now that u_{DWC} is not in-between. Then there exists some point $m \in \mathrm{Subd}(\mathcal{D}) \setminus \mathcal{D}$ such that:

$$u_{\mathrm{DWC}}(m) \notin \cap_{\{p^-,p^+\}\in \mathrm{opp}(m)} \mathrm{intvl}(u_{\mathrm{DWC}}(p^-), u_{\mathrm{DWC}}(p^+)).$$

In other words, there exists two points $a, b \in \mathrm{Subd}(\mathcal{D})$ such as $\{a, b\} \in \mathrm{opp}(m)$ and:

$$u_{\mathrm{DWC}}(m) \notin \mathrm{intvl}(u_{\mathrm{DWC}}(a), u_{\mathrm{DWC}}(b)).$$

Two situations are then possible:

- either $u_{\mathrm{DWC}}(m) < \min(u_{\mathrm{DWC}}(a), u_{\mathrm{DWC}}(b))$ (Case 1)
- or $u_{\mathrm{DWC}}(m) > \max(u_{\mathrm{DWC}}(a), u_{\mathrm{DWC}}(b)$ (Case 2).

Since these two relations are dual, we will study only the first case, the reasoning being the same for the second one.

By hypothesis, $u_{\mathrm{DWC}}(m) < u_{\mathrm{DWC}}(a)$, and then:

$$u^\flat(m) < u^\flat(a), \quad (P1).$$

Also, we know that a and m are $2n$-neighbors in $\mathcal{D}'$ $(P2)$. Finally, since $a \in \mathbb{P}(m)$, $U_+(a) = (\mathcal{I}_{\mathrm{Span}}(u))(a) \subseteq (\mathcal{I}_{\mathrm{Span}}(u))(m) = U_+(m)$ $(P3)$. This way, we have the three properties of Lemma 10 and we can conclude that $u_{\mathrm{DWC}}(a) = u^\flat(a) = \lfloor U_+ \rfloor(a)$.

With the same reasoning applied to b, we obtain that $u_{\mathrm{DWC}}(b) = \lfloor U_+ \rfloor(b)$, which leads to:

$$u_{\mathrm{DWC}}(m) < \min(\lfloor U_+ \rfloor(a), \lfloor U_+ \rfloor(b)).$$

By construction,

$$\lfloor U_+ \rfloor(a) = \min\{u(p)\ ;\ p \in \mathbb{A}(a)\},$$

and

$$\lfloor U_+ \rfloor(b) = \min\{u(p)\ ;\ p \in \mathbb{A}(b)\}.$$

This implies that $u^\flat(m) < \min\{u(p)\ ;\ p \in \mathbb{A}(m)\}$ (since $\mathbb{A}(a) \cup \mathbb{A}(b) = \mathbb{A}(m)$), which is equal to $\lfloor U_+ \rfloor(m)$. However $u_{\mathrm{DWC}}(m) < \lfloor U \rfloor(m)$ is impossible by construction. This concludes the proof.

□

Invariance of u_{DWC}

Note that u_{DWC} should be invariant by translations, $\frac{\pi}{2}$'s rotations and axial symmetries, since the propagation of the front begins at the boundary of the domain of the interval-valued interpolation of the input image, which justifies the following conjecture:

Conjecture 4. *Following the complete process detailed in this section, the interpolation u_{DWC} of the image u is invariant by translations, $\frac{\pi}{2}$'s rotations and axial symmetries.*

4.2.8 An illustration of the complete process

An example of the span-based interpolation is depicted in Figure 4.27. We start from an image u that we interpolate using the digitally well-composed interval-valued interpolation $\mathcal{I}_{\mathrm{Span}}(u)$ at which we add a border to obtain U_+ which is still digitally well-composed. This boundary is displayed in light gray and is filled with a single value $\ell_\infty(u)$, which is actually the median value of the set of values of the boundary of the definition domain of u. We have:

$$\ell_\infty(u) = \mathrm{med}\{\,3,\ 3,\ 5,\ 7,\ 9,\ 11,\ 13,\ 15\,\} = 8.$$

When we take U_+ as input to the FPA, p_∞ can be any point of its boundary. This way, which is similar to [60], we ensure that the propagation starts from the outer boundary of U_+, and that all the points of the inner boundary of u are enqueued. Having $\ell_\infty(-u) = -\ell_\infty(u)$ guarantees that U_+ remains self-dual with respect to u. Then the flattenning process is applied on U_+ and results in a digitally well-composed image $u^\flat$.

9	11	15
7	1	13
3	5	3

(a) u

$\{\mathbf{9}\}$	$[\![9,11]\!]$	$\{\mathbf{11}\}$	$[\![11,15]\!]$	$\{\mathbf{15}\}$
$[\![7,9]\!]$	$[\![1,11]\!]$	$[\![1,11]\!]$	$[\![1,15]\!]$	$[\![13,15]\!]$
$\{\mathbf{7}\}$	$[\![1,7]\!]$	$\{\mathbf{1}\}$	$[\![1,13]\!]$	$\{\mathbf{13}\}$
$[\![3,7]\!]$	$[\![1,7]\!]$	$[\![1,5]\!]$	$[\![3,13]\!]$	$[\![3,13]\!]$
$\{\mathbf{3}\}$	$[\![3,5]\!]$	$\{\mathbf{5}\}$	$[\![3,5]\!]$	$\{\mathbf{3}\}$

(b) $U = \mathcal{I}_{\mathrm{Span}}(u)$

$\{8\}$	$\{8\}$	$\{8\}$	$\{8\}$	$\{8\}$	$\{8\}$	$\{8\}$
$\{8\}$	$\{\mathbf{9}\}$	$[\![9,11]\!]$	$\{\mathbf{11}\}$	$[\![11,15]\!]$	$\{\mathbf{15}\}$	$\{8\}$
$\{8\}$	$[\![7,9]\!]$	$[\![1,11]\!]$	$[\![1,11]\!]$	$[\![1,15]\!]$	$[\![13,15]\!]$	$\{8\}$
$\{8\}$	$\{\mathbf{7}\}$	$[\![1,7]\!]$	$\{\mathbf{1}\}$	$[\![1,13]\!]$	$\{\mathbf{13}\}$	$\{8\}$
$\{8\}$	$[\![3,7]\!]$	$[\![1,7]\!]$	$[\![1,5]\!]$	$[\![3,13]\!]$	$[\![3,13]\!]$	$\{8\}$
$\{8\}$	$\{\mathbf{3}\}$	$[\![3,5]\!]$	$\{\mathbf{5}\}$	$[\![3,5]\!]$	$\{\mathbf{3}\}$	$\{8\}$
$\{8\}$	$\{8\}$	$\{8\}$	$\{8\}$	$\{8\}$	$\{8\}$	$\{8\}$

(c) U_+

8	8	8	8	8	8	8
8	**9**	9	**11**	11	**15**	8
8	8	8	8	8	13	8
8	**7**	7	**1**	8	**13**	8
8	7	7	5	8	8	8
8	**3**	5	**5**	5	**3**	8
8	8	8	8	8	8	8

(d) $u^\flat$

9	9	**11**	11	**15**
8	8	8	8	13
7	7	**1**	8	**13**
7	7	5	8	8
3	5	**5**	5	**3**

(e) u_{DWC}

Figure 4.27: The complete process in detail.

Figure 4.28 depicts the propagation steps: we start from Subfigure (a) where p_∞ is the only point to be enqueued in $Q[\ell_\infty(u)] = Q[8]$. Then, until $Q[8]$ is empty, the propagation continues across the domain of the image, which contains (at least) the ounter boundary, as shown on Subfigure (b) in light gray. The green pixels correspond to the points which have been enqueud during the propagation, and that are not valued yet. Then ℓ is set

at 9, and the same process reiterates, until the whole domain of the image has been enqueued and valued, which results in $u^\flat$ on Subfigure (j).

The final result u_{DWC} which corresponds to $u^\flat$ minus its boundary is digitally well-composed and computed in a self-dual way.

4.2.9 Conclusions about u_{DWC}

As proven in the section before, we finally have the following properties for our interpolation:

$$\begin{cases} u_{\mathrm{DWC}} \text{ is self-dual} \\ u_{\mathrm{DWC}} \text{ is in-between} \\ u_{\mathrm{DWC}} \text{ subdivides the domain only once} \\ u_{\mathrm{DWC}} \text{ has a subdivision factor of 2} \\ u_{\mathrm{DWC}} \text{ is deterministic} \end{cases}$$

Obviously, u_{DWC} is neither ordered not local, but this methods works in n-D, $n \geq 2$.

4.2.10 From $\mathcal{D} \to \mathbb{Z}$ to $\mathcal{D}' \to (\mathbb{Z}/2)$

We can notice that in practice, we will have an integer-valued map u whose values are defined into $\mathbb{Z}$, and then its immersion U will be also defined into $\mathbb{Z}$. When we add a border to the domain of U, we obtain a new function U_+, which is no more defined into $\mathbb{Z}$ but into $\mathbb{Z}/2$, since the median at which we set the border belongs to $\mathbb{Z}/2$. The use of a generic library is then necessary [107] (or we can round the value of ℓ_∞ but we can loose *perfect* self-duality). The consequence is that $u^\flat$ and the final image u_{DWC} will be defined into $\mathbb{Z}/2$. According to us, it is a nice way (and perhaps the only way) to ensure self-duality to an interpolation method starting from an image whose values are defined into $\mathbb{Z}$.

4.2.11 The FPA succeeds where local methods fail

We showed in [26] detailed in the chapter before that no self-dual local interpolation with usual constraints can make any 3D image digitally well-composed with one subdivision. However, our self-dual (non-local) FPA succeeds in making any nD image digitally well-composed thanks to its process in 2 steps: the immersion U and the propagation u_{DWC} (see Figure 4.29).

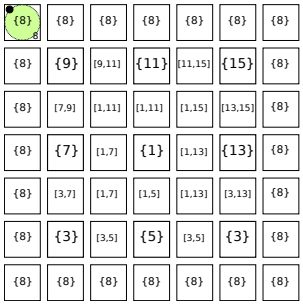

(a) U_+.

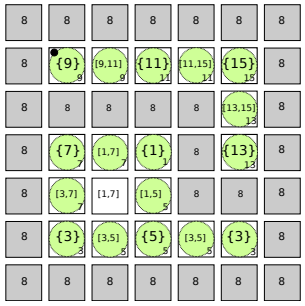

(b) $\ell = 8$.

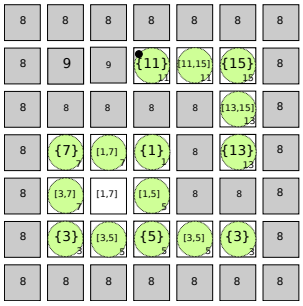

(c) $\ell = 9$.

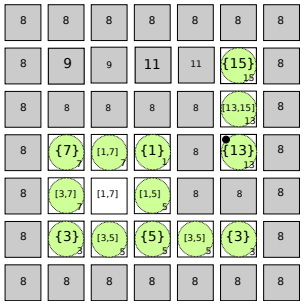

(d) $\ell = 11$.

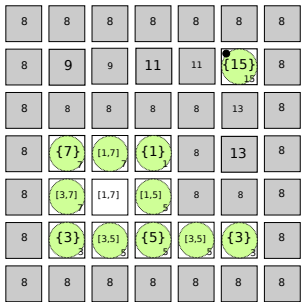

(e) $\ell = 13$.

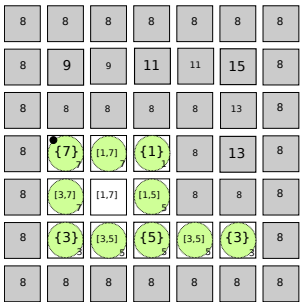

(f) $\ell = 15$.

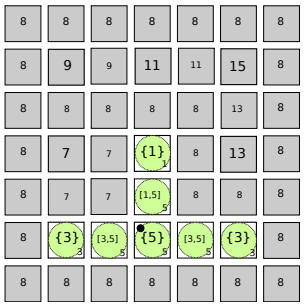

(g) $\ell = 7$.

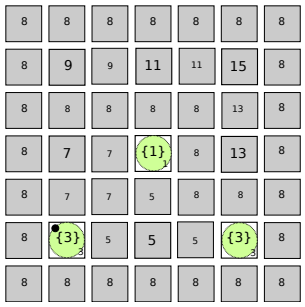

(h) $\ell = 5$.

(i) $\ell = 3$.

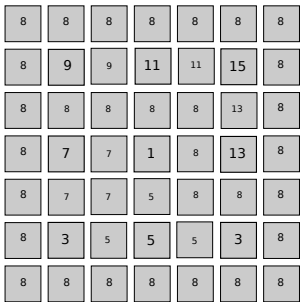

(j) $\ell = 1$.

Figure 4.28: From U_+ to $u^\flat$.

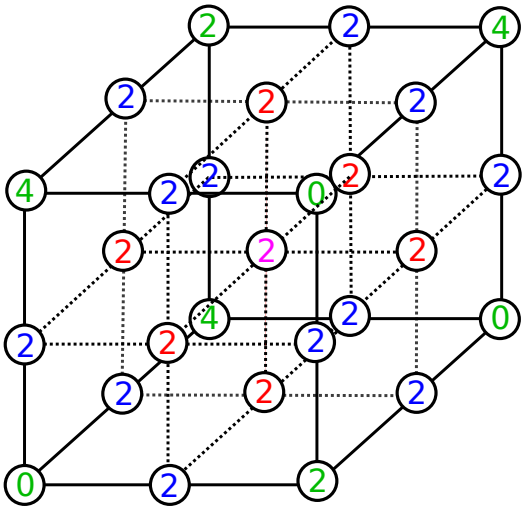

Figure 4.29: A self-dual digitally well-composed interpolation of image of Figure 4.13.

Chapter 5

Some consequences and applications

In this chapter, we explain how we can use the tools we have developed in this thesis to reach our aims: we see in a first time how the self-dual interpolation u_{DWC} of a given image u can be used to obtain pure self-duality using a given self-dual operator, and in a second time, we explain how we can combine this same interpolation and the conjecture that AWCness and DWCness are equivalent on cubical grids to obtain finally a plain map with strong topological properties such as AWCness and continuity. We also show that thanks to the local equivalence of connectivities in a DWC image defined on a cubical grid, the underlying structure of the graph of a well-composed image does not depend anymore on the values in this image. Finally, we observe we have no "ambiguity cases" using the Marching Cubes algorithm on a DWC image, and we conjecture that this property is true in n-D.

5.1 Pure self-duality

A very powerful hierarchical representation, based on the inclusion relationship of the components of an image, exists in mathematical morphology: the tree of shapes [120, 60, 40] (see [117, 177, 178, 179] for some possible applications). It is sometimes seen as the fusion of the *min-tree*, made of the connected components of the lower threshold sets (leaves are the regional minima in the image), and its dual, the *max-tree*, which is made of the connected components of the upper threshold sets (leaves are the regional maxima in

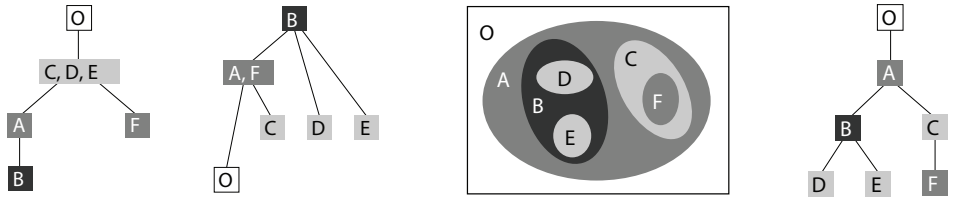

Figure 5.1: In the middle, a gray-level image. On the left, its min-tree and max-tree, and on the right its tree of shapes [60].

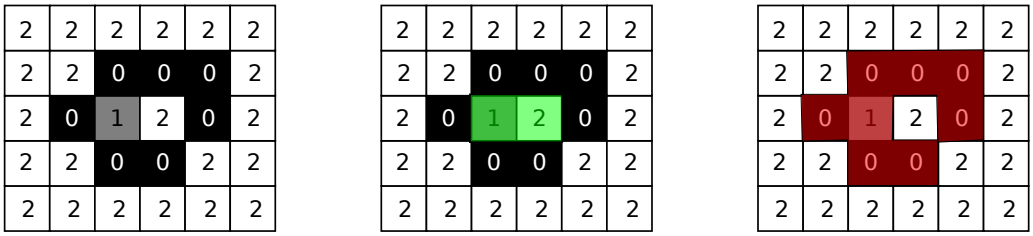

Figure 5.2: Incoherences using 4-connectivity for both upper and lower threshold sets.

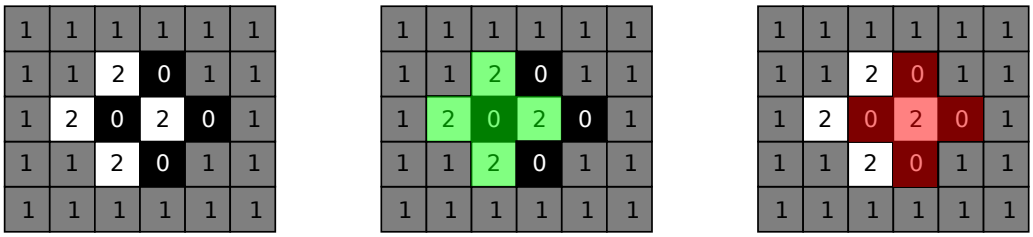

Figure 5.3: Incoherences using 8-connectivity for both upper and lower threshold sets.

the image). Figure 5.1 shows a gray-level image and its component trees.

In fact, this morphological operator is *self-dual* in the sense that it is invariant by contrast: it treats in a similar way bright objects over a dark background or dark objects over a bright background. This is very useful when we do not know a priori the contrast of the object, or if we need to study several objects of different contrasts in the same image.

However, this operator is based on connectivities: we need to associate a connectivity to the upper threshold sets and to the lower threshold sets

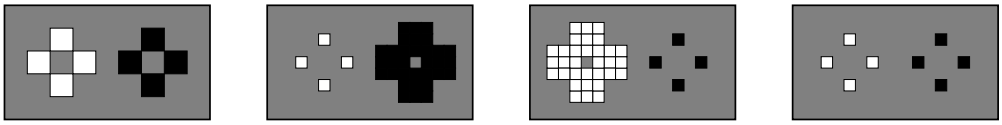

(a) u. (b) u_{min}. (c) u_{max}. (d) u_{DWC}.

Figure 5.4: An image u, its min/max interpolations, and u_{DWC} which is self-dual.

used to compute the saturated connected components, called "shapes", in the image using a "cavity-fill-in" operator.

Theoretically, a tree of shapes is such that if two components overlap, they are nested the one in the other one; in the contrary case, they are disjoint. However, in practice, it can be observed that by associating the $2n$-connectivity (respectively the $(3^n - 1)$-connectivity) to both upper and lower threshold sets, we obtain some abnormalities: we can see on Figure 5.2 (respectively Figure 5.3) that there exist some shapes whose intersection is non-empty and such that they are not included the one in the other one. In these cases, the tree of shapes is a lattice but not a tree: it contains cycles.

To avoid these incoherences, it is common to associate a *Jordan pair of connectivities* [11, 32] to the lower and upper threshold sets. However, the $(4, 8)$- and the $(4, 8)$-trees of shapes of a same 2D image will usually not be exactly the same; in other words, we do not have *unicity* of the tree, which is then ill-defined.

However, using a well-composed image (in the sense that connectivities are equivalent), we can compute the tree of shapes of an image and its negative with exactly the same couple of connectivities (no switch is needed), the result will be the same: Géraud and Najman [60] call this phenomenon "pure self-duality".

Since the front propagation in the computation of the tree of shapes is based on $2n$-connectivity, we can emulate the dual pair of connectivities (c_{2n}, c_{3^n-1}) (which connects the zeros and disconnect the ones) on a min interpolation. In the same way, we can compute the tree of shapes based on the dual pair (c_{3^n-1}, c_{2n}) (which connects the ones and disconnects the zeros) on a max interpolation. So, starting from a given image u, we compute its min, max, and self-dual interpolations as shown on Figure 5.4. Then we compute their respective trees of shapes $\mathcal{T}(u_{min})$, $\mathcal{T}(u_{max})$, and $\mathcal{T}(u_{\mathrm{DWC}})$ as

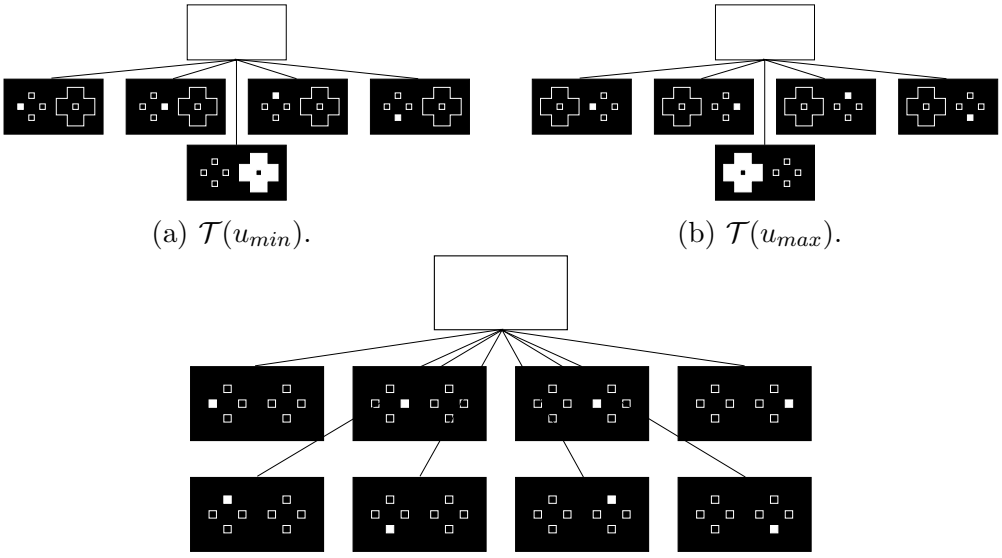

(a) $\mathcal{T}(u_{min})$. (b) $\mathcal{T}(u_{max})$.

(c) $\mathcal{T}(u_{\mathrm{DWC}})$.

Figure 5.5: The tree of shapes of the min, max, and self-dual interpolations.

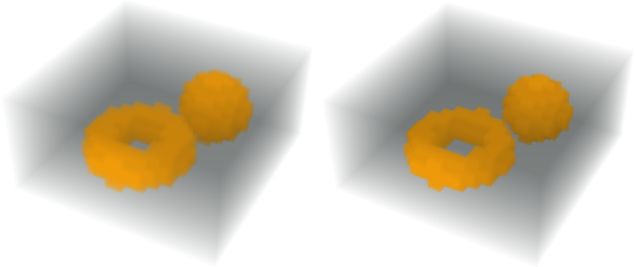

Figure 5.6: The initial image u containing a ball and a full torus and its self-dual interpolation.

shown on Figure 5.5. We can observe that the upper and lower threshold sets are not processed in the same way using the min and max interpolations, contrary to the tree of shapes computed on our self-dual representations u_{DWC} which treats exactly in the same way bright and dark components.

Now, let us show how our self-dual interpolation $u^\flat$ deletes the pinches in the image and let us observe the result we obtain on the tree of shapes. We start from an initial 3D image u showed on the left of Figure 5.6 and we compute its self-dual interpolation $u^\flat$ showed on the right of the same figure.

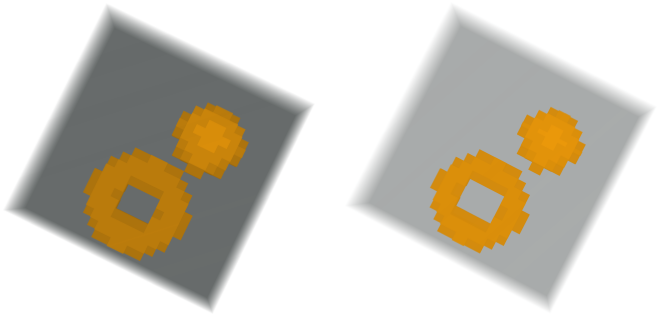

Figure 5.7: On the left, u seen from the top, and on the right, u_{DWC} seen from the top.

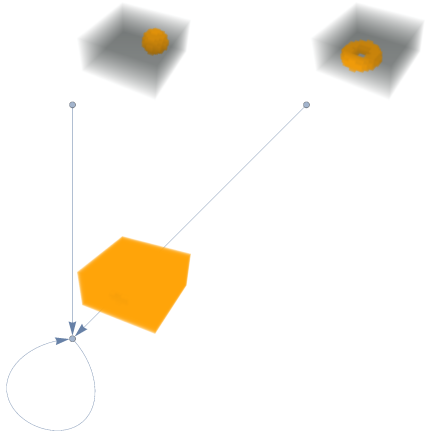

Figure 5.8: The tree of shapes of u.

Figure 5.7 shows the same images seen from the top to see the "pinch". The final result is that the tree of shapes, showed on Figure 5.8, expose the same separation as $u^\flat$ (since the union-find is applied on it).

Note that any self-dual operator which is based on connectivities, derived [31, 178] from the tree of shape (or not), will be purely self-dual on well-composed images. Effectively, an example of self-dual operator derived from the tree of shapes is the *grain filter*, which removes the shapes in the hierarchical representation of an image u whose area is smaller than a given threshold. We can remark easily on Figure 5.9 that using the connectivities

(a) u. (b) $G_{c_4,c_8}(u)$. (c) $G_{c_8,c_4}(u)$. (d) $G(u_{\mathrm{DWC}})$. (e) Emersion of $G(u_{\mathrm{DWC}})$.

Figure 5.9: Grain filtering on an image u: our self-dual representation leads to "pure" self-duality.

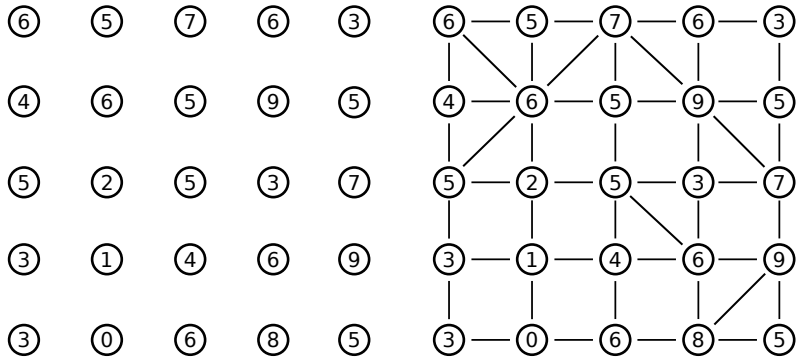

(a) u. (b) Underlying graph structure.

Figure 5.10: From u to its underlying graph structure using the dual pair (c_8, c_4).

(c_4, c_8) or (c_8, c_4) does not lead to the same result. Furthermore, the use of our self-dual representation gives a result which is between the two before, and then shows how our self-dual representation u_{DWC} is "purely" self-dual.

In the same manner, in digital topology, we assume that a Jordan pair of adjacencies, such as (c_{2n}, c_{3^n-1}), is associated to a binary or gray-level image, that is, we associate $2n$-adjacency to the ones (or the upper threshold sets), and $(3^n - 1)$-adjacency to the zeros (or the lower threshold sets). Note that some other Jordan pairs of adjacencies can be considered, as its dual pair $(c_{3^n} - 1, c_{2n})$, depending on the application. In this manner, we obviate connectivity paradoxes. The resulting problem is then that a specific adjacency is considered depending on the values of the pixels in the image, and then the underlying structure of the graph (corresponding to the domain of the image)

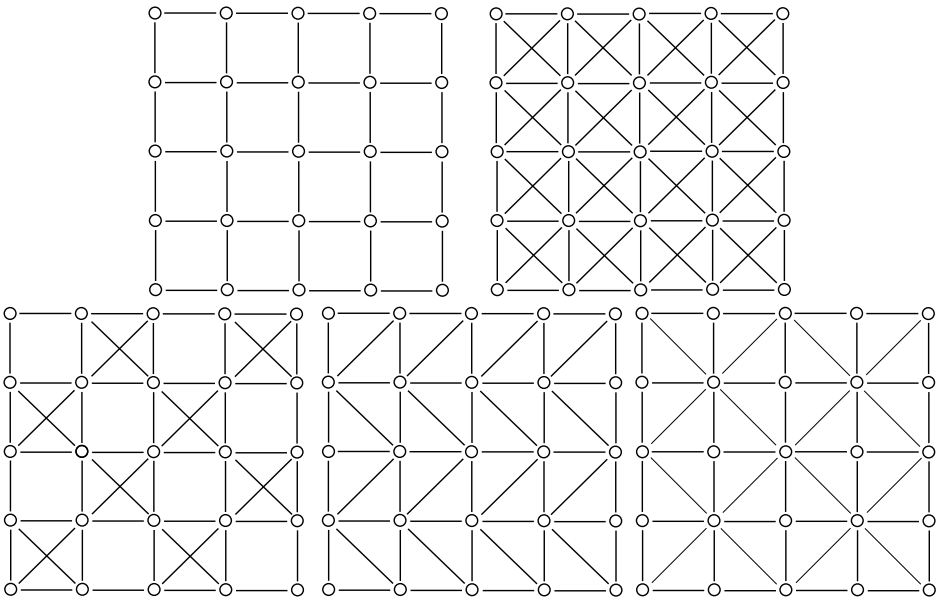

Figure 5.11: All the possible cubical connectivity grids are equivalent on a digitally well-composed image. In the raster scan order, the 4-connectivity grid, the 8-connectivity grid, the perfect fusion grid, a 6-connectivity grid, and the Khalimsky grid.

depends on the location (see Figure 5.10). However, DWC images have their connectivities (locally) equivalent, and then they can be seen as $(2n, 2n)$ images. This way, the underlying graph of the image becomes simpler, regular, 90 degrees rotation and translation invariant, and is not anymore correlated to the values in the image. In fact, since any chosen connectivity for the ones and for the zeros will lead to the same result, we can associate any graph structure to the image. This way, the *perfect fusion grid* [38, 39], the Khalimsky grid [73], and so on (see Figure 5.11) can be associated to a DWC image.

5.2 A new representation of digital images

Note that this section needs some prerequisites of Chapters C and D.

Since we work with images defined on bounded hyperrectangles in a space of finite dimension $n \geq 0$, we can assume that we start from an image

$u : \mathcal{D} \to \mathbb{R}$ where $\mathcal{D} = \otimes_{i \in [\![1,n]\!]} [\![k_i^{\min}, k_i^{\max}]\!]$, with $k^{\min}, k^{\max} \in \mathbb{Z}^n$ the lower and upper bounds of the domain $\mathcal{D}$ of u respectively.

Also, since we are working with subsets of a **finite** spaces, we do not use the topological boundary ∂ but the border Δ instead. We recall that the *border* of a subset X in any Alexandrov space of finite rank $n \geq 0$ (as an order) is the union of the closures of the $(n-1)$-faces that have one n-face as coface.

From $(\mathbb{Z}/2)^n$ to $\mathbb{H}^n$ Now let us define the isomorphism between $(\mathbb{Z}/2)^n$ and $\mathbb{H}^n$ we use to immerse u into any cubical complex subset of $\mathbb{H}^n$. We define the application $\mathcal{H} : (\mathbb{Z}/2) \to \mathbb{H}^1$ such that:

$$\forall z \in (\mathbb{Z}/2), \mathcal{H}(z) = \begin{cases} \{z + 1/2\} & \text{if} \quad z \in (\mathbb{Z}/2) \setminus \mathbb{Z}, \\ \{z, z+1\} & \text{if} \quad z \in \mathbb{Z}, \end{cases} \tag{5.1}$$

from which we deduce using the cartesian product the application $\mathcal{H}_n : \left(\frac{\mathbb{Z}}{2}\right)^n \to \mathbb{H}^n$ such that:

$$\forall z \in (\mathbb{Z}/2)^n, \mathcal{H}_n(z) = \otimes_{i \in [\![1,n]\!]} \mathcal{H}(z_i).$$

We will denote by $\mathcal{Z}_n$ the inverse of the bijection $\mathcal{H}_n$.

Span-based immersions are continuous but not AWC Then, a first idea could be to immerse u into $\mathrm{Imm}_u : \alpha(\mathcal{H}_n(\mathcal{D})) \rightsquigarrow \mathbb{R}$ such that:

$$\forall z \in \alpha(\mathcal{H}_n(\mathcal{D})), \mathrm{Imm}_u(h) = \begin{cases} \{u(\mathcal{Z}_n(h))\} & \text{if } h \in \mathbb{H}_n^n, \\ \mathrm{Span}\left\{u(\mathcal{Z}_n(q)) \ ; \ q \in \beta(h) \cap \mathbb{H}_n^n\right\} & \text{either.} \end{cases}$$

Note that $\alpha(\mathcal{H}_n(\mathcal{D}))$ is a cubical complex (see Definition 70), since it is closed by inclusion, and that any face of any face of this set belongs to this set.

This way, we obtain an USC map as showed on Figure 5.12: the strict upper/lower threshold sets are open and the upper/lower threshold sets are closed.

However, this map is not AWC, as showed on Figure 5.13, in the sense that its *border* in not a disjoint union of $(n-1)$-surfaces.

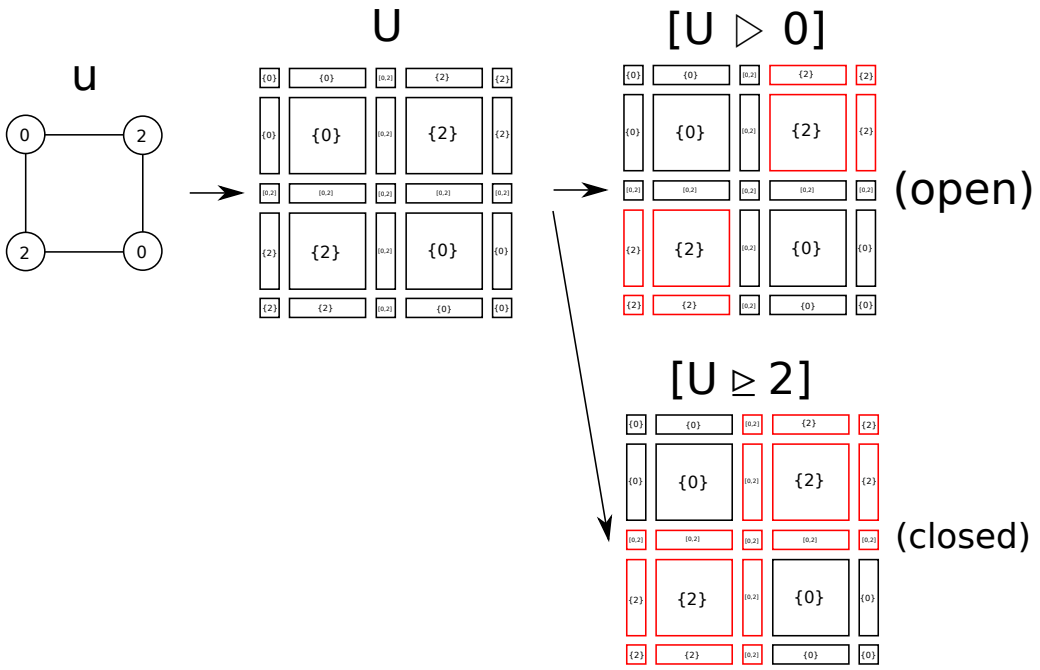

Figure 5.12: Span-based immersion of $u : [\![0,1]\!] \times [\![0,1]\!] \to \mathbb{R}$ into a cubical complex provides continuity properties to the new representation U of u.

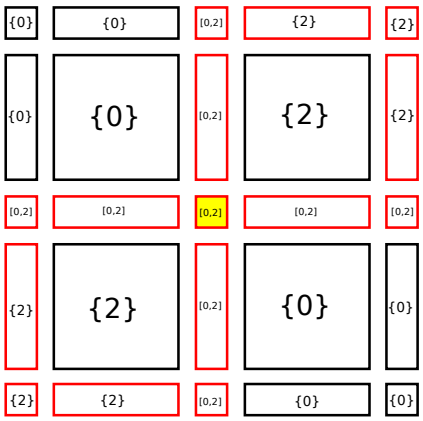

Figure 5.13: $\Delta[U \triangleright 0]$, depicted in red, contains a pinch (in yellow).

An AWC continuous representation on $\mathbb{H}^n$ Note that this section requires the content of Chapter D containing the sketch of the proof that immersions of DWC images on the Khalimsky grids are AWC interval-valued maps.

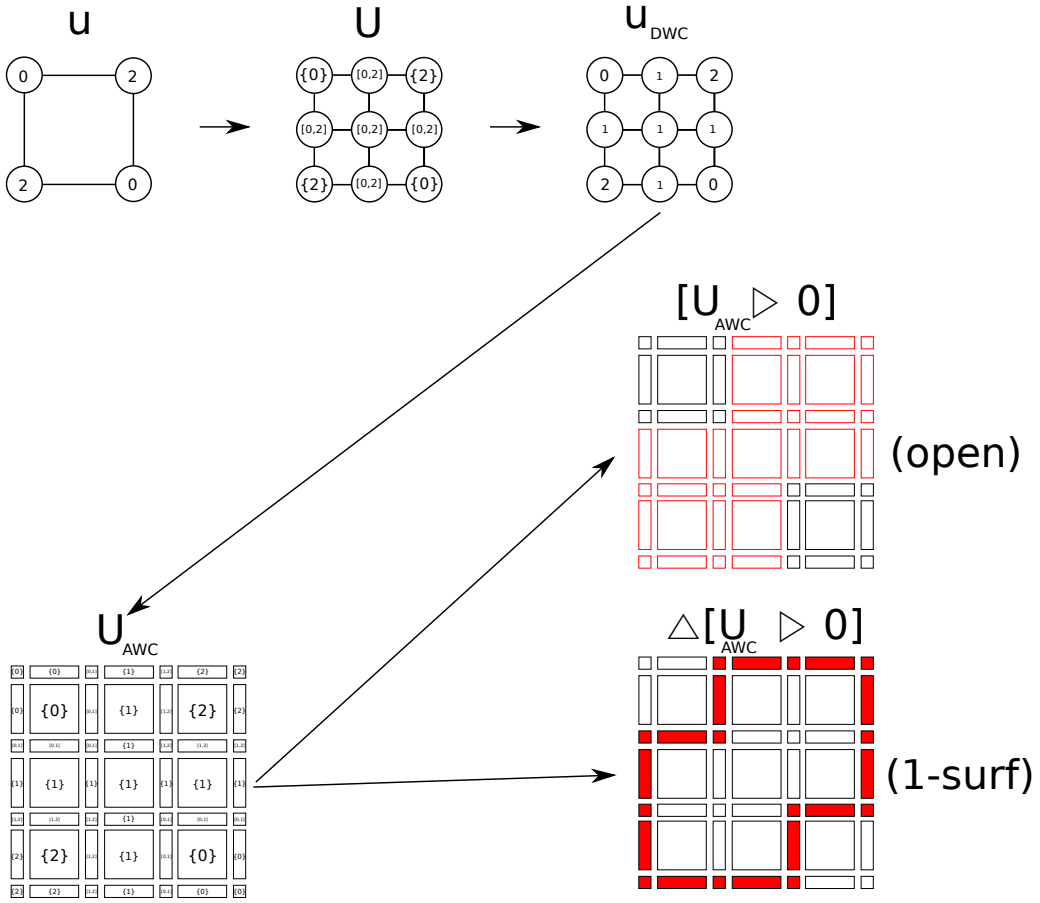

Figure 5.14: Our method to obtain an AWC plain map.

For this reason, we propose the following numerical scheme (see Figure 5.14): we start from an image $u : \mathcal{D} \to \mathbb{R}$ where $\mathcal{D}$ is defined such that:

$$\mathcal{D} = \otimes_{i \in [\![1,n]\!]} [\![2k_i^{\min}, 2k_i^{\max}]\!] \cap (2\mathbb{Z})^n,$$

we compute its span-based interpolation $U : \mathcal{D}_2 \rightsquigarrow \mathbb{R}$ with $\mathcal{D}_2$ defined such that:

$$\mathcal{D}_2 = \otimes_{i \in [\![1,n]\!]} [\![2k_i^{\min}, 2k_i^{\max}]\!],$$

we apply the front propagation $\mathfrak{FP}$ on it to obtain $u_{\mathrm{DWC}} : \mathcal{D}_2 \to \mathbb{R}$, and then we use u_{DWC} to compute its immersion U_{AWC} defined onto $\alpha(\mathcal{H}_n(\mathcal{D}_2)) \subseteq \mathbb{H}^n$ such that $\forall h \in \alpha(\mathcal{H}_n(\mathcal{D}_2))$:

$$U_{\mathrm{AWC}}(h) = \begin{cases} \{u_{\mathrm{DWC}}(\mathcal{Z}_n(h))\} & \text{if } z \in \mathcal{H}_n(\mathcal{D}_2), \\ \mathrm{Span}\,\{u_{\mathrm{DWC}}(\mathcal{Z}_n(q)) \ ; \ q \in \beta(z) \cap \mathcal{H}_n(\mathcal{D}_2)\} & \text{either.} \end{cases}$$

We obtain finally U_{AWC} which is AWC in the sense that the topological boundaries of its threshold sets are either disjoint union of $(n-1)$-surfaces or empty sets (at least in 2D and in 3D, the n-D case, $n \geq 4$, being still not verified).

Following the same idea as Najman and Géraud in [124], and considering that the value image of U is supplied with the usual Euclidian distance, the properties of our self-dual interpolation U_{AWC} will be the following:

- U_{AWC} is AWC,
- U_{AWC} is USC,
- for any $\lambda \in \mathbb{R}$, the threshold sets $[U_{\mathrm{AWC}} \lhd \lambda]$ and $[U_{\mathrm{AWC}} \rhd \lambda]$ are open sets,
- for any $\lambda \in \mathbb{R}$, the threshold sets $[U_{\mathrm{AWC}} \trianglelefteq \lambda]$ and $[U_{\mathrm{AWC}} \trianglerighteq \lambda]$ are closed sets (since $\alpha(\mathcal{H}_n(\mathcal{D}_2))$ is closed by construction),
- U_{AWC} satisfies the *intermediate value theorem*,
- assuming that $\alpha(\mathcal{H}_n(\mathcal{D}_2))$ is *unicoherent*[1], the set of *shapes* [124] $\mathfrak{T}$ of U_{AWC} is a *tree*, that is, two components of $\mathfrak{T}$ are either nested or disjoint; in other words, the tree of shapes is well-defined.

Note: Obviously, a span-based immersion applied on the AWC interpolations described in Chapter E will also lead to AWC continuous maps with these same properties.

[1] A topological space is said to be *unicoherent* iff it is connected and for any two closed connected sets such that their union equals the whole space, their intersection is also connected.

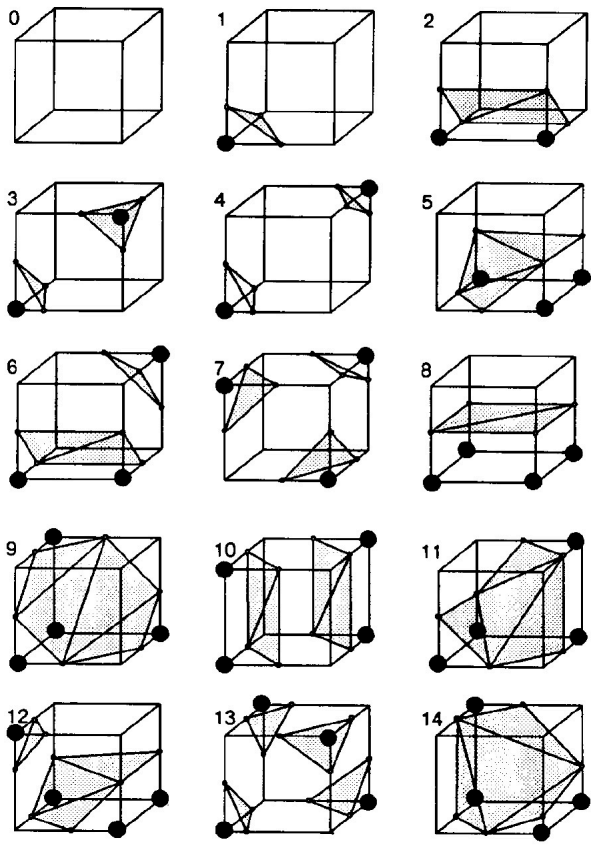

Figure 5.15: Lorensen's Marching Cubes Lookup Table [110]

5.3 n-D Marching-Cubes-like Algorithms

We propose here the conjecture that any n-D MC-like algorithm has no ambiguity cases when the digital gray-level image we are working with is DWC.

The main reference in matter of scientific and experimental visualization of scalar field data on 3D cubical grids is the *Marching Cubes (MC)* algorithm of Lorensen [110]. Assuming that we have a continuous scalar field f whose values are known on the lattice points of a cubical grid, we can visualize the approximate of the implicit surface $[f = \alpha]$ (usually assumed to be a topological 2-manifold), $\alpha \in \mathbb{R}$, using a *triangular mesh*, that is, a simplicial complex, also called the *surface tiling* of the iso-surface. This algorithm

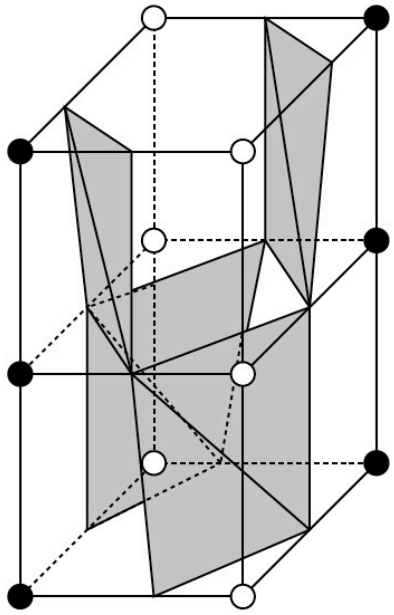

Figure 5.16: The "hole problem" using Marching Cubes ([153])

computes the triangulation cube by cube in this way: each corner c of the cube (the lattice points of the cubical grid) whose value $f(c)$ is superior or equal to the given threshold α is said to be *positive* (they correspond to the inside part of the object), and the other corners of the cubes are said to be *negative* (they correspond to the outside part of the object). A *boundary point* is then created on each edge of the cube using a (trivial or non-trivial) interpolation such that one of its vertices is positive and the other is negative. Then, using a lookup table proper to the MC algorithm [110] as shown on Figure 5.15, boundary points are connected with one or several triangles, making a triangular mesh, connected or not, depending on the configuration of points in the cube. Then the "local" meshes are grouped together to make the final mesh in $\mathbb{R}^3$.

We would then hope that the resulting mesh is an union of disjoint simplical surfaces [24] which separates the positive vertices to the negative vertices. However some *holes/cracks* can appear as shown on Figure 5.16, due to *ambiguities* in some configurations. In this case, the algorithm fails to produce

a piecewise linear manifold: some edges are the face of only one triangle, which means that they draw together the boundary of a hole in the surface. To obviate these ambiguities, Han *et al* [74] use *digital topology*: a couple of connectivities (among the 8-,18-, and 26-connectivities) is then associated to the positive and negative lattice points, to be able to decide which surface tiling has to be drawn (at each cube separatly). As usual, this couple must be a Jordan pair to avoid the connectivity paradox of Rosenfeld. Then there is only one possible tiling at each cube and positive and negative cubes are separated in each cube by the local tiling surface. The resulting mesh is *"digitally" topologically correct* in the sense that the surface tiling correctly reflects the topology of the initial isosurface $[f = \alpha]$ if the connectedness is well chosen. This algorithm is called *connectivity-consistent marching cubes* (CCMC).

Be careful not to amalgamate the topological correctness in the context of digital topology and the *topological correctness* used in isosurface extraction and which means that the approximating isosurface is homeomorphic to piecewise trilinear interpolation of the digitization of the given continuous scalar field.

However it is sometimes difficult to choose which connectivity is the best for the application, and then we would avoid to choose a connectivity, since the resulting mesh depends strongly on this choice. *Digital well-composedness* (in the sense that the sets and its complement do not contain any *critical configurations*) is then salutary: it has been stated in [86] that a cubic cell is unambiguous iff there exists a 6-path of positive (respectively negative) vertices in this cube connecting each pair of positive (respectively negative) vertices of this same cube, which is equivalent to well-composedness in 3D. This way, no choice of connectivity is needed anymore, since whatever the chosen connectivities the result will be the same. Moreover, $[f = \alpha]$ is a PL (*Piecewise Linear*) 2-manifold with no hole, and then its boundary is contained in the boundary of the cubical grid, what is called *topological consistency*.

Furthermore, Siqueira *et al.* proved in [153] that the isosurface resulting from the MC algorithm may reflect the topology of the initial continuous scalar field when the given binary image is well-composed. If for some reason, we are not able to make any well-composed interpolation or to use any topological repairing method, the use of the *Modified Marching Cubes algorithm (MMC)* [162] is a good choice, but it assumes that the digitized object

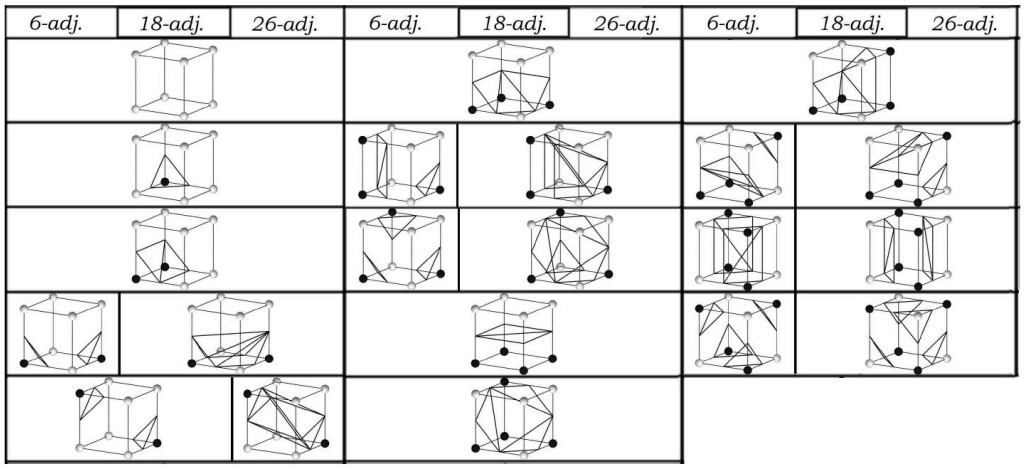

Figure 5.17: Lookup tables of Daragon [42, 43] in the 3D case.

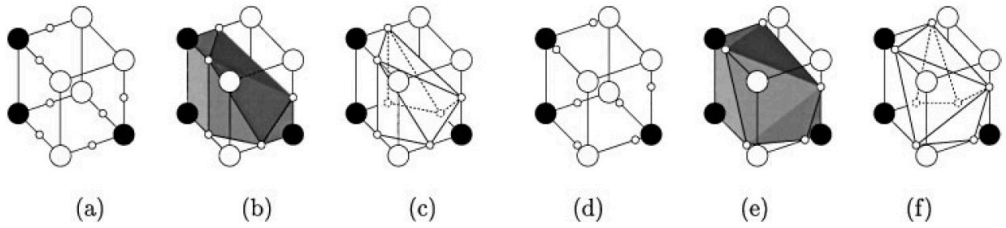

Figure 5.18: n-D approach of Lachaud [94], based on the convex hull.

is r-regular and that the sampling grid has a sufficient resolution.

Note that some very powerful MC-like methods exist for the n-dimensional case, $n \geq 2$, as the *frontier orders* of Daragon [42, 43] based on combinatorial topology and the *continuous analog of the digital boundary* of Lachaud and Montanvert [94] based on digital topology. Both obtain the same surface tilings in the 3D case, as shown on Figure 5.17, showing each possible configuration in the 3D case, assuming that we use 6-,18-, or 26-connectivity for the black points (and a dual connectivity for the white points). In other words, $(6, 18)$-connectivity will join the black points which are 6-connected, and will separate the black points which are only 18- or 26-connected. In the same time, it will join the white points which are 6- or 18-connected, and it will separate the white points which are only 26-connected. Note that the n-D approach of Lachaud is depicted on Figure 5.18, and consists

in computing in each cube separatly the boundary of the convex hull of the set of points made with the black points plus the boundary points (see (a), (b), and(c)). An equivalent approach but using a non trivial interpolating function is showed from (d) to (f). Under reasonable constraints, these two methods provide simplicial surfaces with no "holes", at least in the 3D case.

Finally, we can mention the existence of isosurface simplification algorithms [152, 83] used to reduce the excessive number of triangles produced by the MC algorithm in practice. These methods works particularly well with well-composed images since they preserve the topology of the boundary of the continuous analog of the foreground of a well-composed digital image [153].

Finally, we strongly think that a n-D image which is DWC has no possible local ambiguity. Effectively, assuming that we want to extract the isosurface of a set $X \subset \mathbb{Z}^n$, an ambiguity appears in a block $S \in \mathcal{B}(\mathbb{Z}^n)$ if and only if there exists two points p, p' in $X \cap S$ (respectively in $X^c \cap S$) which are α-connected but not β-connected, where α-connectivity and β-connectivity are two connectivities both implied by $2n$-connectivity, and such that they both imply $(3^n - 1)$-connectivity. However, if the set X is DWC, $(3^n - 1)$-connectivity in S of X (respectively of X^c) implies $2n$-connectivity. In other words, α-connectivity will imply $(3^n - 1)$ connectivity, which implies $2n$-connectivity, which implies β-connectivity, and conversely. In that sense, any pair of connectivities is be equivalent in any block S, and then no ambiguity is possible on the domain of the image. This reasoning leads us to the following conjecture:

Conjecture 5. *Let $u : \mathcal{D} \to \mathbb{R}$ be a real-valued DWC image defined on a domain $\mathcal{D}$. Then, u does not have any ambiguous cases. In other words, no "hole problem" is possible in n-D using DWC images.*

5.4 Tree of shapes of the sign of the DWC morphological Laplacian

In this section, we present some results of Huyhn *et al.* [80] obtained thanks to the computation of the tree of the sign of the (DWC) morphological Laplacian in a self-dual way. Even if it is used here for text detection, this approach can easily be extended to treat n-D signals, such as M.R images, videos, or CT-scans.

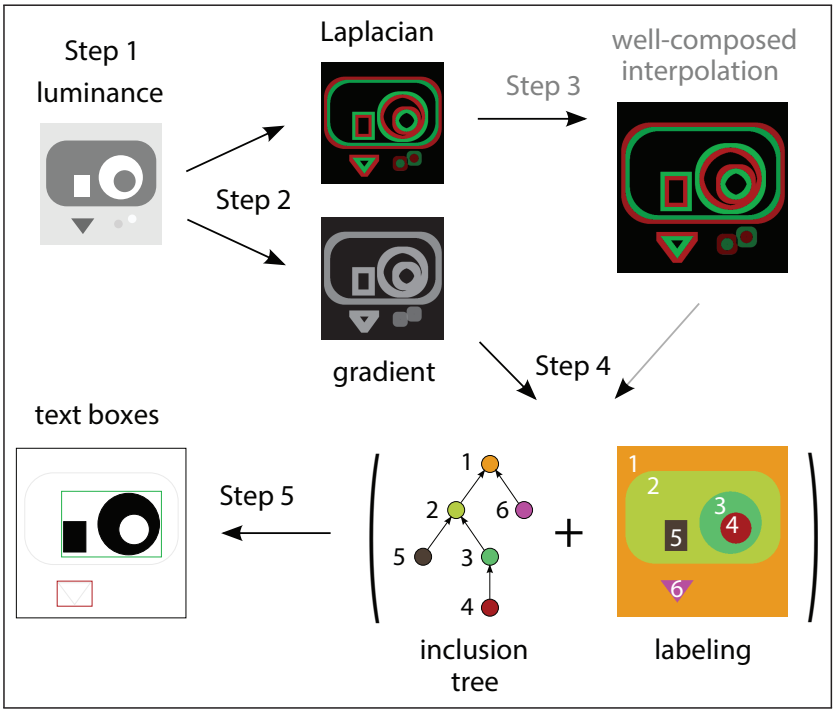

Figure 5.19: Summary of the method used by Huyhn *et al.* [80].

Nowadays, text detection methods [53, 181, 183] are widely used, especially on mobile devices, for recognition tasks. They are generally classified into *connected-components-based approaches*, like *FASText* [30], the *SWT* (Stroke Width Transform) [51], the *TMMS* (Toggle Mapping Morphological Segmentation), and the *MSER* (Maximally Stable Extremal Regions), or into sliding-windows approaches using *SVM* (Support Vector Machines) [36], *AdaBoost* [105], or *CNN* (Convolutional Neural Networks) [174] as classifiers.

The one presented by Huyhn *et al.* [80] is part of the connected-components-based approaches, and consists in transforming an image into a tree-based hierarchical representation (see Figure 5.19), based on adjacency and inclusion relationship between the components in the image.

To proceed, they compute the Laplacian of a given image using a *morphological Laplacian operator* [172, 156, 126], whose *zero-crossings* are known to be very precise contour estimations of the initial image. Using a large-sized structuring element relatively to the size of the text to detect, spurious contours are easily eliminated and salient contours preserved, thanks to the

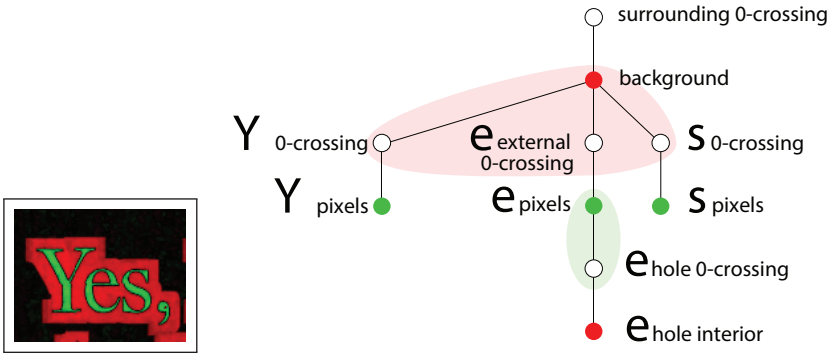

(a) $\Delta^{wc}(u)$. (b) Tree $\mathfrak{S}(\operatorname{sign}(\Delta^{wc}(u)))$.

Figure 5.20: An inclusion tree and its corresponding image [80].

non-linearity of the operator. After that, a self-dual well-composed interpolation (like the one we just presented) of this Laplacian is computed; this way, the zero-crossings of this interpolation are simple closed curves. Using these separated Jordan curves, we can naturally induce a hierarchy [28] in the image: saturation of these curves (whatever the chosen connectivity) are either nested or disjoint. A component labeling of the sign of the Laplacian and the generation of the inclusion tree are then straightforward and very fast (a classical blob labeling algorithm is sufficient).

Thanks to this tree-based representation of the image, they can extract text candidates: a hole of a character or a solid character are leafs of the tree (ss Figure 5.20), and so on. Text grouping is then simply a subtree of this inclusion tree, since characters must be grouped iff they belong to the same background.

Finally, in this context, well-composedness gave access to a very fast (linear time) and efficient self-dual text detection algorithm thanks to the hierarchy induced by the Jordan curves extracted from the well-composed Laplacian.

Chapter 6

Perspectives

In this chapter, we present some future works that seem promising and that are related to well-composedness.

6.1 About the equivalence between AWCness and CWCness on cubical grids

In digital topology, its is generally admitted that in 2D and 3D a finite set $X \subseteq \mathbb{Z}^n$ is continuous well-composed, that is, the boundary of its continuous analog $\mathrm{bdCA}(X)$ is a $(n-1)$-manifold, iff its immersion $\mathcal{IMM}(X) = \mathrm{Int}(\alpha(\mathcal{H}_n(X)))$ in the Khalimsky grids $\mathbb{H}^n$ is well-composed in the sense of Alexandrov, that is, its boundary is a disjoint union of discrete $(n-1)$-surfaces.

Starting from a finite subset $\mathcal{IMM}(X) \subseteq \mathbb{H}^n$, let us recall how we can proceed to build its *underlying polyhedron* into $\mathbb{R}^n$.

Definition 38 (Underlying Polyhedron)**.** *Let h_1 be an element of $\mathbb{H}^1$. We call* underlying polyhedron *of h_1 the set denoted by* $\mathrm{Poly}(h_1)$ *and defined such that:*

$$\mathrm{Poly}(h_1) = \begin{cases} \{a_1\} & \text{if } \exists a_1 \in \mathbb{Z} \text{ s.t.} h_1 = \{a_1\}, \\ [a_1, a_1+1] & \text{if } \exists a_1 \in \mathbb{Z} \text{ s.t.} h_1 = \{a_1, a_1+1\}. \end{cases}$$

In other words, a 0-face becomes a point in $\mathbb{R}$ and a 1-face becomes a closed unitary interval in $\mathbb{R}$. Then, for any face $h \in \mathbb{H}^n$, we define the underlying

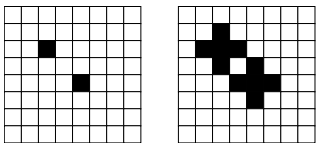

Figure 6.1: Morphological dilation does not preserve digital well-composedness using a structuring element based on 4-connectivity.

polyhedron *of the face h as the cartesian product of the underlying polyhedron of its coordinates:*

$$\mathrm{Poly}(h) = \otimes_{i\in[\![1,n]\!]}\mathrm{Poly}(h_i).$$

Finally, let $X \subseteq \mathbb{H}^n$ be a set of faces, then its underlying polyhedron *is defined as the union of the underlying polyhedron of its elements:*

$$\mathrm{Poly}(X) = \bigcup_{h\in X} \mathrm{Poly}(h).$$

Note that any of these underlying polyhedra are closed into $\mathbb{R}^n$.

This construction seems equivalent to construct the continuous analog in $\mathbb{R}^n$ with unitary n-cubes centered at the points of the set $\mathcal{Z}_n(\mathcal{X})$. Then we propose the following conjecture:

Conjecture 6. *Let X be a finite subset of $\mathbb{Z}^n$ and let $\mathcal{IMM}(X)$ be its immersion in $\mathbb{H}^n$. Then, $\mathcal{IMM}(X)$ is well-composed in the sense of Alexandrov iff X is continuous well-composed, that is, the boundary $\mathfrak{N}$ of $\mathcal{IMM}(X)$ in an disjoint union of (discrete) $(n-1)$-surfaces iff the topological boundary $\partial\mathrm{Poly}(\mathcal{IMM}(X)) = \mathrm{bdCA}(X)$ is a $(n-1)$-manifold.*

As for the equivalence between AWCness and DWCness, we believe that the cartesian product is a property which is essential to prove that CWCness and AWCness are equivalent. Furthermore, we can easily feel that the decomposition of $\mathbb{R}^n$ into $\{\mathrm{Poly}(h)\ ;\ h \in \mathbb{H}^n\}$ has the same structure as $\mathbb{H}^n_n$ whatever the dimension. For these reasons, we think that CWCness and AWCness are equivalent on cubical grids.

6.2 Preservation of Digital Well-composedness

In mathematical morphology, digital well-composedness is not usually "stable": even the simplest morphological operators like the dilation (see Figure 6.1 and Figure 6.2) and the erosion (see Figure 6.3 and Figure 6.4) do

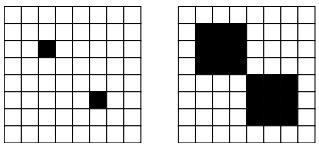

Figure 6.2: Morphological dilation does not preserve digital well-composedness using a structuring element based on 8-connectivity.

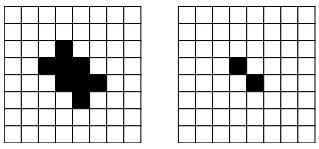

Figure 6.3: Morphological erosion does not preserve digital well-composedness using a structuring element based on 4-connectivity.

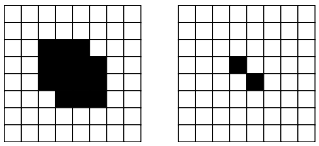

Figure 6.4: Morphological erosion does not preserve digital well-composedness using a structuring element based on 8-connectivity.

not preserve digital well-composedness. It is even worst with second order operators like the morphological Laplacian.

However, we are going to show that there exists some classes of morphological operators that preserve digital well-composedness. Among them, there exist the monotone plannings, a transformation which preserves the order between neighbouring pixels, and the grain filters, a transformation which removes components of small size in the hierarchical representation of the image (computed using the tree of shapes).

6.2.1 Monotone Plannings

In [119], Meyer and Maragos present a strong morphological filter, the *levelings*, whose definition is the following:

Definition 39 (Levelings)**.** *An image* $g : \mathcal{D} \subseteq (\mathbb{Z}/s)^n \to \mathbb{R}$ *is a* leveling *of*

the image $f : \mathcal{D} \to \mathbb{R}$ *iff* $\forall (p, q)$ *2n-neighbors in* $(\mathbb{Z}/s)^n$*:*

$$\{g(p > g(q)\} \Rightarrow \{f(p) \geq g(p) \text{ and } g(q) \geq f(q)\}.$$

The meaning of this definition is that if there exists a difference between two neighboring pixels in the leveling g, there exists an even greater difference in the original image f: "to any contour of a function g corresponds a stronger contour in the function f at the very same location, and the localisation of this contour is exactly the same". In other words, levelings are morphological scale-space filters, with nice properties (see [119]).

In fact, levelings correspond to a particular case of *monotone plannings* [119]:

Definition 40 (Monotone Plannings)**.** *An image* $g : \mathcal{D} \subseteq (\mathbb{Z}/s)^n \to \mathbb{R}$ *is a* monotone planning *of the image* $f : \mathcal{D} \to \mathbb{R}$ *iff* $\forall (p, q)$ *2n-neighbors in* $(\mathbb{Z}/s)^n$*:*

$$\{g(p > g(q)\} \Rightarrow \{f(p) > f(q)\}.$$

This definition called us to mind because monotone plannings constitute a class of transformation which preserves the relation order between neighboring pixels in an image, which is very close to digital well-composedness: if we assume that a 2D image g contains a critical configuration, it means that there exist two points p, p' which are antagonist in a 2D block S such that their value are strictly lower than the two other values in S. By definition of monotone plannings, the original image satisfies then this same order relation, and then the critical configuration is preserved. That means that in 2D, the monotone planning of a digitally well-composed image is digitally well-composed. We can even announce that this property is true in n-D, $n \geq 2$. To prove that, let us introduce some additionnal material.

Definition 41. *Let* z *be a point in* $(\mathbb{Z}/s)^n$*. We define the* 2n-neigborhood of order l*,* $l \geq 1$*, such that* $\mathcal{N}^1_{2n}(x, (\mathbb{Z}/s)^n) = \mathcal{N}_{2n}(x, (\mathbb{Z}/s)^n)$*, and:*

$$\mathcal{N}^l_{2n}(x, (\mathbb{Z}/s)^n) = \bigcup_{v \in \mathcal{N}^{l-1}_{2n}(x, (\mathbb{Z}/s)^n)} \mathcal{N}_{2n}(v, (\mathbb{Z}/s)^n),$$

when $l \geq 2$*. For sake of simplicity, we will also denote for* $l \geq 2$*:*

$$\delta\mathcal{N}^l_{2n}(p, (\mathbb{Z}/s)^n) = \mathcal{N}^l_{2n}(p, (\mathbb{Z}/s)^n) \setminus \mathcal{N}^{l-1}_{2n}(p, (\mathbb{Z}/s)^n).$$

Lemma 11. *Let $u : \mathcal{D} \subset (\mathbb{Z}/s)^n \to \mathbb{R}$ be a real-valued image defined on a bounded hyperrectangle $\mathcal{D}$ in $(\mathbb{Z}/s)^n$. Now, let $S^k \in \mathcal{B}(\mathcal{D})$ be a block of dimension $k \geq 2$ and p be a point in S^k such that $\forall n^1 \in S^k \cap \mathcal{N}_{2n}(p, (\mathbb{Z}/s)^n)$, $u(p) < u(n^1)$ (case 1), or such that $\forall n^1 \in S^k \cap \mathcal{N}_{2n}(p, (\mathbb{Z}/s)^n)$, $u(p) > u(n^1)$ (case 2). Let assume that the restriction of u to S^k is digitally well-composed Then, for any $l \in [\![2, k]\!]$, and for any $n^l \in S^k \cap \delta\mathcal{N}^l_{2n}(p, (\mathbb{Z}/s)^n)$, there exists a block S^l of dimension l included in S_k, such that there exists a $2n$-path $\pi = (p, n^1, \ldots, n^l) \subseteq S^l$ such that $\forall i \in [\![1, l]\!]$:*

$$n^i \in \delta\mathcal{N}^i_{2n}(p, (\mathbb{Z}/s)^n),$$

and:

$$u(p) < u(n^1) \leq \cdots \leq u(n^l), \qquad \textit{(case 1)}$$

or:

$$u(p) > u(n^1) \geq \cdots \geq u(n^l). \qquad \textit{(case 2)}$$

Proof: Let us proceed by induction on $l \in [\![2, k]\!]$ to prove Case 1, the proof of Case 2 being its dual.

Initialization ($l = 2$): Let $n^2 \in S^k \cap \delta\mathcal{N}^2_{2n}(p, (\mathbb{Z}/s)^n)$ be a point. n^2 is then antagonist of p in a 2D block $S^2 \subseteq S^k$. Since the restriction of u to S^2 is digitally well-composed, we have:

$$\text{intvl}(u(p), u(n^2)) \cap \text{Span}\{u(q)\ ;\ q \in S^2 \setminus \{p, n^2\}\} \neq \emptyset,$$

and then $u(n^2) \geq \min\{u(q)\ ;\ q \in S^2 \setminus \{p, n^2\}\}$. This way,

$$\pi = (p, \underset{q \in S^2 \setminus \{p, n^2\}}{\arg\min}\ (v(q)), n_2)$$

is the $2n$-path we are looking for.

Induction ($l \in [\![3, k]\!]$): we assume that the property is true for $(l-1)$. In other words, we assume that for any $n^{l-1} \in S^k \cap \delta\mathcal{N}^{l-1}_{2n}(p, (\mathbb{Z}/s)^n)$, there exists $S^{l-1} \in \mathcal{B}(S^k, (\mathbb{Z}/s)^n)$ and a $2n$-path in $(\mathbb{Z}/s)^n$:

$$\pi = (p, n^1, \ldots, n^{l-1}) \subseteq S^{l-1} \subset S^k$$

such that $u(p) < u(n^1) \leq u(n^2) \leq \cdots \leq u(n^{l-1})$ with $n^i \in S^{l-1} \cap \delta\mathcal{N}^i_{2n}(p, (\mathbb{Z}/s)^n)$ for any $i \in [\![1, l-1]\!]$. Then the following property comes out: $\forall q \in$

$S^k \cap \mathcal{N}_{2n}^{l-1}(p) \setminus \{p\}, u(p) < u(q)$. Let be now $n^l \in S^l \cap \delta\mathcal{N}_{2n}^l(p, (\mathbb{Z}/s)^n)$. If we assume that for any $r \in S^l \cap \mathcal{N}_{2n}(n^l, (\mathbb{Z}/s)^n)$, we have $u(n^l) < u(r)$, then by the induction hypothesis and following the same reasoning as for p in S^{l-1}, we obtain that there exists S_*^l of dimension l such that $p \in S_*^l$ and such that for all $s \in S_*^l \cap \mathcal{N}_{2n}^{l-1}(n^l) \setminus \{n^l\}$, $u(n^l) < u(s)$. In fact, $S^l = S_s(p, n^l) = S_s(n^l, p) = S_*^l$, and then we have that:

$$\max(u(p), u(n^l)) < \min\{u(q) \ ; \ q \in S^l \setminus \{p, n^l\}\},$$

which would imply that u contains a critical configuration into $S^l \subset S^k$, which is impossible. Then there exists $r^* \in S^l \cap \mathcal{N}_{2n}(n^l, (\mathbb{Z}/s)^n)$ such that $u(r^*) \leq u(n^l)$. Since r^* is a $2n$-neighbor of n^l such that it belongs to S^l, $r^* \in S^l \cap \mathcal{N}_{2n}^{l-1}(p)$, and then $(p, n^1, \ldots, n^{l-1} = r^*, n^l)$ is a $2n$-path in S^l as a subset of $(\mathbb{Z}/s)^n$ which satisfies $u(p) < u(n^1) \leq \cdots \leq u(n^l)$. □

Then we can announce our theorem:

Theorem 8. *Let $u : \mathcal{D} \subset (\mathbb{Z}/s)^n \to \mathbb{R}$ be a real-valued image defined on a bounded hyperrectangle $\mathcal{D}$, and let be $u' : \mathcal{D} \to \mathbb{R}$ be a monotone planning of u. If u is digitally well-composed, then u' is digitally well-composed too.*

Proof: Let us proof that if u' is not digitally well-composed and if u is digitally well-composed, we get a contradiction. If u' is not digitally well-composed, there exists a block $S^k \in \mathcal{B}(\mathcal{D}, (\mathbb{Z}/s)^n)$ of dimension $k \geq 2$ such that $p, p' \in S^k$ are antagonist in S^k and we have one of these two cases:

$$\begin{cases} \max(u'(p), u'(p')) < \min\{u'(q) \ ; \ q \in S_k \setminus \{p, p'\}\}, & (1) \\ \max\{u'(q) \ ; \ q \in S_k \setminus \{p, p'\}\} < \min(u'(p), u'(p')). & (2) \end{cases}$$

Let us treat the first case, the reasoning being dual for the second case.

From (1), it follows that:

$$\begin{cases} \forall n^1(p) \in \mathcal{N}_{2n}^*(p) \cap S^k, u'(p) < u'(n^1(p)), \\ \forall n^1(p') \in \mathcal{N}_{2n}^*(p') \cap S^k, u'(p) < u'(n^1(p')), \end{cases}$$

and u' being a monotone planning of u, we have also that:

$$\begin{cases} \forall n^1(p) \in \mathcal{N}_{2n}^*(p) \cap S^k, u(p) < u(n^1(p)), & (A) \\ \forall n^1(p') \in \mathcal{N}_{2n}^*(p') \cap S^k, u(p) < u(n^1(p')). & (A') \end{cases}$$

Figure 6.5: The original Barbara image.

Since u is assumed to be digitally well-composed, we have that the restriction of u to S^k is digitally well-composed. Then (A) implies by Lemma 11 that there exists a $2n$-path $(q^0 = p, \ldots, q^k = p')$ into S^k as a subset of $(\mathbb{Z}/s)^n$ going from p to p' such that $u(p) < u(q^1) \leq \cdots \leq u(p')$, and then $u(p) < u(p')$. From (A'), we obtain using Lemma 11 that $u(p') < u(p)$, which is impossible. We have a contradiction. Then u is not digitally well-composed. □

Obviously, since we have proven that all kind of monotone planning preserves digital well-composedness, it follows that levelings preserve also digital well-composedness.

6.2.2 Grain Filters

We observed that another class of filtering preserves digital well-composedness in morphological analysis: grain filters [31]. The principle is to decompose the image into an hierarchical representations of the shapes in the image, using the tree of shapes [32, 60], and to keep only the components such that their area is greater than a given threshold. Figure 6.5 shows the original Barbara image, Figure 6.6 shows the critical configurations contained in this image, and Figure 6.7 shows our self-dual interpolation of this image.

Figure 6.6: The 44417 critical configurations in the original Barbara image.

Figure 6.7: Our self-dual interpolation of the Barbara image.

Our observation is the following: grain filters preserve digital well-composedness, as depicted on Figure 6.8,Figure 6.9, Figure 6.10 corresponding to filtered DWC interpolations with different thresholds. The result is that any of these images is digitally well-composed.

Our explanation of this phenomenon is that the hierarchical representa-

Figure 6.8: A grain filter of the DWC interpolation of the Barbara image with a threshold $\lambda = 10$.

Figure 6.9: A grain filter of the DWC interpolation of the Barbara image with a threshold $\lambda = 320$.

tion of the interpolation consists in nested or disjoint connected components such that they do no touch each other, since no critical configurations occur in threshold sets of digitally well-composed images. Then, by applying

Figure 6.10: A grain filter of the DWC interpolation of the Barbara image with a threshold $\lambda = 1280$.

the grain filter, we juste remove some shapes, and in this manner we just "simplify" the hierarchical representation of the image, and then the reconstructed image must be digitally well-composed.

6.2.3 Geodesic Dilations/Erosions

We remarked that another class of operations preserves digital well-composedness: geodesic dilations and erosions, much used in mathematical morphology. Geodesic dilation basically consists in starting from a given binary image considered as the *mask*, that we associate to a *marker image* representing the "seeds" lying in this subset. Applying the geodesic dilation is then equivalent to dilate progressively the seeds in the space corresponding to the mask, such that they will completely fill the connected components of the initial set, since dilation outside the set is forbidden. In this manner, geodesic dilation simply extracts some connected components of a set depending on the associated initial marker.

Starting from a digitally well-composed binary image where connected components have Jordan curves as boundaries and do not "touch" each other, geodesic dilation choose among these connected components which ones are kept and which ones are rejected, and in this manner preserves the digital

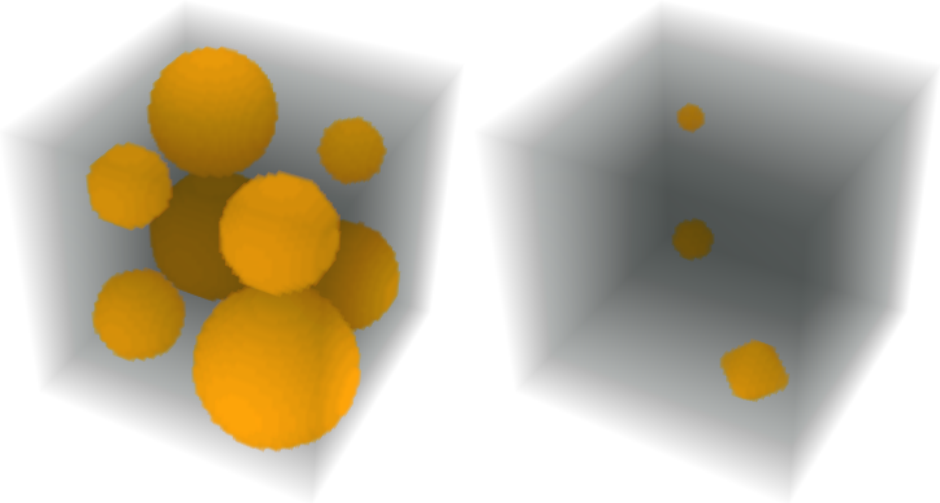

Figure 6.11: A 3D digitally well-composed binary image, the *mask*, and a marker of the same size.

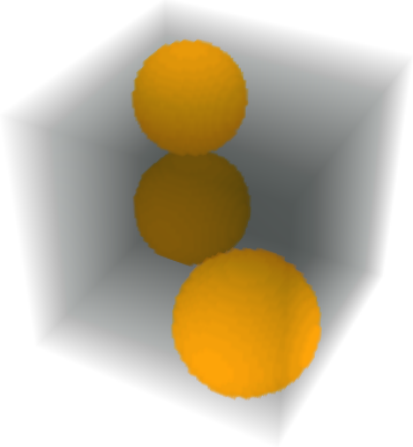

Figure 6.12: The geodesic dilation of the marker in the binary image is also digitally well-composed.

well-composedness of this binary image. Note that this selection of which components the algorithm keeps strongly recalls the grain filters of the section before.

The geodesic erosion is simply the dual of the geodesic dilation, and the geodesic dilation/erosion for graylevel is the natural extension of their

binary version using cross-section topology. For these reasons, we think that geodesic dilations and erosion preserve digital well-composedness.

6.2.4 Conclusion

Finally, as proven by Theorem 8 and showed by the experimental results we obtained with grain filters, the class of transformations which preserve digital well-composedness is much larger that we could believe: monotone plannings, geodesic dilations/erosions, and grain filters, and certainly shapings [178] in general, preserve digital well-composedness in the sense that they only remove shapes in the hierarchical representation of the image.

6.3 Graph-based Characterizations of AWCness and DWCness

These approaches are based on *regional minima* and *regional minima* in graphs, that we define such that:

Definition 42 (Regional extrema)**.** *Let $G = (V, E)$ be a graph valued by a map $u : V \to \mathbb{R}$. We say that a connected component $\mathfrak{P}$ of G is a* plateau *iff there exists $v \in \mathbb{R}$ such that for any element p of $\mathfrak{P}$, the value $u(p)$ is equal to v. We call v the* value *of the plateau. We call a* regional minima *(respectively a* regional maxima*) a plateau $\mathfrak{P}$ of G (associated to its value) such that for any neighbor q of $\mathfrak{P}$ which does not belong to $\mathfrak{P}$, the value $u(q)$ is strictly lower (respectively strictly greater) than the value of $\mathfrak{P}$. Regional minima and maxima are both said to be* regional extrema*.*

6.3.1 Graph-based Characterization of AWCness

Note that this section needs some prerequisites presented into Chapters C and E.

We recall that a partially ordered set $|X| = (X, \alpha)$ is said to be a discrete 0-surface if it made of two points which are not neighbor the one of the other one, and a n-surface, $n \geq 1$, is defined such as it is connected and for any point z belonging to X, the order $|\theta_X^{\square}(x)|$ is a $(n-1)$-surface. It is therefore easy to check if a set is a n-surface with a recursive program. Hence, it is easy to check whether a digital set is well-composed in the sense of Alexandrov

Figure 6.13: A discretized sphere with values on the 2-faces.

in n-D. However, even if a 0-surface or a 1-surface are easy to interpret, it becomes harder to get the intuition of a 2-surface and higher.

Also, assuming that we are able to check in a short time whether a set in an Alexandrov space is AWC, it seems much longer to check if a real-valued, or even integer-valued, image is AWC, in particular in the dynamic of the image is high or if the quantification has a very high resolution: assuming that the domain $\mathcal{D}$ of the image $u : \mathcal{D} \to \mathbb{R}$, made of n-faces, is finite, whatever if it is cubical or not, we should check if, for any λ belonging to the space of the image, the closures of the threshold sets $[u \geq \lambda]$ and $[u \leq \lambda]$ are AWC. Then it can be much interesting to find a characterization of AWCness, like the one of DWCness on bounded hyperrectangles of $(\mathbb{Z}/s)^n$.

Figure 6.13 depicts a triangulated sphere whose 2-faces are valued by a real-valued function. The idea is then to find a new method able to check whether this function is AWC without checking the AWCness of the closure

of every threshold set.

Let us recall that, for any polyhedral complex $\mathfrak{PC}^n$, the set $\mathfrak{PC}^n_n$ denotes the k-faces of this complex, and that in the polyhedral complexes presented here, the infimum between two faces h^1, h^2, assumed to be well-defined when $\alpha(h^1) \cap \alpha(h^2)$ is non-empty, in this complex is denoted $h^1 \wedge h^2$ and is defined as the supremum of the set $\alpha(h^1) \cap \alpha(h^2)$.

Conjecture 7 (Graph-based Characterization of AWCness)**.** *Let $\mathfrak{PC}^n$ be any polyhedral complex of rank $n \geq 2$ which is a n-surface (bordered or not). Let u be any real-valued map defined on the n-faces of this complex. The real map u is AWC iff on $\mathfrak{PC}^n$ iff for any $z \in \mathfrak{PC}^n_k$, $k \in [\![0, n-1]\!]$, the valued graph $\mathcal{G}(u, z) = (V, E)$ defined such that the set of vertices is defined such that:*

$$V = \left\{ u(h) \; ; \; h \in \beta^{\square}_{\mathfrak{PC}^n}(z) \cap \mathfrak{PC}^n_n \right\},$$

and such that the set of edges is defined such that:

$$E = \left\{ (h^1, h^2) \in \mathfrak{PC}^n \times \mathfrak{PC}^n \; ; \; h^1 \wedge h^2 \in \mathfrak{PC}^n_{n-1} \right\},$$

admits exactly one regional maximum and one regional minimum.

Figure 6.14 depicts how we can determine if a 2D image is well-composed in the sense of Alexandrov, and furthermore for which values $\lambda \in \mathbb{R}$ the threshold sets $[u \geq \lambda]$ and $[u \leq \lambda]$ are not well-composed in the sense of Alexandrov: by observing the values of u into the open neighborhood of the 0-face z^1, we can see that the graph $\mathcal{G}(u, z^1)$ contains two maxima, circled in red, and two minima, circled in green. From that, we can respectively deduce that $[u \geq 8]$ and $[u \leq 4]$ are not well-composed in the sense of Alexandrov. Observing the graph $\mathcal{G}(u, z^3)$, we can observe in the same manner that $[u \geq 6]$ and that $[u \leq 2]$ are not well-composed in the sense of Alexandrov.

At the contrary, we can observe that the graph $\mathcal{G}(u, z^2)$ admits one only minimum, which is equal to 1, and one maximum, which is equal to 5. This, way, our conjecture says that this restriction of u to this subcomplex is well-composed in the sense of Alexandrov, and effectively we can depict that the boundary of each threshold sets is a 1-surface as shown on Figure 6.15.

As depicted on the octahedron in Figure 6.16, our method works also in 3D (and more): we have two points in $\mathcal{G}(u, z)$ whose value is one, they are the maxima of $\mathcal{G}(u, z^*)$, and we have only one minima, the connected component

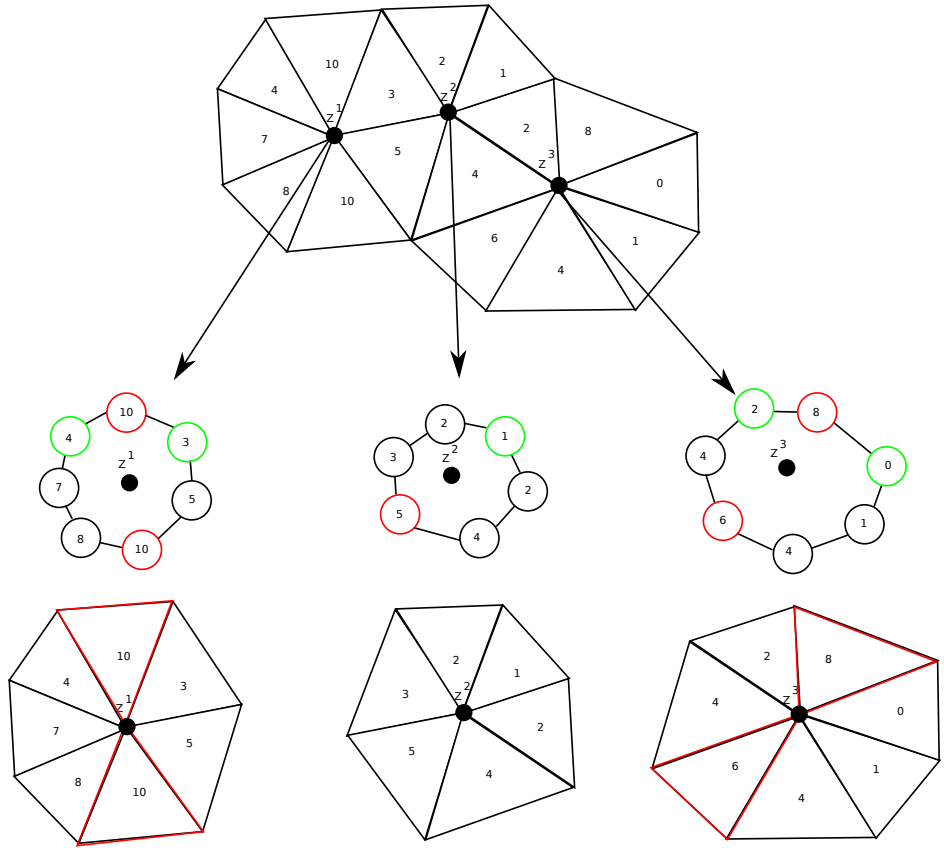

Figure 6.14: How to characterize AWCness in 2D.

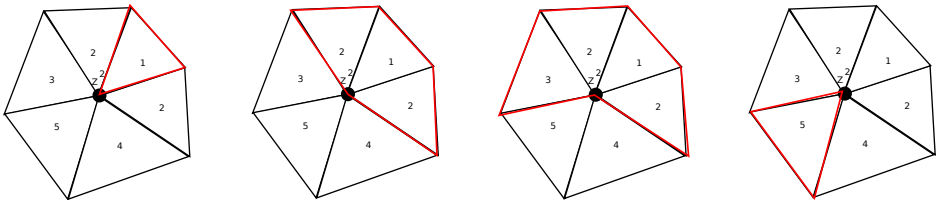

Figure 6.15: Boundaries of the different threshold sets around z^2.

corresponding to the value 0 in $\mathcal{G}(u, z^*)$. This means that u is not AWC. Note that we can observe that it is crucial that we have at the same time one only minimum and only maximum in each graph $\mathcal{G}(u, z)$, since we can have a "pinch" and at the same time one only minimum in $\mathcal{G}(u, z^*)$, where z^* is the point where this pinch occurs.

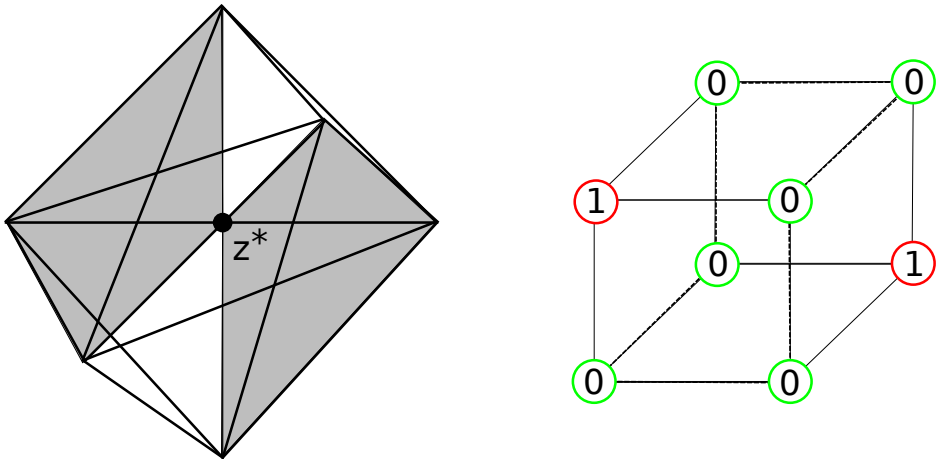

Figure 6.16: A 3D image which is not AWC.

6.3.2 Graph-based Characterization of DWCness

Let us show that we can characterize DWC functions defined on bounded hyperrectangles in $\mathbb{Z}^n$ (and then in $(\mathbb{Z}/s)^n$) using graphs.

Notations 1 (Graph associated to $u\big|_{\mathbb{A}(z)}$)**.** *Let u be a real-valued function on a bounded hyperrectangle $\mathcal{D} \subset \mathbb{Z}^n$ and let $\mathcal{D}'$ be the smallest hyperrectangle containing $\mathcal{D}$ and subset of $\left(\frac{\mathbb{Z}}{2}\right)^n$. For any element $z \in \mathcal{D}'$, the graph $\mathcal{G}(u,z) = (V,E)$ (corresponding to $u\big|_{\mathbb{A}(z)}$) is defined such that:*

$$V = \{(p, u(p)) \; ; \; p \in \mathbb{A}(z)\},$$

and:

$$E = \mathcal{N}_{2n} \cap V \times V.$$

In the sequel, we proceed in two steps: first we show that the digital well-composedness of u is equivalent to say that for any threshold $\lambda \in \mathbb{R}$, and for any z belonging to $\mathcal{D}'$, the sets $[u\big|_{\mathbb{A}(z)} \geq \lambda]$, $[u\big|_{\mathbb{A}(z)} \leq \lambda]$, $[u\big|_{\mathbb{A}(z)} > \lambda]$ and $[u\big|_{\mathbb{A}(z)} < \lambda]$ are $2n$-connected, and then we will prove that this property is equivalent to have for any $z \in \mathcal{D}'$, and for any $\lambda \in \mathbb{R}$, that the valued graph $\mathcal{G}(u,z)$ (see Figure 6.17) admits exactly one maxima and one minima, which corresponds to our new characterization of DWCness.

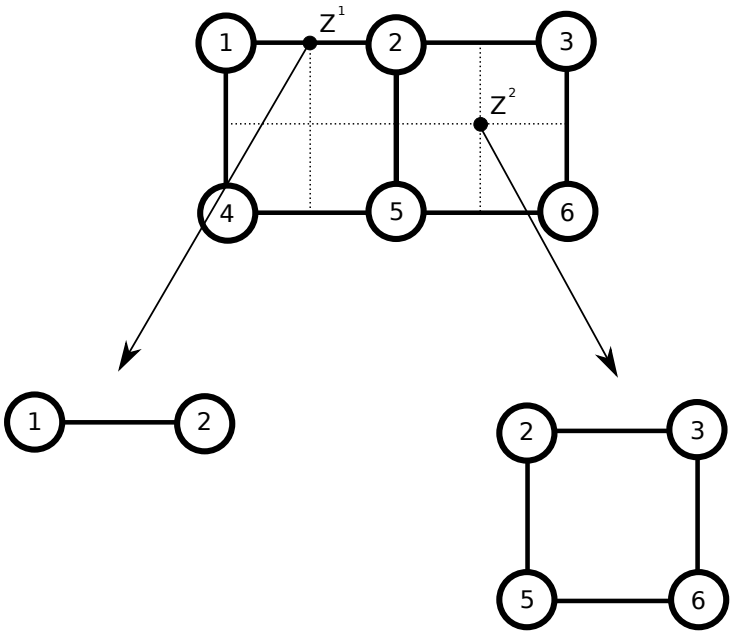

Figure 6.17: Some examples of graphs $\mathcal{G}(u, z)$.

Proposition 22. *Let $u : \mathcal{D} \subset \mathbb{Z}^n \to \mathbb{R}$ be a real-valued image defined on a bounded hyperrectangle $\mathcal{D}$ of $\mathbb{Z}^n$. Then, u is digitally well-composed iff for any value $\lambda \in \mathbb{R}$ and for any block $S \in \mathcal{B}(\mathcal{D}, \mathbb{Z}^n)$, the sets $[u \geq \lambda] \cap S$, $[u \leq \lambda] \cap S$, $[u > \lambda] \cap S$, and $[u < \lambda] \cap S$ are $2n$-connected sets.*

Proof: u is DWC implies that for any value $\lambda \in \mathbb{R}$, $[u \geq \lambda]$, $[u \leq \lambda]$, $[u > \lambda]$, $[u < \lambda]$ are DWC, which implies that for any block $S \in \mathcal{B}(\mathcal{D}, \mathbb{Z}^n)$, $[u \geq \lambda] \cap S$, $[u \leq \lambda] \cap S$, $[u > \lambda] \cap S$, and $[u < \lambda] \cap S$ are $2n$-connected sets: any two points of one of these sets are antagonists in this set and then are connected by a $2n$-path in this set. Conversely, the fact that, for any block $S \in \mathcal{B}(\mathcal{D}, \mathbb{Z}^n)$, the sets $[u \geq \lambda] \cap S$ and $S \setminus [u \geq \lambda] = [u < \lambda] \cap S$ are $2n$-connected implies that u is DWC (because no critical configuration is possible then). □

For the second step, we need to formulate some definitions and lemmas.

Definition 43. *Let $\mathcal{G} = (V, E)$ be a valued graph whose vertices are valued by a real-valued function u. Now, let us define the set of regional maxima $\{M^i\}_{i \in \mathcal{I}}$ such that their respective values are in decreasing order: $\forall i_1, i_2 \in \mathcal{I}, i_1 > i_2 \Rightarrow v_{i_1} \leq v_{i_2}$ where v_{i_1} is the value of M^{i_1} and v_{i_2} is the one of M^{i_2}.*

Then we say that M_1 is the first regional maxima *of $\mathcal{G}$. Also, if* $\mathrm{Card}\,(\mathcal{I}) \geq 2$, *we say that $\mathcal{G}$ admits a second maximal region. M_2 is then called the* second regional maxima *of $\mathcal{G}$. Note that the first and the second regional maxima of a graph can have the same value.*

Definition 44 ($2n$-adjacency)**.** *Let $A \subset \mathbb{Z}^n$ be a subset of $\mathbb{Z}^n$. We say that $x \in \mathbb{Z}^n$ is* $2n$-adjacent *to A iff x does not belong to A and there exists $q \in A$ such that p and q are $2n$-neighbours.*

Definition 45 ($2n$-separated)**.** *Let A, B be two finite subsets of $\mathbb{Z}^n$. We say that A and B are* $2n$-separated *iff the following relation holds:*

$$(\mathcal{N}_{2n}(A) \cap B) \cup (\mathcal{N}_{2n}(B) \cap A) = \emptyset.$$

Lemma 12. *Let $\mathcal{G} = (V, E)$ a graph valued on its vertices $V \subseteq \mathbb{Z}^n$ by a real-valued function $u : V \to \mathbb{R}$, such that* $\mathrm{Card}\,(V) < \infty$ *and G is connected as a graph. We denote then by $M^1 \subseteq V$ the first regional maxima of $\mathcal{G}$, by λ^1 its value, and by p^1 any element of the regional maxima. Then, we obtain:*

$$M^1 = \mathcal{CC}_{2n}([u \geq \lambda^1], p^1).$$

Furthermore, if $\mathcal{G}$ admits a second regional maxima, we denote respectively by $M^2 \subset V$,λ^2 and p^2 this regional maxima, its value, and one of its elements, and we define:

$$M^1_+ = \mathcal{CC}_{2n}([u \geq \lambda^2], p^1).$$

Then we obtain that there exists some $p^2 \in [u \geq \lambda^2] \setminus M^1_+$ such that:

$$M^2 = \mathcal{CC}_{2n}([u \geq \lambda^2], p^2),$$

with $\lambda^2 \leq \lambda^1$ Finally, M^1_+ and M^2 are $2n$-separated.

Proof: Let $\mathcal{G} = (V, E)$ be a graph and let u be a real-valued function defined on V. V is assumed to be $2n$-connected and its cardinal is finite. Now let us denote by $(M^i, \lambda^i)_{i \in \mathcal{I}}$ the family of regional maxima of $\mathcal{G}$ sorted by decreasing order of value λ^i.

Let us say that p^1 belongs to the set $\{p \in V \ ; \ u(p) = \max_{v \in V}\{u(v)\}\}$ and let us show that $M^1 = \mathcal{CC}_{2n}([u \geq \lambda^1], p^1)$ is a first regional maximum of u. Firstly, M^1 is connected by construction. Secundly, the value at each point of M^1 is the same. Thirdly, there does not exist a greater plateau which

contains p^1, and this way, any element $q \in V$ which is $2n$-adjacent to M^1 admits a value $u(q)$ which is strictly lower than $u(p^1)$. Then, M^1 is a first regional maxima of $\mathcal{G}$.

Obviously, for $i, j \in \mathcal{I}$ such that $i \neq j$, M^i and M^j are $2n$-separated: if $M^i \cap \mathcal{N}_{2n}(M^j) \neq \emptyset$, there exists $p^i \in M^i$ and $p^j \in M^j$ such that $u(p^i) \geq u(p^j)$ (because p^i belongs to the regional maxima M^i) and such that $u(p^j) \geq u(p^i)$ (because p^j belongs to the regional maxima M^j). This way, $u(p^i) = u(p^j)$ and $M^i = M^j$, which is impossible.

Now let us admit that $\mathcal{G}$ admits at least two regional maxima, it is clear that $\lambda^2 \leq \lambda^1$, due to the sorting of the family $(M^i, \lambda^i)_{i \in \mathcal{I}}$.

Let us now prove that the second regional maxima M^2 can be written $\mathcal{CC}_{2n}([u \geq \lambda^2], p^2)$ for some $p^2 \in [u \geq \lambda^2] \setminus M^1_+$. If p^2 belongs to M^1_+ which is a connected component of $[u \geq \lambda^2]$, then $\mathcal{CC}_{2n}([u \geq \lambda^2], p^2) = M^1_+$, which means that this component contains M^1, which is impossible. Also, let us assume that p^2 belongs to $[u < \lambda^2]$, it is obvious that $\mathcal{CC}_{2n}([u \geq \lambda^2], p^2) = \emptyset$, which is impossible too. Then, necessarily, p^2 belongs to $[u \geq \lambda^2] \setminus M^1_+$. Let us now show that it is a sufficient condition. Let us assume that p^2 belongs to this set, then $\mathcal{CC}_{2n}([u \geq \lambda^2], p^2)$ is non-empty since $u(p^2) \geq \lambda^2$. Also, this component is a plateau: if there exists a point in this component such that its corresponding value is strictly greater than λ^2, then λ^2 does not correspond to the secund regional maxima in V. Also, for any element q of V which is $2n$-adjacent to this component, $u(q) < \lambda$. Then, $M^2 = \mathcal{CC}_{2n}([u \geq \lambda^2], p^2)$. Let us remark that by definition, M^1 and M^2 are $2n$-separated.

Let us show now that M^1_+ and M^2 are effectively $2n$-separated. If the intersection of M^2 and $\mathcal{N}_{2n}(M^1_+, \mathbb{Z}^n)$ is non-empty, there exists $v^2 \in M^2$ and $v^1 \in M^1_+$ such that $v^1 \in \mathcal{N}_{2n}(v^2, \mathbb{Z}^n)$. This way, $\mathcal{CC}_{2n}([u \geq \lambda^2], p^2) = \mathcal{CC}_{2n}([u \geq \lambda^2], v^2)$ contains v^1 (because $u(v^1) \geq \lambda^2$), and then M^2 contains M^1_+, which would imply that M^2 contains M^1, which is impossible since they are disjoint. A same reasoning will show that $\mathcal{N}_{2n}(M^2, \mathbb{Z}^n) \cap M^1_+ \neq \emptyset$ is impossible too, and then M^2 and M^1_+ are $2n$-separated. □

Lemma 13. *Let $\mathcal{G} = (V, E)$ a graph valued on its vertices $V \subseteq \mathbb{Z}^n$ by a real-valued function $u : V \to \mathbb{R}$, such that* $\mathrm{Card}\,(V) < \infty$ *and G is connected as a graph. We denote then by $m^1 \subseteq V$ the first regional minima of $\mathcal{G}$, by μ^1 its value, and by p^1 any element of the regional minima. Then, we obtain:*

$$m^1 = \mathcal{CC}_{2n}([u \leq \mu^1], p^1).$$

Furthermore, if $\mathcal{G}$ admits a second regional minima, we denote respectively by $m^2 \subset V$, μ^2 and p^2 this regional minima, its value, and one of its elements, and we define:

$$m^1_+ = \mathcal{CC}_{2n}([u \leq \mu^2], p^1).$$

Then we obtain that there exists some $p^2 \in [u \leq \mu^2] \setminus m^1_+$ such that:

$$m^2 = \mathcal{CC}_{2n}([u \leq \mu^2], p^2),$$

with $\mu^2 \geq \mu^1$ Finally, m^1_+ and m^2 are $2n$-separated.

Proof: We can prove this lemma by a reasoning dual to the proof of Lemma 12. □

Notations 2 (Graph associated to $u\big|_S$)**.** *Let u be a real-valued function on a bounded hyperrectangle $\mathcal{D} \subset \mathbb{Z}^n$. For any block $S \in \mathcal{B}(\mathcal{D}, \mathbb{Z}^n)$, the graph $\mathcal{G} = (V, E)$ (corresponding to $u\big|_S$) is defined such that:*

$$V = \{(p, u(p)) \; ; \; p \in S\},$$

and:

$$E = \mathcal{N}_{2n} \cap V \times V.$$

Lemma 14. *Let $u : \mathcal{D} \subset \mathbb{Z}^n \to \mathbb{R}$ be a real-valued image defined on a bounded hyperrectangle $\mathcal{D}$, and let be a block $S \in \mathcal{B}(\mathcal{D}, \mathbb{Z}^n)$. If there exists a value $\lambda \in \mathbb{R}$ such that $[u \geq \lambda] \cap S$ is not $2n$-connected, then u admits strictly more than one maxima on the graph corresponding to $u\big|_S$.*

Proof: Let us assume that there exists some λ such that $[u \geq \lambda] \cap S$ is not $2n$-connected. It is sufficient to show that each $2n$-component of $[u \geq \lambda] \cap S$ contains at least one regional maximum of $u\big|_S$. Let $\{M^i_\lambda\}_{i \in \mathcal{I}} = \mathcal{CC}_{2n}([u \geq \lambda] \cap S)$ be the family of connected components of $[u \geq \lambda] \cap S$. Obviously, $\text{Card}\,(\mathcal{I}) \geq 2$. Let i be an index in $\mathcal{I}$, and let λ^i be the value $\max_{p \in S^i}\{u(p)\}$, we can then choose any point p^i in $\{p \in M^i_\lambda \; ; \; u(p) = \lambda^i\}$ and $M^i = \mathcal{CC}_{2n}([u \geq \lambda^i] \cap S, p^i)$. Let us show that M^i is a regional maxima of u in S. Firstly, M^i is $2n$-connected by definition. Secundly, M^i is a plateau (since λ^i is the maximal value of u in this component), and is maximal for the inclusion by construction. Thirdly, any point q of S which is $2n$-adjacent to M^i satisfies $u(q) < \lambda^i$. Each component M^i is then a regional maximum of u into S.

To prove that there exist more than two regional maxima, let us prove for each $i \in \mathcal{I}$, the component M^i is contained into M^i_λ. Effectively, λ^i is greater than or equal to λ by construction, and then $[u \geq \lambda^i] \subseteq [u \geq \lambda]$, which implies that $[u \geq \lambda^i] \cap S \subseteq [u \geq \lambda] \cap S$. Since $u(p^i) = \lambda^i \geq \lambda$ and $p^i \in S$, p^i belongs to $[u \geq \lambda] \cap S$ and then:

$$\mathcal{CC}_{2n}([u \geq \lambda^i] \cap S, p^i) \subseteq \mathcal{CC}_{2n}([u \geq \lambda] \cap S, p^i),$$

which means that M^i is included into M^i_λ. Based on this observation, we obtain that M^1 and M^2 are two separated regional maxima since:

$$\begin{cases} \mathcal{N}_{2n}(M^1) \cap M^2 \subseteq \mathcal{N}_{2n}(M^1_\lambda) \cap M^2_\lambda = \emptyset, \\ \mathcal{N}_{2n}(M^2) \cap M^1 \subseteq \mathcal{N}_{2n}(M^2_\lambda) \cap M^1_\lambda = \emptyset. \end{cases}$$

□

Lemma 15. *Let $u : \mathcal{D} \subset \mathbb{Z}^n \to \mathbb{R}$ be a real-valued image defined on a bounded hyperrectangle $\mathcal{D}$, and let be a block $S \in \mathcal{B}(\mathcal{D}, \mathbb{Z}^n)$. If there exists a value $\lambda \in \mathbb{R}$ such that $[u \leq \lambda] \cap S$ is not $2n$-connected, then u admits strictly more than one minima on the graph corresponding to $u\big|_S$.*

Proof: the proof is dual to the one of Lemma 14.

Proposition 23. *Let $u : \mathcal{D} \subset \mathbb{Z}^n \to \mathbb{R}$ be a real-valued image defined on a bounded hyperrectangle $\mathcal{D}$ of $\mathbb{Z}^n$. Then, for any $z \in \mathcal{D}'$, the graph $\mathcal{G}(u, z)$ admits exactly one regional maxima and one regional minima iff for any value $\lambda \in \mathbb{R}$ and for any block $S \in \mathcal{B}(\mathcal{D}, \mathbb{Z}^n)$, the sets $[u \geq \lambda] \cap S$, $[u \leq \lambda] \cap S$, $[u > \lambda] \cap S$ and $[u > \lambda] \cap S$ are $2n$-connected sets.*

Proof: Let us assume that for any value $\lambda \in \mathbb{R}$ and for any block $S \in \mathcal{B}(\mathcal{D}, \mathbb{Z}^n)$, the sets $[u \geq \lambda] \cap S$, $[u \leq \lambda] \cap S$, $[u > \lambda] \cap S$ and $[u > \lambda] \cap S$ are $2n$-connected sets, and let us show that for any $z \in \mathcal{D}'$, the graph $\mathcal{G}(u, z)$ corresponding to $u\big|_{\mathbb{A}(z)}$ admits exactly one regional maxima and one regional minima. For that, let us assume that $\mathcal{G}(u, z)$ admits two regional maxima on the block $S = \mathbb{A}(z)$ of $\mathbb{Z}^n$. Since S is $2n$-connected and finite (because n is finite), and since $u\big|_{\mathbb{A}(z)}$ is a real-valued function, we can apply Lemma 12. This way, we obtain that (M^1, λ^1) is the first regional maxima of $\mathcal{G}(u, z)$ such that $M^1 = \mathcal{CC}_{2n}([u \geq \lambda^1] \cap S, p^1)$ with p^1 an element of V such that

$u(p^1) = \lambda^1 = \max_{v \in S}\{u(v)\}$, and (M^2, λ^2) is the second regional maxima of $\mathcal{G}(u, z)$ such that $M^2 = \mathcal{CC}_{2n}([u \geq \lambda^2] \cap S, p^2)$ with p^2 an element of $[u \geq \lambda^2] \setminus M^1_+$, where $M^1_+ = \mathcal{CC}_{2n}([u \geq \lambda^2] \cap S, p^1)$. Furthermore, M^1_+ and M^2 are separated. This means that M^1_+ and M^2 are two disjoint connected components of $[u \geq \lambda^2] \cap S$, which is connected by hypothesis. We obtain a contradiction, and then $u\big|_{\mathbb{A}(z)}$ admits one unique maximum. The same reasoning applies for the minima of $u\big|_{\mathbb{A}(z)}$ by Lemma 13.

Conversely, we assume that for any $z \in \mathcal{D}'$ with $\mathcal{D}'$ the smallest hyperrectangle containing $\mathcal{D}$ in $(\mathbb{Z}/2)^n$, we have that the graph $\mathcal{G}(u, z)$ corresponding to $u\big|_{\mathbb{A}(z)}$ admits one maximum and one minimum. Let us now assume that there exists some $\lambda \in \mathbb{R}$ such that $[u \geq \lambda] \cap \mathbb{A}(z)$ is not $2n$-connected (or equivalently such that $[u > \lambda] \cap \mathbb{A}(z)$ is not $2n$-connected since we work with a finite number of values). Then, by Lemma 14, the restriction of u to $\mathbb{A}(z)$ contains at least two maxima, and then $\mathcal{G}(u, z)$ has at least two maxima too. A dual reasoning using Lemma 15 will show that if $[u \leq \lambda] \cap \mathbb{A}(z)$ is not $2n$-connected (or equivalently if $[u < \lambda] \cap \mathbb{A}(z)$ is not $2n$-connected), the restriction of u to S contains at least two minima, and then $\mathcal{G}(u, z)$ has at least two minima. This proves that for any $\lambda \in \mathbb{R}$, the sets $[u \geq \lambda] \cap \mathbb{A}(z)$, $[u \leq \lambda] \cap \mathbb{A}(z)$, $[u > \lambda] \cap \mathbb{A}(z)$ and $[u < \lambda] \cap V$ are $2n$-connected. □

Theorem 9 (Graph-based characterization of DWCness)**.** *Let $u : \mathcal{D} \subset \mathbb{Z}^n \to \mathbb{R}$ be a real-valued image defined on a bounded hyperrectangle $\mathcal{D}$ of $\mathbb{Z}^n$. Now, let $\mathcal{D}'$ be the smallest hyperrectangle in $(\mathbb{Z}/2)^n$ such that it contains $\mathcal{D}$. Then, u is DWC on $\mathcal{D}$ iff for any element $z \in \mathcal{D}'$, the graph $\mathcal{G}(u, z) = (V, E)$ admits only one regional maxima and only one regional minima.*

Proof: This is the result of Propositions 22 and 23. □

6.4 n-D Segmentation and Parameterization

Combining the conjecture that DWCness and CWCness are equivalent on cubical grids in n-D, and the conjecture that geodesic dilation preserves DWCness in n-D, we can segment gray-level images such that the final segmentation result is CWC. This result permits then to (locally) parameterize the topological boundary of the object (thanks to *coordinate charts* [104]), this one being a topological $(n-1)$-manifold.

(a) u.

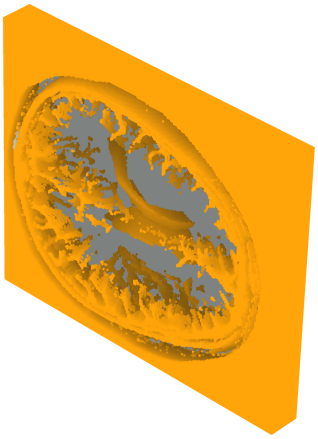

(b) $[u \geq \lambda]$

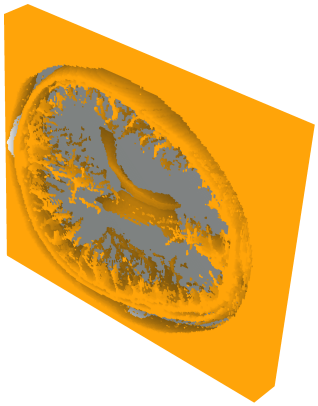

(c) $[u_{\mathrm{DWC}} \geq \lambda]$

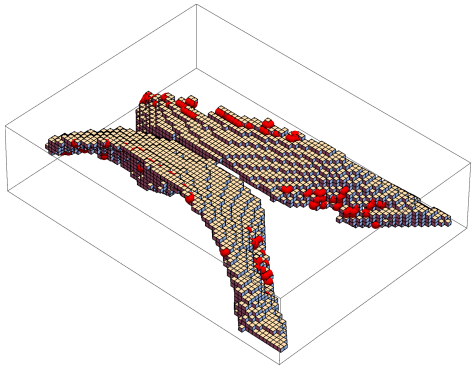

(d) $\partial\delta_{\mathrm{Geod}}[u \geq \lambda]$

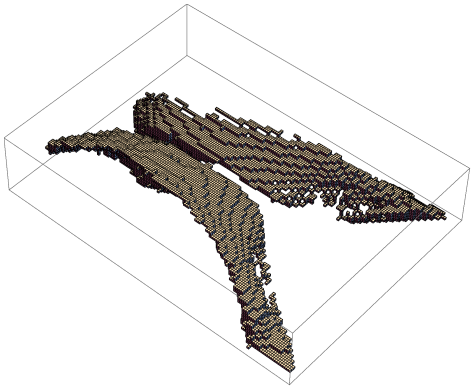

(e) $\partial\delta_{\mathrm{Geod}}[u_{\mathrm{DWC}} \geq \lambda]$

Figure 6.18: Boundary of the well-composed object is a manifold.

On Figure 6.18, we propose to segment the ventricles of the C.S.F. (Cerebro-Spinal Fluid) in a partial M.R.I. (Magnetic Resonance Imaging) of an human

brain (see [61, 112, 37] for more details on brain segmentation using mathematical morphology and digital topology).

Firstly, we binarize the original image u with a threshold $\lambda = 0.2$ (where 0 and 1 are the minimal and maximal luminances of the brain image respectively) and we obtain the set $[u \geq \lambda]$. Then, we proceed to a geodesic dilation of this set using a marker made of a full ellipse of radius $(10, 10, 5)$ at the center of the image (where the C.S.F. is located). We compute then the boundaries of the continuous analog of the geodesic dilation of this marker into $[u \geq \lambda]$. Since this image is not digitally well-composed, we obtain a boundary with a lot of "pinches" which can cause topological issues.

Secundly, we repeat the same process but with the self-dual well-composed interpolation u_{DWC} (proposed in this thesis) instead of u: starting from u_{DWC}, we compute $[u_{\mathrm{DWC}} \geq \lambda]$ which is digitally well-composed since the threshold sets of a well-composed image are well-composed. Then we proceed to a geodesic dilation of the (rescaled) marker into $[u_{\mathrm{DWC}} \geq \lambda]$, resulting then into a digitally well-composed image since geodesic dilations in a digitally well-composed mask results in a digitally well-composed image. Since DWCness and CWCness are equivalent on cubical grids in 3D, the boundary of the resulting segmentation is a 2-manifold.

Chapter 7

Conclusion

Our main contributions are the following: after a differentiation of the various kinds of well-composednesses and their extension to n-D gray-level images, we proved that DWCness implies EWCness in n-D, and we conjectured that DWCness is equivalent to AWCness and to CWCness in n-D on cubical grids. Since we are interested about how to make images DWC, we proved that no self-dual local method making images DWC exists in n-D $n \geq 3$, and then we proposed a non-local self-dual methods (based on front-propagation) which makes images DWC in n-D. We also proposed a way to make images defined on a polyhedral complex AWC. Because it is of much interest to be able to test if an image is well-composed or not, we proposed a characterization of n-D DWC images (on cubical grids) based on interval values and spans, and a characterization of AWC images defined on the n-faces of polyhedral complexes based on graphs.

To conclude this thesis, we will end with an open question: we have seen that DWCness, AWCness, and CWCness seem to be equivalent on cubical grids, but how CWCness and AWCness are related in polyhedral complexes? The counter-example of Daragon [41], stated that the chain complex of the order join of a 0-surface and a torus (see Figure 7.2) is a 3-surface, but not a *combinatorial manifold*[1]. It proves effectively that discrete surfaces are not always (combinatorial) manifolds, but is it enough to ensure that CWCness is stronger than AWCness ?

[1]We recall that a *combinatorial n-manifold* is a (geometric) simplicial complex C of dimension n and such that for each vertex $\{x\} \in C$, the *link* of $\{x\}$ in C is a *combinatorial* $(n-1)$-*sphere*(see p.67 of [41] for more details)

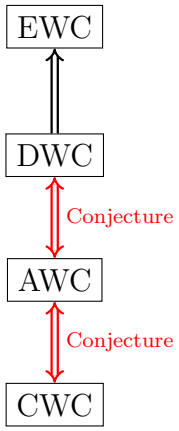

Figure 7.1: Links betweens the different flavors of well-composedness on cubical grids.

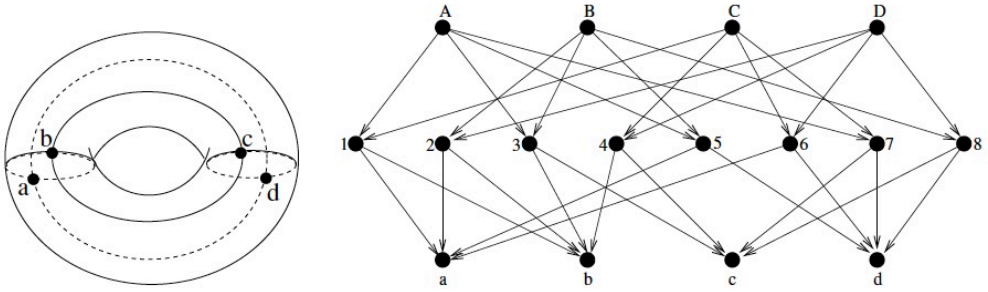

Figure 7.2: A (subdivided) torus and its incidence graph [41] (p.50).

Appendices

Appendix A

Proof that $\mathcal{I}_{\min}(u)$ and $\mathcal{I}_{\max}(u)$ are digitally well-composed

We prove here that Proposition 16 is true, that is, for any real-valued image $u : \mathcal{D} \subset \mathbb{Z}^n \to \mathbb{R}$ defined on a bounded hyperrectangle $\mathcal{D}$, the nD real-valued images $\mathcal{I}_{\min}(u)$ and $\mathcal{I}_{\max}(u)$ are digitally well-composed (their respective duality is obvious).

But before let us present a simple lemma relative to hierarchical subdivisions:

Lemma 16. *Let $z \in \left(\frac{\mathbb{Z}}{2}\right)^n \setminus \mathbb{Z}^n$ be a point. Then $\mathbb{A}(\mathbb{P}(z)) = \mathbb{A}(z)$.*

Proof: Let z be a point in $\left(\frac{\mathbb{Z}}{2}\right)^n \setminus \mathbb{Z}^n$, then:

$$\begin{aligned}
\mathbb{A}(\mathbb{P}(z)) &= \bigcup_{p \in \mathbb{P}(z)} \mathbb{A}(p), \\
&= \bigcup_{p \in \mathbb{P}(z)} \mathbb{P}^{\mathfrak{O}(p)}(p), \\
&= \bigcup_{p \in \mathbb{P}(z)} \mathbb{P}^{\mathfrak{O}(z)-1}(p), \\
&= \mathbb{P}^{\mathfrak{O}(z)-1}(\mathbb{P}(z)), \\
&= \mathbb{A}(z).
\end{aligned}$$

□

Then, the interpolation $\mathcal{I}_{\text{op}}(u)$ of Definition 37 can be reformulated as well:

Proposition 24. *Let $u : \mathcal{D} \to \mathbb{R}$ be an image defined on a bounded hyper-rectangle $\mathcal{D} \subset \mathbb{Z}^n$. Then the interpolation $\mathcal{I}_{\text{op}}(u) : \mathcal{D}' = \text{Subd}(\mathcal{D}) \to \mathbb{R}$ can be reformulated such that:*

$$\forall z \in \mathcal{D}', \left(\mathcal{I}_{\text{op}}(u)\right)(z) = \begin{cases} u(z) & \text{if } z \in \mathcal{D}, \\ \text{op}\{u(p) \ ; \ p \in \mathbb{A}(z)\} & \text{otherwise.} \end{cases}$$

Proof: Let us remark that $\bigcup_{k \in [\![0,n]\!]} \mathbb{E}_k \cap \mathcal{D}' = \mathcal{D}'$, and then we can verify the property for each $z \in \mathbb{E}_k \cap \mathcal{D}'$ with $k \in [\![0, n]\!]$.

The case $z \in \mathbb{E}_0 \cap \mathcal{D}' = \mathcal{D}$ is obvious. For the other points of $\mathcal{D}'$, let us proceed by induction.

Initialization ($k = 1$): Let z be a point in $\mathbb{E}_1 \cap \mathcal{D}'$. Then,

$$\text{op}\{u'(p) \ ; \ p \in \mathbb{P}(z)\} = \text{op}\{u(p) \ ; \ p \in \mathbb{P}(z)\} = \text{op}\{u(p) \ ; \ p \in \mathbb{A}(z)\}$$

Induction ($k \in [\![2, n]\!]$): we assume that for any $p \in \mathbb{E}_{k'} \cap \mathcal{D}'$, $k' \in [\![1, k-1]\!]$, we have the relation $\text{op}\{u'(q) \ ; \ q \in \mathbb{P}(p)\} = \text{op}\{u(a) \ ; \ a \in \mathbb{A}(p)\}$. Let us prove that this relation is still true for $z \in \mathbb{E}_k \cap \mathcal{D}'$:

$$\begin{array}{rcl} \text{op}\{u'(p) \ ; \ p \in \mathbb{P}(z)\} & = & \text{op}\{\text{op}\{u'(q) \ ; \ q \in \mathbb{P}(p)\} \ ; \ p \in \mathbb{P}(z)\}, \\ & = & \text{op}\{\text{op}\{u(a) \ ; \ a \in \mathbb{A}(p)\} \ ; \ p \in \mathbb{P}(z)\}, \\ & = & \text{op}\{u(a) \ ; \ a \in \mathbb{A}(p) \ , \ p \in \mathbb{P}(z)\}, \\ & = & \text{op}\{u(a) \ ; \ a \in \mathbb{A}(\mathbb{P}(z))\}, \\ & = & \text{op}\{u(a) \ ; \ a \in \mathbb{A}(z)\}, \\ & = & \text{op}\{u(a) \ ; \ a \in B_z \cap \mathcal{D}\}. \end{array} ,$$

thanks to Lemma 16. □

This leads to the following proposition:

Proposition 25. *Let $u : \mathcal{D} \to \mathbb{R}$ be an image defined on a bounded hyper-rectangle $\mathcal{D} \subset \mathbb{Z}^n$. Then the interpolation $\mathcal{I}_{\text{min}}(u) : \mathcal{D}' = \text{Subd}(\mathcal{D}) \to \mathbb{R}$ (respectively $\mathcal{I}_{\text{max}}(u) : \mathcal{D}' = \text{Subd}(\mathcal{D}) \to \mathbb{R}$) are digitally well-composed.*

Proof: We will treat only the case of $\mathcal{I}_{\text{max}}$, since $\mathcal{I}_{\text{min}}$ and $\mathcal{I}_{\text{max}}$ are dual. Let $S \in \mathcal{B}(\mathcal{D}', \left(\frac{\mathbb{Z}}{2}\right)^n)$ be a block in the domain of the interpolation $\mathcal{I}_{\text{max}}$. Then there exists a point $z \in \mathcal{D}'$ and a family of vectors $\mathcal{F} = \{f^1, \ldots, f^k\} = \{e^{j_1}, \ldots, e^{j^k}\}$ such that $S = S_2(z, \mathcal{F})$.

Let group together the indices of the vectors of $\mathbb{B}$ that are in $\mathcal{F}$ by denoting $\mathcal{J} = \{j_1, \ldots, j_k\}$. Let be then $\pi = (q^0, \ldots, q^k)$ defined such that:

$$q^0 = z + \sum_{j \in \mathcal{J} \cap \frac{1}{2}(z)} \frac{e^j}{2},$$

and:

$$\forall l \in [\![0, k-1]\!], q^{l+1} = \begin{cases} q^l - \frac{e^{j_{l+1}}}{2} & \text{if } j_{l+1} \in \frac{1}{2}(z), \\ q^l + \frac{e^{j_{l+1}}}{2} & \text{otherwise .} \end{cases}$$

Obivously, q^0 is by definition the point of minimal order into S. Also we can compute that:

$$q^k = q^0 - \sum_{j \in \mathcal{J} \cap \frac{1}{2}(z)} \frac{e^j}{2} + \sum_{j \in \mathcal{J} \setminus \frac{1}{2}(z)} \frac{e^j}{2} = z + \sum_{j \in \mathcal{J} \setminus \frac{1}{2}(z)} \frac{e^j}{2},$$

which shows that q^k is the point of maximal order in S. We can then observe that q^0 and q^k are antagonist in S.

Also, we can remark that $\forall r \in S$, $q^0 \in \mathbb{P}^{\delta_1}(r)$ and $r \in \mathbb{P}^{\delta_2}(q^k)$ for some $\delta_1, \delta_2 \in [\![0, k]\!]$, $u'(q^0) \leq u'(r) \leq u'(q^k)$, which means that $u'(q^0)$ and $u'(q^k)$ are respectively the minimal and maximal values of $u'\big|_S$.

Hence, for any $p, p' \in S$ such that they are antagonist in S, we need to prove:

$$\text{intvl}(u'(p),\, u'(p')) \;\cap\; \text{Span}\{\, u'(p'') \;\big|\; p'' \in S \setminus \{p,\, p'\}\,\} \;\neq\; \emptyset.$$

Two cases are possible: either $p \in \{q^0, q^k\}$, in this case $\{p, p'\} = \{q^0, q^k\}$ and then $\text{intvl}(u'(p),\, u'(p')) = [u'(q^0), u'(q^k)] \supseteq \text{Span}\{\, u'(p'') \;\big|\; p'' \in S \setminus \{p,\, p'\}\,\}$ and the intersection equals $\text{Span}\{\, u'(p'') \;\big|\; p'' \in S \setminus \{p,\, p'\}\,\}$ which is non empty. Or $p \notin \{q^0, q^k\}$, and then q^0 and q^k belong to $S \setminus \{p,\, p'\}$, which means that we have the converse case: $\text{Span}\{\, u'(p'') \;\big|\; p'' \in S \setminus \{p,\, p'\}\,\} = [u'(q^0), u'(q^k)] \supseteq \text{intvl}(u'(p),\, u'(p'))$ and then the intersection equals $\text{intvl}(u'(p),\, u'(p'))$ which is non empty. □

Appendix B

Topological Reparation in n-D

Two approaches exist to make binary images well-composed. The first one is to keep the original space of the image and to change some of the values of the initial image in such a way that the modified image becomes well-composed [154]. The second is to make an interpolation to preserve the topology of the original image [95, 162, 59]. However this second approach needs a subdivision of the original space and measurably increases the computational costs of the algorithms.

In this section, we propose a fast method that we published in [28] and that produces a digitally well-composed image in n-D, $n \geq 2$, by modifying the original values (see an application in Figure B.1). We will also illustrate this algorithm with a 2D application to text detection.

B.1 An Increasing Process Producing Well-Composed Images

B.1.1 Principle

Let $u : \mathcal{D} \subseteq \mathbb{Z}^n \to \mathbb{Z}$ be a given image. We want to find a digitally well-composed image $u^* : \mathcal{D} \subseteq \mathbb{Z}^n \to \mathbb{Z}$ which minimizes the deformation of u,

$$u^* = \arg\min_v \{ ||v - u||_1 \mid v \text{ is DWC} \} \tag{B.1}$$

However, to the best of our knowledge, such a combinatorial problem does not have a solution reachable in a reasonable time. To find an approximate

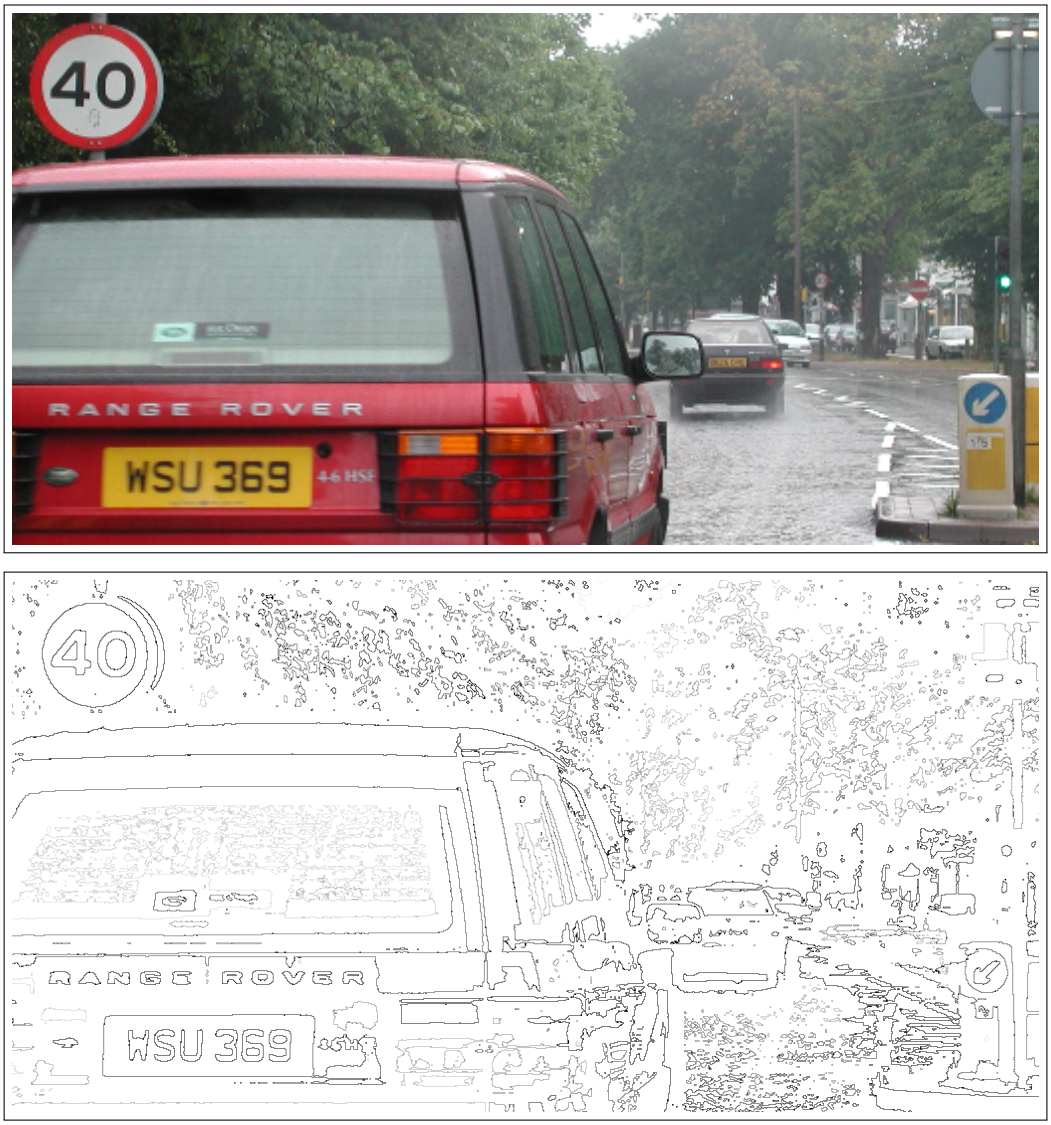

Figure B.1: Hierarchical representation of an image: since component boundaries are simple closed curves on well-composed images, two boundaries are either disjoint or in an inclusion relationship; thus, the delimited regions naturally form a tree. Actually it is a sub-part of the tree of shapes [60].

solution to this problem, we propose to iteratively select critical configurations and correct them, one by one. To prevent oscillation, we impose that, at

each step of the algorithm, the current solution is greater than the previous one. Our process is thus *increasing*.

As we modify a critical configuration, our algorithm is local, in the sense that we only need to look at a block and modify the pixel in the block. However, the modification of the value of a given pixel can create a novel critical configuration in its neighborhood. Hence, there is potentialy a propagation effect, and thus several passes on the image are in principle necessary to achieve convergence.

Due to this propagation effect, the convergence of the algorithm is only ensured if the process is monotone. Indeed, if we allow the modifications to either decrease or increase the image, then oscillation effects could appear.

B.1.2 Correction Step

Algorithm 4: The correction process.

SolveCC (u, S) : p
begin
  $p' \leftarrow \mathrm{antag}_S(p)$
  $m_1 \leftarrow \min(u(p),\, u(p'))$
  $M_1 \leftarrow \max(u(p),\, u(p'))$
  $m_2 \leftarrow \min\{\, u(p'') \mid p'' \in S \setminus \{p, p'\}\,\}$
  $M_2 \leftarrow \max\{\, u(p'') \mid p'' \in S \setminus \{p, p'\}\,\}$
  /* Primary case: */
  if $M_1 < m_2$ **then**
    $p^* \leftarrow \arg\max\{\, u(q) \mid q \in \{p, p'\}\,\}$
    $u(p^*) \leftarrow m_2$
  /* Secondary case: */
  if $M_2 < m_1$ **then**
    $p^* \leftarrow \arg\max\{\, u(p'') \mid p'' \in S \setminus \{p, p'\}\,\}$
    $u(p^*) \leftarrow m_1$
  return p^*

We want to correct a given critical configuration in the block $S \in \mathcal{B}(\mathcal{D}, (\mathbb{Z}/s)^n)$. By definition of a critical configuration, there exists two points $p \in S, p' \in S$

with $p' = \text{antag}_S(p)$, verifying:

$$\text{intvl}(u(p),\, u(p')) \;\cap\; \text{Span}\{\, u(q) \;\big|\; q \in S \setminus \{p, p'\}\,\} \;=\; \emptyset.$$

Then two cases are possible. Either we have:

$$\max(u(p),\, u(p')) \;<\; \min\{\, u(q) \;\big|\; q \in S \setminus \{p, p'\}\,\},$$

and we set:

$$\begin{cases} p^* \leftarrow \arg\max_q\{\, u(q) \;\big|\; q \in \{p, p'\}\,\}, \\ u(p^*) \leftarrow \min\{\, u(q) \;\big|\; q \in S \setminus \{p, p'\}\,\}, \end{cases}$$

or we have:

$$\max\{\, u(q) \;\big|\; q \in S \setminus \{p, p'\}\,\} \;<\; \min(u(p),\, u(p')),$$

then we set:

$$\begin{cases} p^* \leftarrow \arg\max_q\{\, u(q) \;\big|\; q \in S \setminus \{p, p'\}\,\} \\ u(p^*) \leftarrow \min(u(p),\, u(p')). \end{cases}$$

In both cases, u has been made digitally well-composed on S.

B.1.3 Convergence

The convergence of the method is easy to prove. Indeed, let us define $u_{min} = \min\{\, u(p) \,|\, u(p) \in \mathcal{D}\,\}$ and $u_{max} = \max\{\, u(p) \,|\, p \in \mathcal{D}\,\}$. As the algorithm increases the function u by at least one (since we work in $\mathbb{Z}$), we have a maximum of $(u_{max} - u(p))$ corrections for each $p \in \mathcal{D}$. The total number of corrections is then inferior or equal to $\sum_{p\in\mathcal{D}}(u_{max} - u(p)) \leq (u_{max} - u_{min}) \times \text{Card}(\mathcal{D})$. This ensures the convergence of the algorithm, since $\text{Card}(\mathcal{D})$ is finite.

B.1.4 Proposed Algorithm

Given the correction step, the algorithm is straightforward, it is detailed in Algorithm 5. It proceeds in two steps. First, the *initialization step* detects all the critical configurations of the threshold sets $\{[u \geq \lambda]\}_\lambda$ on $\mathcal{D}$ and enqueue them into Q. Second, the *correction step* solves one by one the critical configurations listed into Q using Algorithm 4 and enqueue the new critical configurations which appeared in the neighborhood of the modified value. This algorithm iterates until there is no longer any critical configurations in $\mathcal{D}$; the resulting image u is then digitally well-composed.

Algorithm 5: The increasing nD algorithm.

```
INCREASING (u) : Image
/* Makes the image DWC */
begin
    /* Initialization of the queue: */
    for all S ∈ B(D) do
        if CRITICALCONFIGURATION(S, u) then
            PUSH(Q, S)
    while Q ≠ ∅ do
        S ← POP(Q)
        /* Correction process: */
        p ← SOLVECC(u, S)
        /* Detection of the direction of the propagation: */
        for all S' ∈ B(D) s.t. p ∈ S' do
            if CRITICALCONFIGURATION(S', u) then
                PUSH(Q, S')
```

B.1.5 Experimental Results and Complexity of the 2D Case

We used the test set of 100 natural images of the Berkeley image database [114]. Their sizes are $(\mathrm{sx}, \mathrm{sy})$ with $\mathrm{sx} = 481$ and $\mathrm{sy} = 321$ pixels or the converse. We cropped each image with ten different windows (for each image) to obtain images of various sizes. The size $(\mathrm{newsx}, \mathrm{newsy})$ of the crop window is randomly chosen into $[\![2, \mathrm{sx}]\!] \times [\![2, \mathrm{sy}]\!]$ and its position is randomly chosen into $[\![1, \mathrm{sx} - \mathrm{newsx} + 1]\!] \times [\![1, \mathrm{sy} - \mathrm{newsy} + 1]\!]$.

We experimentally assessed the percentage of critical configurations contained in a given image. Figure B.2 shows that until 24.77% of the domain of the original images is covered by critical configurations. From a statistical point of view, an image contains on average $0.1237(\pm 0.0361)$ critical configuration by pixel. It is rare to have a digitally well-composed image.

Queue initialization. To initialize the queue of critical configurations, we simply have to detect among the $(\mathrm{newsx} - 1) \times (\mathrm{newsy} - 1)$ blocks which one contains a critical configuration, and in this case we insert it in the queue Q. Each detection and each insertion in the queue is in constant time. This

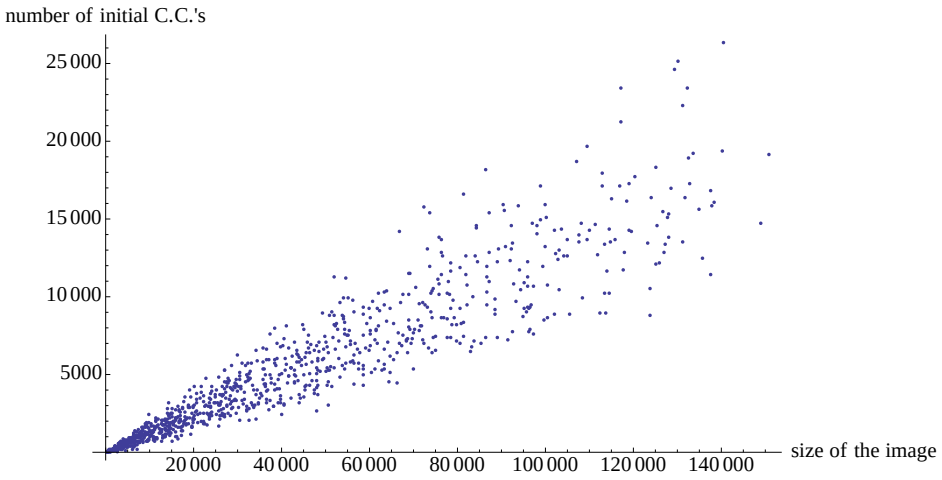

Figure B.2: Number of critical configurations as a function of the size of the image given in number of pixels.

implies that the initialization step is in linear time relatively to the size of the image.

Correction process. Concerning the correction step, we had to proceed to c corrections by pixel, with $c \leq 0.2376$. From a statistical point of view, an average number of $0.1195(\pm 0.0346)$ corrections by pixel has been observed. Numerical experiments show that the correction step is linear on average with respect to the image size.

The number of corrections by initial critical configuration is not a constant: it can be seen on Figure B.3 that the number of corrections is between $m = 86.93\%$ and $M = 108.33\%$ of the number of initial critical configurations. Indeed, a given correction can repair several critical configurations at the same time, which explains that m is less than 100%. Conversely, the propagation effect is responsible for M being greater than 100%. Statistically, we obtain a mean ratio of $0.9659(\pm 0.0338)$ corrections by initial critical configuration.

Detection of the direction of the propagation. For each processed correction, there exists only one position $p \in \mathcal{D}$ such as $u(p)$ is modified in the image, and then the propagation is possible in a bounded number of blocks, *i.e.*, in the blocks containing p. This means that the number of blocks processed in the detection step is proportional to the total number of

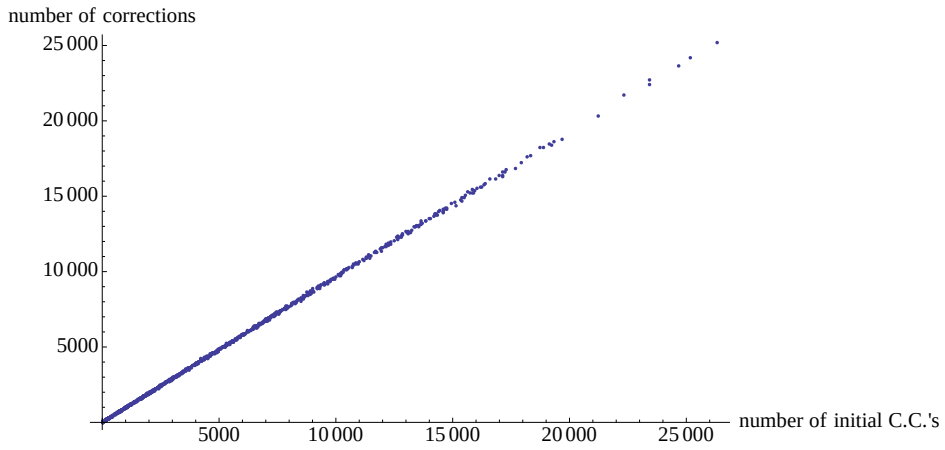

Figure B.3: Number of corrections as a function of the number of initial critical configurations.

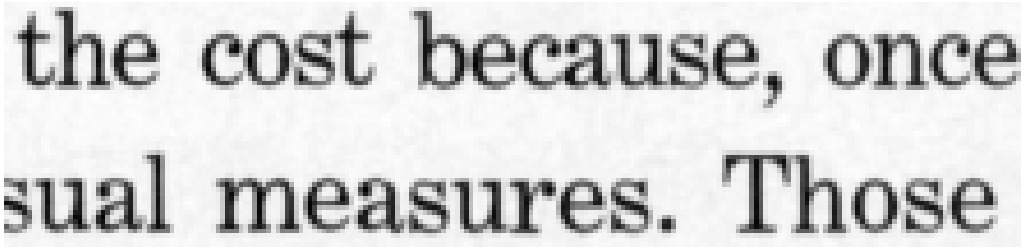

Figure B.4: Original image u.

corrections. Since the correction step is in linear time, so is the detection step.

Complexity. Since the 3 steps of the algorithm are in linear time, the complete algorithm is in linear time with respect to the size of the image (in number of pixels).

B.2 Illustration and Conclusion

We illustrate the interest of well-composedness to text detection with the morphological Laplacian in 2D. Let us recall that the *morphological Laplacian* $\mathcal{L}$ *of a given image* u is defined as $\mathcal{L}_{\text{se}}(u) = \delta_{\text{se}}(u) + \varepsilon_{\text{se}}(u) - 2u$ where se is a given structuring element. The contours of u are the zero-crossing of the

Figure B.5: Zero-crossings of the original Laplacian.

Figure B.6: Zero-crossings of the Laplacian modified by the increasing process.

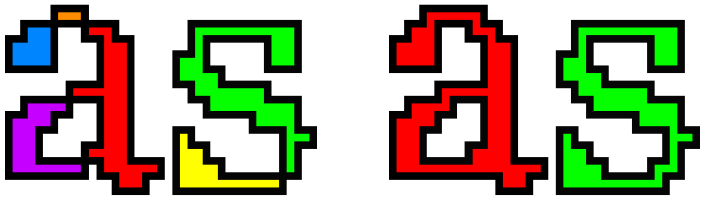

(a) Using the original Laplacian.

(b) Using the DWC Laplacian.

Figure B.7: Text segmentation results.

Laplacian. As they are boundaries of level-sets of the grayscale image, the zero-crossing are closed curves. We can set the gray-level of a given contour to the mean of the gradient of the original image along the contour.

We start from Figure B.4. Without correction, it can be seen on Figure B.5 and Figure B.7a that some characters are broken into several connected components. If we apply the proposed process on the Laplacian image, we observe that the contours are simple. In practice, it can be seen on

Figure B.6 and Figure B.7b that the correction repairs many contours.

B.3 Conclusion

In conclusion, we have presented a new algorithm that produces digitally well-composed images without interpolation. Compare to the interpolation methods, the proposed algorithm is faster and less memory consuming. It can be seen as a natural extension of the algorithm of topological repair of Siqueira *et al.* [154] to gray-valued images.

The source code of the proposed algorithm has been implemented using our image processing C++ library "Milena" [106, 107], which is free software under the GNU Public Licence v2. Since we advocate reproducible research, this source code is released on our web site at:
`http://publications.lrde.epita.fr/boutry.15.icip`.

Appendix C

Axiomatic Digital Topology

Our sources in matter of *Combinatorial Topology* and of *Piecewise Linear Topology* in this chapter are mainly: [48, 16, 2, 41, 79, 2, 7, 4, 108, 41].

C.1 Topology

Definition 46 (Topological spaces [84, 2])**.** *Let X be a set of points, and let $\mathcal{U}$ be a set of subsets of X such that:*

- $X, \emptyset \in \mathcal{U}$, $(TO1)$
- *any union of any family of elements in $\mathcal{U}$ belongs to $\mathcal{U}$,* $(TO2)$
- *any finite intersection of any family of elements in $\mathcal{U}$ belongs to $\mathcal{U}$.* $(TO3)$

Then $\mathcal{U}$ is said to be a topology*, and the couple $(X,\mathcal{U})$ is called a* topological space*. The elements of X are called the* points *of $(X,\mathcal{U})$, and the elements of $\mathcal{U}$ are called the* open sets *of $(X,\mathcal{U})$. We will abusively say that X is a topological space, assuming it is supplied with its topology $\mathcal{U}$.*

An open set which contains a point of X is said to be a *neighborhood* of this point.

Definition 47 (Closed sets and Closure [2])**.** *Let $(X,\mathcal{U})$ be a topological space, and let S be a subset of X. A set $S \subseteq X$ is said* closed *iff it is the complement of an open set in X. The intersection of all the closed sets in X containing M is denoted by $\mathrm{Clo}_{(X,\mathcal{U})}(S)$ and is called the* closure of S*. When no ambiguity is possible, we will abusively denote it $\mathrm{Clo}(S)$.*

Proposition 26 (Properties of the closure [2]). *Let $(X,\mathcal{U})$ be a topological space, and let S,T be subsets of X, then:*

- $\mathrm{Clo}(S \cup T) = \mathrm{Clo}(S) \cup \mathrm{Clo}(T)$,
- $S \subseteq \mathrm{Clo}(S)$,
- $\mathrm{Clo}(\emptyset) = \emptyset$.

Definition 48 (Interior [2]). *Let $(X,\mathcal{U})$ be a topological space. A point p in X is said to be an* interior point *of S relatively to the topology $\mathcal{U}$ iff there exists $U \in \mathcal{U}$ such that $p \in U \subseteq S$. The set of all the interior points of a set $S \subseteq X$ is denoted by $\mathrm{Int}_{(X,\mathcal{U})}(S)$.*

Note that the interior of a set $S \subseteq X$ is an open set in X.

Definition 49 (Topological boundary [2]). *Let $(X,\mathcal{U})$ be a topological space. The* boundary *of a set $S \subseteq X$ is $\mathrm{Clo}(S) \setminus \mathrm{Int}_{(X,\mathcal{U})}(S)$.*

Definition 50 (Relative topology [48]). *Let $(X,\mathcal{U})$ be a topological space and let S be a subset of X. We call* relative topology *induced in S by $\mathcal{U}$ the set of all the sets which can be written $U \cap S$ where $U \in \mathcal{U}$. A set which is open in the relative topology of S is said to be a* relatively open set.

Definition 51 (Connectedness [48]). *Let $(X,\mathcal{U})$ be a topological space. A set $S \subset X$ is said to be* connected *iff there is no decomposition $S = T_1 \cup T_2$ such that $T_1 \cap T_2 = \emptyset$, both $T_1, T_2 \neq \emptyset$, and relatively open sets with respect to S.*

Proposition 27 (Union of non disjoint connected sets [2] (p.14, Prop. 3.13)). *Let $(X,\mathcal{U})$ be a topological space. Let A, B be two connected subsets of X. If $A \cap B \neq \emptyset$, then $A \cup B$ is connected.*

Definition 52 (Components [2]). *Let p a point of a topological space $(X,\mathcal{U})$. The union of all connected sets containing p is connected, is the largest connected set in $(X,\mathcal{U})$ containing p, and is called the* component *of the point p in $(X,\mathcal{U})$. We denote it $\mathcal{CC}(X,p)$ where X represents abusively $(X,\mathcal{U})$.*

Proposition 28 (Continuous functions). *A function f mapping a topological space $(X,\mathcal{U})$ to $(Y,\mathcal{V})$ is said to be* continuous *iff for any set $U \subseteq Y$ which is open in Y, its inverse image:*

$$f^{-1}(U) \equiv \{x \in X \ ; \ f(x) \in U\}$$

is open in X.

Proposition 29 (Image of a connected set)**.** *The image by a continuous mapping of a connected topological space is a connected topological space.*

C.2 Regular open/closed sets

Let $\mathcal{T}$ be a topological space. Then, $\text{Int}_{\mathcal{T}}$ denotes the interior operator and $\text{Clo}_{\mathcal{T}}$ the closure operator in this topological space.

Definition 53. *A set X subset of a topological space $\mathcal{T}$ is said to be a* regular open set *iff* $X = \text{Int}_{\mathcal{T}}(\text{Clo}_{\mathcal{T}}(X))$.

Definition 54. *A set X subset of a topological space $\mathcal{T}$ is said to be a* regular closed set *iff* $X = \text{Clo}_{\mathcal{T}}(\text{Int}_{\mathcal{T}}(X))$.

C.3 $T0$-spaces and Alexandrov Spaces

Definition 55 (Degenerate sets [2])**.** *Let $(X,\mathcal{U})$ be a topological space. A set $M \subseteq (X,\mathcal{U})$ is said to be* degenerate *if it consists of only one point.*

Definition 56 ($T0$ Axiom and $T0$-spaces [5, 84, 2].)**.** *We say that a topological space $(X,\mathcal{U})$ verifies the $T0$* axiom of separation *iff it for any two different points in X, at least one has a neighborhood not containing the other, or equivalently iff two distinct degenerate subsets of X have distinct closures in $(X,\mathcal{U})$. A topological space which verifies the $T0$ axiom of separation is said to be a $T0$-*space*.*

Definition 57 (Discrete Spaces [7])**.** *A topological space $(X,\mathcal{U})$ is said* discrete *iff the intersection of any family of open sets of X is open in X, or equivalently iff the union of any family of closed sets of X is closed in X.*

Definition 58 (Alexandrov Spaces [48])**.** *A discrete T0-space is said to be an* Alexandrov space.

Proposition 30 (Smallest open/closed sets [48])**.** *Let $(X,\mathcal{U})$ be an Alexandrov space. For any point $P \in X$, there exists a* smallest neighborhood *of P is X:*

$$OP = \bigcap_{U \in \mathcal{U} \text{ s.t. } P \in U} U.$$

Due to the symmetry of Alexandrov spaces, there exists also a smallest closed set *containing* P*:*

$$CP = \bigcap_{U \text{ closed in } X \text{ s.t. } P \in U} U.$$

Alexandrov spaces get some interesting properties [48]:

Theorem 10. *Let* $(X, \mathcal{U})$ *be an Alexandrov space, and* P, Q *be two points of* X*.*

1. *if* $P \neq Q$*, then:*
   - $P \in OQ \Rightarrow Q \notin OP$,
   - $P \in CQ \Rightarrow Q \notin CP$,
2. $P \in CQ \Leftrightarrow Q \in OP$,
3. $CP \subseteq CQ \Leftrightarrow OQ \subseteq OP$.

Definition 59 (Locally finite)**.** *A topological space* $(X, \mathcal{U})$ *is said to be* locally finite *if each point* $P \in X$ *has as finite neighborhood and a finite closed set containing* P*.*

Theorem 11 (Path-connectivity and Connectivity in Alexandrov spaces [48].)**.** *Let* $(X, \mathcal{U})$ *be an Alexandrov space. Then* $S \subseteq X$ *is connected iff it is path-connected.*

C.4 Partially ordered sets

Definition 60 (Binary relation [16])**.** *Let* X *be an arbitrary set. A* binary relation R on X *is as subset of the cartesian product* $X \times X$*:*

$$R \subseteq X \times X.$$

Equivalently, a binary relation R *on* X *is a mapping from* $X \times X$ *to* $\{0, 1\}$ *such that* $\forall x, y \in X$*:*

$$\{(x, y) \in R\} \Rightarrow \{R(x, y) = 1\}, \text{ and } \{(x, y) \notin R\} \Rightarrow \{R(x, y) = 0\}.$$

Sometimes will denote by xRy *or by* $y \in R(x)$ *the fact that* $(x, y) \in R$*.*

Definition 61 (Properties of binary relations [16])**.** *A binary relation is said:*

- reflexive *iff,* $\forall x \in X,\ (x,x) \in R$,
- irreflexive *iff,* $\forall x \in X,\ (x,x) \notin R$,
- symmetrical *iff,* $\forall x,y \in X,\ (x,y) \in R \Leftrightarrow (y,x) \in R$,
- asymmetrical *iff,* $\forall x,y \in X,\ (x,y) \in R$ *and* $(y,x) \in R \Rightarrow x = y$,
- transitive *iff,* $\forall x,y,z \in X,\ (x,y) \in R$ *and* $(y,z) \in R \Rightarrow (x,z) \in R$.

Definition 62 (Inverse of a binary relation [16])**.** *Let X be a set, and R a relation order on X. We say that the binary relation R' on X such that $\forall x,y \in X,\ (x,y) \in R \Leftrightarrow (y,x) \in R'$, is the* inverse *of R.*

Notations 3 ($R^{\square}$ [16])**.** *Let X be a set, and R a relation order on X. We will note $R^{\square}$ the relation order defined such that, $\forall x,y \in X$:*

$$\left\{(x,y) \in R^{\square}\right\} \Leftrightarrow \left\{(x,y) \in R \text{ and } x \neq y\right\}.$$

Definition 63 (Order relation [16])**.** *Let $\mathcal{O}$ be a set of arbitrary elements. An* order relation *on $\mathcal{O}$ is a binary relation on X such that R is reflexive, antisymmetric, and transitive.*

Definition 64 (Posets/Orders [16])**.** *A set X of arbitrary elements supplied with an order relation R on X is denoted (X,R) or $|X|$ and is said to be a* partially ordered set (poset) *or simply an* order*. We will also say that the order relation R is* associated *to X, and that X is the* domain *of the poset (X,R).*

Notations 4 (α, β and θ [16])**.** *Let $|X|$ be a partially ordered set. We will usually denote by α_X the order relation associated to its domain X, in such a way that $\mathcal{O} = (X,\alpha_X)$. Also, we will write β_X the inverse of α_X, and $\theta_X = \alpha_X \cup \beta_X$.*

Notations 5 (α, β and θ applied to sets)**.** *By extension, we will define for any X subset of a partially ordered set:*

$$\alpha(X) = \bigcup_{x \in X} \alpha(x),$$

$$\beta(X) = \bigcup_{x \in X} \beta(x),$$

$$\theta(X) = \bigcup_{x \in X} \theta(x).$$

Notations 6 ($\alpha_X(x)$, $\beta_X(x)$, $\theta_X(x)$ [16])**.** *Let $|X|$ be a partially ordered set, and let x be a point in its domain X. Then we denote:*

- $\alpha_X(x) = \{p \in X \ ; \ p \leq x\}$,
- $\beta_X(x) = \{p \in X \ ; \ x \leq p\}$,
- $\theta_X(x) = \alpha_X(x) \cup \beta_X(x)$.

$\alpha_X(p)$ is called the closure *of p in $|X|$ and is the minimal closed set in X containing x, $\beta_X(p)$ is called the* star *of p in $|X|$, and is the minimal open set in X containing X, and $\theta_X(x)$ is called the* neighborhood *of p in $|X|$.*

To forge the intuition let us cite an example [2] of partially ordered sets: the set consisting of the points, staightlines, and planes of an Euclidian space is partially ordered by letting a point (respectively a straight line) precedes any straight line (respectively plane) containing it. In this case, if $p \in \mathcal{O}$ is a point, $\alpha(p)$ is simply the set made of this point $\{p\}$. If p is a straight line, $\alpha(p)$ is this straight line plus all the points lying on this line. If p is a plane, $\alpha(p)$ is this plane, plus all the straightlines lying in this plane, plus all the points lying in this plane. Also, if p is a point, $\beta(p)$ is this point, plus all the straight lines containing this point, plus all the planes containing this point. If p is a straight line, $\beta(p)$ is this straight line, plus all the planes containing this straightline. Finally, if p is a plane, $\beta(p)$ is the set made of this plane.

Note that the set $\mathcal{O}$ of all the subsets of an arbitrary set M:

$$\mathcal{O} = \{A \ ; \ A \subseteq M\},$$

is also a partially ordered set. Futhermore, if $A_1, A_2 \in \mathcal{O}$, $A_1 > A_2$ means that A_2 is a proper subset of A_1, which can be written $A_2 \subset A_1$. The resulting order is called the *natural order* in the collection of set $\mathcal{O}$. It is also called the *order based on the inclusion*. We will see the importance of this order using *Khalimsky grids* in a further subsection.

Definition 65 (Isomorphic orders [16])**.** *Let $|X| = (X, \alpha_X)$ and $(|Y| = (Y, \alpha_Y)$ be two orders. Then, these two orders are said* isomorphic (in the order sense) *iff there exists an* isomorphism in the order sense *between $|X|$ and $|Y|$, that is, a bijection $f : X \to Y$ such that for any couple (x_1, x_2) of elements of X:*

$$\{x_1 \in \alpha_X(x_2)\} \Leftrightarrow \{f(x_1) \in \alpha_Y(f(x_2))\}.$$

Notations 7 (Empty order [41])**.** *Note that all the orders whose domain is empy are isomorph, and we denote them by* $|\emptyset|$*.*

Definition 66 (Suborders [16])**.** *Let* $|X| = (X, \alpha_X)$ *be an order, and let* S *be a subset of* X*. The* suborder *of* $|X|$ *relative to* S *is the order* (S, α_S) *with* $\alpha_S = \alpha_X \cap (S \times S)$*. If no ambiguity is possible, we will write* $(S, \alpha_S) = |S|$*.*

Proposition 31 ($\alpha_S(x)$, $\beta_S(x)$, $\theta_S(x)$ [16])**.** *Let* $(X, \alpha_X) = |X|$ *be an order, and* S *be a subset of* X *inducing a suborder* $(S, \alpha_S) = |S|$*. Then for any* $x \in S$*,* $\alpha_S(x) \equiv \alpha_X(x) \cap S$*,* $\beta_S(x) \equiv \beta_X(x) \cap S$*, and* $\theta_S(x) \equiv \theta_X(x) \cap S$*.*

Definition 67 (Rank [16])**.** *Let* $(X, \alpha_X) = |X|$ *be an order. The* rank $\rho_X(x)$ *of an element* x *in* $|X|$ *is 0 if* $\alpha_X^{\square}(x) = \emptyset$ *and is equal to:*

$$\max_{y \in \alpha_X^{\square}(x)} (\rho_X(y)) + 1$$

either. The rank *of an order* $|X|$ *is denoted by* $\rho(|X|)$ *and is equal to the maximal rank of its elements:*

$$\rho(|X|) = \max_{x \in X}(\rho_X(x)).$$

As underlined by Daragon [41], the notion of dimensions and of ranks are different, even if they often match: the dimension of an object is inherent to an object, when the notion of rank depends of the elements that lie into the neighborhood.

Definition 68 (Point/k-element [16])**.** *Let* $(X, \alpha_X) = |X|$ *be an order. An element of* X *such that* $\rho_X(x) = k$ *is called* point *or* k-element *of* X*.*

C.5 From posets to $T0$-spaces

There comes a much important theorem of Alexandrov [2] relating orders and Alexandrov spaces.

Theorem 12 (Theorem 6.52 [2] (p.28))**.** *Let* $\mathcal{O}$ *be a partially ordered set, and let* A *be a subset of* $\mathcal{O}$*. We shall say that* A *is* closed *iff for any* $p, p' \in \mathcal{O}$*:*

$$\{p \in A \text{ and } p' < p\} \Rightarrow \{p' \in A\}.$$

This topology (based on the closed sets) converts $\mathcal{O}$ into an Alexandrov space $(X,\mathcal{U}) = f(\mathcal{O})$. Conversely, every Alexandrov space $(X,\mathcal{U})$ can be turned into a partially ordered set $\mathcal{O} = \phi((X,\mathcal{U}))$ if, for any two distinct elements $p, p' \in (X,\mathcal{U})$, $p' < p$ is taken to mean that $p' \in \alpha(p)$. It follows that $f(\phi((X,\mathcal{U}))) = (X,\mathcal{U})$ and $\phi(f(\mathcal{O})) = \mathcal{O}$.

As explained by this theorem [2], partially ordered sets can be identified with Alexandrov spaces in such a way that $\alpha_{\mathcal{O}}(p)$ is synonymous with the (topological) closure in the equivalent Alexandrov space $f(\mathcal{O})$, and $\beta_{\mathcal{O}}(p)$ is equal to the minimal (open) neighborhood of the point p in $f(\mathcal{O})$ (where $\beta = \alpha^{-1}$).

C.6 Khalimsky Grids

Definition 69 (Khalimsky Grids [85])**.** *The* Khalimsky grid *of dimension n is denoted $|\mathbb{H}^n| = (\mathbb{H}^n, \supseteq)$ and is defined as the order such that:*

$$\begin{aligned}
\mathbb{H}^1_0 &= \{\{a\}\ ;\ a \in \mathbb{Z}\}, \\
\mathbb{H}^1_1 &= \{\{a, a+1\}\ ;\ a \in \mathbb{Z}\}, \\
\mathbb{H}^1 &= \mathbb{H}^1_0 \cup \mathbb{H}^1_1, \\
\mathbb{H}^n &= \{h_1 \times \cdots \times h_n\ ;\ \forall i \in [\![1, n]\!], h_i \in \mathbb{H}^1\}.
\end{aligned}$$

Definition 70 (Cubical complexes)**.** *Let $\mathcal{X}$ be a subset of $(\mathbb{H}^n, \alpha_{\mathbb{H}^n})$. We say that $\mathcal{X}$ is a* cubical complex *iff its is* closed under inclusion*, that is, for any element h of $\mathcal{X}$, all the elements h' of $\mathbb{H}^n$ such that $h' \subseteq h$ are elements of X. In other words, $X = \alpha_{\mathbb{H}^n}(X)$.*

Figure C.1 shows two usual representations depicting a same cubical complex. On the left, we percieve the elements of $\mathbb{H}^n$ as sets of points of $\mathbb{Z}^n$, and we clearly see when their interection is empty or not. On the right, we percieve elements of $\mathbb{H}^n$ as geometric objects (vertices, edges, squares, cubes, and so on), this is the *splitted representation*, whose name is justified by the fact that even elements whose intersection is non empty are separated on the representation.

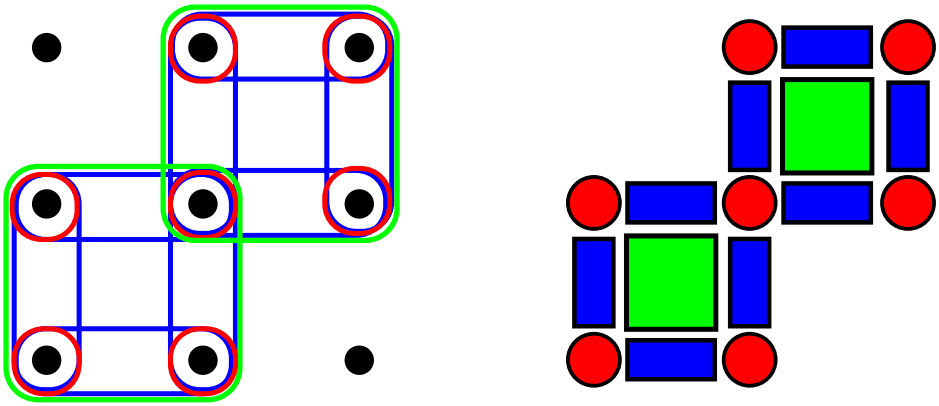

Figure C.1: Different representations of the same cubical complex.

A consequence of Definition 69, showing that $\alpha = \supseteq$, is that for any $h \in \mathbb{H}^n$, we have the following equalities for the closure, the opening, and the neighborhood:

$$\alpha(h) = \{h' \in \mathbb{H}^n \ ; \ h' \subseteq h\},$$

$$\beta(h) = \{h' \in \mathbb{H}^n \ ; \ h \subseteq h'\},$$

$$\theta(h) = \{h' \in \mathbb{H}^n \ ; \ h' \subseteq h \text{ or } h \subseteq h'\}.$$

Obviously, any suborder $|X|$ of $|\mathbb{H}^n|$ verifies that its associated order relation α_X equals $\supseteq \cap X \times X$ which corresponds to the inclusion order restricted to X, and then for any $h \in X$:

$$\alpha_X(h) = \{h' \in X \ ; \ h' \subseteq h\},$$

$$\beta_X(h) = \{h' \in X \ ; \ h \subseteq h'\},$$

$$\theta_X(h) = \{h' \in X \ ; \ h' \subseteq h \text{ or } h \subseteq h'\}.$$

Definition 71 (Dimension and $\mathbb{H}^n_k$)**.** *Any element h of $\mathbb{H}^n$ which is the cartesian product of k elements, with $k \in [\![0, n]\!]$, of $\mathbb{H}^1_1$ and of $(n-k)$ elements of $\mathbb{H}^1_0$ is said to be of* dimension k*, which is denoted by* $\dim(h) = k$*, and the set of all the elements of $\mathbb{H}^n$ which are of dimension k is denoted by $\mathbb{H}^n_k$.*

Property 1. *For any $k \in [\![0, n]\!]$, any element h in $\mathbb{H}^n_k$ is of rank $\rho(h, |\mathbb{H}^n|) =$*

k. In other words, in the Khalimsky grids, the dimension is equal to the rank in $|\mathbb{H}^n|$.

Proof: Let us proceed by induction on the dimension of $h \in \mathbb{H}^n$.

Initialisation ($\dim(h) = 0$): When $\dim(h) = 0$, there exists $a \in \mathbb{Z}^n$ such that $h = \otimes_{i \in [\![1,n]\!]}\{a_i\}$, and then $\alpha(h) = \otimes_{i \in [\![1,n]\!]}\{\{a_i\}\} = \{h\}$, then $\alpha^{\square}(h) = \emptyset$, and then the rank of h in $|\mathbb{H}^n|$ is equal to 0.

Induction ($\dim(h) \in [\![1, n]\!]$): We assume that for any $i \in [\![0, k-1]\!]$, when the dimension of h is lower than or equal to $(k-1)$, the dimension is equal to the rank in $|\mathbb{H}^n|$. Let us now assume that $\dim(h) = k$, we can rearrange the space coordinates such that h can be written:

$$h = \otimes_{i \in [\![1,k]\!]}\{a_i, a_i + 1\} \otimes \otimes_{i \in [\![k+1,n]\!]}\{a_i\},$$

and then by the closure operator we obtain that:

$$\alpha(h) = \otimes_{i \in [\![1,k]\!]}\{\{a_i\}, \{a_i, a_i + 1\}, \{a_i + 1\}\} \otimes \otimes_{i \in [\![k+1,n]\!]}\{\{a_i\}\}.$$

In other words, the only element of $\alpha(h)$ of dimension k is h itself, all the other elements being of dimension in $[\![0, k-1]\!]$, and then:

$$\max\left\{\dim(h') \ ; \ h' \in \alpha^{\square}(h)\right\} = k - 1.$$

When the dimension il lower than or equal to $(k-1)$, the dimension equals the rank in $|\mathbb{H}^n|$, and then we obtain:

$$\max\left\{\rho(h', |\mathbb{H}^n|) \ ; \ h' \in \alpha^{\square}(h)\right\} = k - 1,$$

and then the rank of h is k.

Finally, we obtained that for any value of k, and then for any element of $\mathbb{H}^n$, the dimension equals the rank in $|\mathbb{H}^n|$. □

Proposition 32 (Khalimsky grids are Alexandrov spaces [16])**.** *For any $n \geq 1$, the Khalimsky grids $|\mathbb{H}^n = (\mathbb{H}^n, \alpha)|$ supplied with the order relation $\alpha = \supseteq$, as defined in Theorem 12, is an Alexandrov space.*

Figure C.2, Figure C.3, and Figure C.4 show the different possibles closures/openings/neighborhoods in the case of a "point", an "edge", and a "square" in $\mathbb{H}^2$. We will see next that these *Kovalevsky cells* will be called

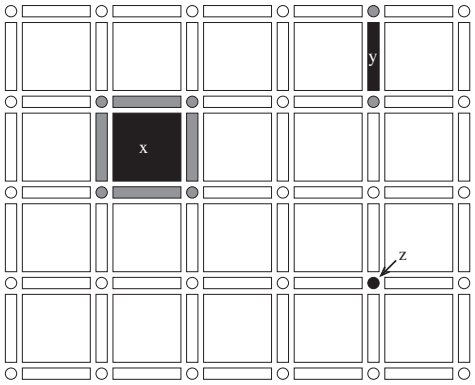

Figure C.2: The closures $\alpha(x)$, $\alpha(y)$, $\alpha(z)$ in $\mathbb{H}^2$ [41] (p. 34)

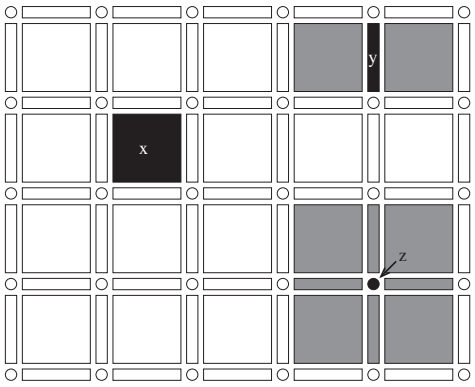

Figure C.3: The openings $\beta(x)$, $\beta(y)$, $\beta(z)$ in $\mathbb{H}^2$ [41] (p. 34)

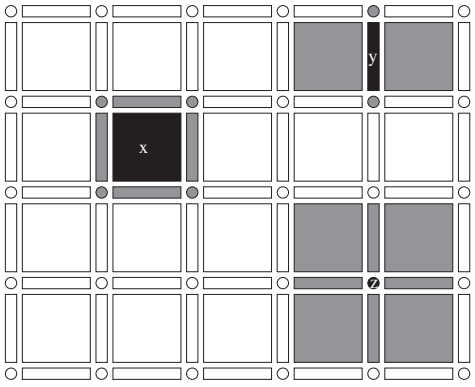

Figure C.4: The neighborhoods $\theta(x)$, $\theta(y)$, $\theta(z)$ in $\mathbb{H}^2$ [41] (p. 34)

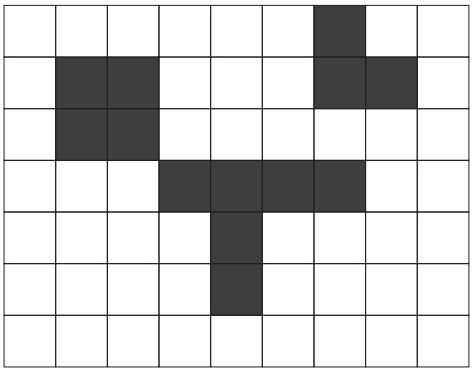

Figure C.5: A binary image u_{bin} in $\mathbb{Z}^2$ [41] (p. 31)

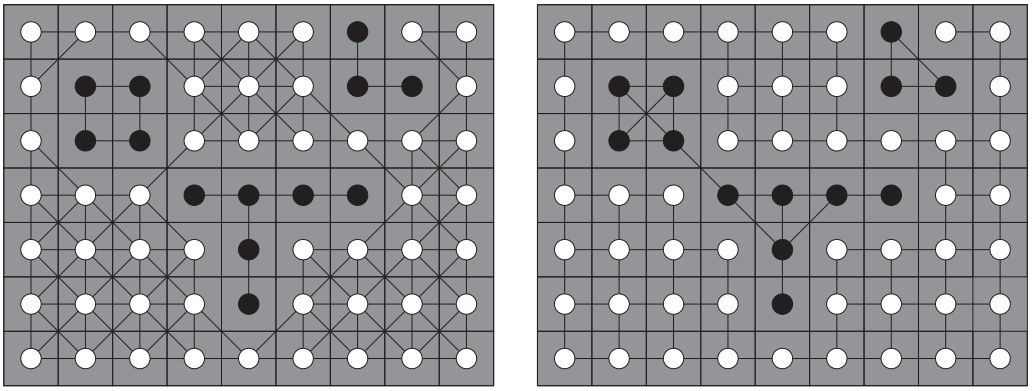

Figure C.6: u_{bin} [41] (p. 31) supplied with the $(4,8)$-topology on the left and with the $(8,4)$-topology on the right (the foreground is in black and the background in white).

respectively 0-*faces*, 1-*faces*, and 2-*faces* and that this notion exists in any finite dimension.

Starting from a binary image u_{bin} or equivalently from a set whose u_{bin} is the characteristical image depicted on Figure C.5, we can supply this image with the $(4,8)$-topology, or the $(8,4)$-topology very usual in digital topology (see Figure C.6). Just observe then the different connected components of the foreground that result from this choice: 3 components in the first choice, and 2 in the second choice.

No, let us immerse the image in $\mathbb{H}^2$ in different manners. In the raster scan order, the first is the most simple, we do a $(1-1)$- mapping between the two

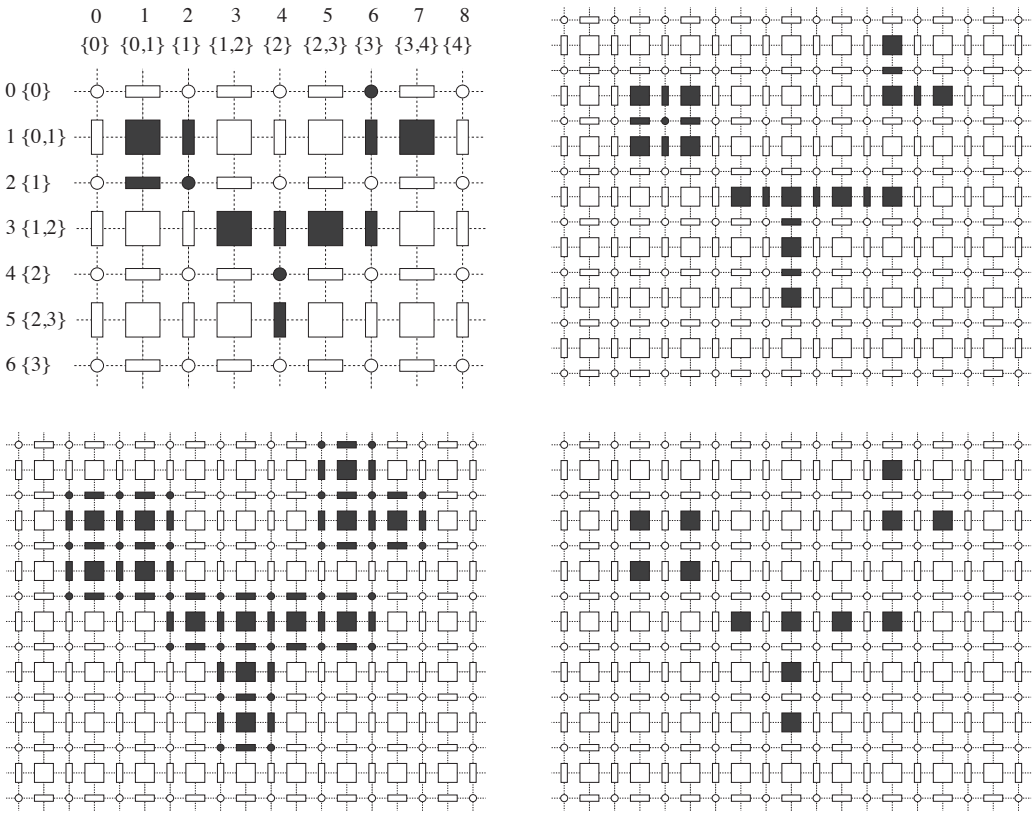

Figure C.7: Different immersions of u_{bin} into $\mathbb{H}^2$ [41] (p. 31).

spaces, but this space is not invariant by translation. The second approach uses the *miss strategy* (which reflects the $(4, 8)$-topology, and that we will use next as *immersions*): the elements of $\mathbb{Z}^2$ are mapped to the squares of $\mathbb{H}^2$, and each point or edge in $\mathbb{H}^2$ whose all the neighboring squares are in the foreground are assigned as foreground too. The third approach uses the *hit strategy* (which reflects the $(8, 4)$-topology): the elements of $\mathbb{Z}^2$ are mapped to the squares of $\mathbb{H}^2$, and each point or edge in $\mathbb{H}^2$ which is a face of a square of the foreground is assigned as foreground too. The fourth approach is like we will proceed next using an *isomorphism*: points become n-cubes.

Definition 72 (Paths [16])**.** *Let $|X|$ be an order. A* path *from $x \in X$ to $y \in X$ is a sequence $(p^0 = x, p^1, \ldots, p^{k-1}, p^k = y)$ of elements of X such that for any $i \in [\![0, k-1]\!]$, $x \in \theta_X(y)$.*

Figure C.8 depicts a path in $\mathbb{H}^2$.

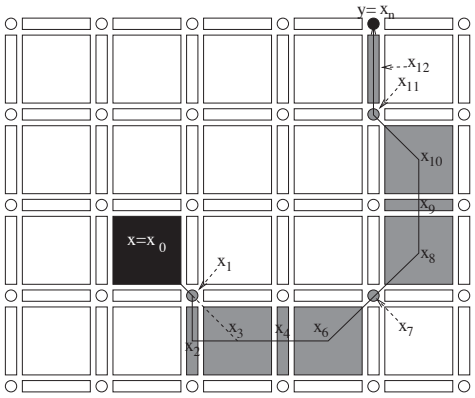

Figure C.8: A path in $\mathbb{H}^2$ [41] (p.34)

Definition 73 (Connectivity of an order [16])**.** *An order, as every topological space, is* connected *iff it cannot be partitioned into two non-empty open sets.*

Effectively, this definition holds since Alexandrov spaces and partially ordered sets are equivalent by Theorem 12 [2].

Definition 74 (Path-connectivity of an order [16])**.** *An order $|X|$ is said* connected by path *or* path-connected *iff for any couple (x, y) of elements of X, there exists a path from x to y into $|X|$.*

Theorem 13 (Connectivity VS path-connectivity [16])**.** *Let $|X|$ be a partially ordered set. Then $|X|$ is connect iff it is path-connected.*

Since the pathwise-connectivity between two points x, y belonging to an order constitutes a binary relation which is reflexive, symmetrical, and transitive, that is, an *equivalence relation* on X, we can define the equivalence classes of X in $\mathbb{H}^n$ as the *connected components* of X in $\mathbb{H}^n$:

Definition 75 (Connected components [16])**.** *Let $|X|$ be an order. A* connected component *C of $|X|$ is a subset of X such that for any couple (x, y) of elements of C, there exists a path from x to y lying entirely into C, and such that C is maximal for this property.*

Definition 76 (Simple closed curve [16])**.** *An order $|X| = (X, \alpha_X)$ is a simple closed curve if for any point $x \in X$, $\mathrm{Card}(\theta^{\square}_X(x)) = 2$ and such that the couple (y, z) of elements of $\theta^{\square}_X(x)$ verifies that $y \notin \theta^{\square}_X(z)$.*

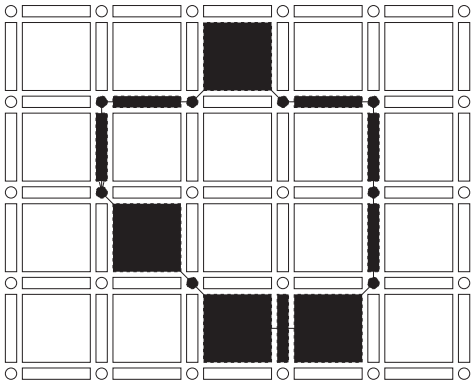

Figure C.9: A simple closed curve in $\mathbb{H}^2$ [41] (p.34)

As proved in [85], a simple closed curve (see Figure C.9) separates $\mathbb{H}^2$ and then satisfies an analog of the Jordan curve theorem in the 2D Khalimsky grids.

C.7 Order Joins

Definition 77 (Order Join [16])**.** *Let* $|X|, |Y|$ *be two orders. It is said that* $|X|$ *and* $|Y|$ *can be* joined *if* $X \cap Y = \emptyset$*. If* $|X|$ *and* $|Y|$ *can be joined, the* join *of* $|X|$ *and* $|Y|$ *is defined as the order:*

$$|X|*|Y| = (X \cup Y, \alpha_X \cup \alpha_Y \cup X \times Y).$$

Some properties [41] of the join are important to remark:

- the empty order $|\emptyset|$ is the neutral element of the join operator: $|X|*|\emptyset| = |\emptyset|*|X| = |X|$,
- the operator $*$ is not commutative,
- the operator $*$ does not create new elements, it adds some order relations between the elements of X and the elements of Y,
- the elements of Y keep their initial rank when the join operation is applied, when the elements of X have a rank which is incremented by the rank of Y plus one.

The construction of an order join can be made in this way: we put on the top each element of X, and at the bottom all the elements of Y. Then we connect the elements of X according to α_X, and then the elements of Y according to α_Y. Finally, we connect each element of X to each element of Y, and we have obtained the Hasse diagram of the order join.

Property 2 (Order join and $\theta^{\square}_X(x)$ [41](Property 1))**.** *Let $|X|$ be an order. Then for any $x \in X$:*

$$|\theta^{\square}_X(x)| = |\beta^{\square}_X(x)| * |\alpha^{\square}_X(x)|.$$

We will see in this section that as is the thesis of Daragon [41], this equilaty is particularily crucial, since it allows to "decompose" the neighborhood of a point of $\mathbb{H}^n$ into two orders which own many very strong topological properties.

Property 3 ($\theta^{\square}_{X*Y}(x)$ [41](Property 2))**.** *Let $|X|$ and $|Y|$ be two orders that can be joined. Then let x be an element of X and y be an element of Y. Then we obtain that $|\theta^{\square}_{X*Y}(x)| = |\theta^{\square}_X(x)| * |Y|$ and $|\theta^{\square}_{X*Y}(y)| = |X| * |\theta^{\square}_Y(y)|$.*

On Figure C.10, three orders of increasing complexity are depicted. Their joins are depicted on Figure C.11 and Figure C.12. Note that the Hasse diagrams are on the top, and the geometrical representation at the bottom. Observe that the rank of these orders is straightforward to compute looking at their Hasse diagrams.

C.8 n-surfaces

Definition 78 (CF-orders [16])**.** *Let $|X| = (X, \alpha_X)$ be a partially ordered set. $|X|$ is said* countable *iff its domain X is countable. Also, $|X|$ is said* locally finite *iff for any element $x \in X$, the set $\theta_X(x) = \{y \in X \ ; \ (x, y) \in \theta_X\}$ is finite. A partially ordered set which is countable and locally finite is said to be a* CF-order*.*

Now let us recall the definition of *discrete surfaces* or *n-surfaces* of Evako, Kopperman and Mukhin [52] which will be essential to define well-composedness in the sense of Alexandrov.

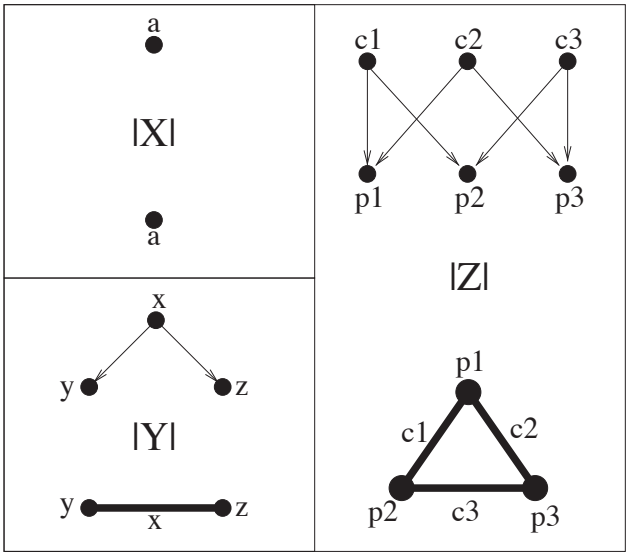

Figure C.10: Three examples of orders $|X|, |Y|, |Z|$ ([41], p.37)

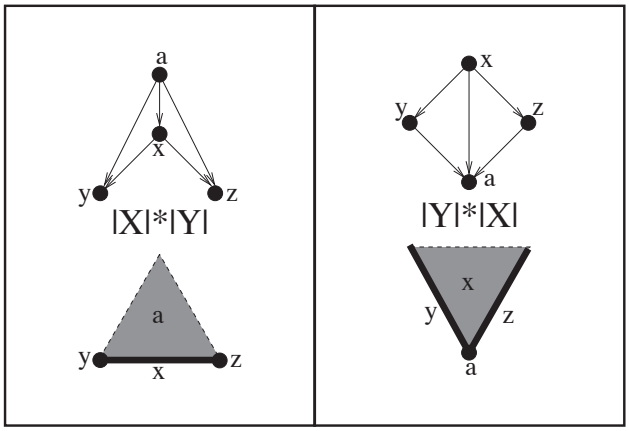

Figure C.11: The join operator $*$ is not commutative ([41], p.37)

Definition 79 (n-surface)**.** *Let $|X| = (X, \alpha_X)$ be a CF-order. The order $|X|$ is said to be:*

- *a (-1)-surface iff $X = \emptyset$,*
- *a 0-surface iff X is made of two elements $x, y \in X$ which are not neighbors the one of the other one: $x \notin \alpha_X(y)$ and $y \notin \alpha_X(x)$,*

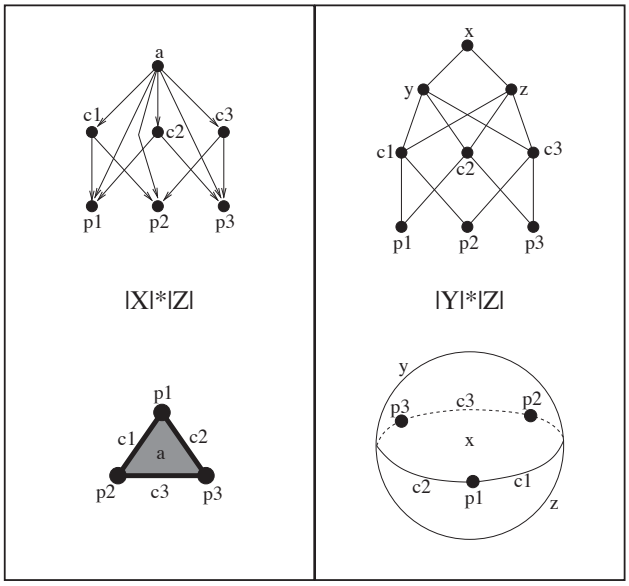

Figure C.12: Some order joins representing a *simplicial complex* on the left and a sphere on the right [41] (p.37)

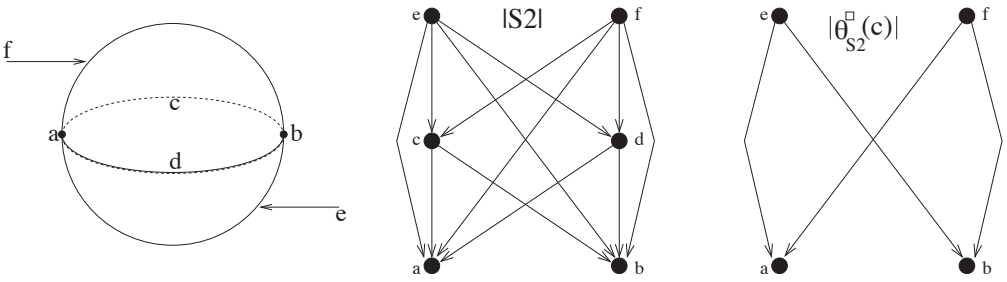

Figure C.13: A 2-surface: the sphere $\mathcal{S}_2$ [41] (p.50)

- *a n-surface, $n \geq 1$, iff $|X|$ is connected and for any $x \in X$, the order $|\theta^{\square}_X(x)|$ is a $(n-1)$-surface.*

To forge the intuition on discrete surfaces, we propose to show an example extracted from [41]. On Figure C.13, we can observe according to Daragon [41] the most simple 2-surface: the *sphere* $|\mathcal{S}_2|$. It is made of 6 elements: $\mathcal{S}_2 = \{a, b, c, d, e, f\}$, and any point $x \in \mathcal{S}_2$ verifies that its neighborhood $|\theta^{\square}_{\mathcal{S}_2}(x)|$ is a 1-surface. Effectively, the neighborhood of any point

$y \in \theta^{\square}_{\mathcal{S}_2}(x)$, we have that $\left|\theta^{\square}_{\theta^{\square}_{\mathcal{S}_2}(x)}(y)\right|$ is made of two points which are not neighbors, that is, is a 0-surface.

Another example of 2-surface is simply $|\mathbb{H}^2|$: the neighborhood of any point of $\mathbb{H}^2$ is a simple close curve. Effectively, as proven by Evako *et al.* in [52]:

Theorem 14. *The order $|\mathbb{H}^n|$ is a (discrete) n-surface.*

Note that this theorem is fundamental and will have many implications later in our study of the relation between well-composedness in the sense of Alexandrov and digital well-composedness.

Also, Daragon [41] proved this following theorem on partially ordered sets:

Theorem 15. *Let $|X|$ and $|Y|$ be two orders that can be joined, and let $n \in \mathbb{N}$ be an integer. The order $|X|*|Y|$ is a $(n+1)$-surface iff there exists some $p \in [\![-1, n+1]\!]$ such that $|X|$ is a p-surface and $|Y|$ is a $(n-p)$-surface.*

The proof of this theorem is based on Property 3 due to Bertrand [16].

Definition 80 (Homogeneity [41])**.** *An order $|X|$ is said* homogeneous *iff for any element $x \in X$, $\theta_X(x)$ contains a n-element.*

Property 4 (Rank of a n-surface [52])**.** *Let $|X|$ be a n-surface. The rank of $|X|$ is equal to n.*

Property 5 (Homogeneity of n-surfaces [41])**.** *Let $|X|$ be a n-surface. Any element x of $|X|$ is θ-neighbor of a n-element of $|X|$.*

Property 6 (Decomposition of a n-surface [41] (Property 10))**.** *Let $|X| = (X, \alpha_X)$ be an order. Then $|X|$ is a n-surface iff for any $x \in X$, $|\alpha^{\square}_X(x)|$ is a $(k-1)$-surface and $|\beta^{\square}_X(x)|$ is a $(n-k-1)$-surface, with $k = \rho(x, |X|)$.*

Since this property will be fundamental next, let us show an example of the $\beta^{\square}$-adherence and of the $\alpha^{\square}$-adherence of a point $x \in \mathbb{H}^3$ of rank 2 in $|\mathbb{H}^3|$ (see Figure C.14). Since x is a 2-element, its $\alpha^{\square}$-adherence is a 1-surface, and its $\beta^{\square}$-adherence is a 0-surface.

Definition 81 (Separation [41])**.** *Let $|X|$ be an order, and let Y be a strict subset of X. Then it is said that $|Y|$* separates *$|X|$ iff $|X \setminus Y|$ is not connected.*

If $|X|$ is a n-surface, and Y is a strict subset of X such that $|Y|$ is a k-surface, then necessarily $k = n-1$ (as in continuous topology using topological n-manifolds).

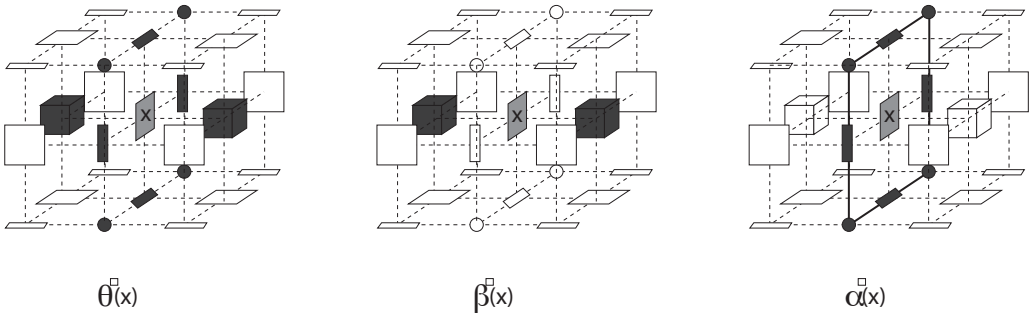

Figure C.14: Different kinds of *adherences* of a 2-element in $\mathbb{H}^3$ [41] (p.54)

C.9 Closed Orders

Definition 82 (Closed orders [41])**.** *Let $|X| = (X, \alpha_X)$ be an order. $|X|$ is said to be* closed *iff for any $z \in X$, and for any $y \in \alpha_X^{\square}(x)$, for any value $i \in]\rho(y, |X|), \rho(x, |X|)[$:*

$$\exists z \in \alpha_X^{\square}(x) \cap \beta_X^{\square}(x) \ s.t. \ \rho(z, |X|) = i.$$

In other words, this relation means that there exists in a closed order elements "between" x and y which are of any rank between the rank of x and the rank of y in the order. It recalls simplicial complexes which are *closed by inclusion* in the sense that for any k-simplex in a simplicial complex S, there exists at least one l-simplex in S which is a face of s for any value l in $[\![0, k]\!]$ (since a simplicial complex contains by definition all the faces of its elements).

Property 7 (n-surfaces are closed orders [41] (Property 20 p.63))**.** *Let $|X|$ be an order. If $|X|$ is a n-surface, $|X|$ is a closed order.*

C.10 Geometric Simplicial Complexes (in $\mathbb{R}^n$)

Since *polyhedral complexes* are made of *convex polyhedral domains* which lies in $\mathbb{R}^n$, let us first recall some basics in linear algebra.

Definition 83 (r-planes and linear independency)**.** *An r-dimensional subspace, $0 \leq r \leq n$, of $\mathbb{R}^n$ is called a* r-plane*. The points $x^0, \ldots, x^r$ are said* linearly independent *iff they are not contained in any k-plane with $k < r$.*

Definition 84 (Affine combination and affinely independency)**.** *Let $u^0, \ldots, u^k$ be $(k+1)$ points in $\mathbb{R}^n$. A point $x = \sum_{i\in[\![0,k]\!]} \lambda_i u^i$ is said to be an* affine combination *of the u^i iff $\sum_{i\in[\![0,k]\!]} \lambda_i = 1$. Also, these $(k+1)$ points are said* affinely independent *iff any two affine combinations $x = \sum_{i\in[\![0,k]\!]} \lambda_i u^i$ and $y = \sum_{i\in[\![0,k]\!]} \mu_i u^i$ are equal iff $\forall i \in [\![0,k]\!], \lambda_i = \mu_i$.*

A consequence is that the $(k+1)$ points $u^0, \ldots, u^k$ are affinely independent iff the k vectors $(u^i - u^0)$, $\forall i \in [\![1,k]\!]$, are linearly independant. In $\mathbb{R}^n$, we can have at most n linearly dependent vectors and then $(n+1)$ affinely independent points.

Definition 85 (Convex)**.** *The straight line defined by two points a, b is the set of all the points of the form $\lambda a + \mu b$, where $\lambda + \mu = 1$. The subset of this straight line defined by the conditions $\lambda \geq 0, \mu \geq 0$ is called the* closed segment *$[ab]$. Then, a set M is said to be* convex *if for any two points a and b in M, it contains also the whole segment $[ab]$.*

Definition 86 (Convex Polyhedral Domains [2] (p. 212))**.** *A bounded nonempty subset of $\mathbb{R}^n$ which is the intersection of a finite number of closed half-planes of $\mathbb{R}^n$ is called a (closed) convex polyhedral domain.*

Definition 87 (Dimension of Convex Polyhedral Domains [2] (p. 210))**.** *The* dimension *of a convex polyhedral domain Q is the maximum number r such that Q contains $(r+1)$ linearly independent points.*

Definition 88 (Supporting planes [2] (p. 213))**.** *Let Q^n be a n-dimensional convex polyhedral domain in $\mathbb{R}^n$. The intersection of every $(n-1)$-plane $R^{n-1} \subset \mathbb{R}^n$ with Q^n is convex. A plane R^{n-1} is called* plane of support *of the polyhedral domain Q^n if $Q^n \cap R^{n-1} \neq \emptyset$ and $R^{n-1} \cap \mathrm{Int}(Q) = \emptyset$ (where $\mathrm{Int}(Q)$ denotes the topological interior of Q).*

Definition 89 (Face of a Convex Polydral Domain [2] (p. 213))**.** *The intersection of every supporting plane R^{n-1} with the topological boundary ∂Q^n of the convex polyhedral domain Q^n coincides with the set $R^{n-1} \cap Q^n$ and is therefore a closed convex polyhedral domain Q^r of dimension $r \leq n-1$; if $r = (n-1)$, Q^r is called a $(n-1)$-face of the polyhedral domain Q^n. Following the same reasoning, the $(n-2)$-faces of the $(n-1)$-faces of Q^n are called the* $(n-2)$-faces *of Q^n, and so on.*

Definition 90 ((Closed) Polyhedral complex)**.** *Let K be a finite set K of (closed) convex polyhedral domains situated in some $\mathbb{R}^n$. K is said to be a a* (closed) polyhedral complex *iff :*

1. *any intersection of two different elements h^1, h^2 of K is an element h^3 of K such that h^3 is a common face of h^1 and h^2,*
2. *every face of every convex polyhedral domain of K is also an element of K.*

Note that tis family of complexes is also known as *convex linear cell complexes* in Hudson's book [79].

Even if these complexes are basically geometric structures, we will see later that they have also very nice topological properties as orders, when they are supplied with the inclusion order $\supseteq$.

Definition 91 (Dimension of a polyhedral complex [2])**.** *The* dimension *of a polyhedral complex is the maximum dimension of its convex polyhedral domains.*

Definition 92 (Convex combinations and Convex hull)**.** *Let $u^1, \ldots, u^n$ be n points in $\mathbb{R}^N$. The sum $\sum_{i\in[\![1,n]\!]} \lambda_i u^i$ such that each λ_i, $i \in [\![1,n]\!]$, is nonnegative, is said to be a* convex combination *of the u^i. The* convex hull *of these points is the set of convex combinations of u^i.*

Definition 93 (Geometric n-simplex, Vertices of a geometric simplex [79])**.** *A* geometric n-simplex *in $\mathbb{R}^N$ is the convex hull of $(n+1)$ linearly independent points, called its* vertices*.*

Definition 94 (Simplicial Complex [79])**.** *A* geometrical simplicial complex *is a polyhedral complex whose convex polyhedral domains are all geometric simplices.*

Definition 95 (Vertex Set of a Geometric Simplicial Complex)**.** *The* vertex set *of a geometric simplicial complex C is denoted by* $\mathrm{Vert}(C)$ *and is equal to:*

$$\{\sigma \in C \,;\, \dim(\sigma) = 0\}\,.$$

Definition 96 (Underlying Polyhedron [79])**.** *If K is any geometric simplicial complex, we denote by* $\mathrm{Poly}(K)$ *the pointwise union in $\mathbb{R}^n$ of all the faces in K, and we call* $\mathrm{Poly}(K)$ *the* underlying polyhedron *of K.*

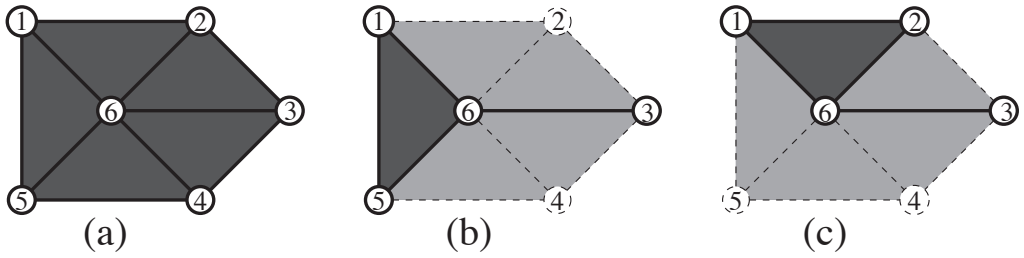

Figure C.15: Examples of simplicial complexes ([41], p.40).

C.11 Abstract Simplicial Complexes

Now, we recall some results in combinatorial topology, mainly applied to *abstract simplices* and *abstract simplicial complexes*.

Definition 97 ((Abstract) Simplex)**.** *Let Λ be a countable space of arbitrary elements. We will say that $s \subseteq \Lambda$ is a* abstract simplex *(in Λ) iff it is a non-empty finite subset of Λ. We will also say that an abstract simplex is an abstract n-simplex (in Λ) if it is made of $(n+1)$ elements of Λ. We will sometimes call it* abstract simplex of dimension n*.*

Definition 98 (Faces)**.** *Let Λ be a countable space of arbitrary elements. We will say that an abstract simplex $f \subseteq \Lambda$ is a* face *of the abstract simplex $s \in \Lambda$ iff $f \subseteq s$, and that it is a* proper/strict face *of s iff $f \subset s$.*

Definition 99 (Abstract Simplicial Complex)**.** *Let Λ be a countable space of arbitrary elements, and let C be a family of simplices if Λ. We will say that C is an* abstract simplicial complex *iff* $\mathrm{Card}\,(C) < \infty$ *and C its* closed by inclusion*, which means that for any face s belonging to C, any of its faces $f \subseteq s$ belongs also to C.*

Note that in this manner, an abstract simplicial complex is a finite set of finite subsets of Λ.

Definition 100 (Support)**.** *Let Λ be a countable space of arbitrary elements, and let C be an abstract simplicial complex in Λ. We will say that the minimal set Λ_C such that any element $s \in C$ is a subset of Λ_C is the* support *of C.*

Definition 101 (Subcomplex)**.** *Let Λ be a countable space of arbitrary elements, and let C be an abstract simplicial complex in Λ of support Λ_C. We will say that the subset K of C such that $\Lambda_K \subseteq \Lambda_C$ is a* subcomplex *of C iff it is an abstract simplicial complex.*

Definition 102 (Full subcomplex)**.** *Let Λ be a countable space of arbitrary elements, let C be an abstract simplicial complex in Λ of support Λ_C, and let be K a subcomplex of C. Then K is said to be a* full *subcomplex of C iff any face $f \in C$ such that $f \subseteq \Lambda_C$ is an element of K.*

Figure C.15 depicts on (a) an abstract simplicial complex C of support $\Lambda_C = [\![1, 6]\!]$. On (b), we can observe a subcomplex K of C of support $\Lambda_K = \{1, 3, 5, 6\}$. Each face of C which is included in Λ_K belongs to K, and in this manner K in full into C. On (c), we can see the subcomplex K' of C, whose support is $\Lambda_{K'} = \{1, 2, 3, 6\}$. The abstract simplex $\{2, 3, 6\}$ belongs to C, is a subset of $\Lambda_{K'}$, but does not belong to K'. In this manner, K' is not full into C.

Definition 103 (Vertex Set of an Abstract Simplicial Complex)**.** *The* vertex set *of an abstract simplicial complex A is denoted by* $\mathrm{Vert}(A)$ *and is equal to:*

$$\bigcup_{s \in A} s.$$

C.12 Abstract VS Geometric Simplicial Complexes

Edelsbrunner defined a *geometric realization* of an abstract simplicial complex in the following manner:

Definition 104 (Geometric Realization and Abstraction [49])**.** *A* geometric realization *of an abstract simplicial complex A is a geometric simplicial complex K together with a bijection $\phi : \mathrm{Vert}(A) \to \mathrm{Vert}(K)$ such that $s \in A$ iff $\mathrm{ConvHull}(\phi(s)) \in K$. Conversely, A is called an* abstraction *of K.*

Roughly speaking, any abstract simplicial complex can be "transformed" into a geometric simplicial complex, by attributing coordinates to its vertices, such that they are equivalent, two geometric simplices will intersect iff their corresponding abstract simplices intersect:

Theorem 16 (Geometric Realization Theorem [50])**.** *Every abstract simplicial complex of dimension d has as geometric realization in $\mathbb{R}^{2d+1}$.*

Proof: The proof we propose here is based on the argumentation of Edelsbrunner in [50].

Let us assume that an abstract simplicial complex A, made of finite sets of finite arbitrary elements in Λ, is of dimension $d \geq 0$ Now, let $\varphi : \mathrm{Vert}(A) \to \mathbb{R}^{2d+1}$ ba an injection such that for any set $\{p^0, \ldots, p^{2d+1}\} \subseteq \Lambda_A$, the set $\{\varphi(p^0), \ldots, \varphi(p^{2d+1})\}$ is affinely independent. Let us define:

$$G = \{\mathrm{ConvHull}(\varphi(a)) \ ; \ a \in A\}.$$

We want to prove: that:

1. for any a in Λ, $a \in A \Leftrightarrow \mathrm{ConvHull}(\varphi(a)) \in G$,
2. $\varphi : \mathrm{Vert}(A) \to \mathrm{Vert}(G)$ is a bijection,
3. G is a geometric simplicial complex.

The first property is simply the consequence of the definition of G. For the second property, let us prove first that the image of $\mathrm{Vert}(A)$ is $\mathrm{Vert}(G)$. Starting from the definition of G, we obtain:

$$\begin{aligned}
\mathrm{Vert}(G) &= \{\mathrm{ConvHull}(\varphi(a)) \ ; \ a \in A, \dim(\mathrm{ConvHull}(\varphi(a))) = 0\}, \\
&= \{\mathrm{ConvHull}(\varphi(p)) \ ; \ \{p\} \in A\}, \\
&= \{\{\varphi(p)\} \ ; \ \{p\} \in A\}, \\
&= \{\varphi(\{p\}) \ ; \ \{p\} \in A\}, \\
&= \{\varphi(a) \ ; \ a \in \mathrm{Vert}(A)\}, \\
&= \varphi(\mathrm{Vert}(A)).
\end{aligned}$$

This way, φ is injective and surjective from $\mathrm{Vert}(A)$ to $\mathrm{Vert}(G)$, and then bijective.

To show that G is a geometric simplicial complex, we first have to show that for any geometric simplex $g \in G$, any face f of g belongs also to G (a), then we have to show that for any pair of geometric simplices g^1, g^2 of G, $g^1 \cap g^2$ is also a geometric simplex of G (b), and then we have to show that $g^1 \cap g^2$ is a common face of g^1 and g^2 (c).

(a): Let g be an element of G, then there exists $a_g \in A$ such that $g = \mathrm{ConvHull}(\varphi(a_g))$, which can be rewritten using $a_g = (a_g^1, \ldots, a_g^k)$ into

$g = \text{ConvHull}\{\varphi(a_g^1), \ldots, \varphi(a_g^k)\}$ where the set $\{\varphi(a_g^1), \ldots, \varphi(a_g^k)\}$ is affinely independent by hypothesis on φ. This way, each face of the geometric simplex g can be written $f = \text{ConvHull}\{\varphi(a_g^{i_1}), \ldots, \varphi(a_g^{i_l})\}$, that is, the convex hull of a subfamily of $\{\varphi(a_g^1), \ldots, \varphi(a_g^k)\}$. In other words, there exists $a_f = \{a_g^1, \ldots, a_g^k\} \subseteq a_b \in A$ such that $f = \text{ConvHull}(\varphi(a_f)) \in G$.

(b): Let g^1, g^2 be two elements of G, then there exists $a^1, a^2 \in A$ such that $g^1 = \text{ConvHull}(\varphi(a^1))$ and such that $g^2 = \text{ConvHull}(\varphi(a^2))$. If $a^1 \cap a^2 = \emptyset$, then $g^1 \cap g^2 = \emptyset$: if there exists $z \in \mathbb{R}^{2d+1}$ such that $z \in g^1 \cap g^2$, then:

$$z = \sum_{p \in a^1} \lambda_p \varphi(p) = \sum_{p \in a^2} \mu_p \varphi(p),$$

which means that there exists $\{\xi_p\}$ not all empty such that:

$$\sum_{p \in a^1 \cup a^2} \xi_p \varphi(p) = 0,$$

which is impossible since the family $\{\varphi(p)\}_{p \in a^1 \cup a^2}$ is made of at most $(2d+2)$ different elements (and then affinely independent). Now, if $a^1 \cap a^2 \neq \emptyset$, then there exists $r \in \Lambda$ such that $r \in a^1 \cap a^2$, and then $\varphi(r) \in \text{ConvHull}(\varphi(a^1)) \cap \text{ConvHull}(\varphi(a^2)) \neq \emptyset$. Then, any element r of $g^1 \cap g^2$ can be written:

$$r = \sum_{p \in a^1} \lambda_p \varphi(p) = \sum_{p \in a^2} \lambda_p \varphi(p),$$

which implies that:

$$\sum_{p \in a^1 \cup a^2} \xi_p \varphi(p) = 0,$$

with:

$$\xi_p = \begin{cases} \lambda_p & \text{if } p \in a^1 \setminus a^2, \\ (-\mu_p) & \text{if } p \in a^2 \setminus a^1, \\ (\lambda_p - \mu_p) & \text{if } p \in a^1 \cap a^2. \end{cases}$$

Since $a^1 \cup a^2$ contains at most $(2d+2)$ elements, then $\{\varphi(p)\}_{p \in a^1 \cup a^2}$ is affinely independent, and then all the coefficients ξ_p are equal to zero, which means that:

$$\begin{cases} \lambda_p = 0 & \text{if } p \in a^1 \setminus a^2, \\ \mu_p = 0 & \text{if } p \in a^2 \setminus a^1, \\ \lambda_p = \mu_p & \text{if } p \in a^1 \cap a^2. \end{cases}$$

Then $r = \sum_{p \in a^1 \cap a^2} \lambda_p \varphi(p)$, with $\sum_{p \in a^1 \cap a^2} \lambda_p = 1$, and $\forall p \in a^1 \cap a^2, \lambda_p \geq 0$. Finally, $g^1 \cap g^2$ is then equal to ConvHull$(\varphi(a^1 \cap a^2))$. Since $a \in A$ and $a^1 \cap a^2 \subseteq a^1$, $a^1 \cap a^2 \in A$, and then ConvHull$(\varphi(a^1 \cap a^2)) \in G$.

(c): since $g^1 = \text{ConvHull}(\varphi(a^1))$ is a simplex, its faces are the convex hulls of any subset of a^1. The same reasoning applies for $g^2 = \text{ConvHull}(\varphi(a^2))$. Then $g^1 \cap g^2 = \text{ConvHull}(\varphi(a^1 \cap a^2))$ is a common face to g^1 and g^2. □

Note that this bound is optimal in the sense that there exists examples of k-complexes which need at least $\mathbb{R}^{2k+1}$ to be realized. For example, the set of all faces of dimension lower than or equal to k (called the *k-skeleton*) of a $(2k+2)$-simplex needs to be realized in $\mathbb{R}^{2k+1}$. Also, the complete graph of five vertices usually denoted by K_5 identified by Kuratowski [93] as being one of the obstruction to graph planarity, is a 1-complex which can only be realized in $\mathbb{R}^3$. Some other examples like these ones are given in [58] and in [171].

For this reason, the definitions and theorems recalled or introduced in the sequel hold for both abstract and geometric simplicial complexes.

C.13 Simplicial Complexes as Orders

Like we did with the Khalimsky grids, we can associate a *canonical order relation* $\alpha = \supseteq$ based on the inclusion to any simplicial complex C: $|C| = (C, \alpha)$. This way, simplicial complexes are partially ordered sets. For this reason, the reader is invited to refer to Section C.4 and to Section C.5 for some recalls in matter of partially ordered sets and Alexandrov spaces.

Now let us recall some properties in simplical complexes extracted from [41].

Property 8. *Let Λ be a countable space of arbitrary elements, and let C be a simplicial complex in Λ. Then the order $|C| = (C, \alpha)$ with $\alpha = \supseteq$ defined as in Theorem 12 where α is the* closure operator*, is an Alexandrov space.*

Property 9. *Let Λ be a countable space of arbitrary elements, and let C be a simplicial complex in Λ. Then for any $s \in C$, $\alpha_C(s)$ does not depend on the structure of the simplicial complex C and then can be written $\alpha(s)$.*

Property 10. *Let Λ be a countable space of arbitrary elements, and let C be a simplicial complex in Λ. Then, for any $s \in C$, the rank of any k-simplex in $|C|$ is $\rho(s, |C|) = k$.*

In other words, the dimension of an abstract simplex equals its rank into the simplicial complex it belongs to.

Property 11. *Let Λ be a countable space of arbitrary elements, and let C be a simplicial complex in Λ. Then, for any $s \in C$, $\alpha(s)$ is a simplicial complex. Also, let S be a subset of C, the set $\alpha(S) = \bigcup_{s \in S} \alpha(s)$ is a simplicial complex.*

Since we have defined the closure α_C in a simplicial complex C, we have induced the definition of its inverse binary relation $\beta_C = \alpha_C^{-1}$, called the *star operator* (in C):

$$\forall s \in C, \beta_C(s) = \{t \in C \ ; \ s \subseteq t\} .$$

Note that, contrary to the closure operator α, we cannot simplify this notation, since $\beta_C(s)$ clearly depends on the structure of the simplicial complex C.

C.14 Simplicial Neighborhoods

Definition 105 (Simplicial neighborhood)**.** *Let Λ be a countable space of arbitrary elements, let C be a simplicial complex in Λ, and let be K a subcomplex of C. We denote by $N(K, C)$ the* simplicial neighborhood *of the subcomplex K into the simplicial complex C, and we defined it such as:*

$$N(K, C) = \bigcup_{s \in K} \alpha(\beta_C(s)).$$

Property 12. *Let C be a simplicial complex and let K be a subcomplex of C. Then then simplicial neighborhoord $N(K, C)$ of K in C is a simplicial complex.*

Figure C.16 depicts in (a) in dark gray a simplicial complex C, and in light gray a simplicial subcomplex K of C. On (b), we can observe in light gray the closure of the star of K in C, that is, $N(K, C)$.

C.15 Chain Complexes

Now that we have defined simplices, simplicial complexes and subcomplexes, we can define the *chain complexes*.

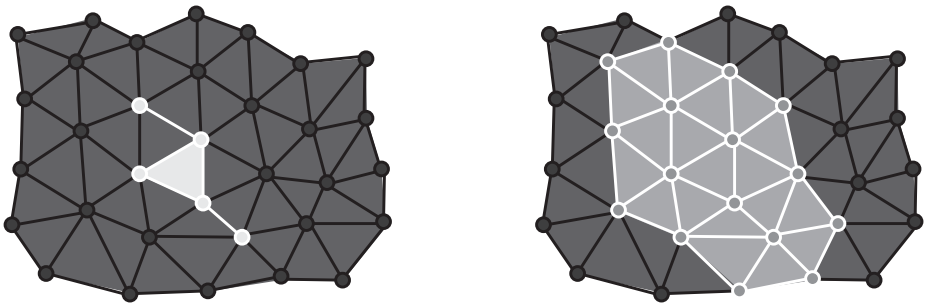

Figure C.16: From a subcomplex to its simplicial neighborhood ([41], p.46).

Definition 106 (Chain)**.** *Let $|X| = (X, \alpha_X)$ be a partially ordered set. Any subset c of X such that $|c| = (c, \alpha_c)$ is totally ordered is called a* chain *of $|X|$.*

Definition 107 (Chain complex)**.** *Let $|X| = (X, \alpha_X)$ be a partially ordered set. Then the set of all the chains of $|X|$ is denoted by $\mathcal{C}^X$ and is called the* chain complex *of $|X|$.*

Property 13. *Let $|X| = (X, \alpha_X)$ be a partially ordered set. Then $\mathcal{C}^X$ is a simplicial complex, and its support is equal to X.*

Effectively, for any element $s \in \mathcal{C}^X$, each face of s belongs to $\mathcal{C}^X$ since it is also a total order. This way, $\mathcal{C}^X$ is closed by the inclusion order, and is a simplicial complex. Also, $\mathcal{C}^X$ is the set of the subsets of X which are totally ordered (in $|X|$), and in this manner its support is the set of the elements in X, that is, X itself.

Figure C.17 shows on the right an order $|X|$ made of all the simplices in $\Lambda = \{a, b, c\}$ and on the right its chain complex $\mathcal{C}^X$. Since any set made of only one element is totally ordered, obviously $\{\{a\}\}$, $\{\{b\}\}$, $\{\{c\}\}$, $\{\{a, b\}\}$, $\{\{b, c\}\}$, $\{\{a, c\}\}$, and $\{\{a, b, c\}\}$ belong to $\mathcal{C}^X$. Also, $\{\{a\}, \{a, b\}\}$ is made of $\{a\}$ and $\{a, b\}$ which belong both to X and are ordered in $|X|$, and then $\{\{a\}, \{a, b\}\}$ belongs to $\mathcal{C}^X$. We can continue this way until we obtain the simplicial complex $\mathcal{C}^X$.

Now that we have defined chain complexes, we can cite a fundamental theorem of Daragon [41], based of prerequisites defined in Section C.8:

Theorem 17 (Theorem 17 (p. 58 of [41]))**.** *Let $|X|$ be an order. Then, $|\mathcal{C}^X|$ is a n-surface iff $|X|$ is a n-surface.*

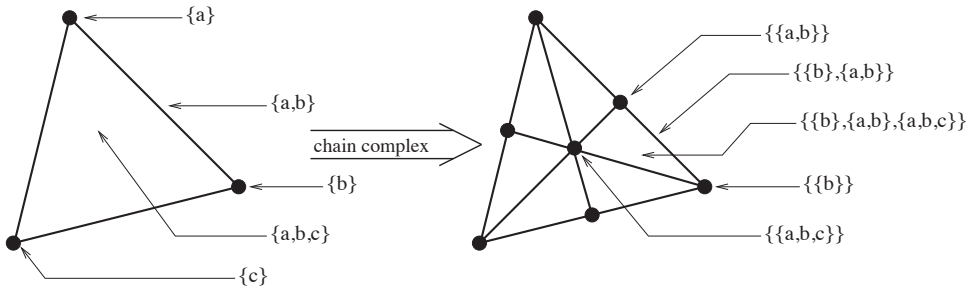

Figure C.17: From an order to its chain comples ([41], p.46).

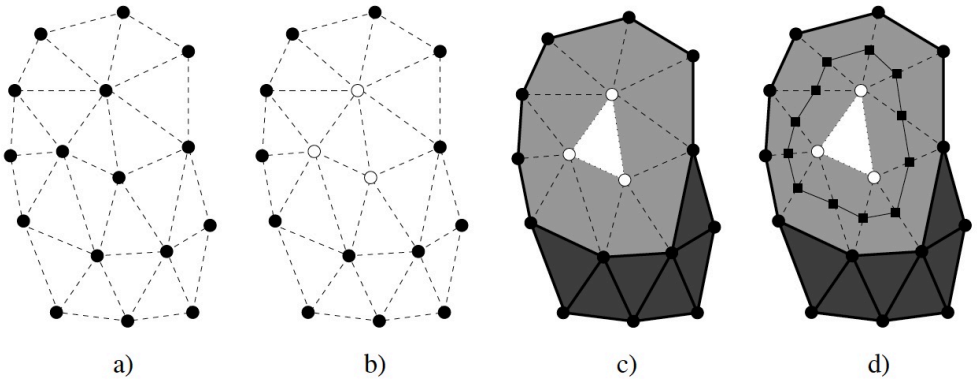

Figure C.18: From a simplicial complex to a frontier order ([41], p. 86).

Intuitively, this theorem means that if an order is a discrete surface, then its "triangulation", that is, its decomposition into triangles, is also a discrete surface.

C.16 Frontier orders

Definition 108 (Frontier Orders [41])**.** *Let C be a simplicial complex, and Λ_C its support. Let us decompose now Λ_C into the union of K the* foreground *and K' the* background*:*

$$\Lambda_C = K \sqcup K'.$$

Then C can be decomposed into 3 disjoint parts: C_K which is the set of the simplices contained into K, $C_{K'}$ which is the set of simplices contained into

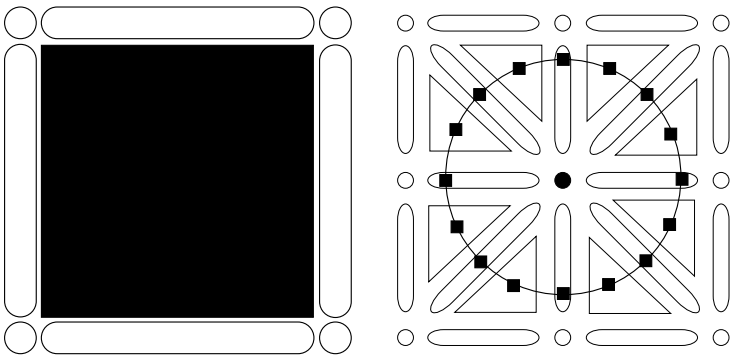

Figure C.19: A cubical complex and the frontier order of the central square into this order.

K', and $C_{K/K'}$ which is the set of simplexes not contained into K and not contained into K'. Then $|C_{K/K'}| = (C_{K/K'}, \supseteq)$ is called the frontier order *of K into Λ_C relatively to C.*

Note that a frontier order is not a simplicial complex: since any vertex belongs either to K or to K', it does not belong to $C_{K/K'}$.

Figure C.18 depicts on (a) a simplicial complex C; on (b) a subset K of the support of C (c.f. the white points); on (c) the tripartition of C into K in white, K' in dark gray, and the frontier order $C_{K/K'}$ in light gray; on (d), we can see the "immersion" of the frontier order represented with black squares and the edges that link them.

The definition of a frontier order exists also for any order [41].

Definition 109. *Let $|X|$ be an order, and let $|Y|$ and $|Y'|$ be two suborders of $|X|$ such that $Y \sqcup Y' = X$. The order $|\mathcal{C}^X_{Y/Y'}| = (\mathcal{C}^X_{Y/Y'}, \supseteq)$, where $\mathcal{C}^X_{Y/Y'}$ denotes the set of simplices of $\mathcal{C}^X$ such that they are not contained into Y and not contained into Y', is called the* frontier order *of $|Y|$ into $|X|$.*

Figure C.19 depicts a cubical complex $|X|$ (on the left), where X is decomposed into $Y \sqcup Y'$. Y is depicted by the black square, and Y' corresponds to $X \setminus Y$ (the white faces of the complex). Then, applying the chain complex on this order, we obtain the right figure, where the complex whose support is Y is made of the black vertex, the complex whose support is Y' is made of the white vertices, and the remaining part of the chain complex is the frontier order $\mathcal{C}^X_{Y/Y'}$ whose immersion is represented with the little squares and the edges linking them.

Theorem 18 (Frontier Orders of a Simplicial Complex [41] (Th. 37 p. 89))**.** *Let C be a simplicial complex which is a n-surface, $n \geq 2$, and let be Λ_C its support. Let K be a strict non-empty subset of Λ_C. Then the order $|C_{K/K'}|$ is an union of disjoint $(n-1)$-surfaces.*

Theorem 19 (Frontier Orders of an Order [41] (Th. 38 p. 90))**.** *Let $|X|$ be an order, and let $|Y|$ be a strict suborder of $|X|$. Then the order $|\mathcal{C}^X_{Y/Y'}|$ is a disjoint union of $(n-1)$-surfaces.*

C.17 Derived Neighborhoods

As we are going to recall, a chain complex can be effectively seen as a triangulation.

Definition 110 (Derived subdivision)**.** *Let C be a simplicial complex. The first* derived subdivision *of C is denoted C^1 and is defined such that:*

$$C^1 = \{\{c_0, \ldots, c_n\} \subseteq C \; ; \; c_0 \subset \cdots \subset c_n\}.$$

The n^{th} derived subdivision *is defined such that:*

$$C^n = (C^{n-1})^1.$$

As we can see, the first derived of a simplicial complex C is simply its chain complex $\mathcal{C}^C$.

Definition 111 (Derived neighborhood)**.** *Let C be a simplicial complex of support Λ_C. Let also K be a full subcomplex of C such that its support Λ_Y satisfies $\Lambda_Y \subseteq \Lambda_X$. The* first derived neigborhood *of K in C is denoted by $N^1(K, C)$ and is equal to the simplicial neighborhood of K^1 into C^1:*

$$N^1(K, C) = \bigcup_{k^1 \in K^1} \alpha(\beta_{C^1}(k^1)).$$

Figure C.20 shows the step-by-step process to compute a derived neighborhood of a subcomplex K which is full in a simplicial complex C. On (a), the entire figure corresponds to the simplicial complex C, and the triangle whose corners are white, with all its faces, corresponds to the full subcomplex K. Then, in (b), a derived subdivision is processed. It is equivalent to compute the chain complex of C. On (c), we can see in light gray the derived neighborhood of K which is equal to the union of the closures of the stars of K^1 into C^1. On (d), we can see the *border* of the derived neighborhood of K in C, its definition will come hereafter.

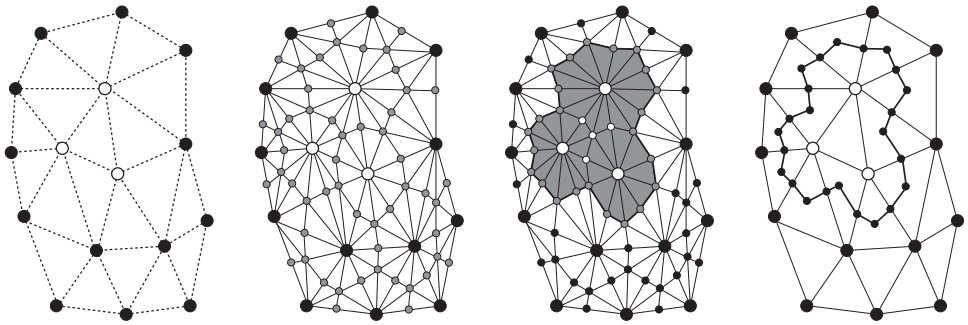

Figure C.20: From a full subcomplex to its derived neighborhood ([41], p. 98).

C.18 Border of a Derived Neighborhood

Let us now recall the definition of a border, since it is the link between a derived neighborhood and a frontier order.

Definition 112 (Border of a derived neighborhood (p.98 [41]))**.** *Let C be a simplicial complex and K be a full subcomplex of C. The* border *of the derived neighborhood of K into C is denoted by $\Delta(K, C)$ and is equal to:*

$$\Delta(K, C) = \left\{ h \in N^1(K, C) \; ; \; \beta_{C^1}(h) \not\subseteq N^1(K, C) \right\}.$$

Theorem 20 (Th. 40 (p.99 [41]))**.** *Let X be a simplicial complex of support Λ_X, let Y be a full subcomplex of X of support K, and let K' be the complement of K into Λ_X. Then $\Delta(Y, X)$ is equal to the chain complex of the frontier order $X_{K/K'}$, that is:*

$$\Delta(Y, X) = [X_{K/K'}]^1.$$

For Theorem 19 and Theorem 21, Daragon deduced then:

Theorem 21 (Th. 42 (p.101 [41]))**.** *Let X be a simplicial complex. If X is a n-surface, $n \geq 1$, and if Y is a subcomplex full in X, then $\Delta(Y, X)$ is a disjoint union of $(n-1)$-surfaces.*

C.19 Plain maps

Let us now recall some mathematical background coming from [10, 124].

Let $\mathcal{A} = (X, \mathcal{U})$ be an Alexandrov space.

Definition 113. *An application $F : X \to \mathcal{P}(\mathbb{R})$ (which is also written $F : X \rightsquigarrow \mathbb{R}$) is said to be a* set-valued map. *The* domain *of F is the set $\mathcal{D}(F) \subseteq X$ such that $\forall x \in X$, $F(x) \neq \emptyset \Leftrightarrow x \in \mathcal{D}(F)$.*

Definition 114. *A set-valued map $F : X \rightsquigarrow \mathbb{R}$ is said to be* upper semi-continuous (USC) *at $x \in \mathcal{D}(F)$, for any neighborhood $\mathcal{U}$ of $F(x)$, $\forall x' \in \beta(x)$, $F(x') \subseteq \mathcal{U}$. A set-valued map is said to be* upper semi-continuous (USC) *iff it is USC at each point $x \in \mathcal{D}(F)$.*

Definition 115. *A set-valued USC map $F : X \rightsquigarrow \mathbb{R}$ is said to be a* (closed) quasi-simple map *iff for any $x \in \mathcal{D}(F)$, $F(x)$ is a closed connected set and furthermore, for any $x \in \mathcal{D}(F)$ such that $\{x\} = \beta(x)$, $F(x)$ is degenerate.*

Definition 116. *A quasi-simple map $F : X \rightsquigarrow \mathbb{R}$ is said to be a* simple map *iff for any quasi-simple map $F_2 : X \rightsquigarrow \mathbb{Z}$ such that $F(x) = F_2(x)$ when $x \in \mathcal{D}$ is such that $\beta(x) = \{x\}$, then for any $x \in \mathcal{D}(F)$, $F(x) \subseteq F_2(x)$.*

Definition 117. *A set-valued map $F : X \rightsquigarrow \mathbb{R}$ is said to be a* plain map *iff it is a closed-valued interval-valued simple map.*

Now, let us assume that A and B are two topological spaces.

Definition 118. *Let $F : A \rightsquigarrow B$ be a set-valued map. We call the* inverse image *of M by F the set $F^-(M) = \{x \in A \; ; \; F(x) \cap M \neq \emptyset\}$. Also, we call* core *of M by F the set $F^+(M) = \{x \in A \; ; \; F(x) \subseteq M\}$.*

Then some properties [10] follow for USC maps:

Proposition 33. *A set-valued map $F : A \rightsquigarrow B$ is USC at x iff the core of any neighborhood of $F(x)$ is a neighborhood of x. Hence, a set-valued map $F : A \rightsquigarrow B$ is USC iff the core of any open subset is open.*

Proposition 34. *If $\mathcal{D}(F)$ is closed, then F is USC iff the inverse image of any closed set is closed.*

Appendix D

About the equivalence between AWCness and DWCness

Today, 4D signals (and beyond) are of primary importance, and then it is crucial to determine the relations between the different definitions in matter of well-composedness. In this section, we investigate the relation between digital well-composedness and well-composedness in the sense of Alexandrov. In fact, if these two definitions are equivalent, it means that well-composed in the sense of Alexandrov images can easily be obtained on cubical grids thanks to digitally well-composed interpolations, and conversely, that digitally well-composed images share the strong topological properties of images that are well-composed in the sense of Alexandrov when they are immersed on Khalimsky grids.

So, in the following sections, after having presented a counter-example showing that this proof is not simple, we will present a sketch of the proof.

Note that the complete proof can be found at the following address:
https://hal-upec-upem.archives-ouvertes.fr/hal-01375621

Note: since this proof has not been verified yet, it will be considered in this thesis as a conjecture.

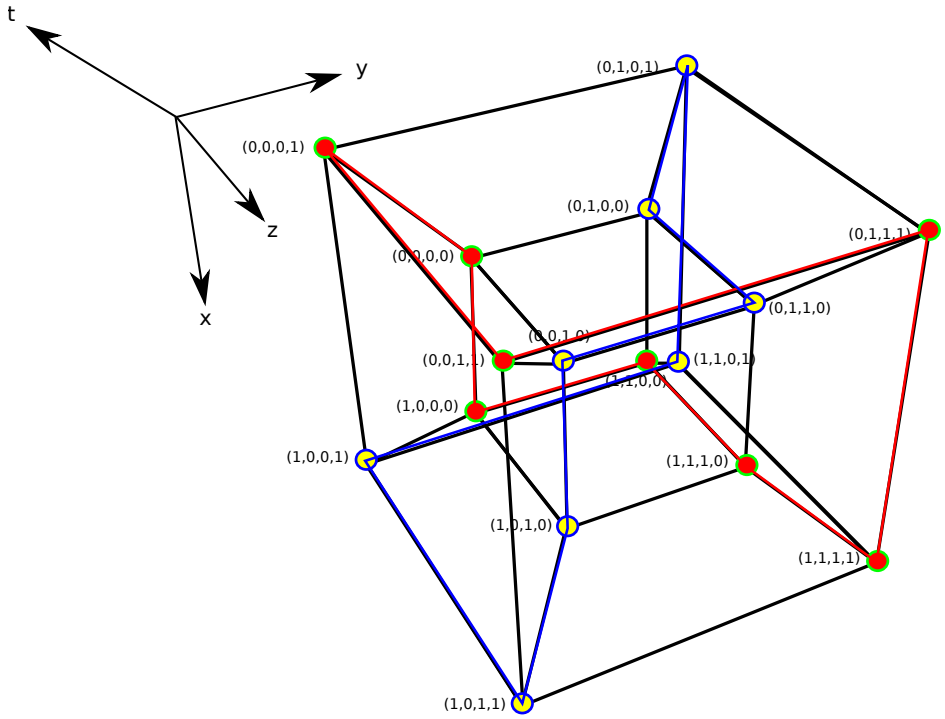

Figure D.1: A 4D digitally well-composed set (depicted in blue) and its complement (in red).

D.1 Preamble

Before beginning the study of the equivalence between these two kinds of well-composednesses, we propose to illustrate the difficulty of this proof with an example showing that the intuition that "a digitally well-composed set should always be the limit of an increasing sequence of digitally well-composed sets" is false. A 4D example of digitally well-composed sets can prove this (see Figure D.1). Effectively, removing/adding any point to this set made of yellow points and blue edges creates a critical configuration of dimension 2, and there there exists no strictly increasing/decreasing sequence of digitally well-composed sets which converges to this set.

D.2 A sketch of the proof

Let us present the main steps of the proof that AWCness (see Section 3.1) and DWCness are equivalent on cubical grids.

From $\left(\frac{\mathbb{Z}}{2}\right)^n$ to $\mathbb{H}^n$ We define the bijection $\mathcal{H} : (\mathbb{Z}/2) \to \mathbb{H}^1$ such that:

$$\forall z \in (\mathbb{Z}/2), \mathcal{H}(z) = \begin{cases} \{z + 1/2\} & \text{if} \quad z \in (\mathbb{Z}/2) \setminus \mathbb{Z}, \\ \{z, z + 1\} & \text{if} \quad z \in \mathbb{Z}. \end{cases} \tag{D.1}$$

We can then deduce the bijection $\mathcal{H}_n : \left(\frac{\mathbb{Z}}{2}\right)^n \to \mathbb{H}^n$ defined such that:

$$\mathcal{H}_n = \otimes_{i \in [\![1,n]\!]} \mathcal{H}(z_i),$$

where z_i denote the i^{th} coordinate of $z \in (\mathbb{Z}/2)$.

We can compute the inverse bijection of $\mathcal{H}$, that we denote by $\mathcal{Z} : \mathbb{H}^1 \to (\mathbb{Z}/2)$, and defined such that:

$$\forall h \in \mathbb{H}^1, \mathcal{Z}(h) = \begin{cases} a & \text{if} \quad \exists a \in \mathbb{Z} \text{ s.t. } h = \{a, a + 1\}, \\ a - 1/2 & \text{if} \quad \exists a \in \mathbb{Z} \text{ s.t. } h = \{a\}. \end{cases} \tag{D.2}$$

We can then deduce the bijection $\mathcal{Z}_n : \mathbb{H}^n \to (\mathbb{Z}/2)$ defined such that:

$$\mathcal{Z}_n = \otimes_{i \in [\![1,n]\!]} \mathcal{Z}(h_i),$$

where h_i denote the i^{th} coordinate of $h \in \mathbb{H}^n$.

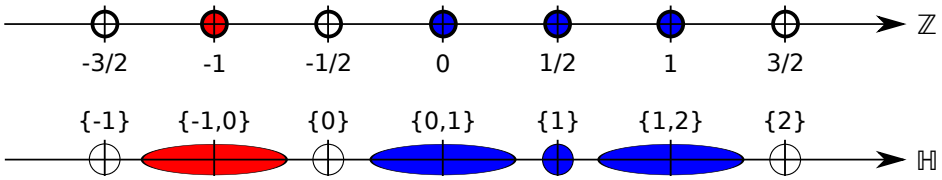

Figure D.2: Bijection between $\mathbb{H}^1$ and $(\mathbb{Z}/2)$

Figure D.2 shows how $(\mathbb{Z}/2)$ is mapped to $\mathbb{H}^1$. Furthermore, it can be shown that supplying $\left(\frac{\mathbb{Z}}{2}\right)^n$ with a particular topology, $\mathcal{Z}_n$ (respectively $\mathcal{H}_n$) is in fact a *topological isomorphism*, that is a bicontinuous bijection, between $\mathbb{H}^n$ and $\left(\frac{\mathbb{Z}}{2}\right)^n$ (respectively between $\left(\frac{\mathbb{Z}}{2}\right)^n$ and $\mathbb{H}^n$). In other words, these two spaces have the same topological structure.

Immersion into Khalimsky Grids Starting from a given digital set $X \subset \mathbb{Z}^n$, we can immerse it into $\mathbb{H}^n$ in the following manner:

$$\mathcal{IMM}(X) \equiv \mathrm{Int}(\alpha(\mathcal{H}_n(X))),$$

where Int it the topological interior in $\mathbb{H}^n$:

$$\mathrm{Int}(X) = \{h \in X \ ; \ \beta(h) \subseteq X\}\,.$$

Stating the problem The context is the following: we have a set X made of points in $\mathbb{Z}^n$, from which we compute its immersion $\mathcal{IMM}(X)$ in the Khalimsky grids. X is digitally well-composed iff it does not contain any critical configuration, and X (or its immersion $\mathcal{IMM}(X)$ by identification) is said well-composed in the sense of Alexandrov iff the topological boundary $\mathfrak{N}$ of $\mathcal{IMM}(X)$ defined such as:

$$\mathfrak{N} = \alpha(\mathcal{IMM}(X)) \cap \alpha(\mathbb{H}^n \setminus \mathcal{IMM}(X)),$$

is made of disjoint discrete $(n-1)$-surfaces.

We want to establish that these two concepts are rigorously equivalent.

Reformulating the topological boundary The topological boundary $\partial\mathcal{IMM}(X)$ can be reformulated as a function of $\mathcal{X} = \mathcal{H}_n(X)$ and the complement $\mathcal{Y} = \mathbb{H}^n_n \setminus \mathcal{X}$ of $\mathcal{X}$ in $\mathbb{H}^n_n$. Effectively, we have the following proposition:

$$\mathfrak{N} = \alpha(\mathcal{X}) \cap \alpha(\mathcal{Y}).$$

Summarily, we can reformulate this way the boundary because these following properties are verified in $\mathbb{H}^n$:

- $\mathbb{H}^n$ is a n-surface and then is homogeneous,
- $\forall z \in \mathbb{H}^n$, $\alpha(\beta(z) \cap \mathbb{H}^n_n) = \alpha(\beta(z))$,
- $\forall z \in \mathbb{H}^n$, $\alpha(z)$ is a regular closed set,
- $\forall z \in \mathbb{H}^n$, $\beta(z)$ is a regular open set.

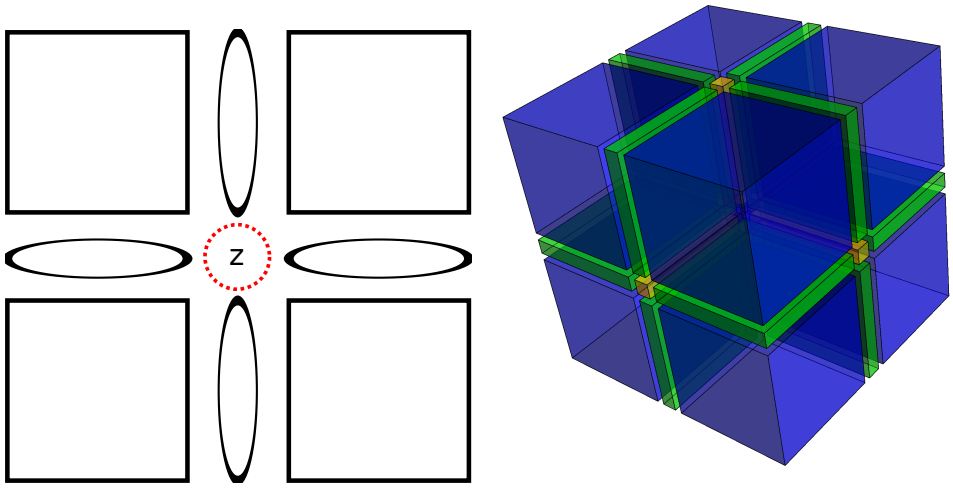

Figure D.3: The subspace $|\beta^{\square}(z)|$ we are working in to study AWCness (2D/3D cases).

Reformulating the problem in a local way We could then directly prove that the fact that $\mathcal{IMM}(X)$ is well-composed in the sense of Alexandrov implies that X is digitally well-composed, and the converse, and we would be done. However, we observed that we can reformulate the condition "$\mathcal{IMM}(X)$ is well-composed in the sense of Alexandrov" with another condition, much simple to handle and manipulate, since it is a local criteria (as digital well-composedness is). Effectively, $\mathcal{IMM}(X)$ is well-composed in the sense of Alexandrov is equivalent to:

$$\left\{\forall z \in \mathfrak{N}, |\beta^{\square}_{\mathfrak{N}}(z)| \text{ is a } (n-2-\dim(z)) - \text{surface}\right\}.$$

Since $|\beta^{\square}_{\mathfrak{N}}(z)|$ is equal to $|\mathfrak{N} \cap \beta^{\square}(z)|$, we understand effectively that we are studying a restriction of the boundary $\mathfrak{N}$ in a small subspace, that is, $|\beta^{\square}(z)|$, depicted on Figure D.3, where we can observe that the point z in the middle of the subspace has been omitted, since it is not taken into account in the local criteria.

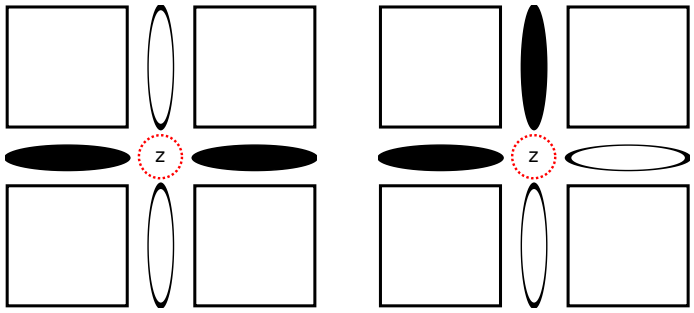

Figure D.4: Examples of 0-surfaces (in black).

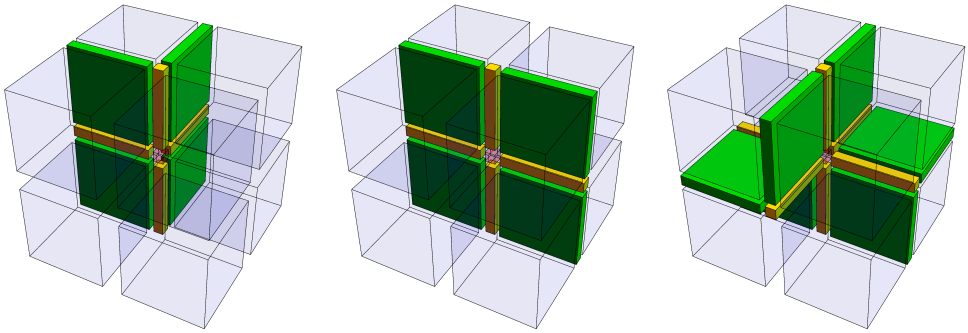

Figure D.5: Examples of 1-surfaces.

The question is then: what does it mean that $|\beta^{\square}_{\mathfrak{N}}(z)|$ is an $(n-2-\dim(z))$-surface? When $\dim(z) = (n-2)$, that is, when $\beta(z)$ is a subspace of dimension 2 as on the left of Figure D.3, it means that $|\beta^{\square}_{\mathfrak{N}}(z)|$ is a 0-surface, that is, the restriction $|\beta^{\square}_{\mathfrak{N}}(z)|$ of the boundary $\mathfrak{N}$ to the subspace $\beta^{\square}(z)$ is made of two elements which are not neighbors the one of the other one (see Figure D.4). When $\dim(z) = (n-3)$, that is when $\beta(z)$ is a subspace of dimension 3 as on the right of Figure D.3, it means that the restriction $|\beta^{\square}_{\mathfrak{N}}(z)|$ of the boundary $\mathfrak{N}$ to the 3D subspace $\beta^{\square}(z)$ is a 1-surface, that is, a simple closed curve (see Figure D.5).

Our aim is then to prove that X is digitally well-composed iff for any element z of the boundary $\mathfrak{N}$, we have that $|\beta^{\square}_{\mathfrak{N}}(z)|$ is a $(n - \dim(z) - 2)$-surface.

Study of the converse sense Let us begin with the converse sense: we admit that for any element z of the boundary $\mathfrak{N}$, we have that $|\beta^{\square}_{\mathfrak{N}}(z)|$ is a $(n - \dim(z) - 2)$-surface, and we want to prove that X is digitally well-composed. For that, we will prove the counterposition: we assume that X is not digitally well-composed, and then contains a critical configuration, and we show that it implies that there exists a "critical point" z^* such that $|\beta^{\square}_{\mathfrak{N}}(z^*)|$ is not a discrete surface.

So, let assume that X contains a primary critical configuration in a block S of dimension $k \geq 2$, that is, $X \cap S = \{p, p'\}$ such that p and p' are antagonist into S (the secondary case follows the same reasoning, by duality of well-composedness in the sense of Alexandrov and digital well-composedness). It is then clear that all the other points of the block S belong to he complement Y of X in $\mathbb{Z}^n$.

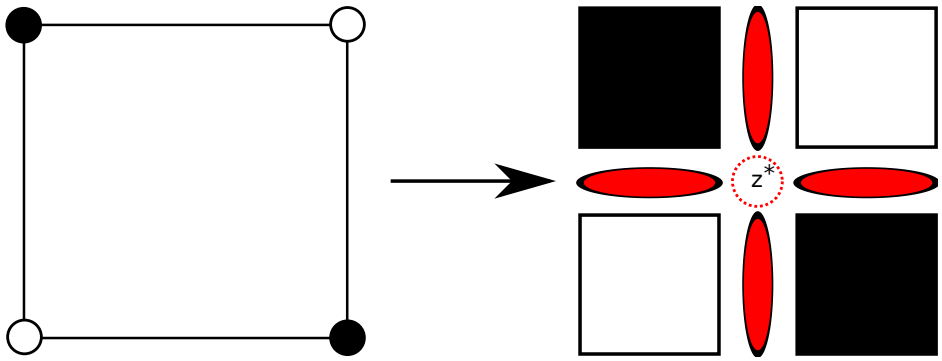

Figure D.6: From a 2D critical configuration in $\mathbb{Z}^2$ to a critical point z^* in $\mathbb{H}^2_0$.

Let us begin with the 2D case, that is, when the block S is of dimension $k = 2$ in $\mathbb{Z}^n$. In this case, its isomorph in $\mathbb{H}^n$, which is in reality made of n-cubes, can be represented using squares, as depicted on Figure D.6. Then, the center of these four squares, that we will call z^*, has a dimension $(n-2)$. Let us show that this point is critical in the sense that $|\beta^{\square}_{\mathfrak{N}}(z)|$ is not a 0-surface. For that, as shown on Figure D.6, we work into the space $\beta^{\square}(z^*)$,

which contains our four colored squares, and we compute their respective closures (into the subspace $\beta^{\square}(z^*)$), their intersection will then be $\beta^{\square}_{\mathfrak{N}}(z^*)$. Effectively, $|\beta^{\square}_{\mathfrak{N}}(z^*)|$ is not a 0-surface, because it is made of 4 points and a 0-surface is made of two points, then z^* is "critical" and we have "proven" the reciprocal sense for $k = 2$.

Let us now proceed to the 3D case, that is, when the block S is of dimension $k = 3$ in $\mathbb{Z}^n$. In this case, its isomorph in $\mathbb{H}^n$ can be represented using cubes, as depicted on Figure D.7. Then, the center z^* of these 8 cubes has a dimension $(n-3)$ and is critical in the sense that $|\beta^{\square}_{\mathfrak{N}}(z^*)|$ is an union of two disjoint 1-surfaces, and then it is not a 1-surface. So we "proved" the case $k = 3$ too.

In fact, for the general case $k \in [\![2, n]\!]$, it can be proven that, if we denote by $\mathfrak{p}$ and $\mathfrak{p}'$ the isomorphisms of the two points p and p' respectively into the cubical complexes $\mathbb{H}^n$, starting from the formulation $\mathfrak{N} = \alpha(\mathcal{X}) \cap \alpha(\mathcal{Y})$, we obtain:

$$\beta^{\square}_{\mathfrak{N}}(z^*) = \left(\alpha^{\square}(\mathfrak{p}) \cup \alpha^{\square}(\mathfrak{p}')\right) \cap \beta^{\square}(z^*),$$

which can be decomposed into two orders $|\alpha^{\square}(\mathfrak{p}) \cap \beta^{\square}(z^*)|$ and $|\alpha^{\square}(\mathfrak{p}') \cap \beta^{\square}(z^*)|$ which are disjoint $(n-2-\dim(z))$-surfaces, and then their union is not a $(n-2-\dim(z))$-surface.

Study of the direct sense Since we have explained how we proceed in the countersense, let us show how we proceed in the direct sense.

We want to prove that if X is digitally well-composed, then $\mathcal{IMM}(X)$ is well-composed in the sense of Alexandrov, which can be proven by the fact that for any element z of the boundary $\mathfrak{N}$, we have that $|\beta^{\square}_{\mathfrak{N}}(z)|$ is a $(n - \dim(z) - 2)$-surface. In fact, we will proceed by induction. We define the property $(\mathcal{P}_k)$ such that if this property is true for any value $k \in [\![1, n]\!]$, then X is well-composed in the sense of Alexandrov:

$$(\mathcal{P}_k) = \left\{\forall z \in \mathfrak{N} \cap \mathbb{H}^n_{n-k},\ |\beta^{\square}_{\mathfrak{N}}(z)| \text{ is a } (n-2-\dim(z)) - \text{surface}\right\}.$$

Obviously, the case $k = 0$ is not necessary, since no point of the boundary $\mathfrak{N}$ is a n-cube.

So let start with $k = 1$: in this case, z is a $(n-1)$-face, and then $\beta^{\square}(z)$ is empty, which means that $|\beta^{\square}_{\mathfrak{N}}(z)|$ is a (-1)-surface since it is the empty order. Let us continue with $k = 2$. In this case, z is a $(n-2)$-face, and

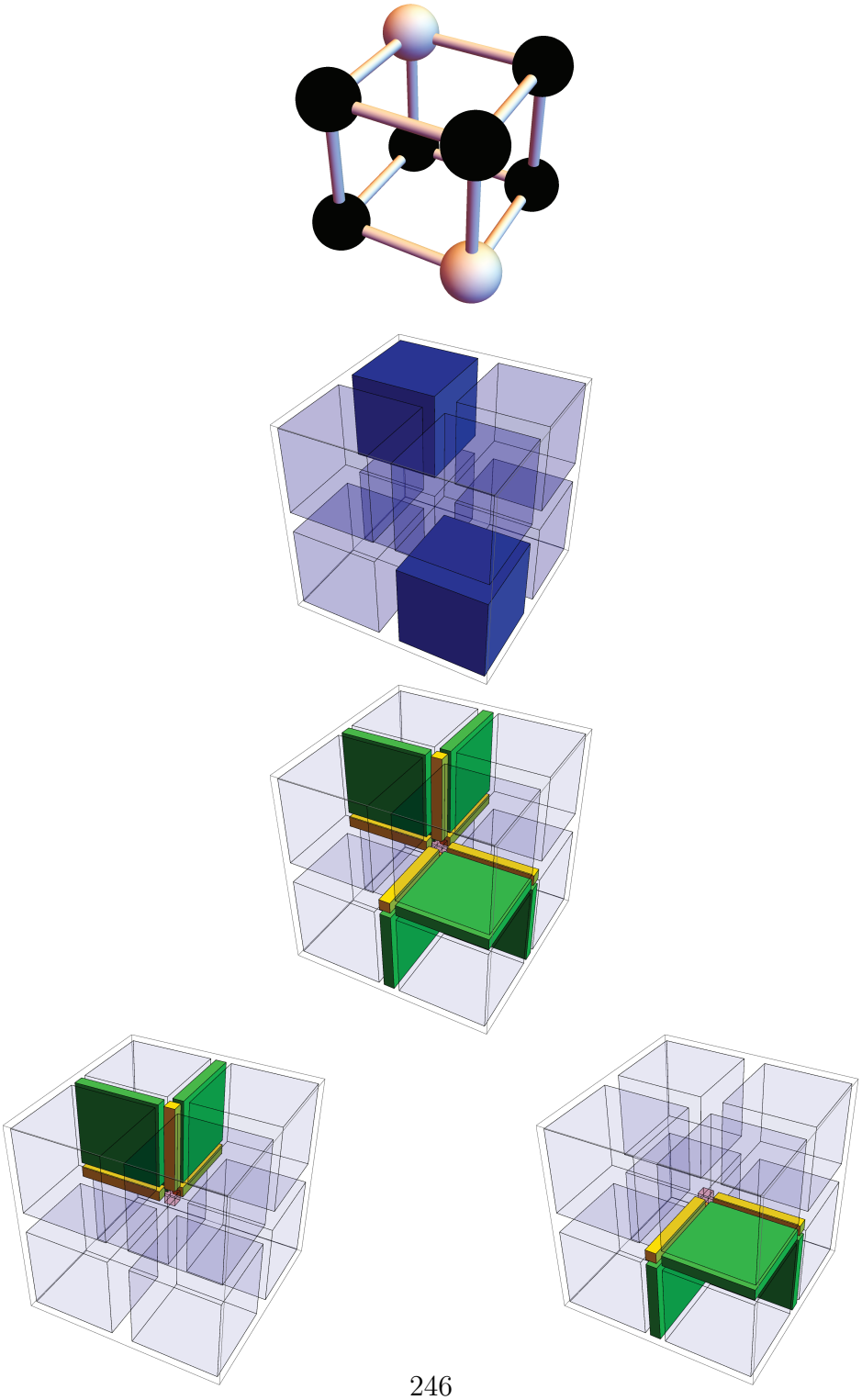

Figure D.7: From the 3D critical configuration to the critical point.

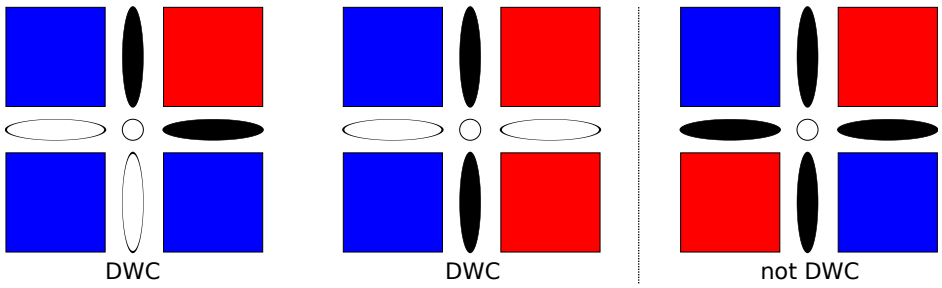

Figure D.8: Assuming that X is DWC, $|\beta^{\square}_{\mathfrak{N}}(z)|$ is a 0-surface when $\dim(z) = n-2$ $(k=2)$.

then it is sufficient to proceed cases by case (modulo symmetry, rotation, and complementation), as shown by Figure D.8. The isomorphism of X restricted to $\beta^{\square}(z)$ is depicted using blue faces, and the isomorphism of $Y = \mathbb{Z}^n \setminus X$ restricted to $\beta^{\square}(z)$ is depicted using red faces. Since we have the relation $\mathfrak{N} = \alpha(\mathcal{X}) \cap \alpha(\mathcal{Y})$, we obtain in the two DWC cases (on the left and at the middle) that the intersection of the closure of the blue faces and the closure of the red faces makes a 0-surface in $\beta^{\square}(z)$ (depicted in black), since its restriction to $\beta^{\square}(z)$ is made of two points which are not neighbors the one of the other one. The case $k = 2$ is then treated.

For the cases $k \in [\![3, n]\!]$, we can proceed by induction on k since the initialization succeeded. So let us assume that $k \in [\![3, n]\!]$ is given and that the property $(\mathcal{P}_l)$ is true for any $l \in [\![1, k-1]\!]$, we want to prove it for k.

In this case, z is a $(n-k)$-face with $k \geq 3$, which means that $\dim(z) \leq (n-3)$, and then $(n-2-\dim(z)) \geq 1$. It is clear then that $|\beta^{\square}_{\mathfrak{N}}(z)|$ is a $(n-2-\dim(z))$-surface iff we have two conditions: (1) $|\beta^{\square}_{\mathfrak{N}}(z)|$ must be connected, and (2) for any point u of $\beta^{\square}_{\mathfrak{N}}(z)$, $|\theta^{\square}_{\beta^{\square}_{\mathfrak{N}}(z)}|$ must be a $(n-3-\dim(z))$-surface.

Even if the secund condition seems to be much more complicated than the first one, it is in fact the converse. Effectively, it it easy to prove by a simple calculus that $|\theta^{\square}_{\beta^{\square}_{\mathfrak{N}}(z)}|$ is equal to:

$$|\beta^{\square}_{\mathfrak{N}}(u)| * \left|\alpha^{\square}(u) \cap \beta^{\square}(z)\right|,$$

which corresponds to an order join of $|\beta^{\square}_{\mathfrak{N}}(u)|$ which is a $(n-2-\dim(u))$-surface by the induction hypothesis and $\left|\alpha^{\square}(u) \cap \beta^{\square}(z)\right|$, from which we can

prove it is a $(\dim(u)-\dim(z)-2)$-surface. Since an order join of a k_1-surface and of a k_2-surface is a (k_1+k_2+1)-surface by Theorem 15, $|\theta^{\square}_{\beta^{\square}_{\mathfrak{N}}(z)}|$ is a $(n-3-\dim(z))$-surface. Then (2) is proven.

To prove (1), we assume that there exists $z \in \mathbb{H}^n_{n-k}$ such that $|\beta^{\square}_{\mathfrak{N}}(z)|$ is not connected. We will see that this hypothesis is essential, since many properties will follow on, until we reach a contradiction.

Assuming $|\beta^{\square}_{\mathfrak{N}}(z)|$ is not connected obviously means that it is made of several connected components, that we will denote by $\{F_i\}_{i\in\mathcal{I}}$. The first fundamental property is that each component F_i, $i \in \mathcal{I}$, is a $(n-2-\dim(z))$-surface because they are connected (by definition) and because we can prove that for any $u \in F_i$, we have $|\theta^{\square}_{F_i}|$ which is equal to $|\theta^{\square}_{\beta^{\square}_{\mathfrak{N}}(z)}|$, which is a $(n-3-\dim(z))$-surface, and then F_i is a $(n-2-\dim(z))$-surface.

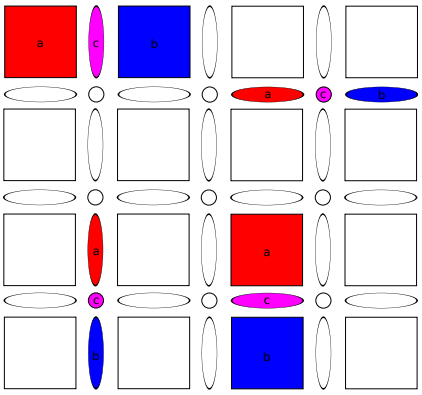

Figure D.9: Examples of opposites in $\mathbb{H}^2$.

Starting from this first property, a secund fundamental property follows on: for $i \in \mathcal{I}$, a same component F_i cannot contain *opposite* faces relatively to z. Roughly speaking, opposite faces are two faces which are symmetrical relatively to a third face (see Figure D.9). Effectively, we can feel that if one first component contains two opposite face in $\beta^{\square}(z)$, it will separate any other component of $|\beta^{\square}_{\mathfrak{N}}(z)|$, which is impossible since each F_i is connected by hypothesis.

Now that we know that each component F_i cannot contain two opposite faces, the third fundamental property can be proven: each of them contains exactly $(n-\dim(z))\ (\dim(z)+1)$ faces of $\beta^{\square}(z)$. For example, in the 3D

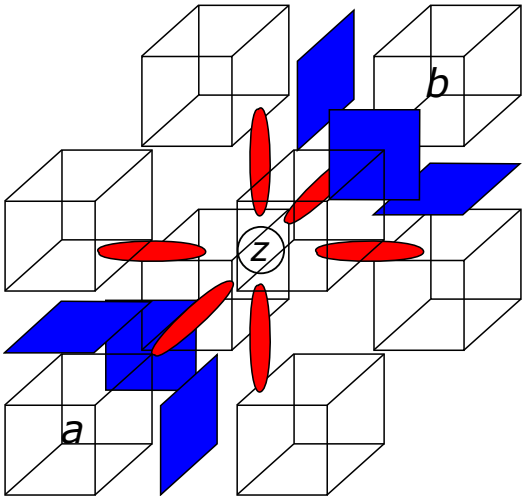

Figure D.10: Structure of $\beta^{\square}_{\mathfrak{N}}(z)$ when we have $(n - \dim(z)) = 3$ assuming that $|\beta^{\square}_{\mathfrak{N}}(z)|$ is not connected.

case, that is for $\dim(z) = (n-3)$ as on Figure D.10, where $(\dim(z)+1)$-faces are depicted in red, each component contains exactly 3 $(\dim(z) + 1)$-faces. Since there are $2(n - \dim(z))$ of these faces in $\beta^{\square}(z)$, $|\beta^{\square}_{\mathfrak{N}}(z)|$ is made of 2 components F_1 and F_2.

Using these three fundamental properties, it can be proven that each of these two components F_1 and F_2 lies in the closure of *characteristical* n-faces $\mathfrak{a}, \mathfrak{b} \in \mathbb{H}^n_n$ that we define here as the supremum of the $(\dim(z) + 1)$-faces contained in each of them. More precisely, $|F_1| \subseteq \left|\alpha^{\square}(\mathfrak{a}) \cap \beta^{\square}(z)\right|$ and $|F_2| \subseteq \left|\alpha^{\square}(\mathfrak{b}) \cap \beta^{\square}(z)\right|$. Furthermore, since we can prove that two k-surfaces which are included the one in the other one are equal and since $\left|\alpha^{\square}(\mathfrak{a}) \cap \beta^{\square}(z)\right|$ and $\left|\alpha^{\square}(\mathfrak{b}) \cap \beta^{\square}(z)\right|$ are two $(n - \dim(z) - 2)$-surfaces like the components F_1 and F_2, we obtain that:

$$\begin{array}{rcl} |F_1| & = & \left|\alpha^{\square}(\mathfrak{a}) \cap \beta^{\square}(z)\right|, \\ |F_2| & = & \left|\alpha^{\square}(\mathfrak{b}) \cap \beta^{\square}(z)\right|. \end{array}$$

On Figure D.10, representing the 3D case $(\dim(z) = n - 3)$, the first component made of red 1-faces and of blue 2-faces on the left lies in the closure of the 3-face a (in the subspace $\beta^{\square}(z)$) and the second component made of red 1-faces and of blue 2-faces on the right lies in the closure of the 3-face b (in the subspace $\beta^{\square}(z)$).

The link between the configuration we obtained in $\mathbb{H}^n_n$ by assuming that $|\beta^{\square}_{\mathfrak{N}}(z)|$ is not connected and a critical conguration is then clear: since $\beta^{\square}_{\mathfrak{N}}(z) \subseteq \mathfrak{N}$, if a belongs to X, then the rest of the block minus b belongs to Y, and then b belongs to X to, and we obtain a critical configuration of primary type in X. The dual reasoning leads to a secundary critical configuration in X. In both cases, we obtain a contradiction. Then $|\beta^{\square}_{\mathfrak{N}}(z)|$ is connected. Finally, $\mathcal{IMM}(X)$ is well-composed in the sense of Alexandrov when X is digitally well-composed.

Conclusion for sets Finally, we obtain the following conjecture:

Conjecture 8. *A set $X \subset \mathbb{Z}^n$ is DWC iff its immersion $\mathcal{IMM}(X)$ into the Khalimsky grids $|\mathbb{H}^n|$ is AWC, that is, is such that its topological boundary $\partial\mathcal{IMM}(X)$ is made of disjoint $(n-1)$-surfaces.*

Conclusion for plain maps Starting from a function $u : \mathbb{Z}^n \to \mathbb{R}$, we can compute its *immersion* $U : \mathbb{H}^n \rightsquigarrow \mathbb{R}$ into the Khalimsky grids, defined such that:

$$\forall h \in \mathbb{H}^n, U(h) = \begin{cases} \{u(\mathcal{Z}_n(h))\} & \text{if } z \in \mathbb{H}^n_n, \\ \text{Span}\,\{U(q)\ ;\ q \in \beta(z) \cap \mathbb{H}^n_n\} & \text{either .} \end{cases}$$

Note that U is a *plain map* (see Section C.19).

On Khalimsky grids, for a given plain map $U : \mathbb{H}^n \rightsquigarrow \mathbb{R}$, the following threshold sets exist [124]:

$$\begin{aligned} [U \trianglerighteq \lambda] &= \{\, z \in \mathbb{H}^n \mid \exists\, v \in U(z),\, v \geq \lambda \,\}, \\ [U \triangleright \lambda] &= \{\, z \in \mathbb{H}^n \mid \forall\, v \in U(z),\, v > \lambda \,\}, \\ .[U \triangleleft \lambda] &= \{\, z \in \mathbb{H}^n \mid \forall\, v \in U(z),\, v < \lambda \,\}, \\ [U \trianglelefteq \lambda] &= \{\, z \in \mathbb{H}^n \mid \exists\, v \in U(z),\, v \leq \lambda \,\}. \end{aligned}$$

Definition 119. *Let $U : \mathbb{H}^n \rightsquigarrow \mathbb{R}$ be a given plain map. We say that this map is* well-composed in the sense of Alexandrov *or* AWC *iff, for any value of $\lambda \in \mathbb{R}$, the connected components of the topological boundary of each of its threshold sets $[U \trianglerighteq \lambda]$, $[U \triangleright \lambda]$, $[U \triangleleft \lambda]$, and $[U \trianglelefteq \lambda]$ are $(n-1)$-surfaces.*

We obtain finally the following conjecture for maps:

Conjecture 9. *A real-valued image $u : \mathbb{Z}^n \to \mathbb{R}$ is DWC iff its immersion $U : \mathbb{H}^n \rightsquigarrow \mathbb{R}$ into the Khalimsky grids is AWC.*

Obviously, we can use functions $u : \mathcal{D} \to \mathbb{R}$ defined on a bounded hyper-rectangle $\mathcal{D}$ as domain, in this case we obtain with the same procedure an immersion $U : \alpha(\mathcal{H}_n(\mathcal{D})) \rightsquigarrow \mathbb{R}$ defined on the closed subset $\alpha(\mathcal{H}_n(\mathcal{D}))$. We will still have that u is DWC iff U is AWC.

Appendix E

Well-composed Interpolations on Polyhedral Complexes

In this chapter, we assume that the domain of the initial function is either the set of n-faces of either a discrete n-surface or what we call a *bordered n-surface* (see the definition below), both in a polyhedral complex. We also assume that this domain is *finite* in the sense that it is made of a finite number of faces, to ensure the convergence of the front propagation we will use on the image defined on this domain. The first interpolation that we propose is based on the derived neighborhoods and the second one is based on the chain complex of the *hierarchical subdivision* (introduced in this thesis). In both cases, we obtain AWC interpolations in the sense that the topological boundaries of the (closure of) threshold sets are disjoint union of $(n-1)$-surfaces. Also, by computing the *underlying polyhedra* of the n-faces of the *dual cells* on which are defined the interpolations, we will see that our interpolations are also *CWC*: the boundaries of underlying polyhedra of their threshold sets are $(n-1)$-manifolds.

E.1 Introducing new mathematical background

In this section, we extend the usual definition of *border* and *interior* to *homogeneous* orders, that we will use to define AWCness for subsets of polyhedral complexes. Then, we follow with the introduction of a combinatorial verison of the *dual cells* of Hudson (coming from PL topology), and with our definition of *(simplicial) cell complexes*. We continue with the natural extension of

AWCness to cell complexes and functions defined of cell complexes, and we finish with the definition of CWCness applied to cell complexes and function defined on them.

E.1.1 Border and Interior

Let us recall the definition of *homogeneity* of an order.

Definition 120 (Homogeneity [41])**.** *Let* $|X| = (X, \alpha_X)$ *be a CF-order of finite rank* $n \geq 0$*. We say that* $|X|$ *is* homogeneous *iff for any element* $f \in X$*, the set* $\beta(f) \cap X_n$ *is non-empty.*

Since orders are in equivalent to Alexandrov spaces, that is, supplied with a topology, we can define the *border* (drew from the *face boundary* of Latecki), and then the *interior*, of an order in this manner:

Definition 121 (Border and Interior of an order)**.** *Let* $|X| = (X, \alpha_X)$ *be an homogeneous CF-order of finite rank* $n \geq 0$*. We denote by* $\mathrm{Char}(X)$ *the* characteristical faces *of* $|X|$ *defined such that:*

$$\mathrm{Char}(X) = \{f \in X_{n-1} \; ; \; \mathrm{Card}\left(\beta(f) \cap X_n\right) = 1\},$$

we can then define the border*, denoted by* ΔX*, of* $|X|$ *such that it is the closure of the characteristical faces of* X*:*

$$\Delta X = \bigcup_{f \in \mathrm{Char}(X)} \alpha_X(f).$$

Then we call the interior of $|X|$ *the set* $|\alpha(X) \setminus \Delta X|$ *and we denote it* $\mathrm{Int}(X)$*.*

Note that we differentiate in this thesis the the topological boundary ∂X, where X is a subset of an Alexandrov space A, from the border ΔX, which does not need a greater space like A to be well-defined. Since we are going to work with Alexandrov spaces which can be finite, we will use borders and not topological boundaries.

Figure E.1 depicts the border of a polyhedral complex being an homogeneous order.

From now on, we will only work with homogeneous orders.

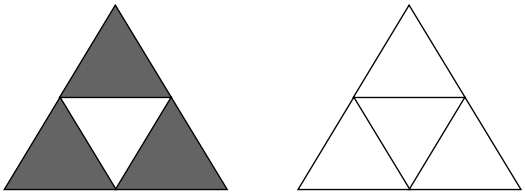

Figure E.1: A polyhedral (simplicial) complex (on the left) and its border.

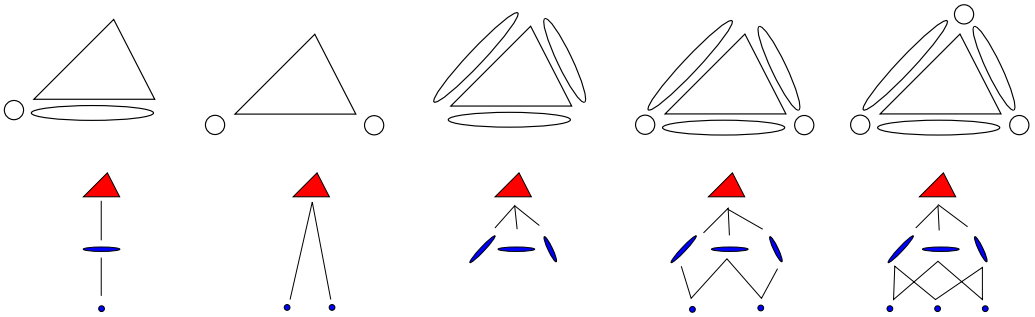

Figure E.2: Among these orders, the only bordered 2-surface is the one on the right.

E.1.2 Bordered n-surfaces

Real signals are always definite on a bounded domain, which justifies the introduction of a definition of (finite) *bordered n-surfaces*, which represent low constrained domains with nice topological properties.

Definition 122 (Bordered n-surfaces)**.** *Let $|X| = (X, \alpha_X)$ be a CF-order, whose cardinal is finite, of rank $n \geq 1$, such that it is connected and such that its border ΔX is non-empty. Then, if, for any $z \in \mathrm{Int}(X)$, $|\theta_X^{\square}(x)|$ is a $(n-1)$-surface, and if ΔX is a disjoint union of $(n-1)$-surfaces, then $|X|$ is said to be a* bordered n-surface*.*

Figure E.2 shows some examples of topological structures that are not bordered n-surfaces except the last one which is a bordered 2-surface. The interior is depicted in red in the Hasse diagrams, and the border is depicted in blue. The first example is a CF-order of rank 2, but its boundary is not a 0-surface since the two faces in it are neighbors. The secund example is a CF-order of rank 1, and then is not a bordered n-surface. The same reasoning holds for the third example. For the fourth example, which is of rank 2, we

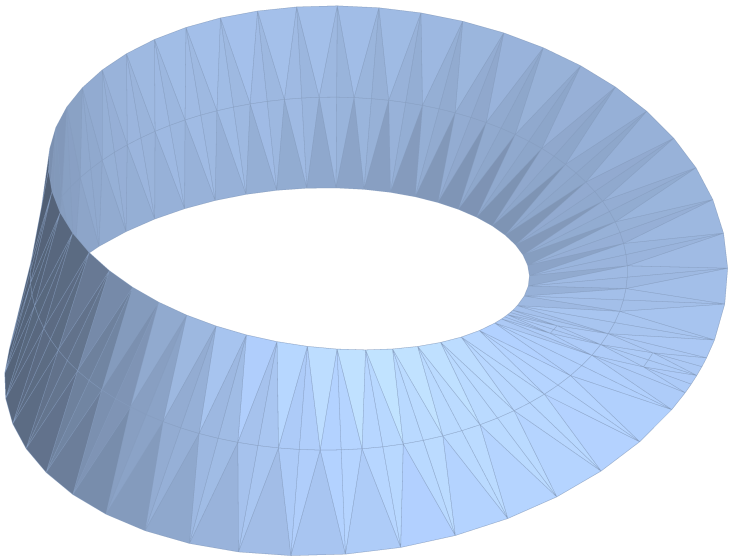

Figure E.3: A triangulated Möbius ruban is a bordered 2-manifold.

can see that the border is connected, but is not a 1-surface, and then this structure is not a bordered 2-surface. Finally, the fifth example verifies all the constraints, and then is a bordered 2-surface.

Also, Figure E.3 shows a Möbius ruban which has been triangulated: it is a bordered 2-surface since its boundary is a 1-surface, and since for any point x at the interior of the ruban, the neighborhood $|\theta^{\square}(x)|$ is a 1-surface.

Finally, note that these examples are made of simplices, but any complex supplied with an order relation can be a bordered n-surface, as shown of Figure E.4. On the left, we have a cubical complex of rank 2, whose border is not a 1-surface: there exists one "critical point" in the boundary such that it admits four neighbors, and then the border is not a 1-surface, which implies that this structure is not a bordered 2-manifold. At the contrary, on the right, we have a connected CF-order of rank 2, with a non-empty border which is made of two disjoint $(n-1)$-surfaces, and such that for any interior point, the $\theta^{\square}$-neighborhood is a 1-surface. Then, this is a bordered 2-manifold.

In fact, we will see in the sequel that these orders seem to be the lowest constrained orders needed to obtain AWC interpolations using our method.

Conjecture 10. *The chain complex of a bordered n-surface is also a bordered*

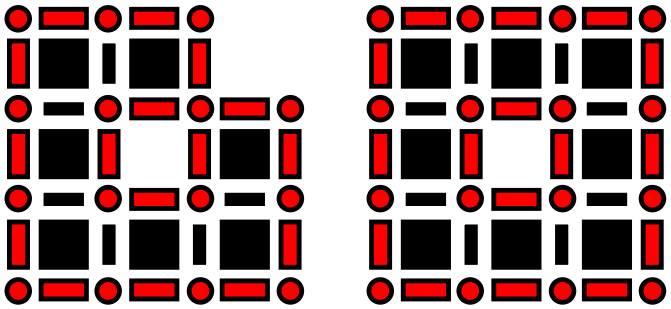

Figure E.4: On the left a topological structure that is not a bordered 2-manifold, and on the right a bordered 2-manifold. Interiors are depicted in black and borders in red.

n-surface.

E.1.3 AWCness on Polyhedral Complexes

Now, let us recall the definition of well-composedness in the sense of Alexandrov according to L. Najman [124] for any polyhedral complex supplied with the canonical order $\supseteq$.

We recall that a polyhedral complex is said *locally finite* iff for any element of this complex, the neighborhood of this point in this complex has a finite cardinality.

Definition 123 (AWC Polyhedral Complexes [124])**.** *Let $|\mathfrak{PC}^n| = (\mathfrak{PC}^n, \alpha)$ be a (locally finite) polyhedral complex of rank $n \geq 0$ supplied with the canonical order $\alpha = \supseteq$, and let $\Delta\mathfrak{PC}^n$ be its border. We say that $|\mathfrak{PC}^n|$ is* well-composed in the sense of Alexandrov *iff its border is a disjoint union of (bordered or not) $(n-1)$-surfaces. Also, we say that a subset $S \subseteq \mathfrak{PC}^n$ is* well-composed in the sense of Alexandrov *if $|\alpha(S)|$ is an AWC simplicial complex.*

By extension, we can define well-composedness in the sense of Alexandrov for functions using threshold sets:

Definition 124 (Threshold Sets on Orders)**.** *Let $|\mathfrak{PC}^n| = (\mathfrak{PC}^n, \alpha)$ be a polyhedral complex of rank $n \geq 0$, and let $\mathcal{D}$ be a subset of $\mathfrak{PC}^n_n$: u is then*

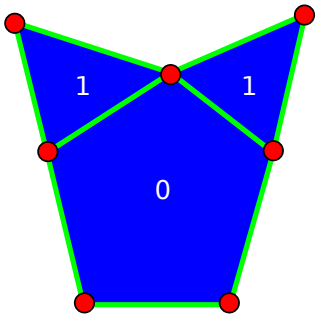

Figure E.5: $[u \leq 0]$ and $[u \leq 1]$ are AWC, but $[u \geq 1]$ is not AWC.

defined only on the n-faces of the polyhedral complex. Then, we define the threshold sets *of* $u : \mathcal{D} \to \mathbb{R}$ *such that:*

$$\begin{aligned}
[u \geq \lambda] &= \{x \in \mathcal{D} \; ; \; u(x) \geq \lambda\}, \\
[u > \lambda] &= \{x \in \mathcal{D} \; ; \; u(x) > \lambda\}, \\
[u \leq \lambda] &= \{x \in \mathcal{D} \; ; \; u(x) \leq \lambda\}, \\
[u < \lambda] &= \{x \in \mathcal{D} \; ; \; u(x) < \lambda\}.
\end{aligned}$$

Definition 125 (AWC Functions on Polyhedral Complexes)**.** *Let* $|\mathfrak{PC}^n| = (\mathfrak{PC}^n, \alpha)$ *be a polyhedral complex of rank* $n \geq 0$ *supplied with the canonical order* $\alpha = \supseteq$*, and let* $\mathcal{D}$ *be a finite subset of* $\mathfrak{PC}^n_n$*. Now let* $u : \mathcal{D} \to \mathbb{R}$ *be a real-valued function defined on* $\mathcal{D}$*. We say that* u *is* well-composed in the sense of Alexandrov *on* $\mathcal{D}$ *iff the border (of the closure in* $|\mathfrak{PC}^n|$*) of any threshold set of* u *is a disjoint union of (bordered or not)* $(n-1)$*-surfaces.*

Let us denote that, without particular constraints on the domain of u, we need to check the AWCness of both upper and lower threshold sets to know if a function u is well-composed in the sense of Alexandrov, as shown on Figure E.5.

E.1.4 Dual Cells

As we will see in the sequel, the following definition, using derivate neighborhoods, will be needed:

Definition 126 (Dual Cells)**.** *Let* K *be a simplicial complex, and* K^1 *its first derived neighborhood. For any element* $A \in K$*. Then, we define* A^**, the* dual

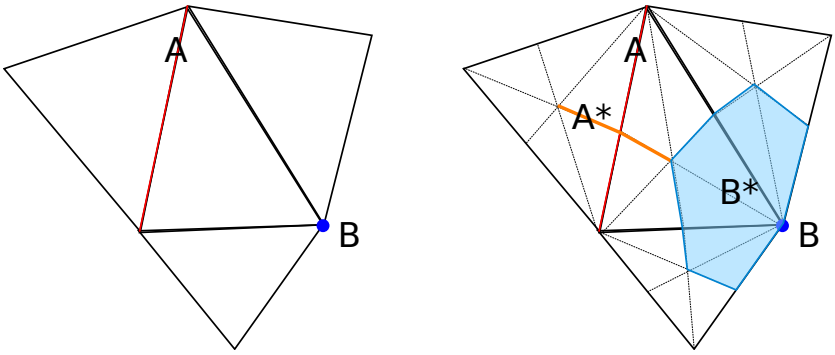

Figure E.6: Dual cells.

cell *of* A*, to be the following subcomplex:*

$$A^* = \bigcap_{\{v\} \subseteq A} \alpha(\beta_{K^1}(\{\{v\}\})).$$

Note that this definition is the combinatorial version of *dual cells* of Hudson [79]. The difference between these two definitions is that in PL topology a point in $\mathbb{R}^n$ is this same point after a subdivision (like a *barycentric subdivision*) when in combinatorial topology, a vertex $\{x\}$ becomes a vertex containing this vertex $\{\{x\}\}$ after having computed a subdivision like the chain complex, which explains this term in Definition 126.

Figure E.6 shows on the left a simplicial complex C, where A is a 1-simplex and where B is a 0-simplex. Both are elements of C. On the right, we subdivided the complex C by computing its first derived C^1, that is, its chain complex, in dotted lines. A^* is then the intersection of the closures of the stars of each 0-simplex contained in A, and is the subcomplex depicted in orange. B^*, the dual cell of B, is computed in the same manner, and is the subcomplex depicted in light blue.

E.1.5 Cell Complexes and AWCness

Definition 127 (k-adjacency)**.** *Let* $|C^n| = (C^n, \alpha)$ *be any simplicial complex of rank* $n \geq 0$ *supplied with the canonical order* $\alpha = \supseteq$*. Two different faces are said* k-adjacent*,* $k \in [\![0, n]\!]$*, iff they share a face of rank equal to* k *but not more.*

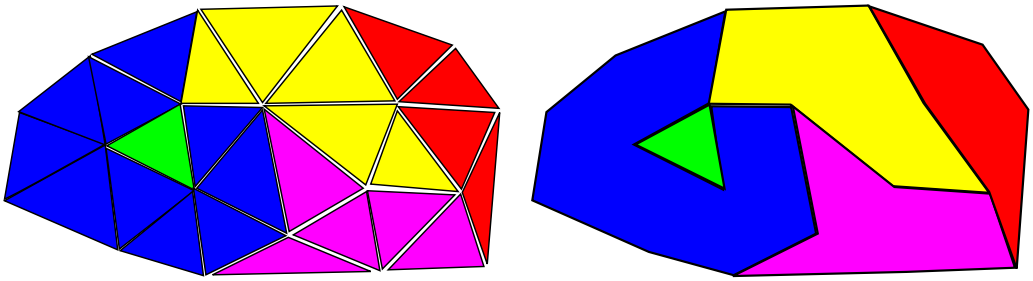

Figure E.7: From a partition of a simplicial complex to its corresponding cell complex (one color by 2-cell).

Definition 128 (Strong Connectedness)**.** *Let $|C^n| = (C^n, \alpha)$ be any simplicial complex of rank $n \geq 0$ supplied with the canonical order $\alpha = \supseteq$. A set S of n-faces of C^n is said* strongly connected *iff for any couple (h^1, h^2) of elements of S, there exists a finite sequence $(q^0 = h^1, \ldots, q^r = h^2)$ of $(r+1)$ elements of S such that for any $i \in [\![0, r-1]\!]$, q^i and q^{i+1} are $(n-1)$-adjacent.*

Since we want to be able to group together simplices of dimension n and their faces into bigger and more complex cells, we propose the following definitions. Effectively a same n-face in the initial polyhedral complex will become during the procedure a vertex and then a simplicial subcomplex. Since all the n-faces of this simplicial subcomplex will be valued the same way, it can be useful to group them together to give back to the initial cell its geometrical structure.

Definition 129 (Cells and Cell Complexes)**.** *Let $|C^n| = (C^n, \alpha)$ be any simplicial complex of rank $n \geq 0$ supplied with the canonical order $\alpha = \supseteq$. Now let be any partition $\{P^i\}_{i \in \mathcal{I}}$ of the set C^n_n of n-faces of C^n:*

$$\bigsqcup_{i \in \mathcal{I}} P^i = C^n_n,$$

such that for any $i \in \mathcal{I}$, P^i is strongly connected. We say that each simplicial subcomplex $\alpha(P^i)$ of C^n is a n-cell *of C with respect to the partition $\{P^i\}_{i \in \mathcal{I}}$. Then, any closure $\alpha(f)$ of any $(n-1)$-face f of the border of a n-cell is a subcomplex of dimension $(n-1)$ that we call* $(n-1)$-cell *with respect to $\{P^i\}_{i \in \mathcal{I}}$, and so on. The set $\mathfrak{CC}^n$ of all these k-cells, $k \in [\![0, n]\!]$, is said to be an* simplicial cell complex *corresponding to the partition $\{P^i\}_{i \in \mathcal{I}}$. Note that we will denote the* k-cells *of the cell complex $\mathfrak{CC}^n$ by $\mathfrak{CC}^n_k$.*

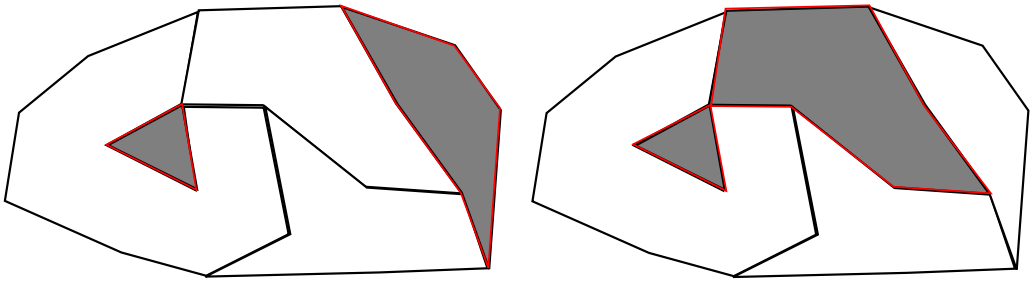

Figure E.8: Families of n-cells: AWC on the left and not AWC on the right.

Figure E.7 depicts a partition of the set of 2-cells of a simplicial complex and its corresponding cell complex.

Definition 130 (AWC Family of n-Cells)**.** *Let $|C^n| = (C^n, \alpha)$ be any simplicial complex of rank n supplied with the canonical order $\alpha = \supseteq$ and let $\mathfrak{CC}^n$ be an cell complex corresponding to any partition of C^n_n. Now let $X = \{S^i\}_{i\in\mathcal{I}}$ be a family of n-cells of $\mathfrak{CC}^n$. Then we say that X is* well-composed in the sense of Alexandrov into C^n *iff the border Δ of the simplicial subcomplex $\bigcup_{i\in\mathcal{I}} S^i$ subset of C^n is a disjoint union of (bordered or not) $(n-1)$-surfaces.*

Figure E.8 shows an AWC family of 2-cells on the left since its boundary is made of a disjoint union of 1-surfaces, and on the right a family of n-cells which is not AWC, since its boundar owns a "pinch".

E.1.6 AWC Functions on Cell Complexes

Definition 131 (Threshold sets on a cell complex)**.** *Let $|C^n| = (C^n, \alpha)$ be any simplicial complex of rank n supplied with the canonical order $\alpha = \supseteq$ and let $\mathfrak{CC}^n$ be an cell complex corresponding to any partition of C^n_n. Now let $u : \mathcal{D} = \mathfrak{CC}^n_n \to \mathbb{R}$ be a real-valued function mapping a real value to any n-cell of C. Then, we define for any $\lambda \in \mathbb{R}$ the* threshold sets *of u on $\mathcal{D}$ such that:*

$$
\begin{aligned}
[u \geq \lambda] &= \{x \in \mathcal{D} \ ; \ u(x) \geq \lambda\},\\
[u > \lambda] &= \{x \in \mathcal{D} \ ; \ u(x) > \lambda\},\\
[u \leq \lambda] &= \{x \in \mathcal{D} \ ; \ u(x) \leq \lambda\},\\
[u < \lambda] &= \{x \in \mathcal{D} \ ; \ u(x) < \lambda\}.
\end{aligned}
$$

In other words, a threshold set is made of families of n-cells, and since we have defined well-composedness for this kind of sets, we can define well-composedness for functions defined on the n-cells of a cell complex.

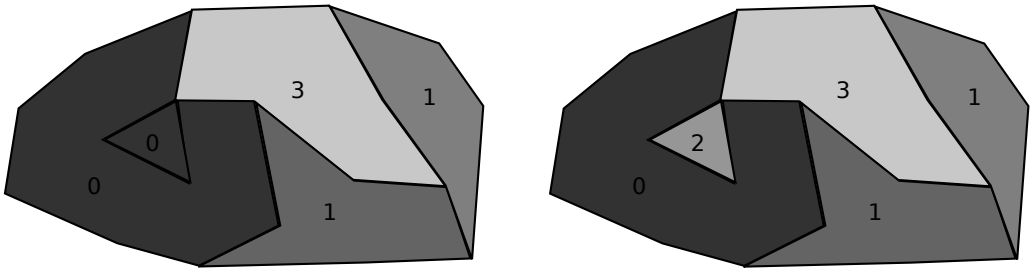

Figure E.9: Functions on cell complexes: AWC on the left and not AWC on the right.

Definition 132 (AWC Functions on Cell complexes)**.** *Let* $|C^n| = (C^n, \alpha)$ *be any simplicial complex of rank* n *supplied with the canonical order* $\alpha = \supseteq$ *and let* $\mathfrak{CC}^n$ *be an cell complex corresponding to any partition of* C^n_n*. Now let* $u : \mathfrak{CC}^n_n \to \mathbb{R}$ *be a real-valued function. Then we say that* u *is* well-composed in the sense of Alexandrov *in* C^n *iff all the closures of the threshold sets of* u *on* $\mathfrak{CC}^n_n$ *are well-composed in the sense of Alexandrov in* C^n*.*

Figure E.9 shows an AWC function defined on a cell complex on the left: any non-empty threshold set is a family of n-cells such that its boundary is made of disjoint 1-surfaces, when on the right, we can observe that the boundary of the threshold set $[u \geq 2]$ of the function u defined on this same cell complex is not made of simple closed curves.

E.1.7 Cell Complexes and CWCness

Let us recall that the definition of an underlying polyhedron of a geometric simplex is given in Definition 96. Also, in the sequel, we will only consider geometric simplices or geometric simplicial complexes.

Definition 133 (Underlying Polyhedron of a Cell Complex)**.** *Let* C^n *be any simplicial complex or subcomplex of rank* $n \geq 0$*. Then its* underlying polyhedron *is denoted by* $\mathrm{Poly}(C^n)$ *and is equal to:*

$$\mathrm{Poly}(C^n) = \bigcup_{s \in C^n} \mathrm{Poly}(s).$$

Definition 134 (CWC Cell Complex)**.** *Let* C^n *be any simplicial complex or subcomplex of rank* $n \geq 0$*. Then,* C^n *is said* continuous well-composed

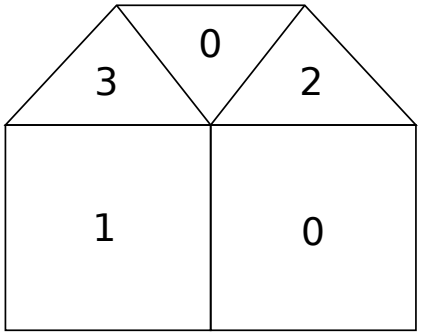

Figure E.10: An image defined u on the n-dimensional convex polyhedral domains of a polyhedral complex.

iff the topological boundary in $\mathbb{R}^n$ *of the underlying polyhedron of* C^n *is a* $(n-1)$*-manifold.*

Definition 135 (CWC Functions on Cell complexes)**.** *Let* $|C^n| = (C^n, \alpha)$ *be any simplicial complex of rank* n *supplied with the canonical order* $\alpha = \supseteq$ *and let* $\mathfrak{CC}^n$ *be a cell complex corresponding to any partition of* C^n_n*. Now let* $u : \mathfrak{CC}^n_n \to \mathbb{R}$ *be a real-valued function. We say that* u *is* continuous well-composed *iff the topological boundary in* $\mathbb{R}^n$ *of the underlying polyhedron of each non-empty thresholds sets is a* $(n-1)$*-manifold.*

E.2 Direct use of these tools fail to produce a self-dual AWC function

Let us now explain how we could have used the existing mathematical tools in matter of combinatorial topology and in piecewise linear topology to extract the boundaries of an function defined on a polyhedral complex such that their boundaries would have been discrete surfaces. We are going to see that these solutions are not satisfying.

Among the different tools we are going to speak about: the chain complexes, the simplicial neighborhoods, the derived neighborhoods, the frontier orders.

Let assume now that a function $u : \mathfrak{PC}^n_n \to \mathbb{R}$ is defined on the n-dimensional convex polyhedral domains of a polyhedral complex which is

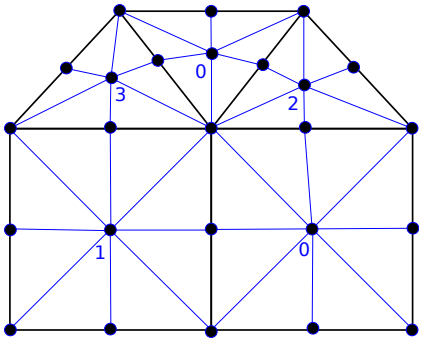

Figure E.11: Chain complex of the initial image.

either a n-surface (as a simplicial subdivision of a sphere or $\mathbb{R}^n$), or a bordered n-surface (which seems more usual). Figure E.10 depicts such an image, which is obviously not well-composed in the sense of Alexandrov: the boundary of the threshold set $[u \leq 1]$ is not a simple closed curve.

If we apply a chain complex on the domain of this image u, we obtain Figure E.11. We can observe that each face becomes a vertex in the chain complex, and then we preserve the geometry of the whole domain, but we loose the one of the convex polyhedral domains which are valued. A solution to give back the geometry to these cells could be that we use the simplicial neighborhoods on the valued vertices, but in this manner we come back to the initial configuration, and the pinches in the images are preserved.

Another available mathematical tool is the simplicial neighborhood, but as we have just seen before, it is the inverse operation of the chain complex, and then it will not permit us to increase the resolution of the cells in such a way that we delete the pinches, and furthermore we need a simplicial structure to use them.

Another possibility is then to use the derived neighborhoods. This structure needs to be applied on a simplicial complex, but the given domain of u is a polyhedral complex. Let us then try to apply the same principle as the one of the derived neighborhood but on the polyhedral complex: we start from the set of n-faces corresponding to some threshold set, let us say $[u \geq 2]$, and then we deduce the corresponding polyhedral subcomplex K as depicted on the left of Figure E.12 in gray. Furthermore, we need this subcomplex to be full (see Theorem 21), which leads to the definition of a new subcomplex, K', as depicted in at the center of Figure E.12 in gray. Then we can compute the

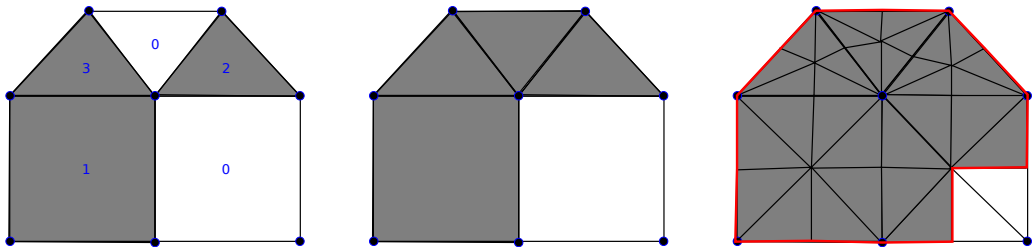

Figure E.12: Using derived neighborhoods directly on the initial domain does not lead to a satisfactory result.

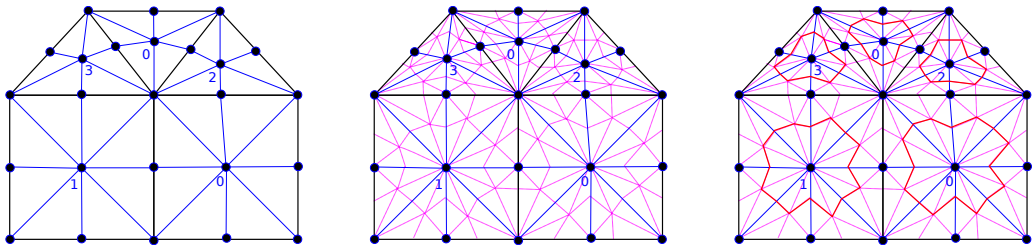

Figure E.13: Using derived neighborhoods on the chain complex of the domain of u does not lead to a satisfactory result neither.

border of its derived neighborhood on the polyhedral complex that we could define as the simplicial neighborhood of the chain complex of K' in the chain complex of the initial polyhedral complex (we have then extended the definition of the derived neighborhood to polyhedral complexes). At the end, we can observe that we effectively obtain a border made of one $(n-1)$-surface, and then we can imagine that in more complex cases, this border will also be made of disjoint union of $(n-1)$-surfaces. However, we have completely destroyed the structure of the initial subcomplex K by making it full, so this solution does not correspond to our needs.

Let us now try another approach with derived neighborhoods, but on simplicial complexes to avoid pathological situations as the one seen just before. Let us then use the chain complex on the polyhedral domain of the image u, and let us transpose the values of the image u onto the new image defined on $\mathcal{C}^u$, which gives a new image u'. We obtain Figure E.13, where we can see that the derived neighborhood of any threshold set has a border made of disjoint $(n-1)$-surfaces. However, we can observe that the border of the derived neighborhood of the threshold set $[u' \geq 0]$ does not cover the

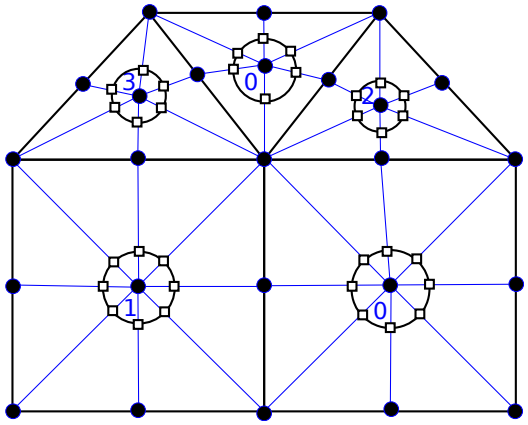

Figure E.14: Using frontier orders on the chain complex of the closure of the domain of the image disconnects the pixels.

whole domain of u, which is problematic. Furthermore, we have lost the connectivity between the initial cells, which means that the contours we will obtain by thresholding u will not be representative. This solution is not good neither.

The last "simple" solution seems then to be the frontier orders. Let us first try them on a simplicial complex, since they can be used either on a simplicial complex or on any partially ordered set. In this case, we have to use it on the chain complex of the (closure of the) domain of u. Like before, even if the borders are disjoint union of $(n-1)$-surfaces, we have disconnected the initial pixels as shown on Figure E.14. Then we have to try the secund solution, which leads finally to the same solution, since using frontier orders on an order which is not a simplicial complex is the same thing as applying it on its chain complex.

Note that if the (closed) domain of u had been a simplicial complex C, we could have used directly the frontier orders as depicted on Figure E.15: we compute the threshold set $[u \geq 1]$ and we deduce its support K. Then K' is the complement of K into the support of C, and we obtain the frontier order depicted by the red line and the squares. The result is a frontier order which overlaps the simplices corresponding to $[u < 1]$, and then this solution is not self-dual: it overemphasizes the ones over the zeros. This solution does not corresponds neither to our needs.

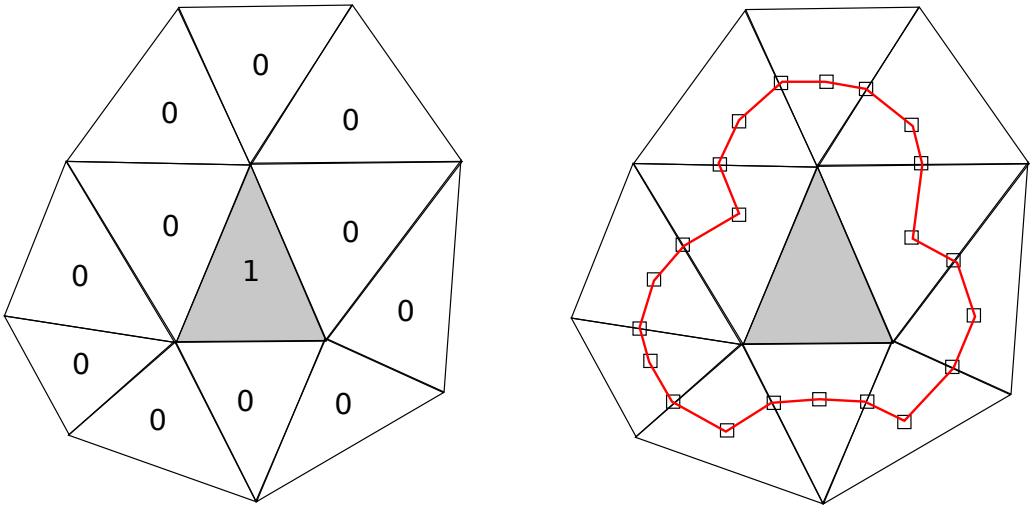

Figure E.15: Using directly frontier orders on a simplicial complex is not self-dual.

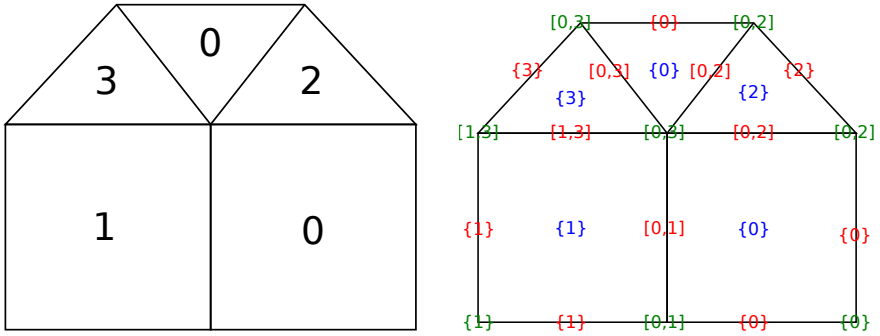

Figure E.16: From u defined on the n-cells of a polyhedral complex to U defined on all the faces of the complex.

E.3 An n-D AWC Interpolation

Now let us present our solution, which finally seems very natural: starting from the observation that derived neighborhoods "disconnect the pixels", we can simply proceed to an (in-between) interpolation on the whole (finite) polyhedral complex, such that the connection between the pixels is preserved.

As for our digitally well-composed self-dual interpolation, we value all the

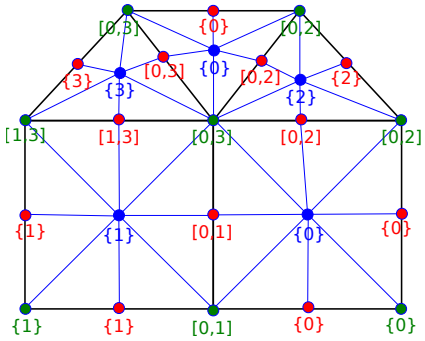

Figure E.17: U' defined on all the 0-faces of the subdivided complex.

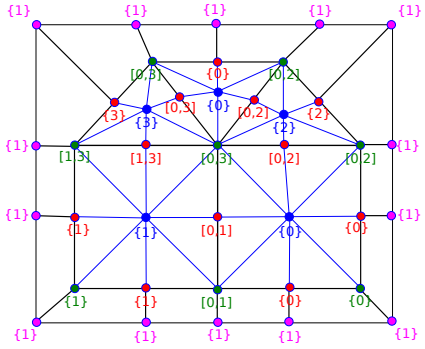

Figure E.18: The same image U' with an additional border.

faces of our polyhedral complex using a new function, U defined such that:

$$\forall z \in \mathfrak{PC}^n,\ U(z) = \begin{cases} \{u(z)\} & \text{if } z \in \mathfrak{PC}^n_n, \\ \text{Span}\,\{u(z')\ ;\ z' \in \beta(z) \cap \mathfrak{PC}^n_n\} & \text{either.} \end{cases}$$

Then we transpose as depicted on Figure E.17 the image U defined on all the cells of the cell complex to its derived subdivision (depicted in blue) by the operation (using the chain complex as described above):

$$\forall \{z\} \in \mathcal{C}^{\mathfrak{PC}^n}, U'(\{z\}) = U(z).$$

Then, to be able to compute a self-dual interpolation, we add a border to the subdivided domain initialized at the median value of the border of the initial image, which leads to Figure E.18.

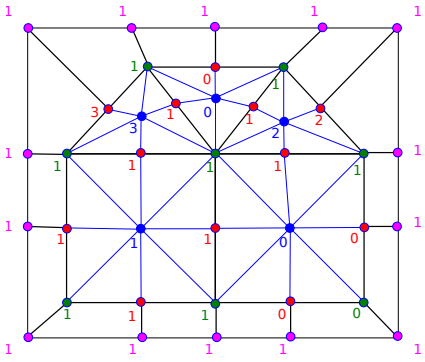

Figure E.19: $u^\flat_+$ (with the temporary border).

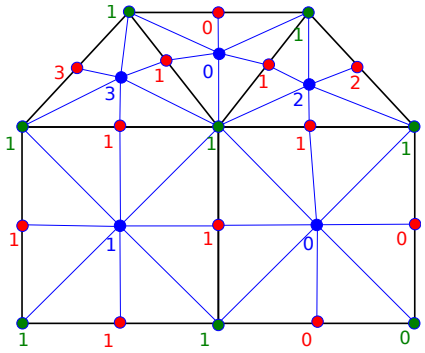

Figure E.20: $u^\flat$ (without the temporary border).

We can finally apply the propagation algorithm explained before (see Algorithm 3), which leads to the image $u^\flat_+$ depicted on Figure E.19, and $u^\flat : (\mathcal{C}^{\mathfrak{P}\mathfrak{C}^n})_0 \to \mathbb{R}$ as depicted on Figure E.20 after we have removed the temporary border.

Note that the front propagation will assurely end since we are working with domains of finite cardinals.

Note that this front-propagation algorithm does not need a structure of cubical grid to be able to proceed: it works on any graph $G = (V, E)$ where V are the vertices, that is, the domain of the propagation, and where E denotes the "directions" of the propagation, that is, the (direct) connectivity between cells.

Since we do not have yet drawn the contours of the future cells, we can

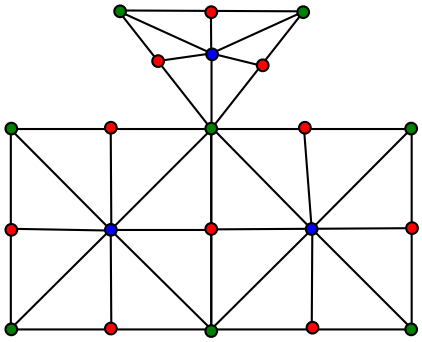

Figure E.21: $\mathcal{F}([u^\flat \leq 1], \mathcal{C}^{\mathfrak{P}\mathfrak{C}^n})$.

define the following subcomplex of $\mathcal{C}^{\mathfrak{P}\mathfrak{C}^n}$ for any $\lambda \in \mathbb{R}$:

$$\mathcal{F}([u^\flat \leq \lambda], \mathcal{C}^{\mathfrak{P}\mathfrak{C}^n}) = \left\{ f \in \mathcal{C}^{\mathfrak{P}\mathfrak{C}^n} \ ; \ f \subseteq [u^\flat \leq \lambda] \right\}.$$

An example of this kind of subcomplex is depicted on Figure E.21 where we drew $\mathcal{F}([u^\flat \leq 1], \mathcal{C}^{\mathfrak{P}\mathfrak{C}^n})$.

Some remarks about this subcomplex:

- it is full into $\mathcal{C}^{\mathfrak{P}\mathfrak{C}^n}$ by construction
- when $\mathfrak{P}\mathfrak{C}^n$ is a bordered n-surface, $\mathcal{C}^{\mathfrak{P}\mathfrak{C}^n}$ is also a bordered n-surface (if Conjecture 10 is true), and then by Theorem 21, the border of the derived neighborhood of the full subcomplex $\mathcal{F}([u^\flat \leq 1], \mathcal{C}^{\mathfrak{P}\mathfrak{C}^n})$ is a disjoint union of $(n-1)$-surfaces.

The second property is depicted on Figures E.22, E.23, and E.24 where $\mathcal{F}([u^\flat \leq \lambda], \mathcal{C}^{\mathfrak{P}\mathfrak{C}^n})$ is drawn in orange and the corresponding border is in red. As we can observe, these boundaries are simple closed curves, that is, 1-surfaces in the derived subdividision of the chain complex of the initial cell complex.

Since this formulation is not particularly easy to manage, we can use the formula of dual cells of Hudson [79]. Then, starting from any element A of $\mathcal{C}^{\mathfrak{P}\mathfrak{C}^n}$, we can compute its dual cell A^* as follows:

$$A^* = \bigcap_{\{x\} \subseteq A} \alpha(\beta_{[\mathcal{C}^{\mathfrak{P}\mathfrak{C}^n}]^1}(\{\{x\}\})),$$

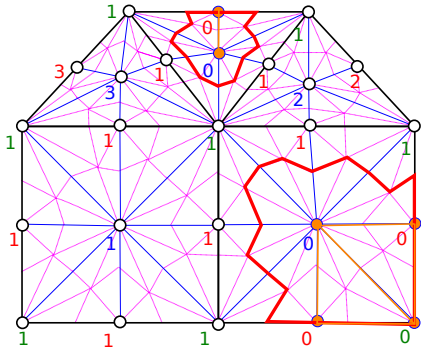

Figure E.22: $\Delta N^1(\mathcal{F}([u^\flat \leq 0], \mathcal{C}^{\mathfrak{P}\mathfrak{C}^n}), \mathcal{C}^{\mathfrak{P}\mathfrak{C}^n})$.

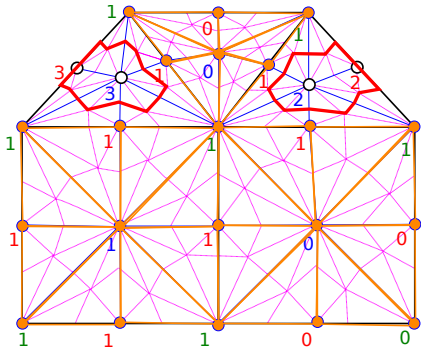

Figure E.23: $\Delta N^1(\mathcal{F}([u^\flat \leq 1], \mathcal{C}^{\mathfrak{P}\mathfrak{C}^n}), \mathcal{C}^{\mathfrak{P}\mathfrak{C}^n})$.

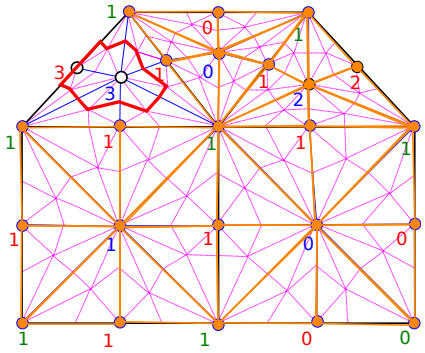

Figure E.24: $\Delta N^1(\mathcal{F}([u^\flat \leq 0], \mathcal{C}^{\mathfrak{P}\mathfrak{C}^n}), \mathcal{C}^{\mathfrak{P}\mathfrak{C}^n})$.

where $[\mathcal{C}^{\mathfrak{P}\mathfrak{C}^n}]^1$ denotes the first derived neighborhood of $\mathcal{C}^{\mathfrak{P}\mathfrak{C}^n}$. A 0-face which is valued in $\mathcal{C}^{\mathfrak{P}\mathfrak{C}^n}$ becomes a simplicial complex of rank n by duality, and we are able to group these simplices into a simplicial n-cell to form a valued cell

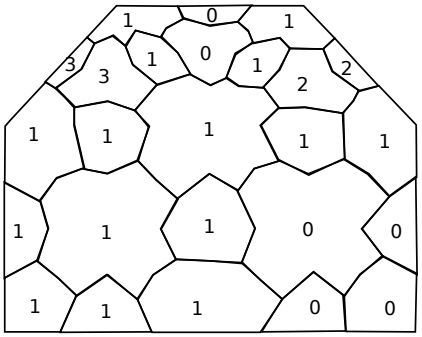

Figure E.25: The new valued cell complex representing an AWC function.

complex which is well-composed in the sense of Alexandrov (since any union of any cells in this cell complex is AWC by construction).

Effectively, since the union of the n-faces of the dual cells of the 0-faces of $\mathcal{C}^{\mathfrak{P}\mathfrak{C}^n}$ covers $[\mathcal{C}^{\mathfrak{P}\mathfrak{C}^n}]^1$, we can partition the set of n-faces of this last set such that: $([\mathcal{C}^{\mathfrak{P}\mathfrak{C}^n}]^1)_n = \sqcup_{A \in \mathcal{C}^{\mathfrak{P}\mathfrak{C}^n}} P(A)$ with $P(A) = (A^*)_n$. Using this partition, we can defined a cell complex $\mathfrak{C}\mathfrak{C}^n_n$ corresponding to $\{P(A)\}_{A \in \mathcal{C}^{\mathfrak{P}\mathfrak{C}^n}}$. This way, we obtain finally $u_{\mathrm{AWC}} : \mathfrak{C}\mathfrak{C}^n_n \to \mathbb{R}$ defined such that $\forall z \in \mathfrak{C}\mathfrak{C}^n_n, u_{\mathrm{AWC}}(z) = u^\flat(C)$ where $C \in (\mathcal{C}^{\mathfrak{P}\mathfrak{C}^n})_0$ is such that $z \in C^*$.

Note that since the function u_{AWC} is only defined on n-cells, the threshold sets of u_{AWC} are sets of n-cells, and then we compute the borders based on the closures of the threshold sets: $\Delta\alpha([u_{\mathrm{AWC}} \geq \lambda])$, $\Delta\alpha([u_{\mathrm{AWC}} < \lambda])$, $\Delta\alpha([u_{\mathrm{AWC}} \leq \lambda])$ and $\Delta\alpha([u_{\mathrm{AWC}} > \lambda])$.

We obtain finally the equalities:

$$\forall \lambda \in \mathbb{R}, \Delta\alpha([u_{\mathrm{AWC}} \geq \lambda]) = \Delta N^1(\mathcal{F}([u^\flat \geq \lambda], \mathcal{C}^{\mathfrak{P}\mathfrak{C}^n}), \mathcal{C}^{\mathfrak{P}\mathfrak{C}^n}),$$

$$\forall \lambda \in \mathbb{R}, \Delta\alpha([u_{\mathrm{AWC}} \leq \lambda]) = \Delta N^1(\mathcal{F}([u^\flat \leq \lambda], \mathcal{C}^{\mathfrak{P}\mathfrak{C}^n}), \mathcal{C}^{\mathfrak{P}\mathfrak{C}^n}),$$

$$\forall \lambda \in \mathbb{R}, \Delta\alpha([u_{\mathrm{AWC}} > \lambda]) = \Delta N^1(\mathcal{F}([u^\flat > \lambda], \mathcal{C}^{\mathfrak{P}\mathfrak{C}^n}), \mathcal{C}^{\mathfrak{P}\mathfrak{C}^n}),$$

$$\forall \lambda \in \mathbb{R}, \Delta\alpha([u_{\mathrm{AWC}} < \lambda]) = \Delta N^1(\mathcal{F}([u^\flat < \lambda], \mathcal{C}^{\mathfrak{P}\mathfrak{C}^n}), \mathcal{C}^{\mathfrak{P}\mathfrak{C}^n}),$$

and for this reason, we propose the following conjecture:

Conjecture 11 (A first AWC/CWC interpolation)**.** *Let n be a finite integer such that $n \geq 2$, and let u be a real-valued image defined on the n-dimensional convex polyhedral domains of a polyhedral complex, which is a*

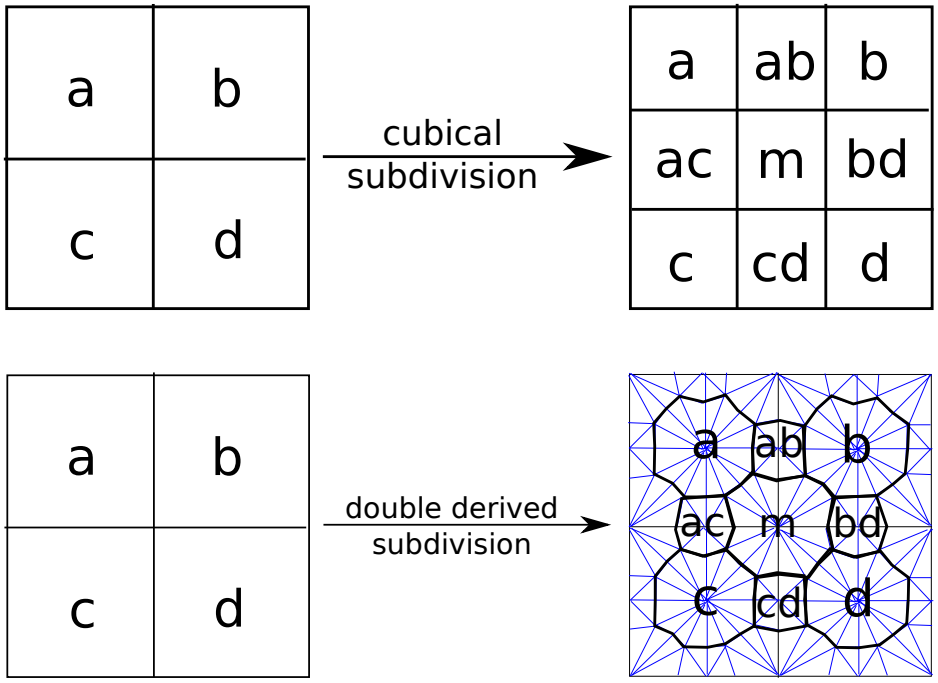

Figure E.26: Cubical subdivision VS double derived subdivision.

n-surface (with or without border). Then, any image u_{AWC} *valued on the cell complex computed like it is described in this section is well-composed in the sense of Alexandrov and continuous well-composed. This method is self-dual.*

Note that the geometry of the cells is not preserved.

E.4 Another n-D AWC Interpolation

We observed that due to the derived neighborhood, the geometry of the cells are not preserved (see Figure E.26), even if we start from a cubical cell complex. Then, we propose an alternative: we still use a sequence of two subdivisions, but the first one is replaced by an *hierarchical subdivision* (introduced hereafter), which attenuates the deformation of the original cells.

E.4.1 Introducing the hierarchical subdivision

We define an hierarchical subdivision as following:

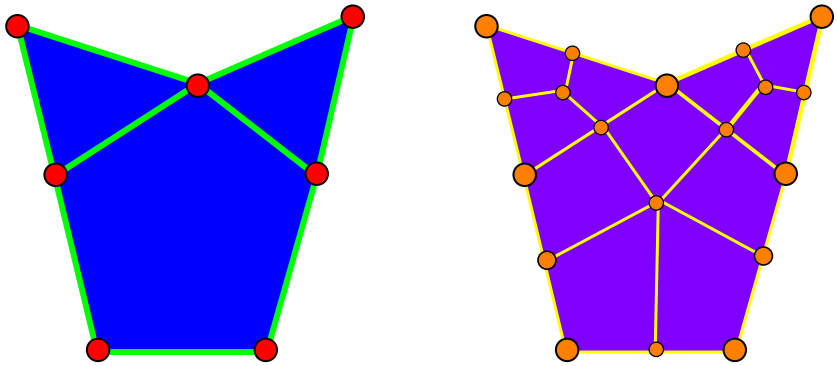

Figure E.27: From a cell complex to its hierarchical subdivision.

Definition 136 (Hierarchical subdivision)**.** *Let* $|\mathcal{O}| = (\mathcal{O}, \alpha)$ *be a partially ordered set. Then we define the* hierarchical subdivision *of the order* $\mathcal{O}$ *as:*

$$\mathcal{SH}(\mathcal{O}) = \{\alpha(a) \cap \beta(b) \ ; \ \exists a, b \in \mathcal{O}, \alpha(a) \cap \beta(b) \neq \emptyset\} \, ,$$

supplied with the canonical relation order $\supseteq$*. Obviously,* $|\mathcal{SH}(\mathcal{O})|$ *is an order.*

E.4.2 An AWC interpolation based on hierarchical subdivision

Applied to a polyhedral complex $|\mathfrak{PC}^n|$, which is closed by inclusion, the hierarchical subdivision provides a new structure that is depicted on Figure E.27. On the left, we draw the initial cell complex, where 2-faces are depicted in blue, 1-faces are depicted in green, and 0-faces are depicted in red. On the right, since any face $h \in \mathfrak{PC}^n$ leads to a 0-face $\alpha(h) \cap \beta(h) = \{h\}$ into $\mathcal{SH}(\mathfrak{PC}^n)$, we represent them using the orange points. Note that the 0-faces in $\mathcal{SH}(\mathfrak{PC}^n)$ which come from 0-faces in $\mathcal{O}$ are depicted using bigger disks. Then, for any couple $(a, b) \in \mathcal{O}$ such that $a \succ b$, it is clear that $\alpha(a) \cap \beta(b) = \{a, b\}$, and since $\rho(\{a, b\}) = 1$, we depict it using an edge (in yellow) linking $\{a\}$ and $\{b\}$. Finally, for the couples (a, b) of elements of $\mathcal{O}$ such that there exists a third element $c \in \mathcal{O}$ such that $a \succ c \succ b$, then $\alpha(a) \cap \beta(b)$ is of rank 2 in $|\mathcal{SH}(\mathcal{O})|$, and then is depicted by a purple polygon.

After we have computed the hierarchical subdivision, we have the "centers" of the new cells, but we still need to draw the cells around these centers. To this aim, we compute the chain complex of $|\mathcal{SH}(\mathcal{O})|$, which results in a

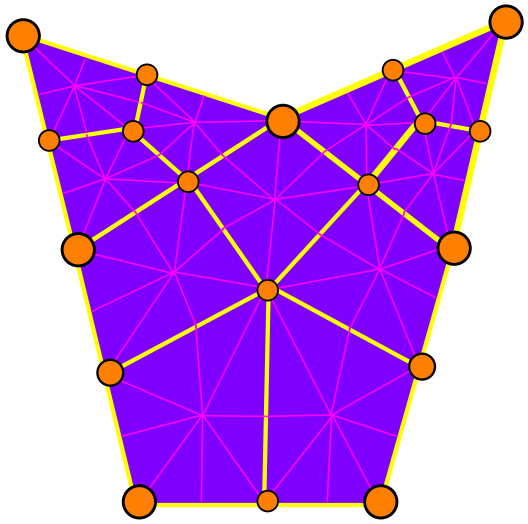

Figure E.28: From the hierarchical subdivision of a polyhedral complex to its chain complex.

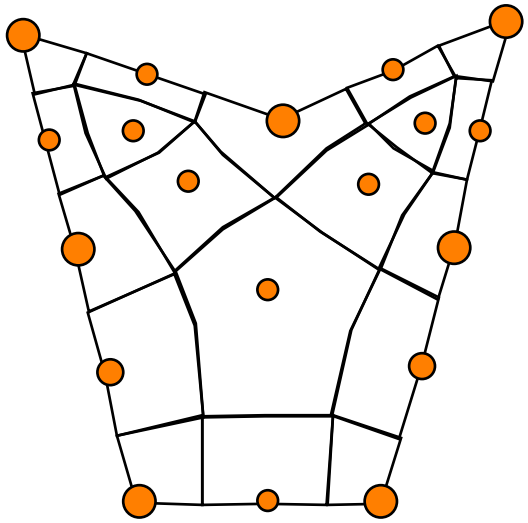

Figure E.29: The cell complex resulting of the chain complex of the hierarchical subdivision: the geometry of the initial cells is preserved.

triangulation of $\mathcal{SH}(\mathcal{O})$. On Figure E.28, this chain complex is depicted in pink.

Now that we have drawn the triangulation of the hierarchical subdivision,

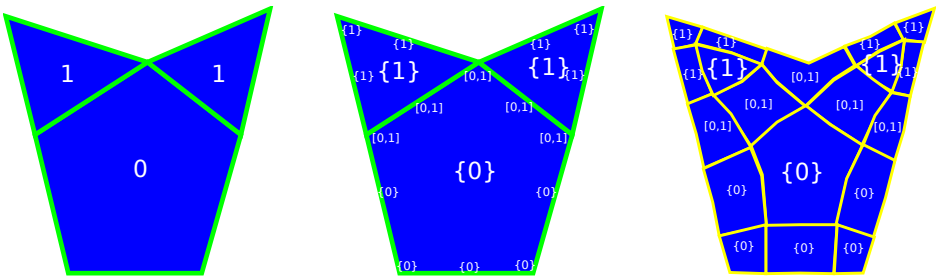

Figure E.30: From u to U.

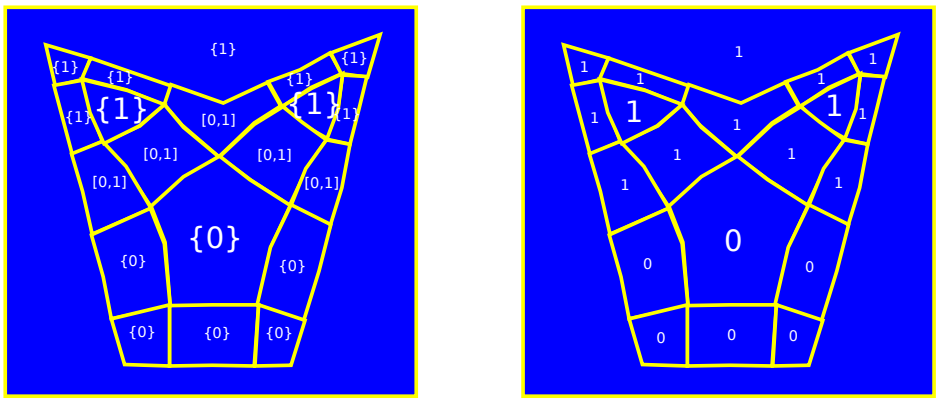

Figure E.31: The propagation.

we are able to compute the dual cells of the orange vertices. For any element $A \in \mathcal{SH}(\mathcal{O})$, its dual cell A^* is the subcomplex resulting from the intersection of the star in the chain complex of the vertices of A in the hierarchical subdivision:

$$A^* = \bigcap_{\{x\} \subseteq A} \alpha(\beta_{\mathcal{CSH}(\mathcal{O})}(\{\{x\}\})).$$

By grouping all these subcomplexes in one set, we obtain a cell complex where the geometry of the cells has been preserved.

Figure E.30 shows that like for the AWC interpolation we presented before, we value each face of the face of the cell complex by the span of the values of the image on the star neighborhood of the face, which makes U. Then, we transpose the computed values on the sudivided domain, and we obtain U'.

Then we are able to proceed to the front propagation, after having added

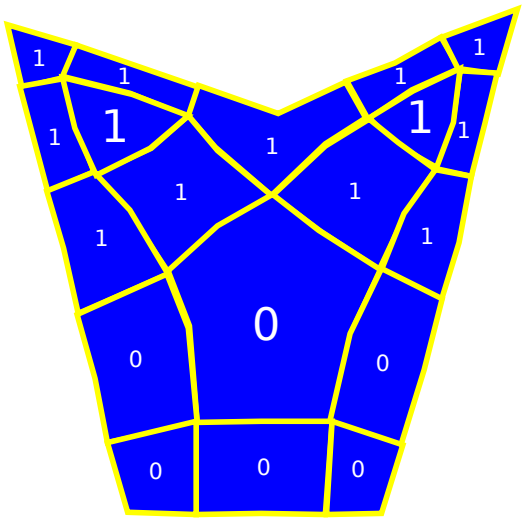

Figure E.32: A self-dual interpolation of u.

the border valued at the median of the border of the initial image (see Figure E.31).

According to us, the resulting image u_{AWC} on the cell complex is well-composed in the sense of Alexandrov, continuous well-composed, and self-dual, since we use the median of the border of the initial image to intialize the outer border before the propagation (as shown on Figure E.32 where the median is equal to 1).

Conjecture 12 (A second AWC/CWC interpolation)**.** *Let n be a finite integer such that $n \geq 2$, and let u be a real-valued image defined on the n-dimensional convex polyhedral domains of a polyhedral domain, which is a n-surface (with or without border). Then, any image u_{AWC} valued on the cell complex computed like it is described in this section is well-composed in the sense of Alexandrov and continuous well-composed. This method is self-dual. Furthermore, the geometry of the cells in the initial domain is preserved.*

E.4.3 Mathematical properties of the hierarchical subdivision

In this section, we denote some remarkable properties of our hierarchical subdivision.

Property 14. *Let $|\mathcal{O}| = (\mathcal{O}, \alpha)$ be a partially ordered set which is connected. Then, its hierarchical subdivision is also connected.*

Proof: Let $|\mathcal{O}|$ be a connected poset, and let $|\mathcal{SH}(\mathcal{O})|$ be its hierarchical subdivision. Now, let x, y be two elements of $|\mathcal{SH}(\mathcal{O})|$ and let show that they are connected. x belongs to $\mathcal{SH}(\mathcal{O})$ and this way there exist a_x, b_x in $\mathcal{O}$ such that $x = \alpha(a_x) \cap \beta(b_x) \neq \emptyset$. For the same reason, there exist a_y, b_y in $\mathcal{O}$ such that $y = \alpha(a_y) \cap \beta(b_y) \neq \emptyset$. Obviously, $\alpha(a_x) \cap \beta(b_x)$ is connected to $\{b_x\}$ into $|\mathcal{SH}(\mathcal{O})|$, and $\alpha(a_y) \cap \beta(b_y)$ is connected to $\{b_y\}$ into $|\mathcal{SH}(\mathcal{O})|$. It is clear that b_x and b_y are connected by hypothesis. Then there exists a path $\pi = (q^0 = b_x, \ldots, q^r = b_y)$ such that for any $i \in [\![0, r-1]\!]$, $q^{i+1} \in \theta^{\Box}_{\mathcal{O}}(q^i)$ joining x and y into $\mathcal{O}$. From this path, we can deduce the following sequence:

$$\pi' = (\{q^0\} = \{b_x\}, \alpha(q^0 \vee q^1) \cap \beta(q^0 \wedge q^1), \{q^1\}, \ldots, \{q^r\} = \{b_y\}),$$

which is clearly a path in $|\mathcal{SH}(\mathcal{O})|$. The existence of this path implies that x and y are connected into $|\mathcal{SH}(\mathcal{O})|$. The proof is done. □

Conjecture 13. *Let $|\mathcal{O}|$ be a non-empty, closed order of finite rank, and let $\mathcal{SH}(\mathcal{O})$ be its hierarchical subdivision. Then $\rho(|\mathcal{SH}(\mathcal{O})|) = \rho(\mathcal{O})$.*

Conjecture 14. *Let $|\mathcal{O}|$ be a non-empty, closed order of finite rank, and let $\mathcal{SH}(\mathcal{O})$ be its hierarchical subdivision. Then, if $|\mathcal{O}|$ is a n-surface, $|\mathcal{SH}(\mathcal{O})|$ is a n-surface too.*

Note that this property is easy to verify for the cases $n = 0$ and $n = 1$ by observing the Hasse diagrams of these n-surfaces and their respective hierarchical subdivision.

Apllied to a convex linear cell complex, we obtain:

Conjecture 15. *Let $|\mathfrak{PC}^n|$ be a convex linear cell complex of dimension n supplied with the order relation $\supseteq$, and let $|\mathcal{SH}(\mathfrak{PC}^n)|$ be its hierarchical subdivision. Then, if $|\mathfrak{PC}^n|$ is a n-surface (respectively a bordered n-surface), $|\mathcal{SH}(\mathfrak{PC}^n)|$ is a n-surface (respectively a bordered n-surface).*

We also observed that the borders of each cells in the new cell complex were 1-surfaces in the 2D case, and we think it can be generalized in n-D. Effectively, starting from a convex linear cell complex such that it is a n-surface, its hierarchical subdivision is also a n-surface. Then, when we

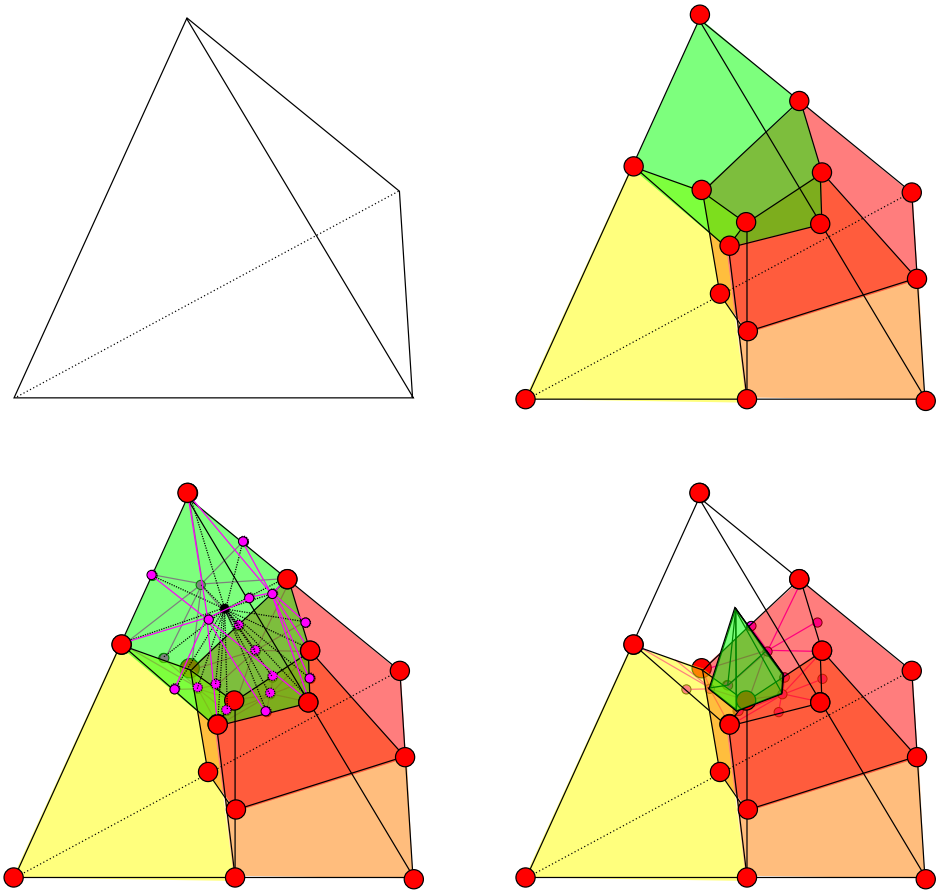

Figure E.33: The dual cell resulting from the chain complex of the hierarchical subdivision.

compute the dual cell of a vertex $\{x\}$ of the hierarchical subidivision, we obtain its dual cell A^* such that:

$$A^* = \alpha(\beta_{\mathcal{C}^{\mathcal{SH}(\mathfrak{PC}^n)}}(\{\{x\}\})),$$

which is equal to the simplicial neighborhood of $\{\{x\}\}$ into $\mathcal{C}^{\mathcal{SH}(\mathfrak{PC}^n)}$ which we assume to be a n-surface and a simplicial complex. For this reason, we think that computing the border of this cell has the same properties as the border of a derived neighborhood, and then is a $(n-1)$-surface.

Conjecture 16. *Let $|\mathfrak{PC}^n|$ be a convex linear cell complex of dimension n supplied with the order relation $\supseteq$, and let $|\mathcal{SH}(\mathfrak{PC}^n)|$ be its hierarchical*

subdivision. Then, if $|\mathfrak{PC}^n|$ is a n-surface (with or without border), then the border of the dual cells of the vertices of the hierarchical subdivision are $(n-1)$-surfaces (in the chain complex of the hierarchical subdivision).

Figure E.33 shows in the raster scan order a convex cell that is a tetrahedron, its hierarchical subdivision, the chain complex of the hierarchical subdivision, and (a part of) the dual cell. The final cell preverves the geometry of the original cell, and its boundary is a $(n-1)$)-surface.

E.5 A self-dual continuous representation on polyhedral complexes

As seen in Section 5.2, we can easily obtain a self-dual plain map (see Section C.19) representing a given image u defined on the n-faces of a cubical complex. This is also true on polyhedral complexes, as depicted on Figure E.34.

Conjecture 17. *Let $u : \mathfrak{PC}^n_n \to \mathbb{R}$ be a real-valued image defined on the n-faces of a polyhedral complex. Using the numerical scheme described in Figure E.34, the image $U_{\mathrm{AWC}} : \mathfrak{CC}^n \to \mathbb{R}$ defined on a cell complex and resulting from a span-based immersion of one of our two self-dual interpolations $u_{\mathrm{AWC}} : \mathfrak{CC}^n_n \to \mathbb{R}$ is an AWC plain map.*

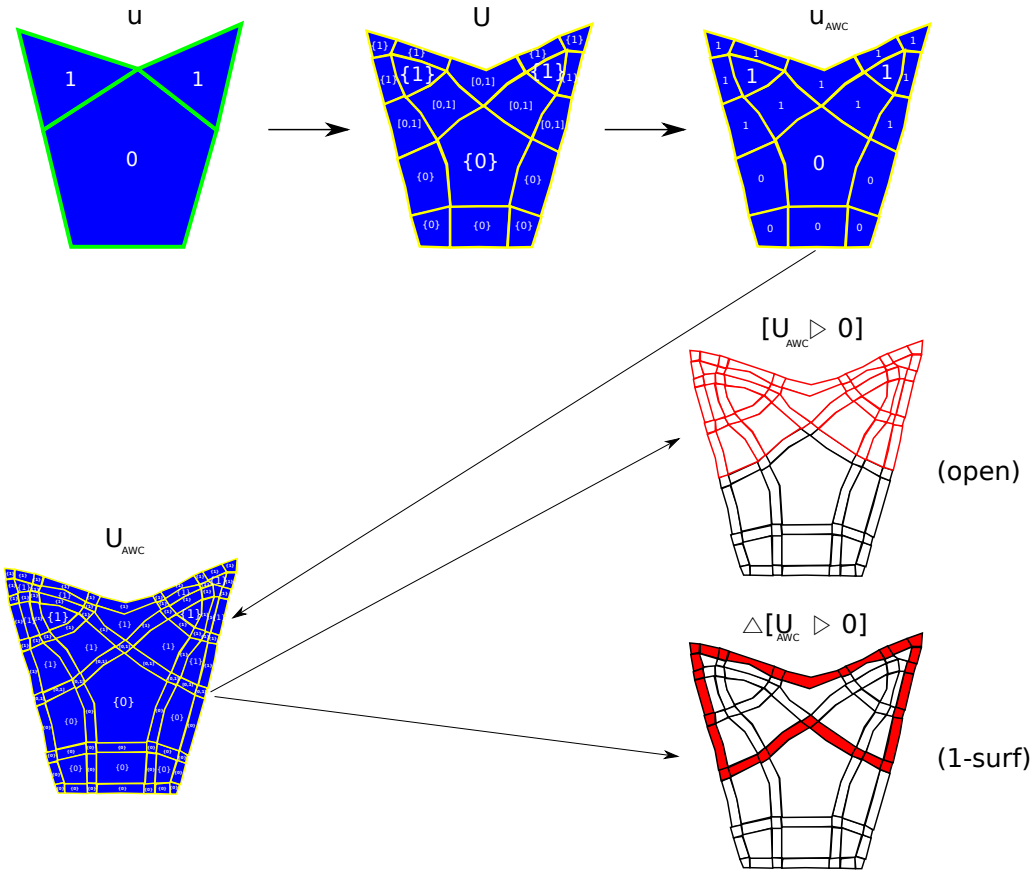

Figure E.34: Our self-dual representation on cell complexes.

List of Publications

Conference Papers

[1] Nicolas Boutry, Thierry Géraud, and Laurent Najman. On making n-D images well-composed by a self-dual local interpolation. In *International Conference on Discrete Geometry for Computer Imagery*, pages 320–331. Springer, 2014.

[2] Nicolas Boutry, Thierry Géraud, and Laurent Najman. Une généralisation du *bien-composé* à la dimension n. Communication at Journée du Groupe de Travail de Géometrie Discrète (GT GeoDis, Reims Image 2014), November 2014. In French.

[3] Nicolas Boutry, Thierry Géraud, and Laurent Najman. How to make n-D functions digitally well-composed in a self-dual way. In *International Symposium on Mathematical Morphology and Its Applications to Signal and Image Processing*, pages 561–572. Springer, 2015.

[4] Nicolas Boutry, Thierry Géraud, and Laurent Najman. How to make n-D images well-composed without interpolation. In *Image Processing (ICIP), 2015 IEEE International Conference on*, pages 2149–2153. IEEE, 2015.

Bibliography

[1] Wisam Al Faqheri and Syamsiah Mashohor. A real-time malaysian automatic license plate recognition (m-alpr) using hybrid fuzzy. *IJCSNS International Journal of Computer Science and Network Security*, 9(2):333–340, 2009.

[2] Pavel S Aleksandrov. *Combinatorial topology*, volume 1. Courier Corporation, 1956.

[3] James W Alexander. A proof and extension of the jordan-brouwer separation theorem. *Transactions of the American Mathematical Society*, 23(4):333–349, 1922.

[4] James W Alexander. The combinatorial theory of complexes. *Annals of Mathematics*, pages 292–320, 1930.

[5] Paul Alexandroff and Heinz Hopf. *Topologie I: Erster Band. Grundbegriffe der Mengentheoretischen Topologie Topologie der Komplexe· Topologische Invarianzsätze und Anschliessende Begriffsbildungen· Verschlingungen im n-Dimensionalen Euklidischen Raum Stetige Abbildungen von Polyedern*. Springer-Verlag, 2013.

[6] Oleg Alexandrov and Fadil Santosa. A topology-preserving level set method for shape optimization. *Journal of Computational Physics*, 204(1):121–130, 2005.

[7] P.S. Alexandrov. Diskrete räume. *Mat. Sb.*, 2(44):501–519, 1937.

[8] Carlo Arcelli. Pattern thinning by contour tracing. *Computer Graphics and Image Processing*, 17(2):130–144, 1981.

[9] Ehud Artzy, Gideon Frieder, and Gabor T Herman. The theory, design, implementation and evaluation of a three-dimensional surface detection algorithm. *Computer graphics and image processing*, 15(1):1–24, 1981.

[10] Jean-Pierre Aubin and Hélène Frankowska. *Set-valued analysis*. Springer Science & Business Media, 2009.

[11] Coloma Ballester, Vicent Caselles, and P Monasse. The tree of shapes of an image. *ESAIM: Control, Optimisation and Calculus of Variations*, 9:1–18, 2003.

[12] Pierre-Louis Bazin, Lotta Maria Ellingsen, and Dzung L Pham. Digital homeomorphisms in deformable registration. In *Biennial International Conference on Information Processing in Medical Imaging*, pages 211–222. Springer, 2007.

[13] G Berg, W Julian, R Mines, and F Richman. The constructive jordan curve theorem. *Journal of Mathematics*, 5(2), 1975.

[14] Giles Bertrand. Simple points, topological numbers and geodesic neighborhoods in cubic grids. *Pattern recognition letters*, 15(10):1003–1011, 1994.

[15] Gilles Bertrand. A boolean characterization of three-dimensional simple points. *Pattern recognition letters*, 17(2):115–124, 1996.

[16] Gilles Bertrand. New notions for discrete topology. In *Discrete Geometry for Computer Imagery*, pages 218–228. Springer, 1999.

[17] Gilles Bertrand, Jean-Christophe Everat, and Michel Couprie. Topological approach to image segmentation. In *SPIE's 1996 International Symposium on Optical Science, Engineering, and Instrumentation*, pages 65–76. International Society for Optics and Photonics, 1996.

[18] Gilles Bertrand, Jean-Christophe Everat, and Michel Couprie. Image segmentation through operators based on topology. *Journal of Electronic Imaging*, 6(4):395–405, 1997.

[19] Gilles Bertrand and Grégoire Malandain. A new characterization of three-dimensional simple points. *Pattern Recognition Letters*, 15(2):169–175, 1994.

[20] Serge Beucher and Christian Lantuéjoul. Use of watersheds in contour detection. 1979.

[21] Serge Beucher and Fernand Meyer. The morphological approach to segmentation: the watershed transformation. *Optical Engineering - New York - Marcel Dekker Incorporated -*, 34:433–433, 1992.

[22] Hanspeter Bieri and Walter Nef. Algorithms for the euler characteristic and related additive functionals of digital objects. *Computer vision, graphics, and image processing*, 28(2):166–175, 1984.

[23] Errett Bishop and Douglas S Bridges. *Constructive analysis*, volume 279. Springer Science & Business Media, 2012.

[24] Ethan D Bloch. *A first course in geometric topology and differential geometry*. Springer Science & Business Media, 1997.

[25] Isabelle Bloch, Henk Heijmans, and Christian Ronse. Mathematical morphology. In *Handbook of Spatial Logics*, pages 857–944. Springer, 2007.

[26] Nicolas Boutry, Thierry Géraud, and Laurent Najman. On making n-D images well-composed by a self-dual local interpolation. In *International Conference on Discrete Geometry for Computer Imagery*, pages 320–331. Springer, 2014.

[27] Nicolas Boutry, Thierry Géraud, and Laurent Najman. How to make n-D functions digitally well-composed in a self-dual way. In *International Symposium on Mathematical Morphology and Its Applications to Signal and Image Processing*, pages 561–572. Springer, 2015.

[28] Nicolas Boutry, Thierry Géraud, and Laurent Najman. How to make n-D images well-composed without interpolation. In *Image Processing (ICIP), 2015 IEEE International Conference on*, pages 2149–2153. IEEE, 2015.

[29] Jean-Pierre Braquelaire and Luc Brun. Image segmentation with topological maps and inter-pixel representation. *Journal of Visual Communication and Image Representation*, 9(1):62–79, 1998.

[30] Michal Buta et al. Fastext: Efficient unconstrained scene text detector. In *2015 IEEE International Conference on Computer Vision (ICCV)*, pages 1206–1214. IEEE, 2015.

[31] Vicent Caselles and Pascal Monasse. Grain filters. *Journal of Mathematical Imaging and Vision*, 17(3):249–270, 2002.

[32] Vicent Caselles and Pascal Monasse. Geometric description of images as topographic maps, ser. *Lecture Notes in Mathematics. Springer-Verlag*, 1984, 2009.

[33] Thomas Christopher Cecil. *Numerical methods for partial differential equations involving discontinuities*. PhD thesis, University of California Los Angeles, 2003.

[34] Li Chen. Genus computing for 3d digital objects: Algorithm and implementation. *arXiv preprint arXiv:0912.4936*, 2009.

[35] Li Chen. Algorithms for computing topological invariants in 2d and 3d digital spaces. *arXiv preprint arXiv:1309.4109*, 2013.

[36] Adam Coates, Blake Carpenter, Carl Case, Sanjeev Satheesh, Bipin Suresh, Tao Wang, David J Wu, and Andrew Y Ng. Text detection and character recognition in scene images with unsupervised feature learning. In *2011 International Conference on Document Analysis and Recognition*, pages 440–445. IEEE, 2011.

[37] Yann Cointepas. *Modélisation homotopique et segmentation tridimensionnelles du cortex cérébral à partir d'IRM pour la résolution des problèmes directs et inverses en EEG et en MEG*. PhD thesis, 1999.

[38] Jean Cousty and Gilles Bertrand. Uniqueness of the perfect fusion grid on $\mathbb{Z}^d$. *Journal of Mathematical Imaging and Vision*, 34(3):291–306, 2009.

[39] Jean Cousty, Michel Couprie, Laurent Najman, and Gilles Bertrand. Grayscale watersheds on perfect fusion graphs. In *International Workshop on Combinatorial Image Analysis*, pages 60–73. Springer, 2006.

[40] Sébastien Crozet and Thierry Géraud. A first parallel algorithm to compute the morphological tree of shapes of nd images. In *2014 IEEE International Conference on Image Processing (ICIP)*, pages 2933–2937. IEEE, 2014.

[41] Xavier Daragon. *Surfaces discrètes et frontières d'objets dans les ordres*. PhD thesis, Marne-la-Vallée, 2005.

[42] Xavier Daragon, Michel Couprie, and Gilles Bertrand. Marching chains algorithm for alexandroff-khalimsky spaces. In *International Symposium on Optical Science and Technology*, pages 51–62. International Society for Optics and Photonics, 2002.

[43] Xavier Daragon, Michel Couprie, and Gilles Bertrand. Discrete surfaces and frontier orders. *Journal of Mathematical Imaging and Vision*, 23(3):379–399, 2005.

[44] Marc Pierrot Deseilligny, Georges Stamon, and Ching Y Suen. Veinerization: a new shape description for flexible skeletonization. *Pattern Analysis and Machine Intelligence, IEEE Transactions on*, 20(5):505–521, 1998.

[45] Tamal K Dey and Sumanta Guha. Computing homology groups of simplicial complexes in r 3. *Journal of the ACM (JACM)*, 45(2):266–287, 1998.

[46] Richard O Duda and John H Munson. Graphical-data-processing research study and experimental investigation. Technical report, DTIC Document, 1967.

[47] Charles R Dyer. Computing the euler number of an image from its quadtree. *Computer graphics and image processing*, 13(3):270–276, 1980.

[48] Ulrich Eckhardt and Longin Latecki. *Digital topology*. Inst. für Angewandte Mathematik, 1994.

[49] Herbert Edelsbrunner. *Geometry and topology for mesh generation*. Cambridge University Press, 2001.

[50] Herbert Edelsbrunner and John Harer. *Computational topology: an introduction*. American Mathematical Soc., 2010.

[51] Boris Epshtein, Eyal Ofek, and Yonatan Wexler. Detecting text in natural scenes with stroke width transform. In *Computer Vision and Pattern Recognition (CVPR), 2010 IEEE Conference on*, pages 2963–2970. IEEE, 2010.

[52] Alexander V Evako, Ralph Kopperman, and Yurii V Mukhin. Dimensional properties of graphs and digital spaces. *Journal of Mathematical Imaging and Vision*, 6(2-3):109–119, 1996.

[53] Jonathan Fabrizio, Myriam Robert-Seidowsky, Séverine Dubuisson, Stefania Calarasanu, and Raphaël Boissel. Textcatcher: a method to detect curved and challenging text in natural scenes. *International Journal on Document Analysis and Recognition (IJDAR)*, 19(2):99–117, 2016.

[54] Sylvain Faisan, Nicolas Passat, Vincent Noblet, Renée Chabrier, and Christophe Meyer. Topology preserving warping of 3-d binary images according to continuous one-to-one mappings. *IEEE Transactions on Image Processing*, 20(8):2135–2145, 2011.

[55] ES Fedorov. Course of crystallography. *Published by RK Rikker, Saint-Petersburg (in Russian)*, 1901.

[56] Christophe Fiorio. *Approche interpixel en analyse d'images, une topologie et des algorithmes de segmentation*. PhD thesis, Technische Universität Wien, 1995.

[57] Christophe Fiorio. A topologically consistent representation for image analysis: the frontiers topological graph. In *Discrete Geometry for Computer Imagery*, pages 151–162. Springer, 1996.

[58] Antonio Flores. Über n-dimensionale komplexe, die im r2n+ 1 absolut selbstverschlungen sind. In *Ergeb. Math. Kolloq*, volume 34, pages 4–6, 1933.

[59] Thierry Géraud, Edwin Carlinet, and Sébastien Crozet. Self-duality and digital topology: links between the morphological tree of shapes and well-composed gray-level images. In *International Symposium on*

Mathematical Morphology and Its Applications to Signal and Image Processing, pages 573–584. Springer, 2015.

[60] Thierry Géraud, Edwin Carlinet, Sébastien Crozet, and Laurent Najman. A quasi-linear algorithm to compute the tree of shapes of nd images. In *International Symposium on Mathematical Morphology and Its Applications to Signal and Image Processing*, pages 98–110. Springer, 2013.

[61] Thierry Géraud, J-F Mangin, Isabelle Bloch, and Henri Maître. Segmenting internal structures in 3d mr images of the brain by markovian relaxation on a watershed based adjacency graph. In *Image Processing, 1995. Proceedings., International Conference on*, volume 3, pages 548–551. IEEE, 1995.

[62] Rocío González-Díaz, María José Jiménez, and Belén Medrano. Cohomology ring of 3d cubical complexes. In *IWCIA Special Track on Applications*, pages 139–150, 2009.

[63] Rocio Gonzalez-Diaz, Maria Jose Jimenez, and Belen Medrano. Cubical cohomology ring of 3d photographs. *International Journal of Imaging Systems and Technology*, 21(1):76–85, 2011.

[64] Rocio Gonzalez-Diaz, Maria-Jose Jimenez, and Belen Medrano. Well-composed cell complexes. In *International Conference on Discrete Geometry for Computer Imagery*, pages 153–162. Springer, 2011.

[65] Rocio Gonzalez-Diaz, Maria-Jose Jimenez, and Belen Medrano. 3d well-composed polyhedral complexes. *Discrete Applied Mathematics*, 183:59–77, 2015.

[66] Rocio Gonzalez-Diaz, Maria-Jose Jimenez, and Belen Medrano. Encoding specific 3d polyhedral complexes using 3d binary images. In *International Conference on Discrete Geometry for Computer Imagery*, pages 268–281. Springer, 2016.

[67] Rocio Gonzalez-Diaz, Javier Lamar, and Ronald Umble. Cup products on polyhedral approximations of 3d digital images. In *International Workshop on Combinatorial Image Analysis*, pages 107–119. Springer, 2011.

[68] Rocio Gonzalez-Diaz and Pedro Real. Towards digital cohomology. In *International Conference on Discrete Geometry for Computer Imagery*, pages 92–101. Springer, 2003.

[69] Rocío González-Díaz and Pedro Real. On the cohomology of 3d digital images. *Discrete Applied Mathematics*, 147(2):245–263, 2005.

[70] Stephen B Gray. Local properties of binary images in two dimensions. *Computers, IEEE Transactions on*, 100(5):551–561, 1971.

[71] Marvin J Greenberg. *Lectures on algebraic topology*, volume 9. WA Benjamin New York, 1967.

[72] Ari Gross and Longin Latecki. Digitizations preserving topological and differential geometric properties. *Computer Vision and Image Understanding*, 62(3):370–381, 1995.

[73] E Halimskii and Uporiadochenie Topologicheskie Prostranstva. Naukova dumka, 1977.

[74] Xiao Han, Chenyang Xu, and Jerry L Prince. A topology preserving deformable model using level sets. In *Computer Vision and Pattern Recognition, 2001. CVPR 2001. Proceedings of the 2001 IEEE Computer Society Conference on*, volume 2, pages II–765. IEEE, 2001.

[75] Xiao Han, Chenyang Xu, and Jerry L Prince. A topology preserving level set method for geometric deformable models. *Pattern Analysis and Machine Intelligence, IEEE Transactions on*, 25(6):755–768, 2003.

[76] Henk J. A. M. Heijmans. Theoretical aspects of gray-level morphology. *IEEE Transactions on Pattern Analysis and Machine Intelligence*, 13(6):568–582, 1991.

[77] Henk JAM Heijmans. Morphological image operators. *Advances in Electronics and Electron Physics Suppl., Boston: Academic Press,—c1994*, 1, 1994.

[78] Gabor T Herman. Discrete multidimensional jordan surfaces. *CVGIP: Graphical Models and Image Processing*, 54(6):507–515, 1992.

[79] John FP Hudson. Piecewise linear topology. *New York*, 1969.

[80] Lê Duy Huynh, Yongchao Xu, and Thierry Géraud. A morphological hierarchical representation with application to text segmentation in natural images. *(to appear)*, 2016.

[81] Ludvik Janos and Azriel Rosenfeld. Digital connectedness: An algebraic approach. *Pattern Recognition Letters*, 1(3):135–139, 1983.

[82] C. Jordan. *Cours d'Analyse de l'Ecole Polytechnique*, volume 3. Gauthier-Villars, Paris, 1887.

[83] Tao Ju, Frank Losasso, Scott Schaefer, and Joe Warren. Dual contouring of hermite data. In *ACM Transactions on Graphics (TOG)*, volume 21, pages 339–346. ACM, 2002.

[84] John L Kelley. General topology. the university series in higher mathematics, 1955.

[85] Efim Khalimsky, Ralph Kopperman, and Paul R Meyer. Computer graphics and connected topologies on finite ordered sets. *Topology and its Applications*, 36(1):1–17, 1990.

[86] RM Kirby, V Pascucci, CT Silva, TJ Peters, J Tienry, C Scheidegger, LG Nonato, and Tiago Etiene. Topology verification for isosurface extraction. *IEEE Transactions on Visualization & Computer Graphics*, (6):952–965, 2012.

[87] T Yung Kong and Azriel Rosenfeld. Digital topology: Introduction and survey. *Computer Vision, Graphics, and Image Processing*, 48(3):357–393, 1989.

[88] T Yung Kong and Azriel Rosenfeld. If we use 4-or 8-connectedness for both the objects and the background, the euler characteristics is not locally computable. *Pattern Recognition Letters*, 11(4):231–232, 1990.

[89] Ralph Kopperman. The khalimsky line as a foundation for digital topology. In *Shape in picture*, pages 3–20. Springer, 1994.

[90] Ralph Kopperman, Paul R Meyer, and Richard G Wilson. A jordan surface theorem for three-dimensional digital spaces. *Discrete & Computational Geometry*, 6(2):155–161, 1991.

[91] Ullrich Köthe. *Generische Programmierung für die Bildverarbeitung*. BoD–Books on Demand, 2000.

[92] Vladimir A Kovalevsky. Finite topology as applied to image analysis. *Computer vision, graphics, and image processing*, 46(2):141–161, 1989.

[93] Casimir Kuratowski. Sur le probleme des courbes gauches en topologie. *Fundamenta mathematicae*, 15(1):271–283, 1930.

[94] Jacques-Olivier Lachaud and Annick Montanvert. Continuous analogs of digital boundaries: A topological approach to iso-surfaces. *Graphical models*, 62(3):129–164, 2000.

[95] LJ Latecki. Well-composed sets. *ADVANCES IN IMAGING AND ELECTRON PHYSICS, VOL 112*, 112:95–163, 2000.

[96] Longin Latecki, Ulrich Eckhardt, and Azriel Rosenfeld. Well-composed sets. *Computer Vision and Image Understanding*, 61(1):70–83, 1995.

[97] Longin J Latecki. Multicolor well-composed pictures. In *Photonics for Industrial Applications*, pages 63–70. International Society for Optics and Photonics, 1995.

[98] Longin Jan Latecki. 3d well-composed pictures. *Graphical Models and Image Processing*, 59(3):164–172, 1997.

[99] Longin Jan Latecki. *Discrete representation of spatial objects in computer vision*, volume 11. Springer Science & Business Media, 1998.

[100] Longin Jan Latecki, Christopher Conrad, and Ari Gross. Preserving topology by a digitization process. *Journal of Mathematical Imaging and Vision*, 8(2):131–159, 1998.

[101] Carole Le Guyader and Luminita A Vese. Self-repelling snakes for topology-preserving segmentation models. *IEEE Transactions on Image Processing*, 17(5):767–779, 2008.

[102] C-N Lee and Azriel Rosenfeld. *Computing the Euler number of a 3D image*. University of Maryland. Computer Science, 1986.

[103] Chung-Nim Lee, Timothy Poston, and Azriel Rosenfeld. Winding and euler numbers for 2d and 3d digital images. *CVGIP: Graphical Models and Image Processing*, 53(6):522–537, 1991.

[104] John Lee. *Introduction to topological manifolds*, volume 940. Springer Science & Business Media, 2010.

[105] Jung-Jin Lee, Pyoung-Hean Lee, Seong-Whan Lee, Alan L Yuille, and Christof Koch. Adaboost for text detection in natural scene. In *ICDAR*, pages 429–434, 2011.

[106] Roland Levillain, Thierry Géraud, and Laurent Najman. Why and howto design a generic and efficient image processing framework: The case of the milena library. In *2010 IEEE International Conference on Image Processing*, pages 1941–1944. IEEE, 2010.

[107] Roland Levillain, Thierry Géraud, and Laurent Najman. Writing reusable digital topology algorithms in a generic image processing framework. In *Applications of Discrete Geometry and Mathematical Morphology*, pages 140–153. Springer, 2012.

[108] William Bernard Raymond Lickorish. Simplicial moves on complexes and manifolds. *Geometry and Topology Monographs*, 2(299-320):314, 1999.

[109] Elon L Lima. The jordan-brouwer separation theorem for smooth hypersurfaces. *The American Mathematical Monthly*, 95(1):39–42, 1988.

[110] William E Lorensen and Harvey E Cline. Marching cubes: A high resolution 3d surface construction algorithm. In *ACM siggraph computer graphics*, volume 21, pages 163–169. ACM, 1987.

[111] Wolfram HHJ Lunscher and Michael P Beddoes. Fast binary-image boundary extraction. *Computer vision, graphics, and image processing*, 38(3):229–257, 1987.

[112] J-F Mangin, Olivier Coulon, and Vincent Frouin. Robust brain segmentation using histogram scale-space analysis and mathematical morphology. In *International Conference on Medical Image Computing and Computer-Assisted Intervention*, pages 1230–1241. Springer, 1998.

[113] Jocelyn Marchadier, Didier Arquès, and Sylvain Michelin. Thinning grayscale well-composed images. *Pattern Recognition Letters*, 25(5):581–590, 2004.

[114] D. Martin, C. Fowlkes, D. Tal, and J. Malik. A database of human segmented natural images and its application to evaluating segmentation algorithms and measuring ecological statistics. In *Proc. of the International Conference on Computer Vision (ICCV)*, volume 2, pages 416–423, 2001.

[115] Loïc Mazo. *Déformations homotopiques dans les images digitales n-aires*. PhD thesis, Université de Strasbourg, 2011.

[116] Loïc Mazo, Nicolas Passat, Michel Couprie, and Christian Ronse. Digital imaging: A unified topological framework. *Journal of Mathematical Imaging and Vision*, 44(1):19–37, 2012.

[117] Enric Meinhardt-Llopis. *Morphological and statistical techniques for the analysis of 3D images*. PhD thesis, Ph. D. thesis, Universitat Pompeu Fabra, Spain (March 2011), 2011.

[118] Fernand Meyer. Skeletons and perceptual graphs. *Signal Processing*, 16(4):335–363, 1989.

[119] Fernand Meyer and Petros Maragos. Morphological scale-space representation with levelings. In *International Conference on Scale-Space Theories in Computer Vision*, pages 187–198. Springer, 1999.

[120] Pascal Monasse and Frederic Guichard. Fast computation of a contrast-invariant image representation. *IEEE Transactions on Image Processing*, 9(5):860–872, 2000.

[121] John P Mylopoulos and Theodosios Pavlidis. On the topological properties of quantized spaces, i. the notion of dimension. *Journal of the ACM (JACM)*, 18(2):239–246, 1971.

[122] JP Mylopoulos and Theodosios Pavlidis. On the topological properties of quantized spaces, ii. connectivity and order of connectivity. *Journal of the ACM (JACM)*, 18(2):247–254, 1971.

[123] Laurent Najman and Michel Couprie. Watershed algorithms and contrast preservation. In *International Conference on Discrete Geometry for Computer Imagery*, pages 62–71. Springer, 2003.

[124] Laurent Najman and Thierry Géraud. Discrete set-valued continuity and interpolation. In *Mathematical Morphology and Its Applications to Signal and Image Processing*, pages 37–48. Springer, 2013.

[125] Laurent Najman and Michel Schmitt. Watershed of a continuous function. *Signal Processing*, 38(1):99–112, 1994.

[126] Laurent Najman and Hugues Talbot. *Mathematical morphology*. John Wiley & Sons, 2013.

[127] Mikio Nakahara. *Geometry, topology and physics*. CRC Press, 2003.

[128] Maxwell Herman Alexander Newman. *Elements of the topology of plane sets of points*. Cambridge, 1939.

[129] Phuc Ngo, Yukiko Kenmochi, Nicolas Passat, and Hugues Talbot. Combinatorial structure of rigid transformations in 2d digital images. *Computer Vision and Image Understanding*, 117(4):393–408, 2013.

[130] Phuc Ngo, Yukiko Kenmochi, Nicolas Passat, and Hugues Talbot. Sufficient conditions for topological invariance of 2d images under rigid transformations. In *International Conference on Discrete Geometry for Computer Imagery*, pages 155–168. Springer, 2013.

[131] Phuc Ngo, Nicolas Passat, Yukiko Kenmochi, and Hugues Talbot. Well-composed images and rigid transformations. In *IEEE International Conference on Image Processing ICIP 2013*, pages 3035–3039, 2013.

[132] Phuc Ngo, Nicolas Passat, Yukiko Kenmochi, and Hugues Talbot. Topology-preserving rigid transformation of 2d digital images. *IEEE Transactions on Image Processing*, 23(2):885–897, 2014.

[133] M Minsky S Papert and ML Minsky. Perceptrons: an introduction to computational geometry. *Expanded Edition*, 1969.

[134] Theodosios Pavlidis. *Algorithms for graphics and image processing*. Springer Science & Business Media, 2012.

[135] Dzung L Pham, Pierre-Louis Bazin, and Jerry L Prince. Digital topology in brain imaging. *IEEE Signal Processing Magazine*, 27(4):51–59, 2010.

[136] Jos BTM Roerdink and Arnold Meijster. The watershed transform: Definitions, algorithms and parallelization strategies. *Fundamenta informaticae*, 41(1, 2):187–228, 2000.

[137] Christian Ronse. Flat morphological operators on arbitrary power lattices. In *Geometry, Morphology, and Computational Imaging*, pages 1–21. Springer, 2003.

[138] Azriel Rosenfeld. Connectivity in digital pictures. *Journal of the ACM (JACM)*, 17(1):146–160, 1970.

[139] Azriel Rosenfeld. Arcs and curves in digital pictures. *Journal of the ACM (JACM)*, 20(1):81–87, 1973.

[140] Azriel Rosenfeld. Adjacency in digital pictures. *Information and Control*, 26(1):24–33, 1974.

[141] Azriel Rosenfeld. Digital topology. *American Mathematical Monthly*, pages 621–630, 1979.

[142] Azriel Rosenfeld. Fuzzy digital topology. *Information and Control*, 40(1):76–87, 1979.

[143] Azriel Rosenfeld. Picture languages-formal model of picture recognition, 1979.

[144] Azriel Rosenfeld. On connectivity properties of grayscale pictures. *Pattern Recognition*, 16(1):47–50, 1983.

[145] Azriel Rosenfeld, T Yung Kong, and Akira Nakamura. Topology-preserving deformations of two-valued digital pictures. *Graphical Models and Image Processing*, 60(1):24–34, 1998.

[146] Azriel Rosenfeld, T Yung Kong, and Angela Y Wu. Digital surfaces. *CVGIP: Graphical Models and Image Processing*, 53(4):305–312, 1991.

[147] Azriel Rosenfeld and John L Pfaltz. Sequential operations in digital picture processing. *Journal of the ACM (JACM)*, 13(4):471–494, 1966.

[148] Philippe Salembier and Jean Serra. Flat zones filtering, connected operators, and filters by reconstruction. *IEEE Transactions on image processing*, 4(8):1153–1160, 1995.

[149] Florent Ségonne. Active contours under topology control—genus preserving level sets. *International Journal of Computer Vision*, 79(2):107–117, 2008.

[150] Jean Serra. *Image analysis and mathematical morphology, v. 1.* Academic press, 1982.

[151] Jean Serra and B Ravi Kiran. Digitization of partitions and tessellations. In *Discrete Geometry for Computer Imagery*, pages 323–334. Springer, 2016.

[152] Raj Shekhar, Elias Fayyad, Roni Yagel, and J Fredrick Cornhill. Octree-based decimation of marching cubes surfaces. In *Visualization'96. Proceedings.*, pages 335–342. IEEE, 1996.

[153] Marcelo Siqueira, Longin J Latecki, and Jean Gallier. Making 3d binary digital images well-composed. In *Electronic Imaging 2005*, pages 150–163. International Society for Optics and Photonics, 2005.

[154] Marcelo Siqueira, Longin Jan Latecki, Nicholas Tustison, Jean Gallier, and James Gee. Topological repairing of 3d digital images. *Journal of Mathematical Imaging and Vision*, 30(3):249–274, 2008.

[155] Lauro Snidaro and Gian Luca Foresti. Real-time thresholding with euler numbers. *Pattern Recognition Letters*, 24(9):1533–1544, 2003.

[156] Pierre Soille. *Morphological image analysis: principles and applications*. Springer Science & Business Media, 2013.

[157] Pierre Soille and Martino Pesaresi. Advances in mathematical morphology applied to geoscience and remote sensing. *IEEE Transactions on Geoscience and Remote Sensing*, 40(9):2042–2055, 2002.

[158] Juan Humberto Sossa-Azuela et al. On the computation of the euler number of a binary object. *Pattern recognition*, 29(3):471–476, 1996.

[159] Juan Humberto Sossa-Azuela, R Santiago-Montero, M Pérez-Cisneros, and E Rubio-Espino. Computing the euler number of a binary image based on a vertex codification. *Journal of applied research and technology*, 11(3):360–370, 2013.

[160] Peer Stelldinger. *Image digitization and its influence on shape properties in finite dimensions*, volume 312. IOS Press, 2008.

[161] Peer Stelldinger and Ullrich Köthe. Towards a general sampling theory for shape preservation. *Image and Vision Computing*, 23(2):237–248, 2005.

[162] Peer Stelldinger and Longin Jan Latecki. 3d object digitization: Majority interpolation and marching cubes. In *Pattern Recognition, 2006. ICPR 2006. 18th International Conference on*, volume 2, pages 1173–1176. IEEE, 2006.

[163] Peer Stelldinger, Longin Jan Latecki, and Marcelo Siqueira. Topological equivalence between a 3d object and the reconstruction of its digital image. *Pattern Analysis and Machine Intelligence, IEEE Transactions on*, 29(1):126–140, 2007.

[164] Peer Stelldinger and Robin Strand. Topology preserving digitization with fcc and bcc grids. In *International Workshop on Combinatorial Image Analysis*, pages 226–240. Springer, 2006.

[165] Lawrence Neff Stout. Two discrete forms of the jordan curve theorem. *The American Mathematical Monthly*, 95(4):332–336, 1988.

[166] Ganesh Sundaramoorthi and Anthony Yezzi. Global regularizing flows with topology preservation for active contours and polygons. *IEEE Transactions on Image Processing*, 16(3):803–812, 2007.

[167] Mohamed Tajine and Christian Ronse. Topological properties of hausdorff discretizations. In *Mathematical Morphology and its Applications to Image and Signal Processing*, pages 41–50. Springer, 2002.

[168] Junichiro Toriwaki and Hiroyuki Yoshida. *Fundamentals of three-dimensional digital image processing*. Springer Science & Business Media, 2009.

[169] Nicholas J Tustison, Brian B Avants, Marcelo Siqueira, and James C Gee. Topological well-composedness and glamorous glue: A digital gluing algorithm for topologically constrained front propagation. *Image Processing, IEEE Transactions on*, 20(6):1756–1761, 2011.

[170] Helge Tverberg. A proof of the jordan curve theorem. *Bull. London Math. Soc*, 12(1):34–38, 1980.

[171] Egbert R Van Kampen. Komplexe in euklidischen räumen. In *Abhandlungen aus dem Mathematischen Seminar der Universität Hamburg*, volume 9, pages 72–78. Springer, 1933.

[172] Lucas J Van Vliet, Ian T Young, and Guus L Beckers. An edge detection model based on non-linear laplace filtering. In *Gelsema, ES, Kanal, LN (eds.), Pattern recognition and artificial intelligence, towards an integration, International workshop, Amsterdam, May 18-20, 1988*. North-Holland, 1988.

[173] K Voss. Images, objects, and surfaces in zn. *International journal of pattern recognition and artificial intelligence*, 5(05):797–808, 1991.

[174] Tao Wang, David J Wu, Adam Coates, and Andrew Y Ng. End-to-end text recognition with convolutional neural networks. In *Pattern Recognition (ICPR), 2012 21st International Conference on*, pages 3304–3308. IEEE, 2012.

[175] Yang Wang and Prabir Bhattacharya. Digital connectivity and extended well-composed sets for gray images. *Computer Vision and Image Understanding*, 68(3):330–345, 1997.

[176] Paul R Wilson. Euler formulas and geometric modeling. *IEEE Computer Graphics and Applications*, 8(5):24–36, 1985.

[177] Yongchao Xu, Thierry Géraud, and Laurent Najman. Context-based energy estimator: Application to object segmentation on the tree of shapes. In *2012 19th IEEE International Conference on Image Processing*, pages 1577–1580. IEEE, 2012.

[178] Yongchao Xu, Thierry Géraud, and Laurent Najman. Morphological filtering in shape spaces: Applications using tree-based image representations. In *Pattern Recognition (ICPR), 2012 21st International Conference on*, pages 485–488. IEEE, 2012.

[179] Yongchao Xu, Thierry Géraud, and Laurent Najman. Two applications of shape-based morphology: Blood vessels segmentation and a generalization of constrained connectivity. In *International Symposium on Mathematical Morphology and Its Applications to Signal and Image Processing*, pages 390–401. Springer, 2013.

[180] Hyun S Yang and Sanjay Sengupta. Intelligent shape recognition for complex industrial tasks. *IEEE Control Systems Magazine*, 8(3):23–30, 1988.

[181] Qixiang Ye and David Doermann. Text detection and recognition in imagery: A survey. *IEEE transactions on pattern analysis and machine intelligence*, 37(7):1480–1500, 2015.

[182] Shigeki Yokoi, Jun-Ichiro Toriwaki, and Teruo Fukumura. An analysis of topological properties of digitized binary pictures using local features. *Computer Graphics and Image Processing*, 4(1):63–73, 1975.

[183] Yingying Zhu, Cong Yao, and Xiang Bai. Scene text detection and recognition: Recent advances and future trends. *Frontiers of Computer Science*, 10(1):19–36, 2016.

Abstract Digitization of the real world using real sensors has many drawbacks; in particular, we loose "well-composedness" in the sense that two digitized objects can be connected or not depending on the connectivity we choose in the digital image, leading then to ambiguities. Furthermore, digitized images are arrays of numerical values, and then do not own any topology by nature, contrary to our usual modeling of the real world in mathematics and in physics. Loosing all these properties makes difficult the development of algorithms which are "topologically correct" in image processing: e.g., the computation of the tree of shapes needs the representation of a given image to be continuous and well-composed; in the contrary case, we can obtain abnormalities in the final result. Some well-composed continuous representations already exist, but they are not in the same time n-dimensional and self-dual. n-dimensionality is crucial since usual signals are more and more 3-dimensional (like 2D videos) or 4-dimensional (like 4D Computerized Tomography-scans), and self-duality is necessary when a same image can contain different objects with different contrasts. We developed then a new way to make images well-composed by interpolation in a self-dual way and in n-D; followed with a span-based immersion, this interpolation becomes a self-dual continuous well-composed representation of the initial n-D signal. This representation benefits from many strong topological properties: it verifies the intermediate value theorem, the boundaries of any threshold set of the representation are disjoint union of discrete surfaces, and so on.

Résumé Le processus de discrétisation faisant inévitablement appel à des capteurs, et ceux-ci étant limités de par leur nature, de nombreux effets secondaires apparaissent alors lors de ce processus; en particulier, nous perdons la propriété d'être "bien-composé" dans le sens où deux objects discrétisés peuvent être connectés ou non en fonction de la connexité utilisée dans l'image discrète, ce qui peut amener à des ambigüités. De plus, les images discrétisées sont des tableaux de valeurs numériques, et donc ne possèdent pas de topologie par nature, contrairement à notre modélisation usuelle du monde en mathématiques et en physique. Perdre toutes ces propriétés rend difficile l'élaboration d'algorithmes topologiquement corrects en traitement d'images: par exemple, le calcul de l'arbre des formes nécessite que la representation d'une image donnée soit continue et bien-composée; dans le cas contraire, nous risquons d'obtenir des anomalies dans le résultat final. Quelques representations continues et bien-composées existent déjà, mais elles ne sont pas simultanément n-dimensionnelles et auto-duales. La n-dimensionalité est cruciale sachant que les signaux usuels sont de plus en plus tridimensionnels (comme les vidéos 2D) ou 4-dimensionnels (comme les CT-scans). L'auto-dualité est nécéssaire lorsqu'une même image contient des objets à contrastes divers. Nous avons donc développé une nouvelle façon de rendre les images bien-composées par interpolation de façon auto-duale et en n-D; suivie d'une immersion par l'opérateur span, cette interpolation devient une représentation auto-duale continue et bien-composée du signal initial n-D. Cette représentation bénéficie de plusieurs propriétés topologiques fortes: elle vérifie le théorème de la valeur intermédiaire, les contours de chaque coupe de la représentation sont déterminés par une union disjointe de surfaces discrètes, et ainsi de suite.